frontiers | Research Topics

Benchmark experiments, development and needs in support of advanced reactor design

Edited by
Mark David DeHart, John Darrell Bess, Michael Fleming and Germina Ilas

Published in
Frontiers in Energy Research

ISSN 1664-8714
ISBN 978-2-8325-3094-8
DOI 10.3389/978-2-8325-3094-8

About Frontiers

Frontiers is more than just an open access publisher of scholarly articles: it is a pioneering approach to the world of academia, radically improving the way scholarly research is managed. The grand vision of Frontiers is a world where all people have an equal opportunity to seek, share and generate knowledge. Frontiers provides immediate and permanent online open access to all its publications, but this alone is not enough to realize our grand goals.

Frontiers journal series

The Frontiers journal series is a multi-tier and interdisciplinary set of open-access, online journals, promising a paradigm shift from the current review, selection and dissemination processes in academic publishing. All Frontiers journals are driven by researchers for researchers; therefore, they constitute a service to the scholarly community. At the same time, the *Frontiers journal series* operates on a revolutionary invention, the tiered publishing system, initially addressing specific communities of scholars, and gradually climbing up to broader public understanding, thus serving the interests of the lay society, too.

Dedication to quality

Each Frontiers article is a landmark of the highest quality, thanks to genuinely collaborative interactions between authors and review editors, who include some of the world's best academicians. Research must be certified by peers before entering a stream of knowledge that may eventually reach the public - and shape society; therefore, Frontiers only applies the most rigorous and unbiased reviews. Frontiers revolutionizes research publishing by freely delivering the most outstanding research, evaluated with no bias from both the academic and social point of view. By applying the most advanced information technologies, Frontiers is catapulting scholarly publishing into a new generation.

What are Frontiers Research Topics?

Frontiers Research Topics are very popular trademarks of the *Frontiers journals series*: they are collections of at least ten articles, all centered on a particular subject. With their unique mix of varied contributions from Original Research to Review Articles, Frontiers Research Topics unify the most influential researchers, the latest key findings and historical advances in a hot research area.

Find out more on how to host your own Frontiers Research Topic or contribute to one as an author by contacting the Frontiers editorial office: frontiersin.org/about/contact

Benchmark experiments, development and needs in support of advanced reactor design

Topic editors

Mark David DeHart — Idaho National Laboratory (DOE), United States

John Darrell Bess — JFoster & Associates, LLC (JFA), United States

Michael Fleming — Organisation For Economic Co-Operation and Development, France

Germina Ilas — Oak Ridge National Laboratory (DOE), United States

Citation

DeHart, M. D., Bess, J. D., Fleming, M., Ilas, G., eds. (2023). *Benchmark experiments, development and needs in support of advanced reactor design*. Lausanne: Frontiers Media SA. doi: 10.3389/978-2-8325-3094-8

Table of contents

frontiers | Frontiers in Energy Research

TYPE Editorial
PUBLISHED 12 July 2023
DOI 10.3389/fenrg.2023.1249428

OPEN ACCESS

EDITED AND REVIEWED BY
Shripad T. Revankar,
Purdue University, United States

*CORRESPONDENCE
Mark D. DeHart,
mark.dehart@inl.gov

RECEIVED 28 June 2023
ACCEPTED 06 July 2023
PUBLISHED 12 July 2023

CITATION
DeHart MD, Bess JD, Fleming M and Ilas G (2023), Editorial: Benchmark experiments, development and needs in support of advanced reactor design. *Front. Energy Res.* 11:1249428. doi: 10.3389/fenrg.2023.1249428

Editorial: Benchmark experiments, development and needs in support of advanced reactor design

Mark D. DeHart[1]*, John Darrell Bess[2], Michael Fleming[3] and Germina Ilas[4]

[1]Idaho National Laboratory, Nuclear Science and Technology Directorate, Idaho Falls, ID, United States, [2]JFoster and Associates, LLC, Idaho Falls, ID, United States, [3]Organisation for Economic Co-Operation and Development, Nuclear Energy Agency, Paris, France, [4]Oak Ridge National Laboratory, Nuclear Energy and Fuel Cycle Division, Oak Ridge, TN, United States

KEYWORDS

nuclear, reactor, validation, experiment, benchmark

Editorial on the Research Topic
Benchmark experiments, development and needs in support of advanced reactor design

Advanced nuclear reactor designs will for the most part be a departure from low enrichment light water reactor (LWR) designs currently operated around the world. Such advanced designs include but are not limited to new TRISO-fueled high temperature gas reactors, heat-pipe cooled micro-reactors, fluoride salt cooled high-temperature reactors, molten salt reactors, lead cooled fast reactors, nuclear thermal propulsion concepts, and include LWR designs with advanced fuel and clad types.

Modeling and simulation methods for advanced reactors is necessary for regulators to approve license requests. However, regulators also require that modeling approaches be validated against experimental measurements. Hence, there is a crucial need for data for advanced reactor systems that will support validation of analysis methods. To this end, this Research Topic includes eleven papers organized into topical seven categories relevant for advanced reactor design.

Experimental facilities

Thompson et al. provide a review of activities at the National Criticality Experiments Research Center (NCERC). NCERC is one of few critical experiment facilities remaining in the United States and regularly performs subcritical, critical and supercritical experiments.

Measurement techniques

Two papers describe measurement techniques and uncertainties associated with measured data. Skifton describes the superposition of both inhomogeneity and drift of

thermocouple elements occurring in high-temperature irradiation-resistant thermocouples. Leclaire and Bess describe two methods to deal with the assessment of the rod positioning uncertainties in a reactor fuel lattice.

Fuel performance

Two papers describe fuel performance measurements. Keiser et al. provides the results of post irradiation examination of a TRIGA fuel element with a high assay low-enrichment uranium-zirconium hydride fuel. Paaren et al. present the results of BISON of metallic fuel against experimental measurements within two fuel experiment databases.

Thermal hydraulics

Gutowska et al. present selected data from experiments performed to fill data gaps in the characteristics pressurized and depressurized conduction cooldown transients.

Shielding

In Iwamoto et al. the validation of the Particle and Heavy Ion Transport System (PHITS) as applied to neutron-shielding experiments for fusion is described. Five sets of measurements with different shielding materials were simulated with PHITS and were found to have acceptable agreement.

Nuclear data

Bostelmann et al. describe an assessment of nuclear data used in analysis of advanced reactor concepts for which operating history is unavailable, while (van der Marck and Koning) make the case for use of fission product cross section measurements performed at the STEK facility.

Benchmark development

Two review papers describe international benchmarking activities that are resources for advanced reactor modeling. Bess et al. describe two benchmark programs: the International Reactor Physics Experiment Evaluation (IRPhE) Project and the International Criticality Safety Benchmark Evaluation Project (ICSBEP). Bess et al. expands on benchmark activities sponsored by the NEA, describing several international benchmark activities.

Summary

The Research Topic entitled *Benchmark Experiments, Development and Needs in Support of Advanced Reactor Design* provides a broad set of research results emphasizing the need for reactor physics benchmarks to support the next-generation of advanced reactors. This Research Topic includes papers on experimental facilities, measurement techniques, fuel performance, thermal hydraulics, shielding, nuclear data, all related to advanced reactor designs, combined with papers describing international efforts to develop Research Topic of benchmarks for reactor physics, criticality safety, fuel performance, spent fuel characterization, thermal hydraulics, shielding and multi-physics computational methods.

Author contributions

All authors approved the submitted version.

Conflict of interest

Author JB is employed by JFoster and Associates.

The remaining authors declare that the research was conducted in the absence of any commercial or financial relationships that could be construed as a potential conflict of interest.

Publisher's note

frontiers | Frontiers in Energy Research

TYPE Methods
PUBLISHED 26 December 2022
DOI 10.3389/fenrg.2022.1058750

OPEN ACCESS

EDITED BY
Yixiang Liao,
Helmholtz Association of German Research Centres (HZ), Germany

REVIEWED BY
Mohammad Alrwashdeh,
Khalifa University, United Arab Emirates
Ian Hill,
Organisation For Economic Co-Operation and Development, France

*CORRESPONDENCE
Nicolas Leclaire,
nicolas.leclaire@irsn.fr

SPECIALTY SECTION
This article was submitted to Nuclear Energy, a section of the journal Frontiers in Energy Research

RECEIVED 30 September 2022
ACCEPTED 12 December 2022
PUBLISHED 26 December 2022

CITATION
Leclaire N and Bess JD (2022), Comparison of two methods for assessment of the rod positioning uncertainty and consequences on the evaluation of correlation factors. *Front. Energy Res.* 10:1058750. doi: 10.3389/fenrg.2022.1058750

Comparison of two methods for assessment of the rod positioning uncertainty and consequences on the evaluation of correlation factors

Nicolas Leclaire[1]* and John Darrell Bess[2]

[1]Institut de Radioprotection et de Sûreté Nucléaire (IRSN), PSN-RES/SNC, Fontenay-aux-Roses, France, [2]JFoster and Associates, LLC (JFA), Idaho Falls, ID, United States

In this paper two major families of methods to deal with the assessment of the rod positioning uncertainty in a lattice are tested: a traditional one described in the *International Handbook of Evaluated Criticality Safety Benchmark Experiments* (IHECSBE) Handbook and the other one consisting in sampling the position of rods with Monte Carlo techniques (ISO Uncertainty Guidelines). They are applied on a benchmark with tight-packed lattice of UO_2 rods that is sensitive to the rod positioning as it is clearly under-moderated. It is shown that the choice of the method has a great impact on the propagated uncertainty, the traditional one leading to a significant overestimation of the overall uncertainty and can also contribute to a bias in the correlation factors that are used for assessing biases due to nuclear data using GLLSM methodologies. The paper briefly describes the tight-packed lattice experimental program performed at the Valduc Research Centre, which is at the origin of these concerns. Then it proposes a simple model on which to apply simulations of rod positioning to be performed with MORET 5 Monte Carlo code using the Prométhée tool. Results demonstrate that use of Monte Carlo methodologies provide more realistic uncertainty estimates in fuel pitch that are consistent with repeatability/reproducibility experiments. The current comparisons use light water reactor systems, which is directly relevant to some small modular reactor designs. However, accurate prediction and estimate of uncertainties in pitch for advanced reactor systems is also relevant. The application of unrealistic uncertainty analysis methods can incur larger margins in advanced reactor design, safety, and operation than are necessary.

KEYWORDS

ICSBEP, Monte Carlo sampling, positioning uncertainty, prométhée, uran

1 Introduction

For several years now, the criticality community has made efforts to provide documented critical experiments with "best-estimate" uncertainties that could be of interest for the validation of criticality codes. A project named International Criticality Safety Benchmark Evaluation Project (ICSBEP) was created in 1992 for that purpose (Briggs, Scott, and Nouri 2003). In that prospect, experiments from diverse laboratories and covering a wide range of applications were evaluated. A part of the evaluation consists of determining the chemical and geometrical uncertainties. Sometimes just a few parameters can drive the overall uncertainty. When designing experimental programs, people in charge of the design of experiments try to select moderation values as close as possible to the moderation optimum. One of the reasons is that the closer the moderation ratio is to the optimum, the lower the uncertainties in rod positioning and fewer rods are needed to reach criticality. However, in the French tight-packed-lattice experiments, LEU-COMP-THERM-071 (Leclaire 2019a), LEU-COMP-THERM-072 (Leclaire 2019b), and LEU-COMP-THERM-073 (Leclaire 2019c), the experiments have pitches smaller than required for optimal moderation, as they were designed to slightly shift the sensitivity of k_{eff} to the epithermal energy range with a view to address the economic needs of nuclear operators with a more compact storage. Therefore, the uncertainty contribution from rod positioning is greater.

In fact, when the spacing between rods corresponds to the fissile medium moderation ratio optimum, the positioning uncertainty is negligible. However, when the spacing between rods is smaller when we get further from the moderation ratio optimum, the impact is much greater. Depending on the pitch between rods, the positioning uncertainty can have a varying effect upon k_{eff}. The situation where the moderation ratio is far from the optimum ratio could be encountered in advanced reactor design concepts, including microreactors. During the design and operations, the uncertainty in the positioning of rods due to the tolerance values of grids' holes and fuel rods is considered in the calculations. A propagation method based on MC sampling can help in determining the best estimate of the overall uncertainty and mitigating overestimation of margins supporting safety and operations.

Moreover, with the growth of advanced tools used to estimate the biases due to nuclear data such as TSUNAMI (Rearden 2004), WHISPER (Brown, Rising, and Alwin 2016), and MACSENS [Fernex], the accurate determination of correlation factors between experimental cases has become an important issue. The determination of such values is conditioned by a thorough evaluation of uncertainties, and the associated random and systematic components of each uncertainty.

To sum this up, different ways of propagating the uncertainty in terms of Δk_{eff} can be envisioned, amongst which what can be called "traditional" ones based on ICSBEP recommendations and other ones based on Monte Carlo (MC) simulations. Depending on the method, the impact on Δk_{eff} can be completely different. The aim of this work is to compare the traditional methods with methods using MC simulations on variable sizes of lattices as proposed in the International Organization for Standardization (ISO) uncertainty guides (referred to in this document as the ISO GUM S1 procedure) (JCGM 2009) (JCGM 2008) and to compare with repeatability/reproducibility experiments allowing access to such uncertainty.

2 Description of the configuration

2.1 Tight-packed lattice pitch program

From 1998 to 1999 a series of critical experiments referred to as the tight-packed lattice experimental program was performed using Apparatus B in the Commissariat à l'Energie Atomique (CEA) Valduc Research Centre in France (Duhamel and Girault 2006). The experimental device, shown in Figure 1A, is commonly used for assembling configurations with epithermal and thermal neutron energy spectra. These experiments, designed by L'Institut de Radioprotection et de Sûreté Nucléaire (IRSN), and funded by COGEMA (also formerly AREVA NC and now Orano Cycle) and IRSN, involved UO_2 rods at a 1.05-, 1.075-, 1.1- or 1.6-cm square pitch and contributed to the validation of uranium cross sections in thermal and epithermal energy ranges. Twenty-seven critical experiments were performed, evaluated, and analyzed with different criticality software packages. The experiments were slightly sub-critical, the water level being raised until $k_{eff} = 1 - (\beta_{eff}/10)$. The water critical level was obtained by extrapolation of the inverse neutron counting rate.

The first step of the program involved lattices of 1.1-cm square pitched UO_2 rods moderated and reflected by water (documented in LEU-COMP-THERM-071). The UO_2 rods were a typical design for a pressurized-water reactor (PWR) with a ^{235}U enrichment of 4.738 wt%. The main characteristics of the fuel rods are given in Table 1 (uncertainties are indicated as 1σ). The uncertainties of the rods are mainly due to the precision of measurement devices and are therefore assumed to be 90% systematic. The UO_2 rods consisted of vertically stacked pellets contained within Zircaloy-4 cladding. The rod diameter corresponded to the industrial fuel pin diameter. The fuel stack length was adjusted to the height of the experimental tank, which was equal to 90 cm. Experimental uncertainties for the rod characteristics are also gathered in Table 1.

Sensitivity studies were performed to assess the impact on k_{eff} of various experimental uncertainties upon the configuration in accordance with the recommendations of the IHECSBE uncertainty guide (Dean 2008). The effects on k_{eff} changes were adopted as the associated components of the k_{eff} uncertainty. In order to compare different methods of rod

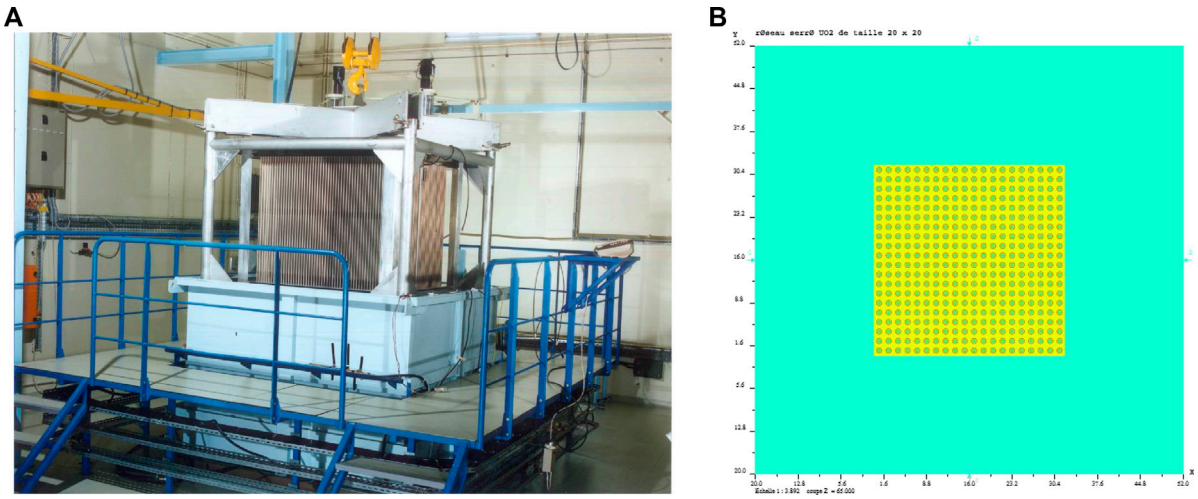

FIGURE 1
(A) Apparatus B Experiment assembly. **(B)** Simple benchmark model of a fuel lattice.

TABLE 1 Primary experiment parameters and uncertainties for LEU-COMP-THERM-071 (Leclaire 2019a).

Parameters	Value	Uncertainty
UO_2 rods		
Uranium Vector (wt%)		
^{234}U	0.0302	0.0005
^{235}U	4.7376	0.0020
^{236}U	0.1362	0.0005
^{238}U	95.0959	0.0010
Oxide impurities (ppm)	204	204
Fuel Pellet	0.78919	0.00176
Diameter (cm)		
Fuel Density (g/cm^3)	10.38	0.073
Inner Clad	0.836	0.005
Diameter (cm)		
Outer Clad	0.94924	0.00044
Diameter (cm)		
Density (g/cm^3)	10.38	0.22
Experiment Data		
Temperature (°C)	20	2
Rod Positioning (Pitch and Grid Hole Diameter) (cm)	1.1	0.023

positioning uncertainty, the uncertainties of two revisions (0 and 1) of the LEU-COMP-THERM-071 benchmark are reported in Table 2. The main components of the k_{eff} errors are shown in Table 2 for the first series of experiments along with the overall propagated uncertainty, calculated as the square root from sum of squares of its individual components. The differences between revision 0 and revision 1 are mainly associated with the fact that random uncertainties were ignored in revision 0 and are taken into account in revision 1. Moreover, the rod position being the source of large uncertainty, its treatment has been modified using Monte Carlo sampling in revision 1, contributing to a reduction of its propagated value. It can also be seen that for cases with a small pitch the rod positioning has a non-negligible effect on the overall uncertainty.

TABLE 2 Evaluated Experimental 1σ Uncertainties (in pcm) for LEU-COMP-THERM-071 Experiments.

Uncertainty component	Revision 0	Revision 1	Type of uncertainty
UO_2 Rods			
Isotopic Content	6	6	Systematic (precision of device)
Oxide Impurities	17	17	Systematic (tolerance level)
Pellet Diameter	2	22	Mixed (Measurement of 53 pellets + device uncertainty)
Fuel Density	Negligible	42	Mixed (Measurement of 1261 rods + precision of device)
Inner Clad Diameter	18	23	Systematic (tolerance value)
Outer Clad Diameter	1	29	Mixed (Measurement of 300 pellets and precision of device)
Experiment Data			
Temperature	7	5	Systematic (variation of temperature range)
Rod Positioning (Pitch and Grid Hole Diameter)	67	20	Mainly random (position of rod inside grid)
Total	**72**	**66**	

The bold values are the total uncertainty, which was derived from the individual component uncertainties listed above them in the table.

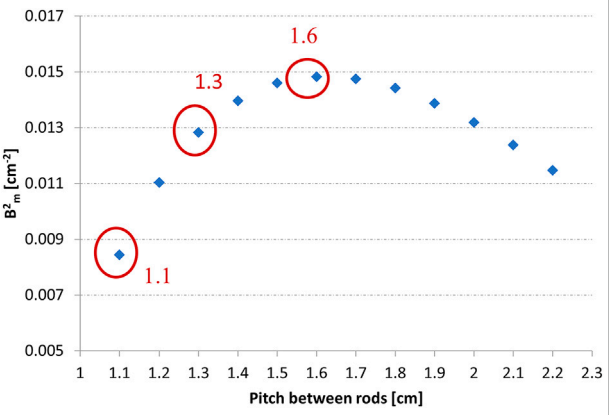

FIGURE 2
Material buckling *versus* pitch between rods. The pitch between rods correspond with the distance between the centers of two neighboring rods. B^2m is the material buckling.

TABLE 3 Array dimension *versus* moderation ratio.

Array dimension	Pitch (cm)	V_{mod}/V_{ox}
35 × 35	1.1	1.028
25 × 25	1.3	1.823
17 × 17	1.6	2.032

2.2 Simple model

To test efficiently the different methods, it seems reasonable to define a simple benchmark, shown in Figure 1B, with which they can be tested. This benchmark is made of three different lattices of UO_2 rods having the same characteristics as the Valduc rods (see Section 2.1). The variable parameter is the pitch between rods (1.1, 1.3, and 1.6 cm). The smallest pitch corresponds to an under-moderated lattice and the largest pitch to the moderation optimum as can be seen in Figure 2, where is reported the material buckling (B_m^2) *versus* the pitch between rods. The moderation ratio, V_{mod}/V_{ox}, values are reported in Table 3.

In order to have a k_{eff} close to 1, the number of fuel rods is adjusted accordingly. The 1.1-cm pitch lattice comprises an array of 35 × 35 rods, the 1.3-cm lattice an array of 25 × 25 rods and the 1.6-cm pitch lattice an array of 17 × 17 rods. It is to be noticed that the moderation optimum corresponds to a pitch of 1.6 cm between rods for a 4.738 wt% ^{235}U enrichment. The rod plugs were not considered in the model; only the fissile column surrounded by its cladding was retained. The height of rods was then set equal to 89.765 cm. The lattices were centered in a parallelepiped box, containing water, of 130-cm height and side dimensions corresponding to the lattice size plus 20 cm.

3 Calculation tools

Calculations were performed using the MORET 5 Monte Carlo code (Cochet, et al., 2015) and the computing environment Prométhée (Richet et al., 2007).

3.1 The MORET 5 monte carlo code

Calculations were performed using the MORET 5 continuous energy Monte Carlo code. It is a 3D MC code for neutron transport developed at IRSN for criticality safety assessments. It employs continuous energy cross sections derived from JEFF-3.1 evaluated nuclear data files (Koning et al., 2006). Typically, each calculation k_{eff} was run to achieve a precision of ±.00010 Δk_{eff} (±10 pcm).

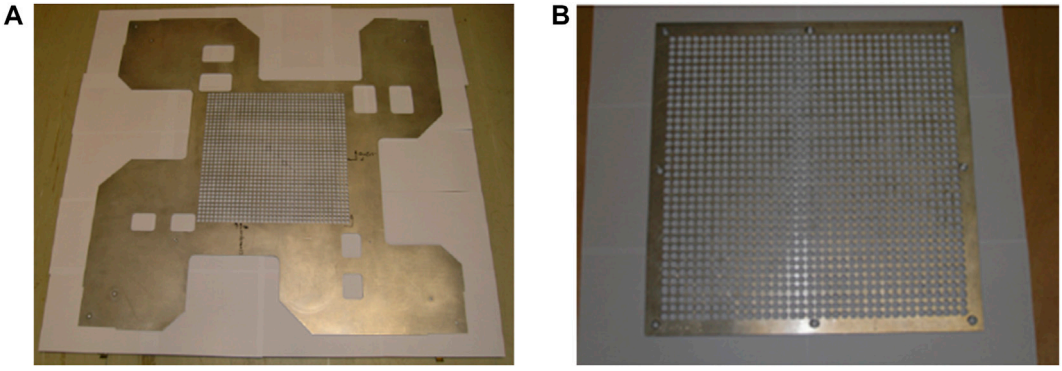

FIGURE 3
Upper **(A)** and lower **(B)** grids of LEU-COMP-THERM-071 experiments.

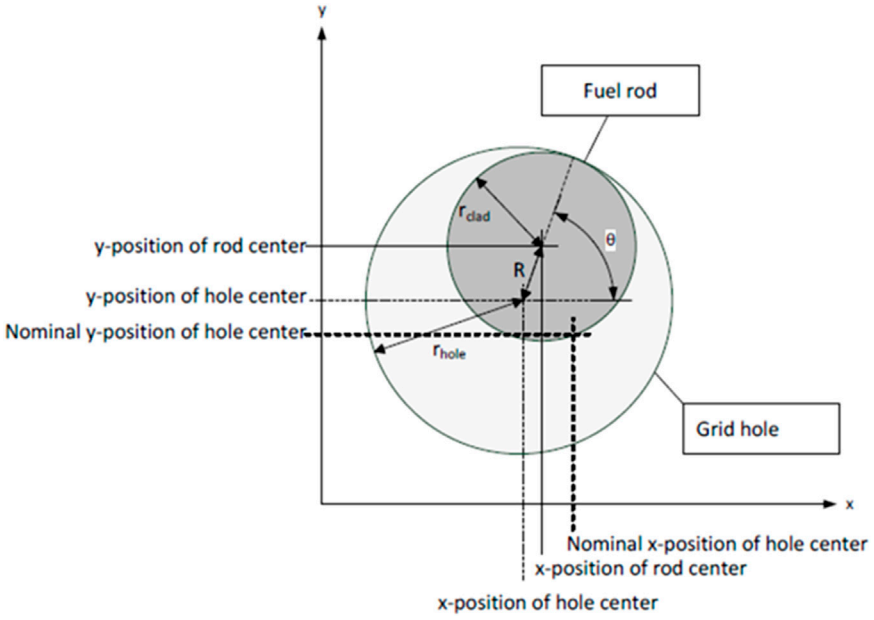

FIGURE 4
Rod location uncertainty: Detail of a rod in its grid hole.

3.2 Description of prométhée tool

Prométhée is a grid computing environment designed to provide engineering methodologies relevant for any available code. The Prométhée system is composed of a Graphical User Interface (GUI) designed to provide ergonomics features for a computing software input data engineering algorithms (for instance uncertainties propagation methods). Then, calculations are remotely performed on servers. The parameterization of rods' location in the lattice was performed using Prométhée.

4 Description of the different methods to assess the rod positioning uncertainty

At first look, the origin of the rod positioning uncertainty is mainly linked with the presence of two grids (both upper (A) and lower (B) are shown in Figure 3) drilled with holes with a slightly higher diameter; the spacing between rods is conditioned by the grid plate holes. These two grids ensure the mechanical rigidity of the lattice.

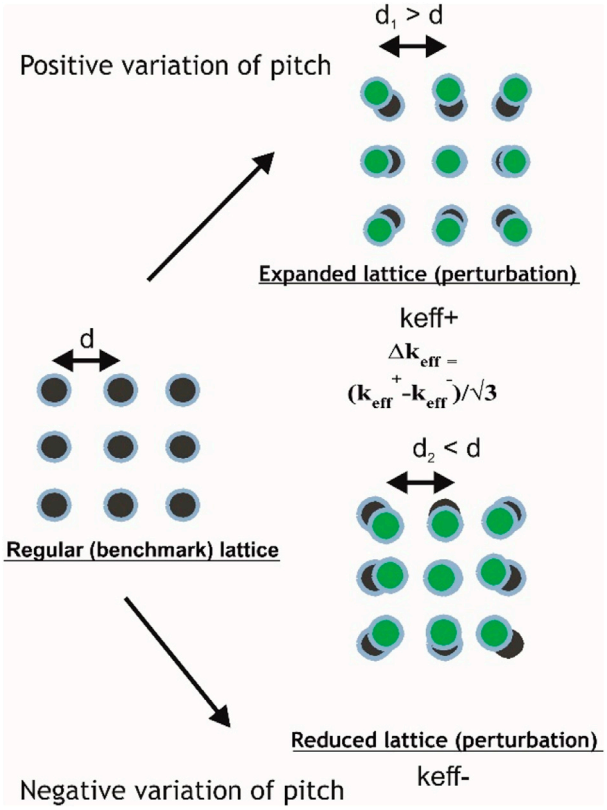

FIGURE 5
Traditional method for evaluation of pitch uncertainty. d is the pitch, d_1 correspond with a positive variation of pitch; keff+ is the resulting keff; d_2 correspond with a negative variation of pitch. keff– is the resulting keff.

As illustrated in Figure 4, The uncertainty of rods' positioning is composed of:

- Hole position uncertainty due to error in adjustment of the grid hole piercing device: ±.001 cm manufacturing tolerance;
- The uncertainty of the outer diameter of the rod cladding: ±.00044 cm (1σ);
- The uncertainty of the grid holes' diameter: ±.0085 cm (1σ); and
- The uncertainty of the gap between the rod and the edge of the grid hole (tolerance of ±.0407 cm): corresponds to a 1σ-uncertainty of ±.023 cm.

All in all, a total 1σ-uncertainty of ±.033 cm is obtained. The different components of the spacing uncertainty are converted in an increase or decrease of the distance between rods.

4.1 Traditional method

The way the uncertainty in rod positioning is propagated varies from one evaluator to another and from one calculation code to another. One of the examples given to evaluators in the IHECSBE consists of varying the spacing between all rods from plus or minus the uncertainty of the gap. The reactivity difference between these two calculations divided by two times the square-root of three (representing the correction from a two-sided bounding uncertainty with uniform probability distribution to a standard 1σ Gaussian uncertainty) determines the effective uncertainty in k_{eff}. The resultant value is then divided by square root of total number of rods. Historically, this method derived from the use of cell codes to evaluate this type of uncertainty.

As shown in Figure 5, this method was applied by shifting the rods nearer or further away from each other. The spacing between two neighboring rods was assumed to be the same throughout the lattice. Thus, the moderation ratio was varied by the same amount for all the lattice rods. For each lattice size, 2 MC calculations were performed: one, increasing the spacing between rods of a given quantity and another decreasing the spacing by the same amount. The variation was chosen in order to remain within the linearity domain of k_{eff} variations yet still large enough not to be influenced by the MC standard deviation of the calculation.

Then, the obtained k_{eff} value was scaled to 1σ and, divided by square-root of the number of rods. This factor was derived in Eq. 1:

$$\sigma^2\left(\Delta k_{eff}\right) = \sum_i \sigma^2\left(\Delta k_{rod,i}\right), \tag{1}$$

which assimilated the overall uncertainty to the sum of each rod uncertainty. When assuming that the independent contribution of each rod to the overall uncertainty is the same, the formula can be written as shown in Eq. 2:

$$\sigma^2\left(\Delta k_{lattice}\right) = N \times \sigma^2\left(\Delta k_{rod}\right). \tag{2}$$

The last assumption consists in saying that the variance of the lattice is the total variance divided by N as described in Eq. 3:

$$\sigma^2\left(\Delta k_{lattice}\right) = \frac{\sigma^2\left(\Delta k_{eff}\right)}{N}. \tag{3}$$

For large lattices of rods, assuming that the contribution of the uncertainty of each rod is the same leads to a biased estimation of the uncertainty. A calculation separating the assembly in two zones (internal and peripheral) and assessing separately uncertainties on these two zones should ideally be considered. However, it will not be investigated in this paper.

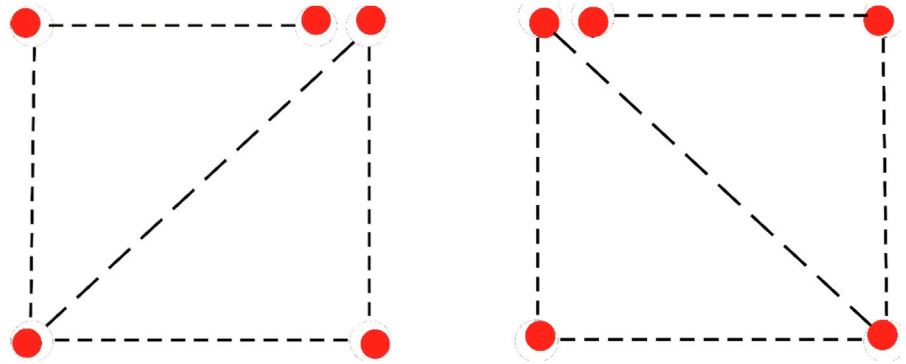

FIGURE 6
Extreme positions of rods within a lattice.

4.2 Refined traditional method

The "refined traditional" method is a variant of the basic traditional method. The only difference is that the Δk_{eff} is divided by the square-root of an additional factor (k_R) to account for the fact that the position of rods is constrained within a grid and that there is a compensation effect for the simultaneous variation of pitch between all rods. This factor (Ivanova, Ivanov, and Bianchi 2014) is called the peak-to-average ratio and is typically constrained between the values of 1.3 and 1.5.

4.3 Extreme lattice bounds

Another variant of traditional methods leans upon the fact that the rod position is constrained within the grids. The rods cannot move outside their grid holes. As a consequence, it is impossible to impose the maximum shift to all the rods at the same time. The average rod position is constrained between two extreme positions that are demonstrated in Figure 6. For that reason, the method could be called "extreme lattice bounds." The mean variation of rod position is equal to the difference of width between these two lattices divided by the square-root of the total number of rods in the lattice. In fact, in the X direction for instance, only the distance separating the two last rows of rods at the periphery is modified. The modification is equal to the gap between the rod and the grid hole multiplied by $\sqrt{2}$. As a consequence, the average rod position shift is the gap $\times$ $\sqrt{2}/\sqrt{N}$ with N being the total number of rods in the lattice. When propagated in terms of Δk_{eff}, this variation leads to results comparable to traditional methods but slightly lower.

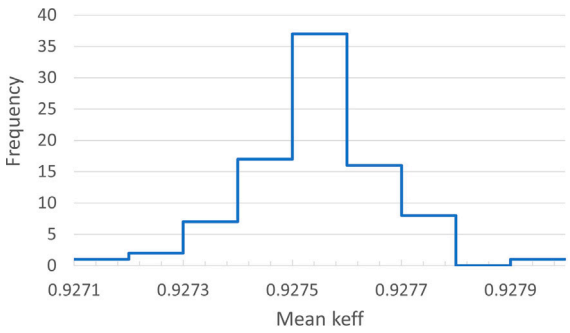

FIGURE 7
Distribution of k_{eff} Results.

4.4 Monte Carlo sampling with MORET 5/ Prométhée

Two kinds of MC simulations were tested during this work. The first one uses the MORET 5 code combined with the Prométhée workbench to do the MC sampling. A first step consisted in comparing the traditional method varying the pitch value according with a chosen distribution law. The variation was then propagated in terms of Δk_{eff} for 100 different rod positioning maps corresponding to 100 different simulations. Then, the distribution of k_{eff} was observed.

A second step consisted in comparing the traditional method with a simulation on the position of rod according to ISO GUM S1 standard procedure. Instead of increasing artificially the distance between rods of the same quantity, the position of

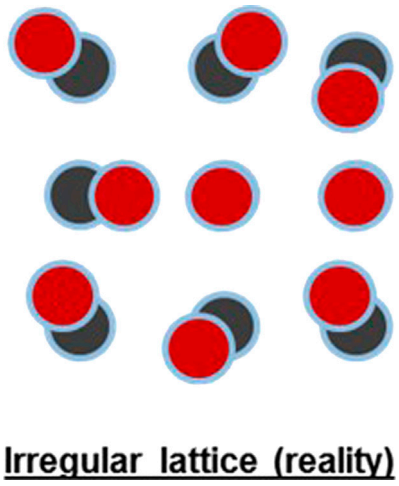

FIGURE 8
Example of rod positioning *via* simulations with prométhée.

rods in their holes was sampled independently 100 times (this number was chosen arbitrarily but was found sufficient to have a Gaussian distribution, as shown in Figure 7, which was confirmed by the value of the bootstrap) for the 35 × 35 array and propagated in terms of Δk_{eff} using the ISO GUM S1 standard procedure, which corresponded to a more realistic approach. For this method, the position of each rod was chosen independently from its neighbors. The Δk_{eff} was observed and its statistical parameters (mean and variance) were estimated(Figure 8).

4.4.1 Sampling of rod positioning

In this section, the position of rods varies independently from the position of neighboring rods (Figure 9), which is more realistic than the use of traditional methods. The position of rods is constrained since they are held by two grids (lower and upper). As explained at the beginning of section IV, the rods can move within their grid holes. Their uncertain position pertains to the external diameter of claddings, the precision of the piercing of grid holes, and to the gap existing between the rods and the grid holes. In fact, with the increase of water level during a critical approach, the rods can move inside their grid holes and their respective positions can be correlated. The overall positioning uncertainty was chosen to follow a uniform distribution. Each rod position was supposed to be completely uncorrelated from that of its neighbors. Thus, the distance between rods was not the same throughout the lattice. The parameterized variable was the position of rods. For each lattice, the input listings were automatically generated with Prométhée tool.

The rods position shifts are given by Eqs 4, 5 in the X and Y lattice directions, respectively. The maximum shift was estimated as being equal to 2 × .0439 cm between two neighboring rods.

$$\Delta X = 0.0439 \times r_1^{\frac{1}{2}} \times cosine(2 \times \pi \times t_1)\cdot \quad (4)$$

$$\Delta Y = 0.0439 \times r_1^{\frac{1}{2}} \times sine(2 \times \pi \times t_1)\cdot \quad (5)$$

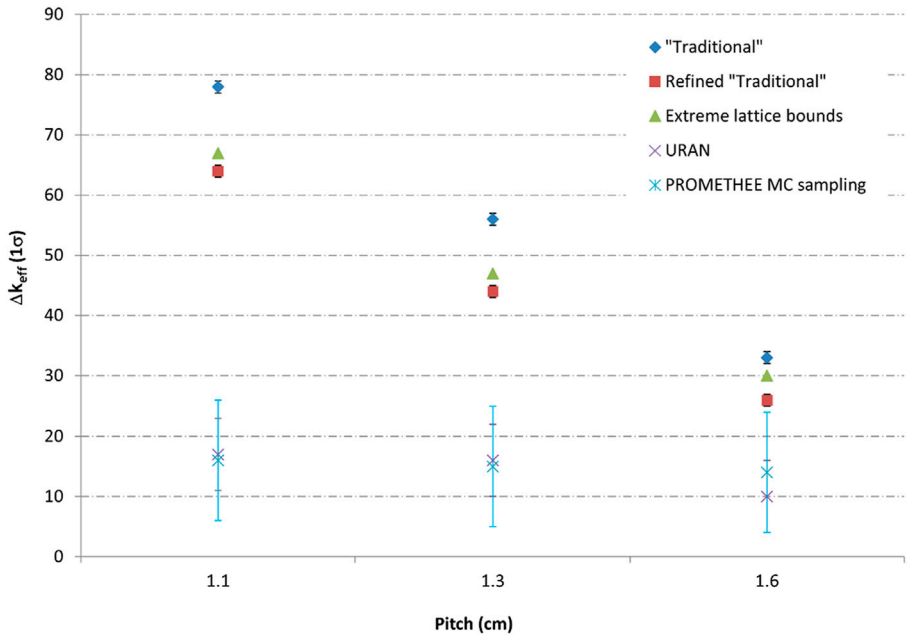

FIGURE 9
Results comparison of the different methods with MORET 5 code.

The variables r_1 and t_1 were chosen randomly according with an equiprobable distribution law. This assumption is over-predicting the uncertainty propagation in comparison with a triangular or Gaussian distribution law. By default, this option was retained. The size of the modeled lattice is chosen accordingly with the pitch between rods as defined in section 2.2.

For each lattice, a batch of 100 calculations corresponding to 100 different values of (r_1, t_1), with a MC precision of ±0.00010 Δk, was launched on 100 different computing nodes *via* the Prométhée plugin. A fixed number of neutrons per lattice (10,000) was chosen. It has been checked that this number had hardly any impact upon k_{eff}. It should be noticed that the observed variance is the sum of both code k_{eff} estimate variance (MC codes) and studied rod positioning effect variance. These two random variables being independent, the rod variance is estimated as the difference of observed variance and code variance.

Moreover, the value is known with a small standard deviation (<3 pcm) (Davison, Hinkley, and Schechtman 1986) due to the sample size of 100. The obtained value is far lower than the one obtained using the traditional method. Even if the comparison has been done on a simple benchmark model, the ratio obtained between the uncertainty given by the traditional method and that obtained from the ISO GUM S1 simulations can be transmitted to a configuration close to that model. This procedure applies for the tight-packed lattice program. A rod positioning uncertainty of about 70 pcm is obtained with the traditional method for a 4.738 wt% ^{235}U enrichment and a 35 × 35 rods lattice. For the same rods at the same moderation ratio, the "best estimate" value of the rod uncertainty can be assessed as being closer to 20 pcm.

4.4.2 Limits of the method

It should be stressed that the validity of the method leans mainly on the MC sampling. It is conditioned by the number of neutrons per batch and per volume in the geometry. A comparison with a deterministic method would be needed to definitively validate it without potential deviation due to MC sampling of neutrons (including MC Markov chain initial transient).

4.5 Monte Carlo simulations with URAN card in MCNP

Another approach consists in using the Monte Carlo N-Particle (MCNP) code, version 6, with the URAN card (Goorley et al., 2013). This card allows selecting universes to randomly translate the geometry inside a lattice cell. The Universe corresponding to the main cell of the lattice is then selected and the rods are randomly shifted within its cell. The same .0439 cm variation is defined as for the previous method involving random sampling. The position of rods is shifted of the following quantities in the *X* and *Y* directions according to Eqs 6, 7, respectively.

$$\Delta X = (2t_1 - 1) \times \delta_1. \quad (6)$$

$$\Delta Y = (2t_2 - 1) \times \delta_2. \quad (7)$$

Here, t_1 and t_2 are random variables comprised between 0 and 1, and δ1 and δ2 are user-defined variations.

5 Results

5.1 Traditional and refined traditional methods

The MORET 5 results for the three lattice pitches of the benchmark are given in Table 4. The JEFF-3.1 evaluation is used for the nuclear data library. Quite similar results are obtained with the two traditional methods, the results of the refined traditional being a little lower. Moreover, for a same pitch variation, the propagated 1σ uncertainty is greater for the lowest pitch, which was predictable since a tight-packed lattice of rods is more sensitive to a pitch variation than a lattice at the moderation optimum.

5.2 Results of Monte Carlo sampling and URAN

The calculations were performed for the two methods (MC sampling with MORET 5/Prométhée and URAN card with MCNP) for a rod positioning uncertainty of ± 0.04 cm. The results are reported in Table 4. It can be shown that there is no great influence of the pitch value and that the two methods are quite consistent since there is no significant difference between the results.

5.3 Comparison of the different methods

For the three pitches of the benchmark and a shift of the position of rods corresponding to the 1σ uncertainty of rod position, calculations were performed with the continuous energy Monte Carlo MORET 5 code and the various methods presented beforehand. These results are reported in Figure 9. It can be shown that the traditional methods lead to higher Δk_{eff} values than the methods based on MC sampling or the URAN card in MCNP6. The reduced uncertainty using the URAN card with MCNP is consistent with similar comparison studies performed for the Neutron Radiography (NRAD) reactor (Bess, Maddock, and Marshall 2014). The discrepancy is more important for smaller pitches. In fact, at moderation optimum, the MC sampling methodology is not necessary since quite

TABLE 4 Comparison of Methods for Pitch 1σ Uncertainty (in pcm).

Pitch uncertainty (cm)	Traditional	Refined	Extreme lattice bounds	Monte Carlo sampling	URAN
Pitch = 1.1 cm					
.02	38	31	67	17	16
.04	78	64			
.08	158	129			
Pitch = 1.3 cm					
.02	28	22	47	16	15
.04	56	44			
.08	112	91			
Pitch = 1.6 cm					
.02	16	13	30	10	14
.04	33	26			
.08	74	53			

consistent results are obtained. This is not the case for tight-packed lattices of rods, however. Moreover, it should be pointed out that the results obtained with MC sampling and those using the URAN card in MCNP6 are perfectly consistent. The question now is to know which method better predicts the uncertainty.

5.4 Comparison with experimental results

A way to have access to this information is to make comparisons with experimental results. Repeatability/reproducibility experiments can allow such comparison. This was done for another proprietary program called MIRTE (Matériaux en Interaction et Réflexion Toutes Epaisseurs) (Leclaire et al., 2014) whose aim was the validation of the calculation of structural materials in thermal energy spectrum. This program involved the same UO_2 rods, with a 1.6-cm square pitch (moderation optimum). The reproducibly experiment consisted in draining the water level from the tank, unloading the baskets containing the rod lattices, shake them, reload them and then perform a new critical approach. Such experiments addressed different uncertainties amongst them such as the critical height uncertainty and the rod position uncertainty. The critical level difference observed between the two experiments, when propagated in terms of Δk_{eff}, corresponded to an insignificant reactivity worth (less than 20 pcm). This value was clearly lower than what was highlighted using traditional methods. It demonstrates that traditional methods are clearly overestimating rod positioning uncertainty. Moreover, the same order of magnitude was obtained as with the MC sampling method. As a result, the results obtained with the MC sampling method or with the URAN card of MCNP 6 are not without experimental validation. One can be confident in the results they provide.

6 Consequences of correlation factors

6.1 Definition of correlation factors

Correlation factors between experiments or between cases of an experimental series are key values for the determination of biases due to nuclear data. For many years now, various tools such as TSURFER for the SCALE 6 package (Wieselquist, Lefebvre, and Jessee 2020), WHISPER for MCNP, and MACSENS (Fernex and Leclaire, 2022) for the CRISTAL package (Gomit et al., 2015) have implemented (or are implementing for MORET) a sensitivity on k_{eff} capability and the Generalized Linear Least Squares Methodology (GLLSM) to evaluate biases due to nuclear data (Broadhead et al., 1999). To correctly assess the bias, one needs to know the correlation between experiments (or cases). These values strongly influence the result of the adjustment procedure and therefore the bias. Very accurate-value correlation factors are needed. And for that, a thorough evaluation of uncertainties is required. For each parameter source of uncertainty, it is necessary to know the random and systematic components of the uncertainty to clearly demonstrate the shared uncertainty between cases. Eqs 8–11 show how these factors are calculated.

6.2 Calculation of correlation factors

Establishment of correlations between the uncertainties of a pair of benchmark experiments (called experimental correlations hereafter) is not a trivial task. If an uncertainty component is wholly or partially common for a pair of experiments, the problem is reduced to estimating the component correlation coefficient related to that specific component of the uncertainty.

TABLE 5 Comparison of 1σ Uncertainties (in pcm) for LEU-COMP-THERM-071 using Two Scenarios.

Uncertainty component	Traditional (case 1)	Traditional (case 4)	MC sampling (case 1)
UO_2 rods			
Isotopic Content	6	6	6
Oxide Impurities	17	17	17
Pellet Diameter	22	22	22
Fuel Density	42	42	42
Inner Clad Diameter	23	18	23
Outer Clad Diameter	29	27	29
Experiment Data			
Temperature	5	7	5
Rod Positioning (Pitch and Grid Hole Diameter)	58	67	20
Total	**86**	**90**	**66**

The bold values are the total uncertainty, which was derived from the individual component uncertainties listed above them in the table.

$$r^i_{m,n} = \frac{\delta^{i(s)}_m \delta^{i(s)}_n}{\delta^i_m \delta^i_n}. \quad (8)$$

$$\left[\delta^i_n\right]^2 = \left[\delta^{i(s)}_n\right]^2 + \left[\delta^{i(r)}_n\right]^2. \quad (9)$$

$$[\delta_n]^2 = \sum_i \left[\delta^i_n\right]^2. \quad (10)$$

$$r_{m,n} = \frac{1}{\delta_m \delta_n} \sum_i \delta^i_m \delta^i_n r^i_{m,n}. \quad (11)$$

Where, δ_n is the total uncertainty of the nth experiment; δ^i_n is the ith component of the total uncertainty of the n^{th} experiment; $\delta^{i(s)}_n$ and $\delta^{i(s)}_n$ are the systematic, i.e., common, and random parts of the ith component for n^{th} experiment's total uncertainty, respectively; $r^i_{m,n}$ is the component correlation coefficient for the ith uncertainty component for experiments m and n; and the coefficient $r_{m,n}$ varies between 0.0 and 1.0, i.e., between non-correlated and fully correlated systems, respectively.

In order to demonstrate that correlation factors between experiments are dependent upon the evaluation of experimental uncertainties, an application case is chosen. The tight-packed lattice program, LEU-COMP-THERM-071, is chosen for that aim. We will show how the evaluation of the rod positioning uncertainty can influence the value of correlation factors. Two cases are selected: one with a 1.1-cm square pitch (case 1 of Table 5) and the other with a 1.075-cm square pitch (case 4 of Table 5). The detail of experimental uncertainties is provided with in Table 5. Two scenarios are retained concerning the evaluation of the rod positioning uncertainty: traditional method or Monte Carlo sampling. Cross cut views of the two model lattices are reported in Figure 10.

The rod positioning uncertainty appears to be driving the overall uncertainty. The correlation factors were calculated assuming that the uncertainties pertaining to all parameters are 100% systematic (in fact, the random part of the uncertainty is negligible when compared to the systematic part), except for the rod positioning uncertainty where it is supposed to be random for both scenarios. Even if there is some systematic uncertainty on the grid hole position due to the manufacturing procedure, the rod positioning uncertainty is mainly random. Indeed, the rods are inserted manually in the grids' holes and lean on their bottom plug. Once positioned in the grids' holes, they can move randomly within the holes during the critical approach due to the increase of the water level or can even move due to vibrations. Moreover, the positions of rods being not marked in the lattice, from one case to another, the position is resampled, and the positioning uncertainty is random. When looking now at the correlation matrix below, one can see that the correlation factor is strongly dependent on the chosen scenario, for tight-packed lattices of rods. It would not be the case for lattices of rods at moderation optimum.

$$\begin{matrix} \text{TraditionalMC} \\ \begin{pmatrix} 1 & 0.449 \\ 0.449 & 1 \end{pmatrix} \end{matrix} \qquad \begin{matrix} \text{Sampling} \\ \begin{pmatrix} 1 & 0.859 \\ 0.859 & 1 \end{pmatrix} \end{matrix}$$

6.3 Discussion

In this section a first attempt to understand the difference between the traditional methods and the ones using MC simulations (ISO GUM S1) is provided. It is to be noted that it is implicitly assumed while using the traditional methods that the rods are non-correlated in the contribution to overall k_{eff}. The traditional methods make the assumption that each rod contributes independently from its neighbors to the overall k_{eff}. However, the factor k_R (peak to average ratio) is

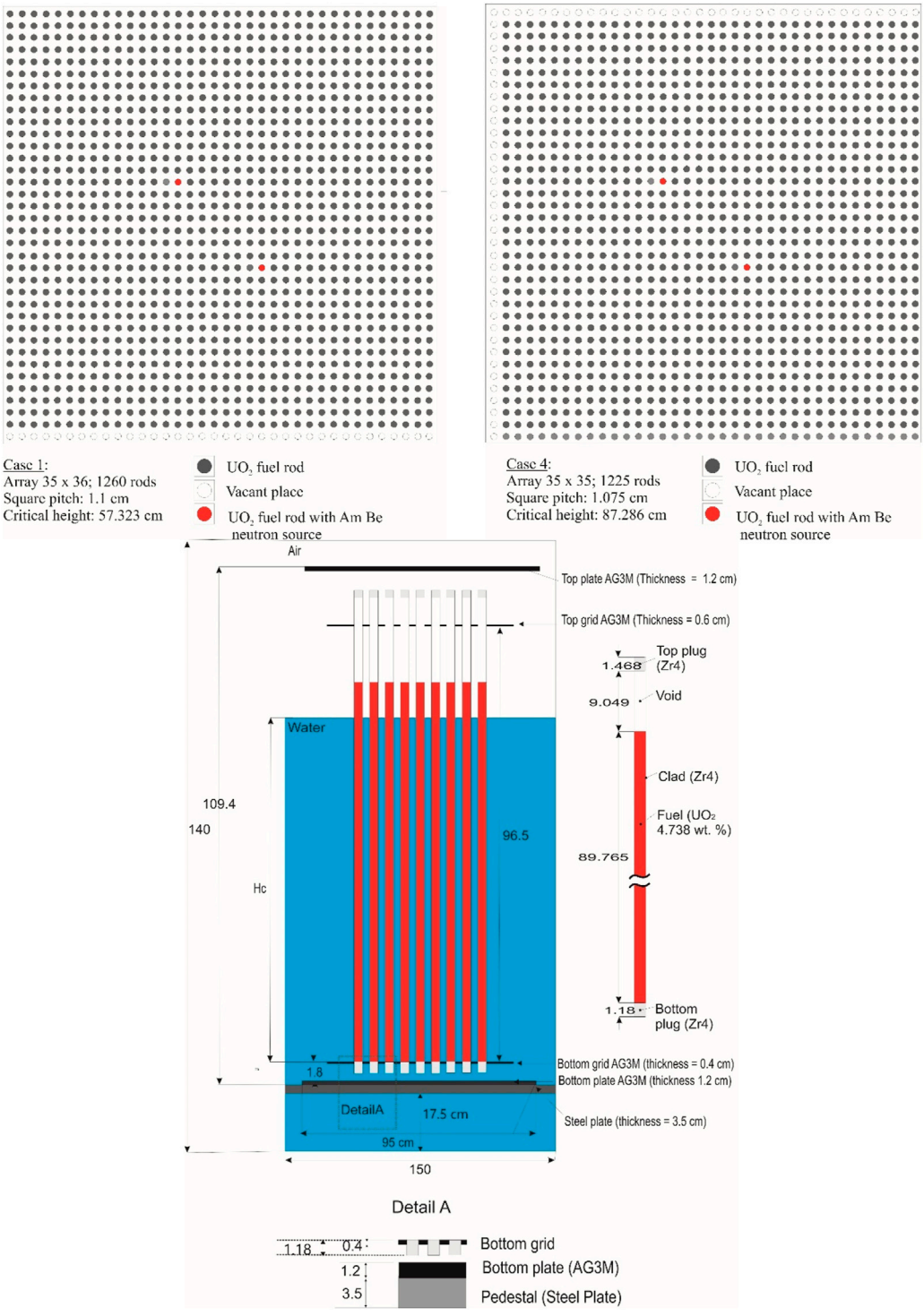

FIGURE 10
Horizontal and vertical cross-cut views of rod lattices (LEU-COMP-THERM-071).

introduced to compensate for that by taking the correlations into account. This factor is purely empirical and depends on the rod lattice size and moderation ratio. In fact, the position of rods is correlated since it is constrained by the presence of grids maintaining them. With the mean free path of neutrons being around 1–2 cm in a thermal spectrum, the neutrons produced in

each rod interact with at least two neighbors. Consequently, some covariance terms should contribute negatively to the uncertainty propagation. This is what is observed when doing calculations using MC sampling.

7 Consequences on criticality safety, reactor physics, and advanced reactor systems

It can be easily concluded from previous sections that the choice of the rod location uncertainty propagation methodology can have a significant impact on the overall uncertainty, especially when the fuel is under-moderated, as it is the case for LEU-COMP-THERM-071. The objective for a good assessment of calculation bias and uncertainty is not necessarily to overestimate this quantity. In criticality-safety assessment, the uncertainty in the positioning of rods due to the tolerance values of grids' holes and fuel rods is taken into account in the calculations. The same problematics applies on reactor physics design and operations. A propagation method based on MC sampling can help in determining the best estimate of the overall uncertainty, avoiding overestimation of the uncertainty with the traditional method which has historically been used.

Direct applicability of this work applies towards some of the light water small modular reactor and microreactor concepts such as the ACP100 (Danrong et al., 2021), Nuward (OECD, 2021) and Nuscale designs (Weber and Mullin 2020). As the quantity and diversity of these types of reactors expands, questions remain in not just how the uncertainties in pitch will impact reactor physics performance, but also in other core performance parameters including desired uses beyond power generation such as process heat generation for desalination, hydrogen production, or other industrial processes (IAEA 2017).

Overprediction of pitch uncertainties in advanced reactor design could lead to larger than necessary margins required for safety and operations. A simple means to understand this potential impact is to relook at the conversion of the NRAD reactor from highly enriched to low-enriched fuel (Bess, Maddock, and Marshall 2014). The initial critical mass necessary for the converted core was physically greater than computationally predicted, resulting in post-conversion accommodations to incorporate additional fuel rods into a restricted design space to enable the reactor to achieve and maintain at-power operations. While control rod worth and coefficient measurements were not significantly different from their estimates, the available core excess reactivity for operations was much less than the maximum allowed within the safety limits of the technical specifications, and nearly insufficient to enable necessary reactor operations. Uncertainties in the experiment were evaluated, including those for pitch, to estimate the impact upon the bias between computational models and the freshly refueled reactor. Should significantly large uncertainties have been included in the design due to pitch, or any other parameter, the margins between operations and safety would have been even more significantly discrepant, possibly to the point of reactor inoperability.

Therefore, an improved approach is also of interest for advanced reactor designs such as pebble bed reactors using tri-isotropic (TRISO) fuel or other high-temperature gas-cooled reactors (HTGRs), for which the fuel-to-moderator ratio and fuel-to-fuel pitches are random; a sampling MC methodology would help evaluating the uncertainty pertaining to the fuel location. The traditional approach to column and channel pitch in prismatic HTGRs could be on the order of 0.1 $\%\Delta k_{eff}$ (Bess and Fujimoto 2010). While this uncertainty could be minor compared to some more significant uncertainties such as graphite and fuel properties, as manufacturing processes are improved, the approach towards treatment of geometric uncertainties becomes more prominent. However, implementation of a MC sampling methodology for TRISO particle packing in pebbles contributes insignificantly to the overall uncertainty, as expected (Çolak and Seker 2005)(Bess and Dolphin 2013). Similar expectations would apply towards fluoride salt-cooled high-temperature reactor (FHR) designs (Qualls, et al., 2017).

In fast reactor systems, significant contributors to changes in pitch can be seen in thermal expansion or bowing effects (Lum, 2018). Random rod displacement effects are mitigated and negligible if the core assemblies are suitably constrained; however, thermal expansion of grid plates and assemblies further add to the complexity in the evaluation of core neutron leakage and reactivity effects (Pope and Lum 2021). In liquid fuel systems, such as a molten salt reactor (MSR) the impact on pitch could derive from uncertainties in placement of moderator channels and blocks, if used, which can also be more suitably addressed using MC evaluative techniques (Shen, 2019), and should be further investigated as a component of evaluating technological gaps and safety requirements supporting MSR design and deployment (Forsberg 2006)(Elsheikh 2013).

A key aspect in regulation and operation of advanced nuclear reactors will require those designing and deploying the reactors to demonstrate to those regulating the operation and safety of these reactors that all aspects of systems will perform as expected. The impact of uncertainties in rod positioning is only one component of many that will need to be properly understood to satisfy regulatory requirements prior to advanced reactor deployment and operations. Ultimately, the uncertainties addressed in this paper might improve assessment of modular transportation of microreactors or fuel and their ultimate disposal; understanding biases and associated uncertainties when utilizing various methodologies and codes is imperative (Tardy, 2019).

8 Conclusion

The impact of rod positioning has been tested with various methods: the traditional one recommended historically by the ICSBEP working group, modifications to the traditional method, MC sampling using the MORET 5 code and the Prométhée computing environment, and the MCNP6 code with the URAN card to simulate the uncertain position of rods inside their grids. These methods have been applied on a benchmark involving three critical lattices of Valduc UO_2 rods with various pitches (1.1-cm, 1.3-cm or 1.6-cm square pitch) corresponding to different moderation ratios. It has been shown that the traditional methods commonly used by benchmark evaluators does not underestimate the contribution of the rod positioning uncertainty, as it was originally thought. On the contrary, for tight-packed lattices of rods (pitch 1.1 cm), a noticeable positive discrepancy with MC simulations (ISO GUM S1) is highlighted. Moreover, with a good consistency between MC sampling with MORET 5/Prométhée and MCNP 6/URAN being obtained, one can be quite confident in the result. To better estimate such a small effect, it would be necessary to perform calculations with a deterministic code.

At last, the validity of MC sampling calculations is ensured by the comparison with experimental results. Indeed, repeatability/reproducibility experiments were performed in the framework of the MIRTE (Matériaux en Interaction et Réflexion Toutes Epaisseurs) program involving similar rods in a 1.6-cm square-pitched lattice. It can be shown that the uncertain position of rods in their baskets leads to a Δk_{eff} less than ± 0.00020, which is in accordance with the results obtained *via* MC sampling with MORET 5/Prométhée or MCNP6/URAN. Monte Carlo sampling techniques show improvement in better prediction of actual uncertainties in light water reactor systems, which is directly applicable to many small modular reactor concepts in development. However, the application of such methodologies can apply towards advanced reactor design concepts, including microreactors, to mitigate overestimation of margins supporting safety and operations.

Data availability statement

The raw data supporting the conclusion of this article will be made available by the authors, without undue reservation.

Author contributions

NL is the main author of the paper. JB added sections to highlight the interest of such methodology for advanced reactor and complemented the lis references.

Acknowledgments

The authors wish to thank Yann Richet for the support on the use of the Prométhée tool and are grateful to the Bertrand Cochet for his advice on the use of the code and Alexis Jinaphanh for its support on the calculations.

Conflict of interest

The authors declare that the research was conducted in the absence of any commercial or financial relationships that could be construed as a potential conflict of interest.

Publisher's note

References

Bess, J. D., and Dolphin, B. H. (2013). HTR-PROTEUS pebble bed experimental program cores 1, 1A, 2, and 3: Hexagonal close packing with a 1:2 moderator-to-fuel pebble ratio. *PROTEUS-GCFR-EXP-001, Rev. 1.*

Bess, J. D., and Fujimoto, N. (2010). Evaluation of the start-up core physics tests at Japan's high temperature engineering test reactor (Fully-Loaded core). *HTTR-GCR-RESR-001, Rev. 1.*

Bess, J. D., Maddock, T. L., and Marshall, M. A. (2014). Fresh-core reload of the neutron Radiography (NRAD) reactor with uranium(20)-erbium-zirconium-hydride fuel. *NRAD-FUND-RESR-001, Rev. 2.*

Briggs, J. B., Scott, L., and Nouri, A. (2003). The international criticality safety benchmark evaluation project. *Nucl. Sci. Eng.* 145 (1), 1–10. doi:10.13182/NSE03-14

Broadhead, B. L., Hopper, C., Childs, R. L., and Parks, C. V. (1999). *Sensitivity and uncertainty analyses applied to criticality safety validation: Methods development*, 1. Washington, DC: U.S. Nuclear Regulatory Commission. NUREG/CR-6655.

Brown, F. B., Rising, M. E., and Alwin, J. L. (2016). *MCNP-WHISPER methodology for for nuclear criticality safety validation. LA-UR-16-23757.* Los Alamos, New Mexico, USA: Los Alamos National Laboratory.

Cochet, B., Jinaphanh, A., Heulers, L., and Jacquet, O. (2015). Capabilities overview of the MORET 5 Monte Carlo code. *Ann. Nucl. Energy* 82, 74–84. doi:10.1016/j.anucene.2014.08.022

Çolak, Ü., and Seker, V. (2005). Monte Carlo criticality calculations for a pebble bed reactor with MCNP. *Nucl. Sci. Eng.* 149 (2), 131–137. doi:10.13182/NSE04-17

Danrong, S., Qing, L., Dong, Q., Gaojian, D., Chang, Z., Renjie, X., et al. (2021). Key Technology of ACP100: Reactor core and safety design. *Nucl. Power Eng.* 42 (4), 1–5. doi:10.13832/j.jnpe.2021.04.0001

Davison, A. C., Hinkley, D. V., and Schechtman, E. (1986). Efficient bootstrap simulation. *Biometrika* 73, 555–566. doi:10.2307/2336519

Dean, V. (2008). *ICSBEP guide to the expression of uncertainties. Rev. 5.* Paris, France: OECD Nuclear Energy Agency.

Duhamel, I., and Girault, E. (2006). "Criticality experiments with tightly packed lattices of low-enriched UO_2 rods," in Proceeding of the PHYSOR 2006: Advances in Nuclear Analysis and Simulation, Vancouver, September 10-14. Available from: https://www.ans.org/store/item-700323/)

Elsheikh, B. M. (2013). Safety assessment of molten salt reactors in comparison with light water reactors. *J. Radiat. Res. Appl. Sci.* 6 (2), 63–70. doi:10.1016/j.jrras.2013.10.008

Fernex, F., and Leclaire, N. (2022). *A new IRSN tool for nuclear data bias assessment: MACSENS V3.0 GLLSM module. NCSD2022.* Anaheim.

Forsberg, C. W. (2006). "Molten-salt-reactor Technology gaps," in International Congress on Advances in Nuclear Power Plants (ICAPP '06), Reno, NV, USA, June 4-8. Available at: https://www.ans.org/store/item-700324/.

Gomit, J.-M., Duhamel, I., Entringer, A., Magnaud, C., Damian, F., and Riffard, C. (2015). "Cristal V2.0: A new-generation criticality package," in Proceeding of the International Conference on Nuclear Criticality Safety (ICNC 2015), Charlotte, NC, September 13-17. Available at: https://www.ans.org/store/item-700400/.

Goorley, T., James, M., Booth, T., Brown, F., Bull, J., Cox, L. J., et al. (2013). *Features of MCNP6. LA-UR-13-28114.* Los Alamos, NM: Los Alamos National Laboratory.

IAEA (2017). *Opportunities for cogeneration with nuclear energy. NP-T-4.1.* Vienna, Austria: International Atomic Energy Agency.

Ivanova, T., Ivanov, E., and Bianchi, G. E. (2014). Establishment of correlations for some critical and reactor physics experiments. *Nucl. Sci. Eng.* 178 (3), 311–325. doi:10.13182/NSE14-24

JCGM (2009). "Evaluation of measurement data – an introduction to the "guide to the expression of uncertainty in measurement" and related documents," in *JCGM 104:2009. Joint committee for guides in metrology* (Sèvres, France: Bureau International des Poids et Mesures).

JCGM (2008). "Evaluation of measurement data – supplement 1 to the "guide to the expression of uncertainty in measurement" – propagation of distributions using a Monte Carlo method," in *JCGM 101:2008. Joint committee for guides in metrology* (Sèvres, France: Bureau International des Poids et Mesures).

Koning, A., Forrest, R., Kellett, M., Mills, R., Henriksson, H., and Rugama, Y. (2006). *The JEFF-3.1 nuclear data library*. Paris, France: OECD Nuclear Energy Agency.

Leclaire, N., Duhamel, I., Dauphin, F. X. L., Briggs, B., Piot, J., Rennesson, M., et al. (2014). The MIRTE experimental program: An opportunity to test structural materials in various configurations in thermal energy spectrum. *Nucl. Sci. Eng.* 179 (4), 429–445. doi:10.13182/NSE14-29

Leclaire, N. (2019a). *Low moderated 4.738-wt.%-Enriched uranium dioxide fuel arrays. LEU-COMP-THERM-071, rev. 2.*

Leclaire, N. (2019b). *Under-moderated 4.738-wt.%-Enriched uranium dioxide fuel rod arrays reflected by water or polyethylene. LEU-COMP-THERM-072, rev. 2.*

Leclaire, N. (2019c). *Water-reflected under-moderated 4.738-wt.%-Enriched uranium dioxide fuel rod arrays with heterogeneities. LEU-COMP-THERM-073, rev. 1.*

Lum, E. S. (2018). *Evaluation of run 138B at experimental breeder reactor II, a prototypic liquid metal fast breeder reactor. EBR2-LMFR-RESR-001.*

OECD (2021). *Nuclear Technology development and economics 2021, small modular reactors: Challenges and opportunities.*

Pope, C., and Lum, E. (2021). "Nuclear reactor thermal expansion reactivity effect determination using finite element analysis coupled with Monte Carlo neutron transport analysis," in *Finite element methods and their application*. Editors M. Baccouch and IntechOpen (London, UK. doi:10.5772/intechopen.93762

Qualls, A. L., Betzler, B. R., Brown, N. R., Carbajo, J. J., Greenwood, M. S., Hale, R., et al. (2017). Preconceptual design of a fluoride high temperature salt-cooled engineering demonstration reactor: Motivation and overview. *Ann. Nucl. Energy* 107, 144–155. doi:10.1016/j.anucene.2016.11.021

Rearden, B. T. (2004). Perturbation theory eigenvalue sensitivity analysis with Monte Carlo techniques. *Nucl. Sci. Eng.* 146 (3), 367–382. doi:10.13182/NSE03-03

Richet, Y., Heulers, L., Bernard, F., and Gauluet, F. (2007). A flexible calculation environment for criticality parametric modeling, In Proceeding of the International Conference on Nuclear Criticality Safety (ICNC 2007), Saint Ptersburg, Russia.

Shen, D. (2019). *Molten-salt reactor experiment (MSRE) zero-power first critical experiment with ^{235}U. MSRE-MSR-EXP-001.*

Tardy, M. (2019). *Criticality codes biases and associated uncertainties determination for fissile nuclear material transportation using different approaches* in 18th International Symposium on the Packaging and Transportation of Radioactive Materials (PATRAM 2019), New Orleans, LA, USA, August 4-9. Available at: https://resources.inmm.org/.

Weber, S. J., and Mullin, E. M. (2020). Severe accident phenomena: A comparison among the NuScale smr, other advanced lwr designs, and operating LWRs. *Nucl. Technol.* 206, 1351–1360. doi:10.1080/00295450.2020.1756160

Wieselquist, W. A., Lefebvre, R. A., and Jessee, M. A. (2020). "ORNL/TM-2005/39, version 6.2.4," in *SCALE code system* (Oak Ridge, Tennessee, USA: Oak Ridge National Laboratory).

Nomenclature

Acronyms

CEA Commissariat à l'Energie Atomique

FHR Fluoride salt-cooled High-temperature Reactor

GLLSM Generalized Linear Least Squares Methodology

GUI Graphical User Interface

HTGR High-Temperature Gas-cooled Reactor

ICSBEP International Criticality Safety Benchmark Evaluation Project

IHECSBE *International Handbook of Evaluated Criticality Safety Benchmark Experiments*

IRSN L'Institut de Radioprotection et de Sûreté Nucléaire

ISO International Organization for Standardization

JFA JFoster and Associates

MC Monte Carlo

MCNP Monte Carlo N-Particle

MIRTE Matériaux en Interaction et Réflexion Toutes Epaisseurs

MSR Molten Salt Reactor

NRAD Neutron Radiography

PWR Pressurized Water Reactor

TRISO Tri-Isotropic

frontiers | Frontiers in Energy Research

TYPE Review
PUBLISHED 05 January 2023
DOI 10.3389/fenrg.2022.1082389

OPEN ACCESS

EDITED BY
Michael Fleming,
Organisation for Economic Co-Operation and Development, France

REVIEWED BY
Nicolas Leclaire,
Institut de Radioprotection et de Sûreté Nucléaire, France
Michael Zerkle,
Naval Nuclear Laboratory, United States

*CORRESPONDENCE
Nicholas W. Thompson,
nthompson@lanl.gov

SPECIALTY SECTION
This article was submitted to Nuclear Energy, a section of the journal Frontiers in Energy Research

RECEIVED 28 October 2022
ACCEPTED 29 November 2022
PUBLISHED 05 January 2023

CITATION
Thompson NW, Maldonado A, Cutler TE, Trellue HR, Amundson KM, Rao Dasari V, Goda JM, Grove TJ, Hayes DK, Hutchinson JD, Kistle HM, Kostelac CM, Lamproe JR, Matthews C, McKenzie G, McMath GE, McSpaden AT, Sanchez RG, Stolte KN, Walker JL, Weldon R and Whitman NH (2023), The National Criticality Experiments Research Center and its role in support of advanced reactor design.
Front. Energy Res. 10:1082389.
doi: 10.3389/fenrg.2022.1082389

The National Criticality Experiments Research Center and its role in support of advanced reactor design

Nicholas W. Thompson[1]*, Alexis Maldonado[2], Theresa E. Cutler[1], Holly R. Trellue[2], Kelsey M. Amundson[1], Venkateswara Rao Dasari[3], Joetta M. Goda[1], Travis J. Grove[1], David K. Hayes[1], Jesson D. Hutchinson[1], Hadyn M. Kistle[1], Cole M. Kostelac[1], Juliann R. Lamproe[1], Christopher Matthews[4], George McKenzie[1], Garrett E. McMath[1], Alexander T. McSpaden[1], Rene G. Sanchez[1], Kristin N. Stolte[1], Jessie L. Walker[1], Robert Weldon[1] and Nicholas H. Whitman[1]

[1]Los Alamos National Laboratory, Nuclear Engineering and Nonproliferation, Advanced Nuclear Technology (NEN-2), Los Alamos, NM, United States, [2]Los Alamos National Laboratory, Nuclear Engineering and Nonproliferation Systems Design and Analysis (NEN-5), Los Alamos, NM, United States, [3]Los Alamos National Laboratory, Civilian Nuclear Programs, Los Alamos, NM, United States, [4]Los Alamos National Laboratory, Materials Science and Technology, Materials Science in Radiation and Dynamics Extremes (MST-8), Los Alamos, NM, United States

The National Criticality Experiments Research Center (NCERC) located at the Nevada National Security Site (NNSS) in the Device Assembly Facility (DAF) and operated by Los Alamos National Laboratory (LANL) is the only general purpose critical experiments facility in the United States. Experiments from subcritical to critical and above prompt critical are carried out at NCERC on a regular basis. In recent years, NCERC has become more involved in experiments related to nuclear energy, including the Kilopower/KRUSTY demonstration and the recent Hypatia experiment. Multiple nuclear energy related projects are currently ongoing at NCERC. This paper discusses NCERC's role in advanced reactor design and how that role may change in the future.

KEYWORDS

nuclear, criticality, reactor, experiments, critical, demonstration

1 Introduction

The National Criticality Experiments Research Center (NCERC) located at the Nevada National Security Site (NNSS) in the Device Assembly Facility (DAF) and operated by Los Alamos National Laboratory (LANL) is the only general purpose critical experiments facility in the United States. NCERC consists of four critical assemblies;

Comet, Planet, Flattop, and Godiva IV. Using these critical assemblies and the large quantities of nuclear materials stored at NCERC, an almost limitless combination of experiments can be performed.

NCERC has its roots in the Manhattan Project at the Pajarito Site and later TA-18, both at LANL (Loaiza and Gehman, 2006; Hutchinson et al., 2021a). For decades, criticality experiments were performed at LANL, known as the Los Alamos Critical Experiments Facility (LACEF) (Paxton, 1978, Paxton, 1981, Paxton, 1983). In the early 2000s, some of the critical assemblies were moved out to NNSS to the DAF and reconstituted as NCERC. For over 10 years since that move, criticality experiments have been performed at NCERC. This also includes many subcritical experiments. These experiments have been documented in a special issue of Nuclear Science and Engineering (Hutchinson et al., 2021b; Thompson et al., 2021b; Goda et al., 2021; Hayes et al., 2021; Sanchez et al., 2021).

1.1 Criticality experiments

Criticality experiments are experiments where fissile material is arranged in a way that generates meaningful and measurable neutron multiplication. These experiments can be a subcritical bare sphere of material or can scale all the way up to a full scale demonstration of a reactor. Criticality experiments are typically low power (a few kW and below), although burst experiments can have instantaneous powers of many GW for a very short amount of time. A typical criticality experiment is used to measure the reactivity of the system or other nuclear parameters. At NCERC, we often use the term "criticality experiments" over "critical experiments" as "critical" implies a k_{eff} of 1.0, whereas the experiments we perform can range from very subcritical to critical and above prompt supercritical. Each of the critical assemblies at NCERC use different means of reactivity control and various detectors so that important parameters such as reactivity and delayed critical configurations can be measured with high accuracy.

The main sponsor for NCERC experiments is the Nuclear Criticality Safety Program (NCSP). NCERC (and LACEF before that) has performed many benchmark critical and subcritical experiments which are now part of the International Criticality Safety Benchmark Evaluation Project handbook (ICSBEP) (OECD-NEA, 2022). The ICSBEP benchmarking process is extremely rigorous; each benchmark includes dimensions of each component, material compositions, temperature information, isotopics for fuel and other relevant components, and uncertainties for each of these values. These uncertainties are used to estimate the uncertainty in the experiment, the uncertainty in the benchmark model, and biases between the experiment and benchmark model. Due to their high quality, these benchmarks are crucial for validating nuclear data and ensuring nuclear criticality safety. Major nuclear data libraries such as ENDF/B-VIII.0, JEFF-3.3, and JENDL-4.0 make extensive use of criticality benchmarks for validating nuclear data and benchmarking the performance of the nuclear data library compared to other libraries (van der Marck, 2006, 2012; CHIBA et al., 2011; SHIBATA et al., 2011; Brown et al., 2018; Plompen et al., 2020). In fact, nuclear data libraries are sometimes adjusted to match these benchmarks, for example, nubar for ^{239}Pu and ^{235}U respectively were adjusted to match k_{eff} of Jezebel and Godiva in ENDF/B-VIII.0 (Peterson, 1953; Peterson and Newby, 1956; LaBauve, 2002; Favorite, 2016; Brown et al., 2018; Chadwick et al., 2018; Kimpland et al., 2021).

Recently, NCERC has performed a number of experiments related to nuclear energy and advanced reactors, some of which will be covered in **Section 4**. Given NCERC's unique capabilities, experiments can be performed on relatively accelerated timelines, and often without major changes to the facility. This allows NCERC to fill an interesting niche for performing criticality testing on fuels and components, and even small scale, low power demonstrations of advanced reactor designs.

2 NCERC capabilities

NCERC has four critical assemblies, Planet, Comet, Flattop, and Godiva IV. Planet and Comet are vertical lift assemblies, meaning a portion of the reactor is placed on a lower, movable platen, while another portion is affixed to a stationary platform above. When the lower platen is inserted, reactivity of the system is increased and a critical experiment can be conducted. **Figures 1**, **2** show photos of the Planet and Comet assemblies respectively. Comet has a much higher lifting capacity and overall weight limit than Planet, so much of this paper will focus on the Comet assembly.

Flattop has a highly enriched uranium (HEU) or weapons grade Pu spherical core, surrounded by one metric ton of natural uranium, which is split into a stationary hemisphere and two movable quarter spheres. The stationary hemisphere also has control rods made of natural uranium which can be inserted to increase reactivity. Flattop is primarily used for activation analyses and as a training tool. **Figure 3** is a photo of the Flattop assembly.

Godiva IV is a fast burst assembly made of HEU. It has a cylindrical core with roughly 65 kg of HEU and is used for many experiments, including testing criticality accident alarm system, measuring prompt fission neutron spectrum, and activation analyses. **Figure 4** is a photo of the Godiva IV assembly.

NCERC also has a large selection of fuels. The most commonly used are the HEU "Jemima" plates (so named due to their pancake like shape) and the Pu Zero Power Physics Reactor (ZPPR) plates. **Figures 5**, **6** show photos of the Jemima plates and ZPPR plates. The ZPPR plates came

FIGURE 1
Photo of the Planet assembly.

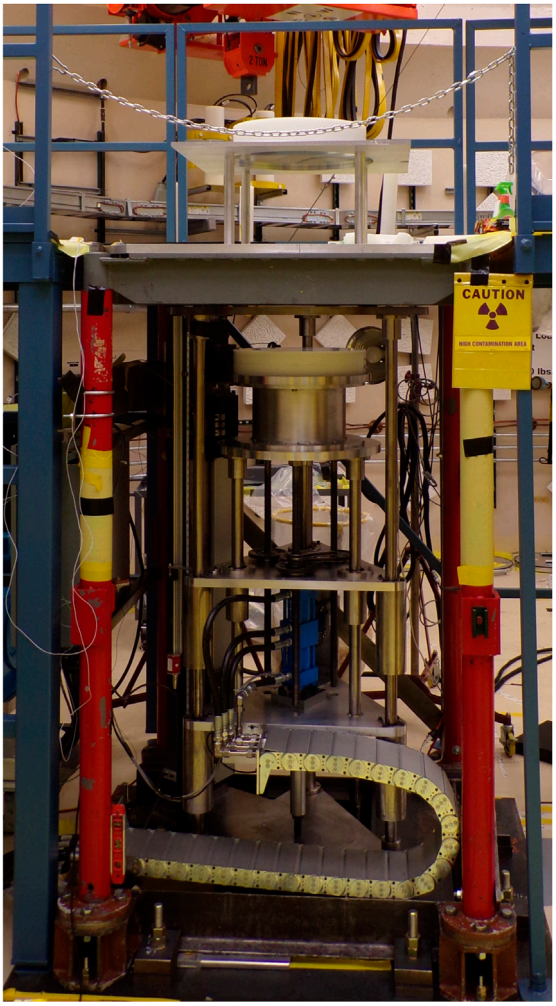

FIGURE 2
Photo of the Comet assembly.

from the original ZPPR which was located at Idaho National Laboratory (Shuck et al., 1967). NCERC also has other materials, including the "Rocky Flats Shells", HEU hemi-shells which were produced at the Rocky Flats plant (seen in **Figure 7**) (Rothe, 2005, Rothe, 2003), the HEU "C-Disks" (Brewer, 1998) (used in the SPEC-MET-FAST-004 benchmark and the Hypatia experiment discussed in **Section 4.2**, seen in **Figure 8**), and the Compact Nuclear Power Source (CNPS) fuel (Hansen and Palmer, 1989). The CNPS experiment used high-assay low enriched uranium (HALEU) Tri-structural Isotropic (TRISO) fuel, making NCERC one of the few facilities in the world with appreciable amounts of HALEU TRISO fuel. **Figure 9** shows an example of one of the CNPS HALEU TRISO fuel compacts.

There are a number of detector systems that are used during experiments at NCERC. These include startup (He^3) and linear channel (compensated ion chambers) detectors for monitoring neutron flux, organic and inorganic scintillators for measuring neutron and gamma responses, and many other detectors. These other systems are used for gamma spectroscopy, neutron noise measurements, neutron leakage spectra measurements, and others. In addition to the critical assemblies, NCERC also has a count room that is routinely used for counting irradiated samples from NCERC measurements. This includes HPGe detectors,

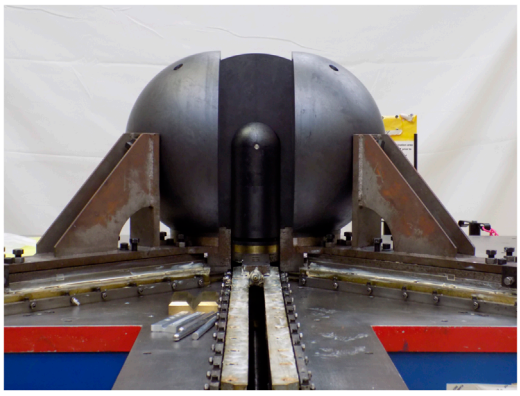

FIGURE 3
Photo of the Flattop assembly.

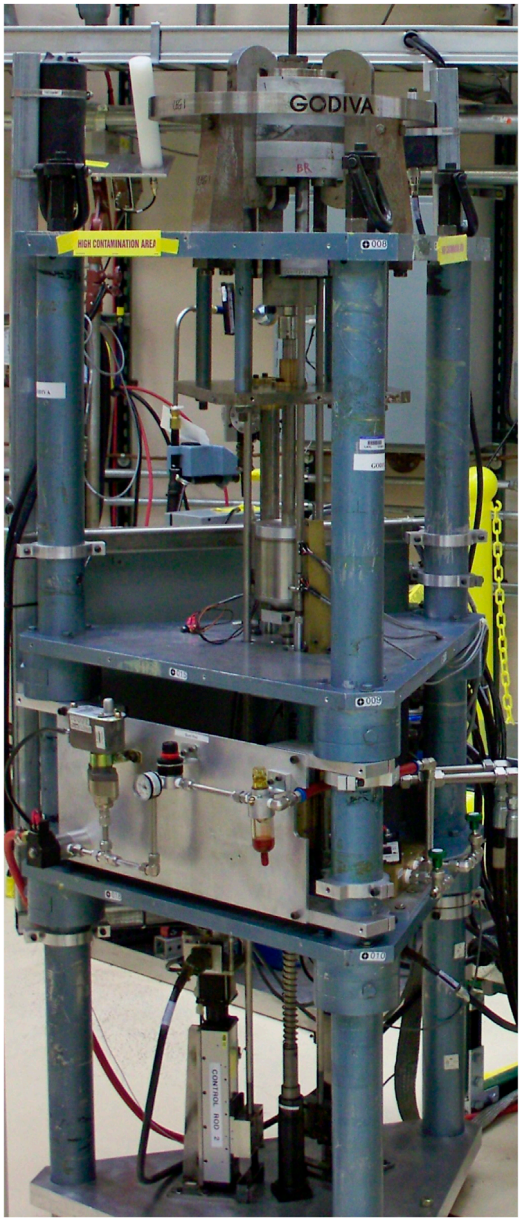

FIGURE 4
Photo of the Godiva assembly.

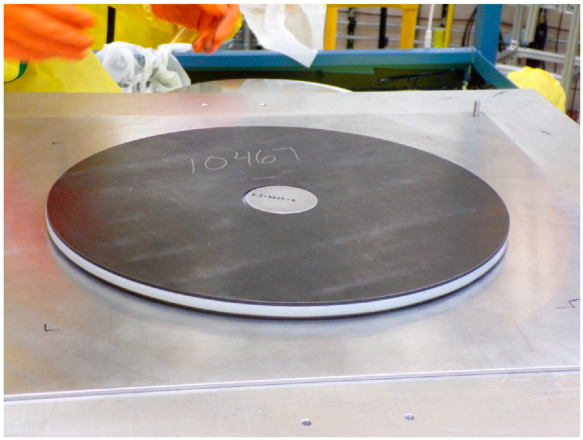

FIGURE 5
Photo of a Jemima plate during an NCERC experiment.

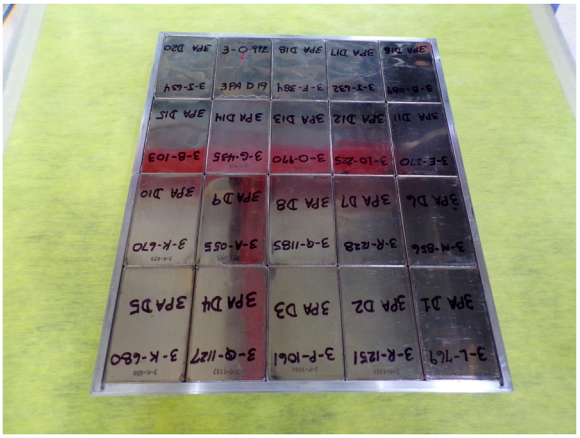

FIGURE 6
Photo of an array of ZPPR plates during the Chlorine Worth Study.

alpha spectroscopy equipment, and dosimetry equipment for determining dose.

3 Nuclear criticality safety

Many of the experiments performed at NCERC are funded by NCSP. These experiments usually focus on one material (e.g., nickel or iron) or one application (e.g., Hanford waste tanks). In the case of a material, there is often a specific concern about nuclear data. One example of this is the upcoming CERBERUS experiment which is designed to be highly sensitive to copper cross sections in the 100 keV–900 keV energy region (Amundson et al., 2022). The end goal of this experiment is to validate copper cross sections which will help improve existing benchmarks that are sensitive to copper, particularly the Zeus benchmarks. The Zeus experimental series were the first to use the large copper reflector on the Comet critical assembly, and these benchmarks are used often in validating nuclear data (Mosteller et al., 2004; Mosteller, 2005; Hayes and Sanchez, 2006).

In cases where an experiment is designed to match an application, the experiment is designed to match the sensitivity profile of the application, using tools such as

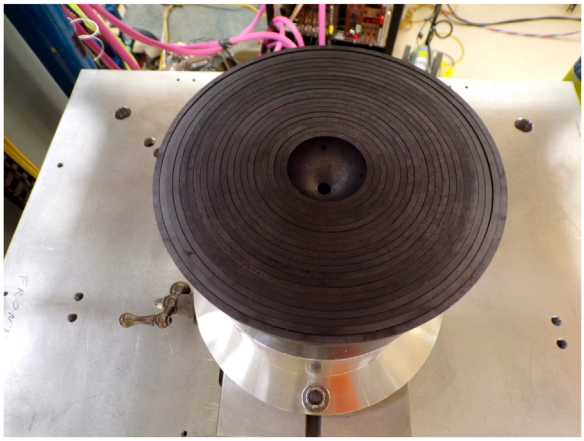

FIGURE 7
Photo of Rocky Flats shells during the MUSiC experiment.

the particle transport code MCNP®[1] (Werner et al., 2017) and the sensitivity/uncertainty analysis code WHISPER (Kiedrowski et al., 2015). MCNP can be used to generate sensitivity profiles, and the WHISPER code can then compare those profiles to existing benchmarks or applications, generating similarity coefficients for each benchmark based on the "sandwich rule." Much more has been written and published about this topic and code. Both of these methodologies (designing to test a material or designing to match an application) are extremely relevant for advanced reactors.

4 Selection of relevant past experiments

NCERC has performed a number of recent experiments that are highly relevant to advanced reactors, below are just a sample.

4.1 KRUSTY/Kilopower

In 2012, the Demonstration Using Flattop Fission (DUFF) experiment was performed (Poston, 2013). This experiment used the Flattop assembly with a heatpipe inserted in the center of the core attached to a Stirling engine. This experiment was the predecessor to the KRUSTY/Kilopower experiment, which was performed in late 2017 and early 2018.

FIGURE 8
Photo of the core stack during the Hypatia experiment.

The KRUSTY/Kilopower experiment was a demonstration of a space nuclear reactor being developed with NASA. The experiment itself was a collaboration between NASA, NCSP, and NNSA. The motivation was to ensure high reliability by minimizing moving parts as much as possible, while also maximizing the power to weight ratio. The final experiment used an HEU core about the size of a roll of paper towels, surrounded by a BeO reflector, on the Comet critical assembly (seen in Figure 10). The HEU core was new and designed specifically for this experiment and manufactured at Y-12. Eight heatpipes were

1 MCNP® and Monte Carlo N-Particle® are registered trademarks owned by Triad National Security, LLC, manager and operator of Los Alamos National Laboratory. Any third party use of such registered marks should be properly attributed to Triad National Security, LLC, including the use of the designation as appropriate. For the purposes of visual clarity, the registered trademark symbol is assumed for all references to MCNP within the remainder of this paper.

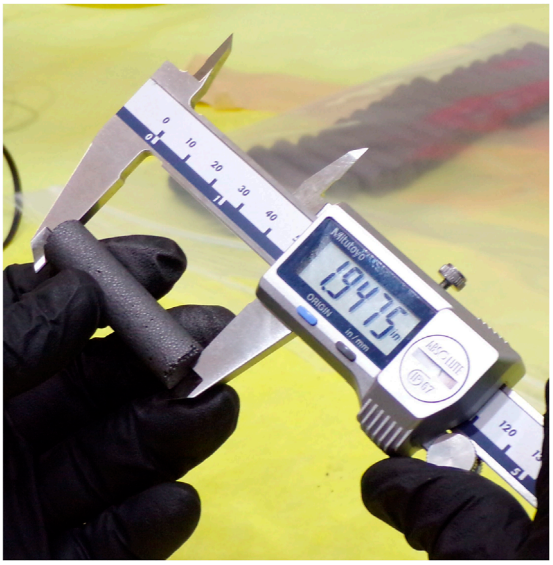

FIGURE 9
Photo of a pellet from the CNPS experiment being measured.

FIGURE 10
Photo of the KRUSTY experiment on the Comet assembly.

also connected to the core, which were cooled by Stirling engines and simulated Stirling engines. To simulate space conditions, the core, heatpipes, and Stirling engines were enclosed in a large vacuum chamber.

Weeks of tests were performed to bring the system critical and measure reactivity of components. The final test included a 28 h "high power" test, averaging 3 kW of power and an average core temperature of 800°C while undergoing many transients (startup, loss of cooling, reactivity insertions, shutdown, etc.). These tests showed the capability for the system to load-follow (match power to a desired electrical load) with no operator input. Much more has been written about this experiment in a special issue of Nuclear Technology, along with other publications (McClure et al., 2020b; Poston et al., 2020a; Gibson et al., 2020; McClure et al., 2020a; Sanchez et al., 2020; Grove et al., 2020; Poston et al., 2020b, Poston et al., 2020c; Stolte et al., 2022). The KRUSTY experiment has been approved and has been included as a benchmark in the 2021 ICSBEP Handbook and will be useful for validating Be nuclear data.

4.2 Hypatia

Hypatia was an experiment conducted in early 2021 that was focused on performing a heated critical experiment with yttrium-hydride (YH_x). YH_x has been proposed by many as a potential neutron moderator in micro-reactors, due to its high hydrogen density and low hydrogen loss even at high temperatures (Trellue et al., 2021). However, until the Hypatia experiment, there had never been a critical experiment performed with YH_x.

There was a large effort at LANL to develop YH_x samples large enough to work in a critical experiment (Trellue et al., 2022). Once the YH_x samples were produced, they were sealed and shipped to NCERC. The Hypatia core was a combination of HEU disks (C-Disks), graphite pieces, electric heaters, and YH_x samples, all surrounded by Be as a reflector and moderator.

During this test, the YH_x samples were heated to roughly 300°C and reactivity was measured as a function of temperature. This was the first experiment to demonstrate and measure the positive temperature coefficient of reactivity for YH_x, meaning that as the temperature of the YH_x increased, the reactivity also increased. This effect has been seen before in ZrH_x in the Topaz reactor (Buden, 1993), and was predicted based on new thermal scattering laws for YH_x in ENDF/B-VIII.0 (Zerkle and Holmes, 2017; Zerkle et al., 2021; Brown et al., 2018) and new experimental data on YH_x scattering (Mehta, 2020; Mehta et al., 2022). The positive temperature coefficient of reactivity for YH_x may have design implications for advanced reactors seeking to utilize this moderator (Ade et al., 2022). Additional information on the Hypatia experiments can be

found in publications by Trellue and Cutler (Trellue et al., 2021, Trellue et al., 2022; Cutler et al., 2022b).

4.3 MUSiC

The Measurement of Uranium Subcritical and Critical (MUSiC) experiment was performed in 2020 and 2021 at NCERC using the "Rocky Flats Shells" (McSpaden et al., 2019a; Weldon et al., 2021, Weldon et al., 2020; Darby et al., 2021; McSpaden et al., 2021). **Figure 11** is a photo of the experimental setup. The goal of the experiment was to perform high quality measurements of HEU systems with many detector types, from very subcritical to critical. Since the Rocky Flats Shells are nesting HEU hemishells, systems of different size spheres of HEU were made by varying which shells were used in the experiment. The MUSiC experiment included some measurements with a ^{252}Cf source, some with a pulsed deuterium-tritium neutron generator, and some with no external neutrons. Similar subcritical measurements are often made at NCERC, but this was the first time at NCERC a system like this was measured from subcritical to critical. Two MUSiC critical experiments will be submitted as benchmarks to the ICSBEP Technical Review Group in 2023. Other subcritical experiment benchmarks will follow in the years to come. Ultimately, this data will be used by nuclear data evaluators to validate ^{235}U nuclear data in the fast energy region, which is extremely important for many advanced reactor designs. Additionally, due to uncertainties in the original "Lady Godiva" benchmark, MUSiC may become the new standard for ^{235}U validation (Bess et al., 2013; Hutchinson et al., 2022b).

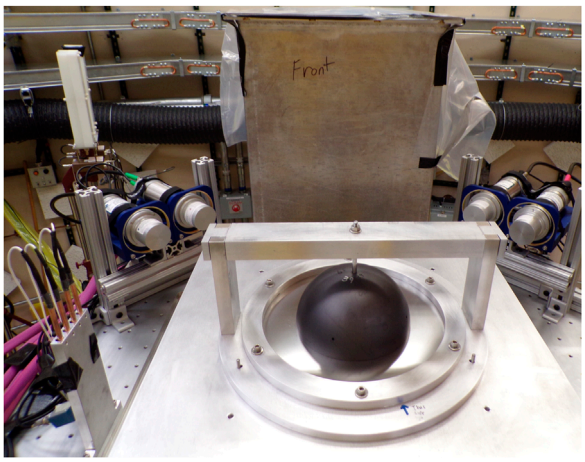

FIGURE 11
Photo of the experimental setup during the MUSiC experiment.

4.4 Japan Atomic Energy Agency collaboration experiments

From 2015 to 2019, a series of experiments in collaboration with the Japan Atomic Energy Agency (JAEA) was performed, specifically focused on lead void coefficients of reactivity. The JAEA was interested in created an Accelerator Driven System (ADS) for spent fuel transmutation. Three configurations were built and operated, a Plutonium system (also known as Jupiter), an HEU system, and an effectively Intermediate Enriched Uranium (IEU) system (Fukushima et al., 2018, Fukushima et al., 2019). The "IEU" system combined natural and HEU Jemima plates to create an "effective enrichment" of 22.9 weight percent. Each of the systems had a large amount of lead (Pb), and multiple experiments were performed where the amount of lead in the system was varied while keeping the fuel concentration constant. This allowed for measurements of the void coefficient of reactivity of lead for each system. The HEU/Pb and IEU/Pb systems used the Jemima plants for fuel, and the Pu system (Jupiter) used ZPPR plates. There was also a Jupiter configuration which utilized ZPPR plates with higher ^{240}Pu content. The HEU/Pb system had a negative lead void coefficient of reactivity, but the IEU/Pb had a positive lead void coefficient; this behavior was predicted in MCNP simulations, but it highlights the importance of demonstration experiments to prove that models are performing correctly (Goda et al., 2015; Goda et al., 2019, Thompson et al., 2021b). Work is ongoing to submit these experiments to the ICSBEP as benchmarks (McSpaden et al., 2019b, McSpaden et al., 2020; Amundson et al., 2020).

5 Upcoming NCERC experiments

NCERC also has some upcoming experiments that are highly relevant to advanced reactor development and deployment.

5.1 EUCLID

Experiments Underpinned by Computational Learning for Improvements in Nuclear Data (EUCLID) is a LANL Laboratory Directed Research & Development project focused on identifying and resolving compensating errors in nuclear data (Hutchinson et al., 2022a; Neudecker et al., 2022a; Neudecker et al., 2022b; Clark et al., 2022; Kleedtke et al., 2022; Rising and Clark, 2022). As part of this project, an experiment series at NCERC was designed using machine learning tools. This experiment was specifically focused on ^{239}Pu scattering using two different configurations: one that maximizes neutron leakage, and one that minimizes leakage. Because of the large differences in leakage, there are large differences in sensitivities to both elastic and inelastic scattering. Even for a well known isotope

such as ^{239}Pu, different nuclear data libraries (ie. ENDF/B-VIII.0 and JEFF-3.3) have very different ^{239}Pu elastic and inelastic scattering cross sections. This experiment should assist in resolving some of the issues between nuclear data libraries for ^{239}Pu and this methodology of experiment design will be used for other experiments in the future.

5.2 Westinghouse eVinci

NCERC is currently partnering with Westinghouse to potentially perform a small scale demonstration of their eVinci microreactor. A portion of the eVinci core will be placed on the movable platen of Comet, and surrounded by graphite fueled with the CNPS fuel. The setup will be designed to accommodate measurements in the temperature range of 20–1,200°C and will contain materials to be tested. The current plan includes 1/M approach to criticals for the different configurations, component critical tests (testing reactivity of various components), and heated tests with various core configurations. This data will be used by Westinghouse to validate their simulation codes, reduce uncertainties, and to help support their safety case to their regulator. It is to be determined whether this data will stay proprietary or will become an official benchmark in the ICSBEP or IRPhEP handbooks (OECD-NEA, 2022, OECD-NEA, 2019).

6 NCERC and advanced reactors

As demonstrated from the experiments mentioned above, there are two key ways experiments at NCERC can support the development and deployment of advanced reactors - through low power demonstrations, and experiments designed to validate key nuclear data.

6.1 Low power demonstrations

The KRUSTY/Kilopower experiment summarized in **Section 4.1** is a great example of a low power demonstration that can be performed at NCERC. However, one downside to the KRUSTY experiment was neutron activation; even with shielding around the core, the room remained unusable for other experiments for months. Given the high demand for the NCERC facility, being unable to operate key critical assemblies for over a month is not currently an option. As a lesson learned from KRUSTY, experiments in the future will have to be lower power, which often necessitates electric heating as opposed to nuclear heating.

There is still an enormous amount of information that can be gained from low power demonstrations, such as reactor physics parameters, system reactivity, reactivity of components, temperature coefficients, flux distributions, neutron spectra *via* activation foils, leakage spectra, multiplicity, shielding performance, control rod/drum worth, and much more. These are exactly the types of measurements being planned for the Westinghouse eVinci demonstrations.

Today many of these parameters are simulated without adequate validation data, especially for novel systems such as advanced reactors that often plan to use new coolants, fuels, moderators, or other materials. Additionally, there are even fewer validation experiments at the high temperatures many of these reactors are planning to operate at. It is important we make high quality measurements of these systems and materials so that when these systems are actually built, they operate as they are designed.

6.2 Nuclear data

Nuclear data is extremely important for advanced reactors, and in some cases, the quality of the nuclear data today is still lacking. One rather important example that has gotten a lot of attention is the ^{35}Cl (n,p) cross section at high energies. As was shown by Oak Ridge National Laboratory, TerraPower, and Moltex Energy, the ^{35}Cl (n,p) has a huge impact on the reactivity of Molten Chloride Fast Reactors (Bostelmann et al., 2020; Kolos et al., 2022; Taylor et al., 2022). In fact, changes in recent nuclear data libraries have resulted in differences of thousands of pcm. Additionally, uncertainty/covariance data for ^{35}Cl (n,p) in ENDF/B-VIII.0 is missing above ~1 MeV, meaning some analysis techniques which rely on covariance data to estimate nuclear data uncertainties will not attribute any nuclear data uncertainty to this reaction. In this way, covariances can be just as important as the underlying cross sections. This topic has already generated multiple papers and a request to the NEA Nuclear Data High Priority Request List.

This is an example of a material and energy range that could be targeted with a well designed critical experiment at NCERC. In fact, NCERC recently completed the Chlorine Worth Study (CWS) experiment (Cutler et al., 2022a) - this experiment was focused on the reactivity worth of chlorine at low energies, specifically related to aqueous chloride operations. While this CWS experiment is not very helpful for validating the ^{35}Cl (n,p) cross section in the fast energy region, another measurement could be designed to test just that. As was mentioned before, many experiments at NCERC are designed specifically to validate nuclear data.

Another relevant example of an experiment designed to validate nuclear data is the Critical Unresolved Region Integral Experiment (CURIE). CURIE was originally designed to validate the unresolved resonance region (URR) of ^{235}U (Cutler et al., 2018). Around the same time CURIE was taking place, the Nuclear Data Machine Learning team lead by Denise Neudecker at LANL found some rather large discrepancies in

nuclear data for ^{19}F (Neudecker et al., 2020). CURIE used the large copper reflectors form ZEUS and teflon (PTFE) moderator plates to create an energy spectrum highly sensitive to the URR of ^{235}U, making CURIE also highly sensitive to ^{19}F in this energy region (Cutler et al., 2020; Thompson et al., 2021a). Because of this, CURIE is currently being used by members of the Cross Section Evaluation Working Group (CSEWG) and the International Nuclear Data Evaluation Network (INDEN) to validate and improve ^{235}U, ^{19}F, and ^{63,65}Cu nuclear data (Trkov and Capote, 2022). Work is ongoing to submit this experiment as an ICSBEP benchmark.

Many other experiments have been performed at NCERC specifically focused on nuclear data validation, including the TEX HEU and TEX Pu series, the Zeus series, and others (Percher and Norris, 2019; Percher and Norris, 2020, Norris and Araj, 2021; Mosteller et al., 2004; Mosteller, 2005; Hayes and Sanchez, 2006). These experiments are detailed in the NCERC Ten Year Papers and other publications (Hutchinson et al., 2021b; Thompson et al., 2021b; Goda et al., 2021; Hayes et al., 2021; Sanchez et al., 2021).

7 Future of NCERC

Recently at LANL, a meeting was held to discuss the future of NCERC, aptly named NCERC Futures. A report on the meeting is currently being written, but many ideas for new buildings/facilities, critical assemblies, measurements, and fuels were presented. One notable mention here is the possibility of adding a horizontal split table to NCERC. This would add the capability to perform much larger experiments at NCERC. Currently experiments are limited by the size and weight limits of the Comet assembly. A horizontal split table would have a much larger area for experiments and a much larger weight limit, which would allow for experiments similar to the ones done at the original ZPPR (near full scale reactor experiments). It should be noted that LACEF previously had multiple horizontal split table reactors, "Big Ten," which operated intermittently from 1971 to 1996 and "Honeycomb" which operated from 1956 to 1990 (Loaiza and GehmanPaxton, 2006; Paxton, 1983).

Other notable mentions include a new Jezebel (unreflected Pu system), another Comet assembly, and new fuels such as Pu nesting hemishells. Many of these new assemblies would require NCERC to expand into a new building: this is currently being investigated.

8 Conclusion

NCERC can play a crucial role in supporting the development and deployment of advanced reactors. Small scale demonstrations can be built and tested. Key nuclear data parameters can be measured and validated. NCERC has done many experiments in the past that have helped to constrain important nuclear data.

NCERC has also performed demonstrations of advanced reactors, and experiments are currently in the planning process to perform additional demonstration experiments. Since NCERC is a low power facility, experiments can often be done much faster and cheaper than it would cost to build a full scale demonstration, while providing much of the same experimental data. The future is bright for advanced reactors as long as experimental facilities like NCERC are open to perform crucial experiments to demonstrate reactor designs, demonstrate key nuclear physics, and validate nuclear data.

Author contributions

NT wrote most of the article, is the PI of the Westinghouse eVinci project, and is part of the NCERC team. AM is a member of the Westinghouse eVinci team at LANL, specializing in neutronics and thermal analysis, and also helped write the article. TC was the NCERC lead on the Hypatia experiment and the Chlorine Worth Study. HT managed the Hypatia experiment and also leads other advanced reactor and micro-reactor activities at LANL. VD is the head of the Civilian Nuclear Program office at LANL and has been involved in both the Hypatia and Westinghouse projects. CM is involved in managing all technical projects with Westinghouse. JG is the NCERC team leader, and is also the PI for the Godiva assembly. DH is the NCERC Chief Engineer, the PI for Flattop, and has been involved in nearly every experiment performed at NCERC since its founding. RS is the PI on the Comet and Planet assemblies, was the NCERC lead on the KRUSTY/Kilopower experiment, and has also been involved in nearly every project at NCERC since its founding. KA, TG, JH, HK, CK, JL, GMcK, GMcM, AM, KS, JW, RW, and NW are all members of the NCERC team and have worked on many of the projects mentioned in this article. All of the authors gave comments and suggestions for the article.

Funding

This work was supported by the U.S. Department of Energy through the Los Alamos National Laboratory. Los Alamos National Laboratory is operated by Triad National Security, LLC, for the National Nuclear Security Administration of U.S. Department of Energy (Contract No. 89233218CNA000001). Much of the work discussed was supported by the DOE Nuclear Criticality Safety Program, funded and managed by the National Nuclear Security Administration for the Department of Energy. Other sources of funding include the Los Alamos National Laboratory Laboratory Directed Research and Development Program, NASA, and DOE-NE.

Acknowledgments

The authors would like to acknowledge the technicians of NCERC, Kenny Valdez and Justin Martin in particular, for their tireless help getting these experiments up and running. The authors would also like to thank NCERC-FO for their support of NCERC activities, the RCTs at NCERC for constantly ensuring our safety and minimizing our contamination while working with hazardous materials. A special thanks to the NEN-2 Design Engineering team for making these experiments a reality. The authors would also like to thank the NEN management for their forward thinking an openness to expanding NCERC activities and scope.

Conflict of interest

The authors declare that the research was conducted in the absence of any commercial or financial relationships that could be construed as a potential conflict of interest.

Publisher's note

All claims expressed in this article are solely those of the authors and do not necessarily represent those of their affiliated organizations, or those of the publisher, the editors and the reviewers. Any product that may be evaluated in this article, or claim that may be made by its manufacturer, is not guaranteed or endorsed by the publisher.

References

Ade, B. J., Betzler, B. R., Burns, J. R., Chapman, C. W., and Hu, J. (2022). Reactor physics considerations for use of yttrium hydride moderator. *Nucl. Sci. Eng.* 0, 1–20. doi:10.1080/00295639.2022.2035157

Amundson, K., Cutler, T., and Thompson, N. (2022). "CERBERUS integral experiment design," in Proceedings of the nuclear criticality safety division topical meeting (NCSD 2022), Anaheim, CA, June 12–16, 2022, 305–314. Available at: https://www.ans.org/pubs/proceedings/article-51948

Amundson, K., et al. (2020). Fast-spectrum critical assemblies with a pb-heu core surrounded by a copper reflector. *Trans. Am. Nucl. Soc.* 123, 817.

Bess, J., Briggs, J., and Marshall, M. (2013). "What if lady Godiva was wrong?" in *International conference on nuclear data for science and Technology*. ND 2013).

Bostelmann, F., Ilas, G., and Wieselquist, W. A. (2020). *Key nuclear data impacting reactivity in advanced reactors*. Oak Ridge, TN: Oak Ridge National Laboratory. Tech. Rep. ORNL/TM-2020/1557. doi:10.2172/1649145

Brewer, R. (1998). "Critical experiments performed using plate of plutonium-242, HEU, and plutonium-239," in *International handbook of evaluated criticality safety benchmark experiments* (Paris: OECD Nuclear Energy Agency).

Brown, D., Chadwick, M., Capote, R., Kahler, A., Trkov, A., Herman, M., et al. (2018). ENDF/B-VIII.0: The 8th major release of the nuclear reaction data library with CIELO-project cross sections, new standards and thermal scattering data. *Nucl. Data Sheets* 148, 1–142. doi:10.1016/j.nds.2018.02.001

Buden, D. (1993). Summary of space nuclear reactor power systems. Tech. Rep. INEL/MISC-93085 Available at: https://www.osti.gov/biblio/10151265.

Chadwick, M., Capote, R., Trkov, A., Herman, M., Brown, D., Hale, G., et al. (2018). CIELO collaboration summary results: International evaluations of neutron reactions on uranium, plutonium, iron, oxygen and hydrogen. *Nucl. Data Sheets* 148, 189–213. doi:10.1016/j.nds.2018.02.003

Chiba, G., Okumura, K., Sugino, K., Nagaya, Y., Yokoyama, K., Kugo, T., et al. (2011). JENDL-4.0 benchmarking for fission reactor applications. *J. Nucl. Sci. Technol.* 48, 172–187. doi:10.1080/18811248.2011.9711692

Clark, A., Alwin, J., Cutler, T., Grosskopf, M., Haeck, W., Hutchinson, J., et al. (2022). "How can a diverse set of integral and semi-integral measurements inform identification of discrepant nuclear data?" 15th International Conference on Nuclear Data for Science and Technology (ND2022).

Cutler, T., Amundson, K., Hutchinson, J., Kleedtke, N., and Wynne, N. (2022a). "The CWS experiments - an experimental study of the effects of chloride on thermal neutron absorption," in *Proceedings of the nuclear criticality safety division topical meeting. NCSD 2022)*.

Cutler, T., et al. (2020). Critical unresolved region integral experiment execution. *Trans. Am. Nucl. Soc.* 123, 828.

Cutler, T., et al. (2018). Curie preliminary design. *Trans. Am. Nucl. Soc.* 119, 728–730.

Cutler, T., Trellue, H., Blood, M., Grove, T., Luther, E., Thompson, N., et al. (2022b). The Hypatia experiment: Yttrium hydride and highly enriched uranium critical experiment. *Nucl. Technol.*, 1–17. doi:10.1080/00295450.2022.2027146

Darby, F. B., Hutchinson, J. D., Hua, M. Y., Weldon, R. A., McKenzie, G. E, Lamproe, J. R., et al. (2021). Comparison of neutron multiplicity counting estimates with trans-stilbene, EJ-309, and He-3 detection systems. *Trans. Am. Nucl. Soc.* 125, 602–605. doi:10.13182/T125-36636

Favorite, J. (2016). "Bare sphere of plutonium-239 metal," in *International handbook of evaluated criticality safety benchmark experiments [DVD]/Nuclear energy agency* (Paris: OECD Nuclear Energy Agency). (NEA;7328). doi:10.1787/e2703cd5-en

Fukushima, M., Goda, J., Bounds, J., Cutler, T., Grove, T., Hutchinson, J., et al. (2018). Lead void reactivity worth in two critical assembly cores with differing uranium enrichments. *Nucl. Sci. Eng.* 189, 93–99. doi:10.1080/00295639.2017.1373520

Fukushima, M., Goda, J., Oizumi, A., Bounds, J., Cutler, T., Grove, T., et al. (2019). Systematic measurements and analyses for lead void reactivity worth in a plutonium core and two uranium cores with different enrichments. *Nucl. Sci. Eng.* 194, 138–153. doi:10.1080/00295639.2019.1663089

Gibson, M. A., Poston, D. I., McClure, P. R., Sanzi, J. L., Godfroy, T. J., Briggs, M. H., et al. (2020). Heat transport and power conversion of the kilopower reactor test. *Nucl. Technol.* 206, 31–42. doi:10.1080/00295450.2019.1709364

Goda, J., Bravo, C., Cutler, T., Grove, T., Hayes, D., Hutchinson, J., et al. (2021). A new era of nuclear criticality experiments: The first 10 Years of Godiva IV operations at NCERC. *Nucl. Sci. Eng.* 195, S55–S79. doi:10.1080/00295639.2021.1947103

Goda, J., et al. (2015). "Void reactivity worth in uranium/lead systems," in *Proceedings of the PHYSOR 2015*. Sun Valley, Idaho, May 1-5).

Goda, J., Grove, T., and McKenzie, G. (2019). "Improvements in void reactivity worth measurements using a load cell as pressure sensor," in *ICNC 2019 - 11th internation conference on nuclear criticality safety* (Paris, France. September 15-20).

Grove, T., Hayes, D., Goda, J., McKenzie, G., Hutchinson, J., Cutler, T., et al. (2020). Kilowatt reactor using stirling TechnologY (KRUSTY) cold critical measurements. *Nucl. Technol.* 206, 68–77. doi:10.1080/00295450.2020.1712950

Hansen, G. E., and Palmer, R. G. (1989). Compact nuclear power source critical experiments and analysis. *Nucl. Sci. Eng.* 103, 237–246. doi:10.13182/NSE89-A23674

Hayes, D., Bredeweg, T., Cutler, T., Goda, J., Grove, T., Hutchinson, J., et al. (2021). A new era of nuclear criticality experiments: The first 10 Years of Flattop operations at NCERC. *Nucl. Sci. Eng.* 195, S37–S54. –S54. doi:10.1080/00295639.2021.1947104

Hayes, D., and Sanchez, R. (2006). "Zeus: Fast-Spectrum critical assemblies with an iron - HEU core surrounded by A copper reflector," in *International handbook of evaluated criticality safety benchmark experiments* (Paris: OECD Nuclear Energy Agency).

Hutchinson, J., Alwin, J., Clark, A. R., Cutler, T., Grosskopf, M. J., Haeck, W., et al. (2022a). "Euclid: A new approach to improve nuclear data coupling optimized experiments with validation using machine learning," 15th International Conference on Nuclear Data for Science and Technology (ND2022). Nuclear Data.

Hutchinson, J., Alwin, J., McSpaden, A., Myers, W., Rising, M., and Sanchez, R. (2021a). Criticality experiments with fast 235U and 239Pu metal and hydride systems during the manhattan project. *Nucl. Technol.* 207, S62–S80. doi:10.1080/00295450.2021.1908076

Hutchinson, J., Bounds, J., Cutler, T., Dinwiddie, D., Goda, J., Grove, T., et al. (2021b). A new era of nuclear criticality experiments: The first 10 Years of radiation test object operations at NCERC. *Nucl. Sci. Eng.* 195, S80–S98. –S98. doi:10.1080/00295639.2021.1918938

Hutchinson, J., Goda, J., Hayes, D., Sanchez, R., Smith, T., and McSpaden, A. (2022b). "Why lady Godiva should be replaced as the default validation experiment for U-235 nuclear data," in *Transactions of the American nuclear society. 2022 ANS winter meeting*.

Kiedrowski, B. C., Brown, F. B., Conlin, J. L., Favorite, J. A., Kahler, A. C., Kersting, A. R., et al. (2015). Whisper: Sensitivity/Uncertainty-Based computational methods and software for determining baseline upper subcritical limits. *Nucl. Sci. Eng.* 181, 17–47. doi:10.13182/NSE14-99

Kimpland, R., Grove, T., Jaegers, P., Malenfant, R., and Myers, W. (2021). Critical assemblies: Dragon burst assembly and solution assemblies. *Nucl. Technol.* 207, S81–S99. doi:10.1080/00295450.2021.1927626

Kleedtke, N., Hutchinson, J., Cutler, T., Michaud, I., Rising, M., Hua, M., et al. (2022). "Data assimilation using non-invasive Monte Carlo sensitivity analysis of reactor kinetics parameters," in 15th International Conference on Nuclear Data for Science and Technology (ND2022). Available at: https://indico.frib.msu.edu/event/52/contributions/990/.

Kolos, K., Sobes, V., Vogt, R., Romano, C. E., Smith, M. S., Bernstein, L. A., et al. (2022). Current nuclear data needs for applications. *Phys. Rev. Res.* 4, 021001. doi:10.1103/PhysRevResearch.4.021001

LaBauve, R. (2002). "HEU-MET-FAST-001: Bare, highly enriched uranium sphere (Godiva)," in *International handbook of evaluated criticality safety benchmark experiments [DVD]/Nuclear energy agency* (Paris: OECD Nuclear Energy Agency). (NEA;7328). doi:10.1787/e2703cd5-en

Loaiza, D., and Gehman, D. (2006). End of an era for the Los Alamos critical experiments facility: History of critical assemblies and experiments (1946–2004). *Ann. Nucl. Energy* 33, 1339–1359. doi:10.1016/j.anucene.2006.09.009

McClure, P. R., Poston, D. I., Clement, S. D., Restrepo, L., Miller, R., and Negrete, M. (2020a). KRUSTY experiment: Reactivity insertion accident analysis. *Nucl. Technol.* 206, S43–S55. doi:10.1080/00295450.2020.1722544

McClure, P. R., Poston, D. I., Gibson, M. A., Mason, L. S., and Robinson, R. C. (2020b). Kilopower project: The KRUSTY fission power experiment and potential missions. *Nucl. Technol.* 206, S1–S12. doi:10.1080/00295450.2020.1722554

McSpaden, A., Bravo, C., Cutler, T., Goda, J., Haeck, W., Hutchinson, J., et al. (2021). "Preliminary NoMAD results of the MUSiC experiment," in *Transactions of the American nuclear society* (ANS Winter Meeting), 125, 598.

McSpaden, A., Cutler, T., Hutchinson, J., Myers, W., McKenzie, G., Goda, J., et al. (2019a2019). Music: A critical and subcritical experiment measuring highly enriched uranium shells. *Int. Conf. Nucl. Crit.*

McSpaden, A., et al. (2019b). Jupiter: A proposed benchmark for lead void worth with plutonium. *Trans. Am. Nucl. Soc.* 121, 1055–1058.

McSpaden, A., et al. (2020). Update on the benchmark analysis of the jupiter experiments: Plutonium moderated by lead. *Trans. Am. Nucl. Soc.* 123, 824–827.

Mehta, V. (2020). *Investigating the response of yttrium hydride moderator due to changes in stoichiometry and temperature*. Atlanta, GA: Georgia Institute of Technology. Ph.D. thesis.

Mehta, V. K., Vogel, S. C., Kotlyar, D., and Cooper, M. W. D. (2022). A modeling and neutron diffraction study of the high temperature properties of sub-stoichiometric yttrium hydride for novel moderator applications. *Metals* 12, 199. doi:10.3390/met12020199

Mosteller, R., Brewer, R., and Sapir, J. (2004). "The initial set of Zeus experiments : Intermediate-spectrum critical assemblies with a graphite-HEU core surrounded by a copper reflector," in *International handbook of evaluated criticality safety benchmark experiments* (Paris: OECD Nuclear Energy Agency).

Mosteller, R. (2005). "The unmoderated Zeus experiment: A cylindrical HEU core surrounded by a copper reflector," in *International handbook of evaluated criticality safety benchmark experiments* (Paris: OECD Nuclear Energy Agency).

Neudecker, D., Alwin, J., Clark, A. R., Cutler, T., Gibson, N., Grosskopf, M. J., et al. (2022a). Uncovering where compensating errors could hide in ENDF/B-VIII.0. Nuclear data 2022.

Neudecker, D., Grosskopf, M., Alwin, J., Clark, A., Cutler, T., Frankle, S., et al. (2022b). *Understanding the impact of nuclear-data covariances*. EPJ Web of Conferences, online.

Neudecker, D., Grosskopf, M., Herman, M., Haeck, W., Grechanuk, P., Vander Wiel, S., et al. (2020). Enhancing nuclear data validation analysis by using machine learning. *Nucl. Data Sheets* 167, 36–60. doi:10.1016/j.nds.2020.07.002

Norris, J., and Araj, R. (2021). "TEX-HEU baseline assemblies: Highly enriched uranium plates with polyethylene moderator and polyethylene reflector," in *International handbook of evaluated criticality safety benchmark experiments* (Paris: OECD Nuclear Energy Agency).

OECD-NEA (2022). *International handbook of evaluated criticality safety benchmark experiments*. Paris: Nuclear Energy AgencyOECD Nuclear Energy Agency. Tech. Rep. NEA;7592.

OECD-NEA (2019). *International handbook of evaluated reactor physics benchmark experiments*. Paris: Nuclear Energy AgencyOECD Nuclear Energy Agency. Tech. Rep. NEA 7496.

Paxton, H. (1983). *A history of critical experiments at Pajarito site*. Los Alamos, NM: Los Alamos National Laboratory. Tech. Rep. LA-09685-H.

Paxton, H. (1978). *Thirty years at Pajarito canyon site*. Los Alamos, NM: Los Alamos Scientific Laboratory. Tech. Rep. LA-7121-H.

Paxton, H. (1981). *Thirty-five years at Pajarito canyon site*. Los Alamos, NM: Los Alamos Scientific Laboratory. Tech. Rep. LA-07121-H-REV.

Percher, C., and Norris, J. (2020). "TEX plutonium assemblies with tantalum: Plutonium-aluminum metal alloy plates with varying thicknesses of polyethylene moderator, interstitial tantalum and a thin polyethylene reflector," in *International handbook of evaluated criticality safety benchmark experiments* (Paris: OECD Nuclear Energy Agency).

Percher, C., and Norris, J. (2019). "TEX plutonium baseline assemblies: Plutonium/aluminum metal alloy plates with varying thicknesses of polyethylene moderator and a thin polyethylene reflector," in *International handbook of evaluated criticality safety benchmark experiments* (Paris: OECD Nuclear Energy Agency).

Peterson, R. (1953). *Lady Godiva; an unreflected uranium-235 critical assembly*. Los Alamos, NM: Los Alamos Scientific Laboratory. *LA-01614*.

Peterson, R., and Newby, G. (1956). An unreflected U-235 critical assembly. *Nucl. Sci. Eng.* 1 (2), 112–125. doi:10.13182/nse56-1

Plompen, A. J. M., Cabellos, O., Jean, C. D. S., Fleming, M., Algora, A., Angelone, M., et al. (2020). The joint evaluated fission and fusion nuclear data library, JEFF-3.3. *Eur. Phys. J. A* 56, 181. doi:10.1140/epja/s10050-020-00141-9

Poston, D. (2013). Criticality and dynamic benchmarking of the DUFF reactor test. *Trans. Am. Nucl. Soc.* 108, 697.

Poston, D. I., Gibson, M. A., Godfroy, T., and McClure, P. R. (2020a). KRUSTY reactor design. *Nucl. Technol.* 206, S13–S30. doi:10.1080/00295450.2020.1725382

Poston, D. I., Gibson, M. A., McClure, P. R., and Sanchez, R. G. (2020b). Results of the KRUSTY warm critical experiments. *Nucl. Technol.* 206, S78–S88. doi:10.1080/00295450.2020.1727287

Poston, D. I., Gibson, M. A., Sanchez, R. G., and McClure, P. R. (2020c). Results of the KRUSTY nuclear system test. *Nucl. Technol.* 206, S89–S117. doi:10.1080/00295450.2020.1730673

Rising, M., and Clark, A. (2022). Development of a new fixed-source sensitivity tally capability in the MCNP code. *Nucl. Data* 2022.

Rothe, R. E. (2005). *A technically useful histoy of the critical mass laboratory at Rocky Flats*. Los Alamos, NM: Los Alamos National Laboratory. Tech. Rep. LA-UR-05-3247.

Rothe, R. E. (2003). The critical mass laboratory at Rocky Flats. *Nucl. Sci. Eng.* 145, 161–172. doi:10.13182/NSE03-A2372

Sanchez, R., Cutler, T., Goda, J., Grove, T., Hayes, D., Hutchinson, J., et al. (2021). A new era of nuclear criticality experiments: The first 10 Years of Planet operations at NCERC. *Nucl. Sci. Eng.* 195, S1–S16. doi:10.1080/00295639.2021.1951077

Sanchez, R., Grove, T., Hayes, D., Goda, J., McKenzie, G., Hutchinson, J., et al. (2020). Kilowatt reactor using stirling TechnologY (KRUSTY) component-critical experiments. *Nucl. Technol.* 206, 56–67. doi:10.1080/00295450.2020.1722553

Shibata, K., Iwamoto, O., Nakagawa, T., Iwamoto, N., Ichihara, A., Kunieda, S., et al. (2011). JENDL-4.0: A new library for nuclear science and engineering. *J. Nucl. Sci. Technol.* 48, 1–30. doi:10.1080/18811248.2011.9711675

Shuck, A. B., Jelinek, H. F., Hins, A. G., Carson, N. J.Jr, Denst, A. A., and Steele, T. A. (1967). *The development of a design and fabrication method for plutonium-bearing zero-power reactor fuel elements*. Lemont IL: Argonne National Laboratory. Tech. Rep. ANL-7313. doi:10.2172/4564458

Stolte, K. N., Favorite, J. A., McKenzie, G. E., Cutler, T. E., Hutchinson, J. D., Thompson, N. W., et al. (2022). Benchmark of the kilowatt reactor using stirling TechnologY (KRUSTY) component critical configurations. *Nucl. Technol.* 208, 625–643. doi:10.1080/00295450.2021.1945357

Taylor, T., Ballard, A., Fernandez, A., Cao, Y., Yang, W. S., Feng, B., et al. (2022). "Sensitivity to chlorine nuclear data in molten chloride fast reactors," in *41st annual conference of the Canadian nuclear society ant 46th annual CNS/CNA student conference* (Canadian Nuclear Society, virtual).

Thompson, N., Cutler, T., Grove, T., Amundson, K., Hayes, D., Favorite, J., et al. (2021a). "The CURIE experiment and nuclear data," in Transactions of the 2021 American nuclear society winter meeting. 125, 652–655.

Thompson, N., Sanchez, R., Goda, J., Amundson, K., Cutler, T., Grove, T., et al. (2021b). A new era of nuclear criticality experiments: The first 10 Years of Comet operations at NCERC. *Nucl. Sci. Eng.* 195, S17–S36. doi:10.1080/00295639.2021.1947105

Trellue, H. R., Long, A. M., Luther, E. P., Carver, D. T., and Mehta, V. K. (2021). Effects of hydrogen redistribution at high temperatures in yttrium hydride moderator material. *J. Minerals, Metals Mater. Soc.* 73, 3513–3518. doi:10.1007/s11837-021-04898-2

Trellue, H., Taylor, C., Luther, E., Cutler, T., Shivprasad, A., Jewell, J. K., et al. (2022). Advancements in yttrium hydride moderator development. *Nucl. Technol.* 0, 1–13. doi:10.1080/00295450.2022.2043088

Trkov, A., and Capote, R. (2022). Contribution to the validation of the INDEN evaluated data files. *Tech. Rep*.

van der Marck, S. C. (2006). Benchmarking ENDF/B-VII.0. *Nucl. Data SheetsEvaluated Nucl. Data File ENDF/B-VII.0* 107, 3061–3118. doi:10.1016/j.nds.2006.11.002

van der Marck, S. C. (2012). Benchmarking ENDF/B-VII.1, JENDL-4.0 and JEFF-3.1.1 with MCNP6. *Nucl. Data Sheets* 113, 2935–3005. doi:10.1016/j.nds.2012.11.003

Weldon, R. A.Jr, Cutler, T. E., Goda, J. M., Hutchinson, J. D., Myers, W. L., McKenzie, G. E., et al. (2021). Preliminary RAM-RODD results for the MUSiC subcritical configurations. *Trans. Am. Nucl. Soc.* 125, 585. doi:10.13182/T125-37007

Weldon, R., Cutler, T., Hutchinson, J., McKenzie, G., Misurek, L., and Sorensen, E. (2020). *Rossi alpha measurements - rapid organic (n,γ) discrimination detector (RAM-RODD) system capabilities*. Los Alamos, NM: Los Alamos National Laboratory. Tech. Rep. LA-UR-20-28902.

Werner, C., Armstrong, J., Brown, F., Bull, J., Casswell, L., Cox, L., et al. (2017). *MCNP users manual*. Los Alamos, NM: Los Alamos National Laboratory. Code Version 6.2. Tech. Rep. LA-UR-17-29981.

Zerkle, M., and Holmes, J. (2017). A thermal neutron scattering law for yttrium hydride. *EPJ Web Conf.* 146, 13005. doi:10.1051/epjconf/201714613005

Zerkle, M. L., Holmes, J. C., and Wormald, J. L. (2021). Re-evaluation of the tsl for yttrium hydride. *EPJ Web Conf.* 247, 09015. doi:10.1051/epjconf/202124709015

frontiers | Frontiers in Energy Research

TYPE Original Research
PUBLISHED 24 January 2023
DOI 10.3389/fenrg.2023.1088070

OPEN ACCESS

EDITED BY
Mark David DeHart,
Idaho National Laboratory (DOE),
United States

REVIEWED BY
Palash Kumar Bhowmik,
Idaho National Laboratory (DOE),
United States
Carlos Estrada,
Idaho National Laboratory (DOE),
United States

*CORRESPONDENCE
Izabela Gutowska,
gutowski@oregonstate.edu

SPECIALTY SECTION
This article was submitted to Nuclear Energy, a section of the journal Frontiers in Energy Research

RECEIVED 03 November 2022
ACCEPTED 11 January 2023
PUBLISHED 24 January 2023

CITATION
Gutowska I, Woods BG and Halsted J (2023), Developing PCC and DCC integral effects test experiments at the High Temperature Test Facility.
Front. Energy Res. 11:1088070.
doi: 10.3389/fenrg.2023.1088070

Developing PCC and DCC integral effects test experiments at the High Temperature Test Facility

Izabela Gutowska*, Brian G. Woods and Joshua Halsted

School of Nuclear Science and Engineering, Oregon State University, Corvallis, OR, United States

Among the Next-Generation Nuclear Plant (NGNP) designs, the High-Temperature Gas-Cooled Reactors (HTGRs) are very attractive, due to their inherent safety features, high power conversion efficiency, and potential of providing high-temperature process heat. To perform a thorough safety study and to license these types of reactors, sufficient information needs to be provided about the phenomena that occur during accident scenarios. While several experimental research efforts have been dedicated in the past to investigate accident scenarios, knowledge gaps still exist in the phenomena characteristic of pressurized and depressurized conduction cooldown (PCC/DCC) transients as well as for normal operation scenarios. This paper summarizes the Oregon State University High Temperature Test Facility (HTTF) test matrix, experimental campaign, and selected tests results. High Temperature Test Facility is a scaled Integral Test Facility (IET) that is capable of mimicking scaled dimensions and operational conditions of the Modular High-Temperature Gas Cooled Reactor (MHTGR). The goal of the High Temperature Test Facility is to provide experimental data on the DCC, PCC and normal operating scenarios of the reference Modular High-Temperature Gas Cooled Reactor design. The DCC, PCC, mixing, heat up and cooldown tests described in this paper were performed at prototypical Modular High-Temperature Gas Cooled Reactor temperatures, scaled initial pressure conditions (~200 kPa), and thermal power input of less than 70 kW. Presented test data show temperature distributions in the High Temperature Test Facility core, upper plenum, cross duct, or lower plenum. Based on these temperature profiles attempts to investigate stratified flow, natural convection flow, heat up, cooldown and mixing phenomena are made. Furthermore, this paper evaluates the performed test campaign in the light of the Very High Temperature Gas-cooled Reactor Phenomena Identification and Ranking Table (PIRT) and proposes experiments to complement the existing PCC/DCC testing database for the validation of the thermal-hydraulic codes.

KEYWORDS

HTGR, PCC, DCC, SET, gas-cooled reactor, thermal-hydraulic codes

1 Introduction

The Very High Temperature Gas-cooled Reactor (VHTR) is one of the most mature Generation IV reactor concepts under development today. Moreover, it offers several advantages to the well-established Generation III reactor designs. The high temperature of the gas coolant exiting the reactor core enables high thermal efficiency for electricity generation, and among other applications, can serve as process heat for hydrogen production.

Due to VHTRs significant departure from the light water reactors (LWR) technologies, such as the use of high-temperature helium primary coolant or graphite moderator, the applicability

of existing, nuclear reactors legacy modeling and simulation tools to VHTR modeling, simulation, and safety analyses needs to be carefully evaluated with appropriate experimental data.

The experimental data are fundamental for supporting the development and demonstrating the reliability of computer codes in simulating the behavior of a nuclear power plant (NPP) during postulated accident scenarios or normal operations: in general, this is a regulatory requirement.

It is indeed one of the greatest challenges of designing and licensing the VHTR to confirm that the intended VHTR analysis tools can be used confidently to make decisions on the design and licensing of the gas cooled reactors.

The overall VHTR methods development process is outlined in the Next-Generation Nuclear Plant Methods Research and Development Technical Program Plan (Schultz et al., 2008). The requirements associated with scenario identification, defining the phenomena identification and ranking tables (PIRT), and performing the necessary verification and validation studies must all be completed before performing the required analyses confidently and using analyses outcomes to inform licensing. Verification studies ensure that the computer code correctly performs the mathematical operations specified in the numerical model used while the validation efforts are used to certify that computed variables reflect the experimental data with acceptable accuracy (ASME V&V 20-2009, 2016).

To demonstrate whether or not the analysis software is capable of simulating the HTGR design and beyond design basis transients and plant integral behavior, several countries around the world are involved in experimental work that accounts for different core designs, and operational specifications. For instance, HTR-10 is a 10 MWth prototype for HTR-PM (High Temperature Pebble Bed Modular Nuclear Reactor) and was built at Tsinghua University in China. This design incorporates helium coolant with pressure around 3 MPa and inlet/outlet temperatures respectively: 250°C/700°C. The main features of this facility are the use of spherical fuel elements containing enriched uranium fuel with TRISO-coated particles. Several transient and normal operation tests were executed at this reactor to obtain data for neutronic and thermal hydraulic codes validation. The testing campaign scoped loss of forced cooling, loss of offsite power, power increase, steady state full operation, reactivity insertion and post-scram natural convection tests (Chen et al., 2014).

High Temperature Test Reactor (HTTR) was introduced by Japan Atomic Energy Agency (JAERI). Unlike competing pebble bed reactor concepts, this design uses prismatic block (hexagonal) fuel elements. HTTR also incorporates helium as a reactor coolant. Coolant pressure and temperatures are as follows: 4 MPa and 395°C/850°C–950°C. Thermal output reaches 30 MW (Maruyama et al., 1994). Based on the HTTR project, JAERI is developing the Gas Turbine High Temperature Reactor (GT-HTR) of thermal power up to 600 MWt per module. One of the experiments performed by JAERI was the investigation of DEGB (Double ended guillotine break) in the coaxial pipe connected vertically to the bottom of the reactor vessel. In this setup, the main phenomena leading to air ingress into the reactor core are molecular diffusion and subsequent natural circulation (lack of density gradients that cause stratified exchange flow) (Hishida et al., 1993).

Another tests facilities were built in South Africa under the PBMR project. High Temperature Test Unit (HTTU) was operated at high temperatures and low pressure (1,200°C and 100 kPa) with noth helium and nitrogen coolants in contrast to the High Pressure Test Unit (HPTU) which was run at lower temperatures (~35°C) and a high-pressure range (100 kPa-5 MPa) with nitrogen only. Experimental results were used to validate models of heat transfer and flow phenomena in pebble bed cores (Rousseau and van Staden, 2008).

Furthermore, up to July 2022, there were over 29 completed and ongoing United States Department of Energy Office of Nuclear Energy Nuclear Energy University Program (DOE NEUP) projects focusing on HTGR related research. These projects scopes, associated test facilities, test matrixes, and main findings are outlined in the INL Report: "High-Temperature GasCooled Reactor Research Survey and Overview: Preliminary Data Platform Construction for the Nuclear Energy University Program" (Qin et al., 2022). As a part of these efforts, Oregon State University (OSU), under the auspices of the Idaho National Laboratory (INL) and the United States Department of Energy (DOE), assembled an integral test facility, the High Temperature Test Facility (HTTF) that delivered experimental data to validate thermal-hydraulic system codes used for nuclear reactors safety analyses. These codes, such as RELAP5-3D, are expected to simulate the scope of phenomena identified in the PIRT prepared for the VHTR (Ball and Fisher, 2008). The HTTF uniquely complements the other gas-cooled reactors related research efforts in the United States since it is the only test facility that is capable of delivering integral effects test data (IET) at prototypic MHTGR operating temperatures. IET results allow for analyzing different sub-systems interactions during simulated scenarios (for instance primary, secondary, reactor cavity cooling or auxiliary systems) in contrast to the separate effects test (SET) facilities that scope operation of only a selected reactor component or subsystem.

The objective of this paper is to outline the testing campaign performed at the HTTF, provide a basic description of tests progression, discuss hardware limitations and evaluate the performed test matrix in the light of the VHTR PIRT. Finally, this work proposes experiments to complement the existing HTTF pressurized and depressurized conduction cooldown (PCC and DCC) testing database for the validation of the thermal-hydraulic codes.

The remainder of this document will present the HTTF technical description (Section 2), HTTF test matrix (Section 3), description of the performed tests (Sections 3.1–3.6), experimental data uncertainty, and limitations (Section 3.7). Conclusion and suggestions for future work are outlined in Section 4.

2 High Temperature Test Facility (HTTF)

The OSU HTTF is an integral test facility configured to test a variety of VHTR postulated depressurized (DCC) and pressurized conduction cooldown (PCC) accidents as well as normal system operation. The facility (Figure 1B) is a reduced scale model (1:4 in height and diameter) of the General Atomics Modular High Temperature Reactor (MHTGR) design and is designed to provide data at temperatures similar to those expected in a loss of forced convection accident. HTTF also features 1: 8 pressure scale and can operate at 0.8 MPa. The nominal working fluid is helium and accidents are simulated with a break gas utilization of nitrogen. During normal operation, helium is driven down through the core coolant channels by forced convection (Figure 1A). Figure 1B shows the main facility components: Reactor Cavity Storage Tank (RCST), cross ducts, break valves and the reactor pressure vessel. Not shown in this figure is the Reactor Cavity Cooling System (RCCS) that is also

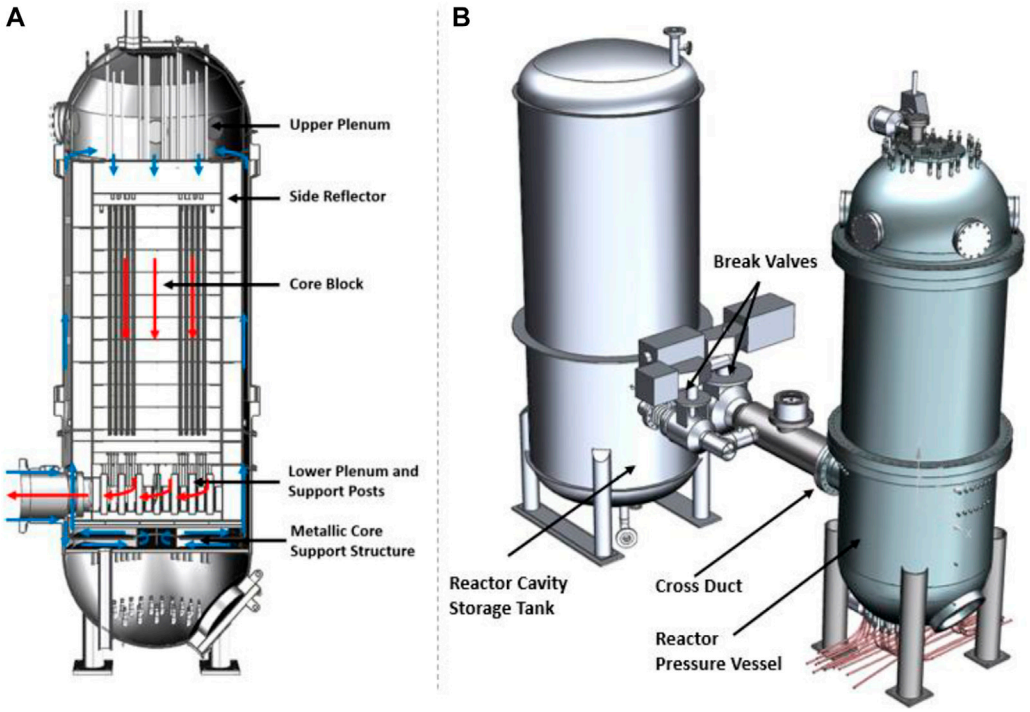

FIGURE 1
(A) Section view of the HTTF RPV showing the helium flow path; **(B)** HTTF system CAD model.

present at the HTTF. It consists of forced water-cooled panels that surround the reactor vessel. The HTTF RCCS is not a scaled version of an actual HTGR design but rather is used to specify the boundary conditions to control radiation heat transfer from the vessel wall.

Graphite prismatic block structure in the MHTGR is simulated by ceramic blocks in the test facility to capture prototypical core temperature profiles. The HTTF reactor core is built of 10 hexagonal core blocks that are made of a cast ceramic, Greencast 94-F (96.5% Alumina). The reactor core is surrounded by several reflectors on each side (two upper reflectors, three bottom reflectors, and side reflectors). The side reflectors are made of a cast ceramic, ShotTech SiC 80 (78% Silicon Carbide, 10.5% Silica, 8.3% Alumina) while the top and bottom reflectors are also made of Greencast 94-F. For the MHTGR the permanent side reflectors are made of a different grade of graphite (Stackpole 2020) than the rest of the reflectors and core (H-451 Graphite). These have very different thermal conductivities and thus needed a different ceramic material to scale appropriately. There are also three separate structures designed to model the core exit chamber: lower plenum roof, lower plenum (the chamber that houses 163 support posts), and lower plenum floor. The HTTF core block cross section is shown in Figure 2A. 516 coolant channels and 210 heaters channels are shown in the core block cross section view, indicated by five different colors. Coolant flow channels are shown as blue, green or yellow (depending on the channel diameter) while the voids where the heater rods are placed are shown in red (Figure 2A). Core bypass flow is restricted by the graphite plate placed on the top of upper reflector and instead is accounted for by 6 inner and 36 outer bypass core channels. Core sections denoted as primary, secondary, and tertiary are the only instrumented regions within a single core block. HTTF inlet plenum shroud (Figure 2B) is assembled with 39 guide tubes that hold thermocouples and gas capacitance sensors in place. A total of 42 thermocouples and 6 gas capacitance sensors are placed in the upper head region (Woods, 2018).

The facility does not use nuclear fuel to produce power, it is equipped with a network of electrically heated graphite rods (graphite grade G-348) that produce approximately 2.2 MWth. There are 210 heater rods arranged in 10 heater banks, with 3 heater legs per heater bank. Each heater leg consists of 7 heater rods. During a heat-up test in the fall of 2017, several spots within the ceramic core melted. This was because arcing occurred at the interface between graphite rodlets, spiking the local temperatures that exceeded the ceramic melting point. This arcing occurred because the blocks' thermal expansion at elevated temperatures caused the blocks to shift in position, affecting the contact points between graphite rodlets and misaligning the heating channels. In response to this, several new core blocks were installed, all thermocouples had to be reinstalled, and only four heater banks (103, 104, 107, and 108) were utilized for the tests. There was also a change in the type of heater design to preserve a relatively uniform surface contact area. The consequences of having to implement new core blocks and heaters, as well as reinstall instrumentation, were significant. OSU and INL agreed to only have four heater banks installed, limiting the number of shakedown and possible matrix tests to be performed. Many of the matrix tests planned were supposed to be low power (below 350 kW), but often, the tests typically had power outputs below 150 kW. Additionally, having only four banks resulted in localized (and asymmetric) heating within the core, requiring OSU test engineers to carefully monitor heat up rates during test preparation. In general, limiting the decay power impacted efforts to investigate the effects of core power on

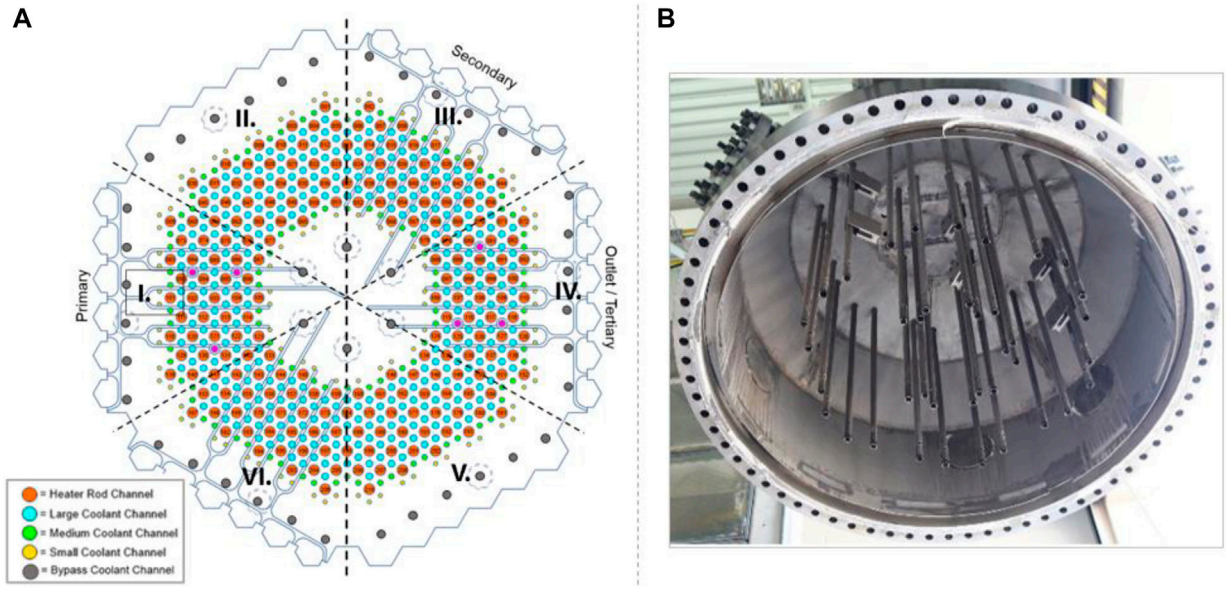

FIGURE 2
(A) Arrangement of coolant channels, bypass channels, and heater rods channels in the HTTF core block; **(B)** HTTF upper head with instrumented guide tubes.

system behavior. Non-etheless, tests were completed for various loss of forced cooling (LOFC) events, as well as normal operations.

3 HTTF testing matrix and tests description

In the VHTR PIRT, the Nuclear Regulatory Commission (NRC) identified three main phenomena of interest concerning the safety aspects of the HTGR: primary system cooldown phenomena, core power and temperature distributions, and postulated air-ingress accidents (Ball and Fisher, 2008).

Of particular note, the designer of the HTGR must provide validation of key passive safety phenomena to prove that the design can withstand postulated accidents *via* passive heat removal. Three types of postulated accidents that the HTTF was designed to examine are PCC and DCC, and DCC with air ingress. The purpose of the testing campaign was to complete integral-level thermal-fluid tests at the HTTF to investigate the phenomenological behavior of conduction cooldown events at a system level.

Table 1 lists tests performed at the HTTF. Tests 1 through 6 focused on characterizing the facility's operational parameters. Subsequent tests delivered data on the DCC with varying gas temperatures and power levels. PCC, gas mixing, heat up and cooldown tests were also executed. Detailed test acceptance reports providing test data, initial conditions, and limitations are available at https://www.osti.gov/.

3.1 Characterization tests

The objective of the characterization testing was to establish a well-defined operational envelope of the facility and to demonstrate the ability of the HTTF to safely and reliably perform its designed matrix tests. The following list outlines the purpose of each of the executed characterization tests.

- PG-01 Pre-Operation Test (OSU-HTTF-TEST-001)—developed to verify the control of critical components at the Operator Control Center (OCC).
- PG-02 Circulator and System Form Loss Characterization Test (OSU-HTTF-TEST-002)—developed to measure the forced flow differential pressure across components and regions of interest within the primary system over the expected primary gas flow rate range.
- PG-06 Facility Gas Conditioning (OSU-HTTF-TEST-006)—developed to perform all the necessary steps to condition the gas in the test facility for the initial conditions of other design tests.
- PG-07A Primary Loop and RCST Volume Determination (OSU-HTTF-TEST-007)—executed to measure the gas volume needed to bring the system to full pressure.
- PG-08 Break Valve Characterization (OSU-HTTF-TEST-008)—developed to simulate four large break valves blowdown effects.
- PG-09 Steam Generator Secondary Side Volume Determination (OSU-HTTF-TEST-009)—executed to measure the volume of the steam generator vessel.

3.2 DCC tests

The DCC typically involves a break in the pressure boundary of the reactor system resulting in a depressurization. The transient can be divided into three distinct stages: 1) depressurization, 2) gas-ingress (if present), and 3) natural circulation. The gas ingress stage can be further divided into gas-ingress by exchange flow, gas-ingress by molecular diffusion, and gas-ingress by inflow due to coolant

TABLE 1 HTTF- list of performed tests.

Test	Start date	Procedural guide (PG)	Test title	Phenomena
1	01/27/2017	PG-01	Pre-Operation	Characterization
2	02/20/2017	PG-02	Circulator and System Form Loss Characterization	Characterization
3	5/10/2017	PG-06	Facility Gas Conditioning	Characterization
4	4/17/2017	PG-07A	Primary Loop and RCST Volume Determination	Characterization
5	04/20/2017	PG-08	Break Valve Characterization	Characterization
6	08/09/2017	PG-09	Steam Generator Secondary Side Volume Determination	Characterization
7	06/06/2017	PG-21	Lock Exchange Flow and Diffusion Test with 500°C average Gas Temp	DCC
8	03/30/2017	PG-22	Lock Exchange Flow and Diffusion Test with 125°C average Gas Temp	DCC
9	4/4/2017	PG-23	Lock Exchange Flow and Diffusion Test with 375°C average Gas Temp	DCC
10	5/11/2017	PG-24	Lock Exchange Flow and Diffusion Test with 250°C average Gas Temp	DCC
11	5/30/2019	PG-26	Low Power (<350 kW) Double Ended Inlet-Outlet Crossover Duct Break, 2 Heaters	DCC
12	4/23/2019	PG-27	Low Power (<350 kW) Complete Loss of Flow, 2 Heaters	PCC
13	7/24/2019	PG-28	Low Power (<350 kW) Lower Plenum Mixing	Mixing
14	7/24/2019	PG-29	Low Power (<350 kW) Double Ended Inlet-Outlet Crossover Duct Break, Hybrid Heater	DCC
15	8/29/2019	PG-30	Low Power (<350 kW) Lower Plenum Mixing, Constant Temperature	Mixing
16	8/30/2019	PG-31	Low Power (<350 kW) Pressure Vessel Bottom Break with Restored Forced Convection Cooling	DCC
17	8/28/2019	PG-32	Low Power (<350 kW) Asymmetric Core Heatup	Heat up
18	8/31/2019	PG-33	Zero Power Long Term Cooldown	Cooldown
19	7/31/2019	PG-34	Low Power (<350 kW) Asymmetric Core Heatup Full Hybrid Heater	Heat up
20	6/3/2019	PG-35	Low Power (<350 kW) Zero Power Crossover Duct Exchange Flow and Diffusion	DCC

contraction during the subsequent cooldown phase. The extent to which the prototypical plant experiences, if at all, gas-ingress by exchange flow or diffusion depends on the location and the size of the break. While the HTTF is capable of performing a variety of transient and normal operation scenarios that happen in the VHTR, it was primarily designed and scaled to mimic the DCC event. Therefore, the majority of experiments performed at the facility aimed at varying core power levels or average temperature differences between the upper plenum floor average and lower plenum inlet jet, which can impact the progression and severity of the DCC stages.

Tests PG-21, 22, 23, and 24 focused on testing the progression of the lock exchange flow between the RPV and RCST, and diffusion air ingress stages with varying average helium temperatures (500, 125, 375, and 250°C). These test results and the impact of varying initial temperature conditions on the air ingress progression were assessed by Glass (2017).

During the execution of the heated DCC tests performed in 2017, the performance of the graphite heaters was closely monitored and observed to degrade with each test until heat could be no longer produced. This was caused by several factors, including core blocks thermal expansion and water accumulation in the RPV ceramic structures. Thermal expansion caused lateral movement of core blocks that impacted graphite rodlets' alignment and contact. When the contact between rodlets was imperfect or lost, then either arcing or electric circuit failure occurred. Subsequently, large temperatures associated with arcing caused localized graphite sublimation, melting of alumina and blocks cracking. Moreover, the C-Type thermocouples located in the inner core region were degraded due to exposition to temperatures that exceeded the instrument's maximum temperature (2,315°C). Before the testing campaign was resumed, the graphite rods were redesigned and the facility underwent major maintenance. The original annular graphite rodlets were replaced with bone-shaped ones (with ball and socket endings to facilitate rodlets contact in case of lateral blocks translation caused by thermal expansion). Only four new heater legs (out of 10 that were originally installed) were located in the core. Although the maximum power output was reduced to 880 kW, it allowed for benchmarking the new heating system with a reduced number of legs. In addition, cracked core blocks were replaced, C-Type thermocouples were replaced with R-Type thermocouples. New operation and maintenance procedures to reduce the heat up rate and increase the coolant flow rate during each test were also written. Water accumulation in the ceramic structures is an inherent property of the core and reflectors' structural material and its removal became a permanent part of the facility conditioning before the matrix testing execution.

In 2019, after the facility was reassembled and conditioned for testing, four additional DCC tests (PG-26, PG-29, PG-31, and PG-35) were executed at varying core power distributions or break locations. To provide an example of the DCC test progression, PG-29 will be described in more detail. This test modeled a break in the HTTF inlet/outlet ducts. It was initiated when the average core temperature was between 550 and 590°C, with the peak temperature being between 780 and 820°C. The pressure was kept at a steady-state (170 kPa), and the outlet temperature on the secondary side was kept consistent at around 118°C. The transient would be initiated by stopping the gas circulator,

TABLE 2 PG-29 test initial conditions.

Property/Component	Desired initial condition	Test initial condition
Primary loop pressure	~200 kPa Helium	212.2 kPa
RCCS pressure	~200 kPa Nitrogen	211.3 kPa
Cooling water system	Filled with water at ambient pressure	35.1°C, 101.3 kPa
Steam Generator	Between 60% and 80%	74.7%
RCCS tank	Filled with water at ambient pressure	35.1°C, 101.3 kPa

shutting the steam generator isolation valve, opening the break valves located in the concentric duct, and following the decay heat power curve across four heater banks during the natural convection phase. This was revised during the test, to only incorporate one hybrid heater providing constant power and was initiated with conditions listed in Table 2. The hybrid heater layout is presented in Figure 9A. The test began on 7/24/2019 and was completed on 7/26/2019.

The break valves were opened at just over 80 h into the test, about a minute after the circulator was shut off, and the diffusion phase started approximately a minute later. Break valves characteristics are listed in Table 3. The break diameter was scaled as 1:4 (referring to the reference MHTGR design). This ratio is in line with the vessel diameter scaling to reduce test facility to MHTGR similarity group numbers distortions. The break location (shown in Figure 1A) near the RCCS enables counter-current flow development and investigation of the RPV gas ingress *via* lock-exchange flow.

The power output during PG-29 was supposed to be kept at a maximum of 48 kW for approximately 80 min to ensure that the ceramic did not exceed the heat-up limit, as well as to preserve the scaled decay heat curve. After this period, the transient natural circulation phase started. Once the DCC was initiated, the steam generator was allowed to cool down. After the initial dumping of steam, the pressure was kept steady at about 120 kPa, and the water inventory was kept at just above 70%. The heaters failed approximately 89 h into the test, prohibiting the operators from following the decay curve. This implies that the core would have lost heat at a faster rate than what was anticipated to happen. The test ended when the motor speed drive for the RCCS pump was set to zero, at approximately 14 h after the start of the natural circulation phase.

After break valves were opened, the hot helium flowed into the RCST as the cold nitrogen flowed toward the PPV. The gases flowed in a counter-current fashion, where the top half of the hot duct contained hot helium flowed in one direction and cold nitrogen propagated towards RPV occupying the bottom half of the duct. The stratified temperature trend indicating the counter-current flow can be observed in Figure 3, where after hour 80 the measurements of TF-3202 and TF-3203 are shown to increase. These two thermocouples are in the middle and upper regions of the hot (outlet) duct, downstream of the vessel (at the entrance to the RCST). In contrast, TF-3201 (placed in the lower section of the hot leg) shows the lowest temperature and relatively steady behavior. It should be noticed that when break valves were opened, the RCST temperatures dropped uniformly to approximately 20°C (that is also observed by looking at the TF-3201 and TF-3202 trends in Figure 3). It is anticipated that this was caused by a pressure difference between the primary loop and RCST. Although the procedure aimed at performing the test at equalized pressure of ~200 kPa, a pressure difference of several kPa could have existed between the PPV and RCST due to the vulnerability of the system to helium leaks.

If natural circulation was to occur, the expectation is that the thermocouples at the top of the core would register a temperature that is higher than at the bottom of the core. Figure 4 shows the inlet (within core block 9) and outlet core coolant temperatures (thermocouples located in the inlet to the lower plenum). Based on these temperatures, it appears that natural circulation might be occurring, since the thermocouples at the inlet become substantially higher than that observed within the lower plenum.

One additional indication that fluid is flowing upwards through the core is to look at the fluid thermocouple readings in the upper plenum (Figure 5). If natural convection is occurring, and hot gas is flowing upward through the core, gas temperatures in the upper plenum should and are increasing throughout the transient. The temperatures in the uppermost part of the upper plenum are observed to increase at a faster rate, which may imply that the radiative and convective heat transfer from the RPV to the RCCS panels is not occurring at a rate sufficient enough to maintain steady-state conditions. The upper plenum gas temperature profile presents a small drop in temperature when valves are opened, leveling out after approximately 2 hours and rising from hour 82 onward. Gas appears to be well mixed as there is little to no temperature difference between the upper and lower regions.

3.3 PCC tests

During the PCC event, forced circulation is lost and the pressure boundary remains intact, preventing any significant system depressurization and outside gas ingress into the primary system. Following the loss of pumping power, it is expected that flow reversal

TABLE 3 HTTF cross-ducts break valve characteristics.

Valve location	Model	Size (cm)	Stroke time (s)	Flow area (cm^2)	Loss coefficient (Cv)
Cold duct	Mogas Ball	20.32	4	313.9	8,985
Hot Duct	Mogas Ball	30.48	14.5	699.4	20,857

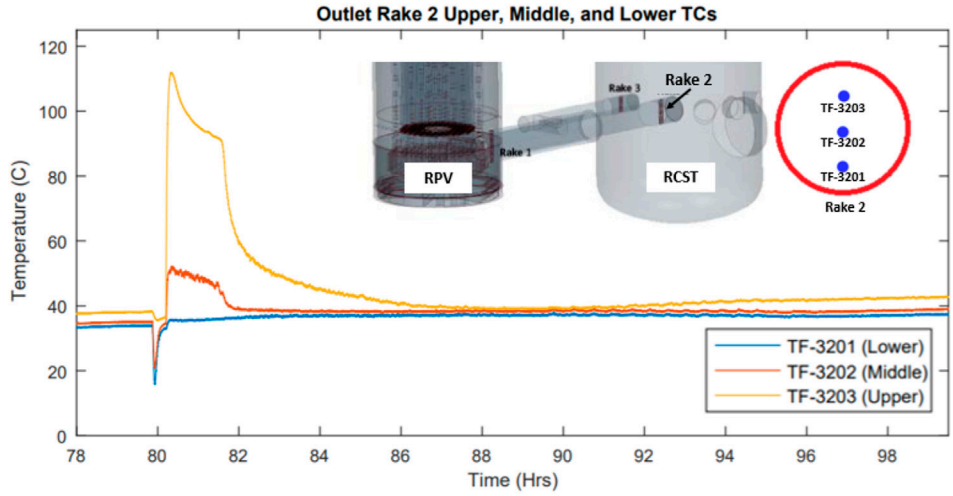

FIGURE 3
Hot leg's Rake 2 thermocouples readings starting in the 78th hour of the PG-29 test (Woods, 2019).

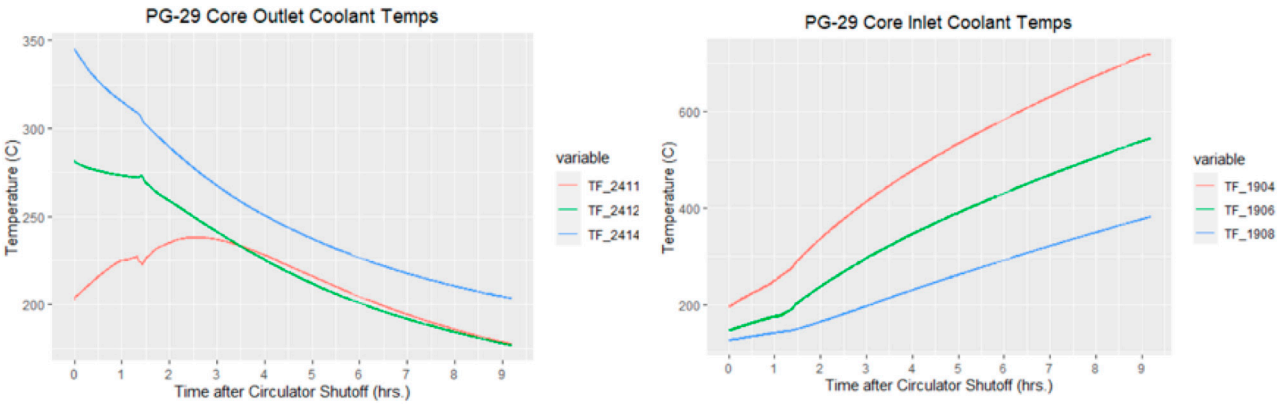

FIGURE 4
PG-29 core outlet (left) and inlet (right) coolant temperatures.

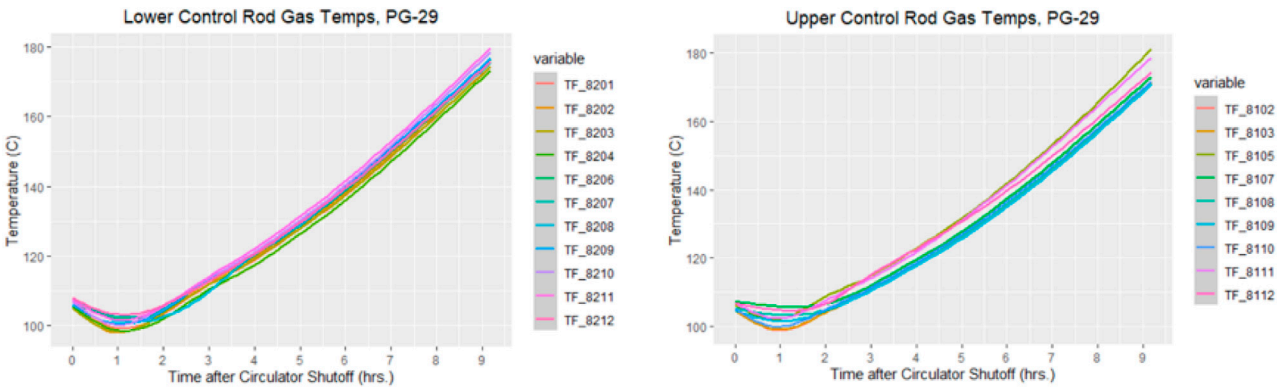

FIGURE 5
PG-29 upper plenum, lower (left) and upper (right) control rod gas temperatures.

TABLE 4 PG-27 test initial conditions.

Property/Component	Desired initial condition	Test initial condition
Primary loop pressure	>130 kPa helium	206.72 kPa
RCCS pressure	>101 kPa helium	195.87 kPa
Cooling water system	Filled with water at ambient pressure	20.9°C, 101.3 kPa
Steam Generator	Between 60% and 80%	76%
RCCS tank	Filled with water at ambient pressure	20.9°C, 101.3 kPa

will occur as the original coolant inertia is overcome by buoyant and frictional losses. This is similar to all of the DCC events. This phenomenon is expected since coolant travels downwards through the core channels during normal operations, and after some time, frictional and buoyant forces overcome the coolant's momentum to reverse the flow pattern. The helium coolant expands as it travels upward through the core channels, cools as it interacts with the upper plenum structural materials, then flows downwards through the upcomer. Determining the onset of phenomena and how coolant velocity behavior will help determine its effect on the core temperature profile, as well as the peak core temperature.

Once flow reversal occurs, it is expected that intracore natural circulation would occur since the steam generator's thermal center is placed below the core thermal center. This would generate a thermosyphoning effect where some coolant channels experience coolant flowing upwards, and somewhere it flows down. Rather than striking the lower plenum, the hot jets should strike the upper plenum structures, and these structures should be cooled predominantly through radiative heat transfer. In the HTTF, however, the SG thermal center is placed above the core thermal center, and there should be natural convection observed throughout the loop.

Natural circulation in many parallel vertical channels with different heat inputs is quite complicated because the flow rate and direction depend on the time history of the heat input of each channel. It is desirable to know at what point the fluid buoyancy becomes significant (onset of mixed convection) and predict the threshold of flow instabilities (Gutowska and Woods Brian, 2019). It is also desirable to determine what the temperature behavior is like in the core channels and upper plenum to witness this thermosyphoning event. This is done *via* the PG-27 test, which does not exactly replicate the same chronological events that would occur within the VHTR or GA-MHTGR. For one, the circulator in the GA-MHTGR has a coast-down period; the HTTF would immediately cease forced convection, resulting in almost near-instantaneous flow stagnation. To establish the desirable initial conditions for the transient, the cold valve on the secondary side of the steam generator was closed during the test to limit the loop natural convection flow to the intracore natural convection flow. The PG-27 test initial conditions are listed in Table 4. Another hybrid heater configuration (Figure 6A) with two heater banks (102 and 104) was operated during the test with a power output of approximately 66 kW for each bank.

During the PCC test, the coolant flowing through the HTTF core successfully stagnated. It is apparent, however, that none of the coolant channels investigated (3 channels located at different core radial locations shown in Figure 6B, analyzed for all three instrumented sectors) explicitly showed a thermosyphoning effect. A sample of this observation is given in Figure 7 : the vast majority of thermocouples had relatively hot

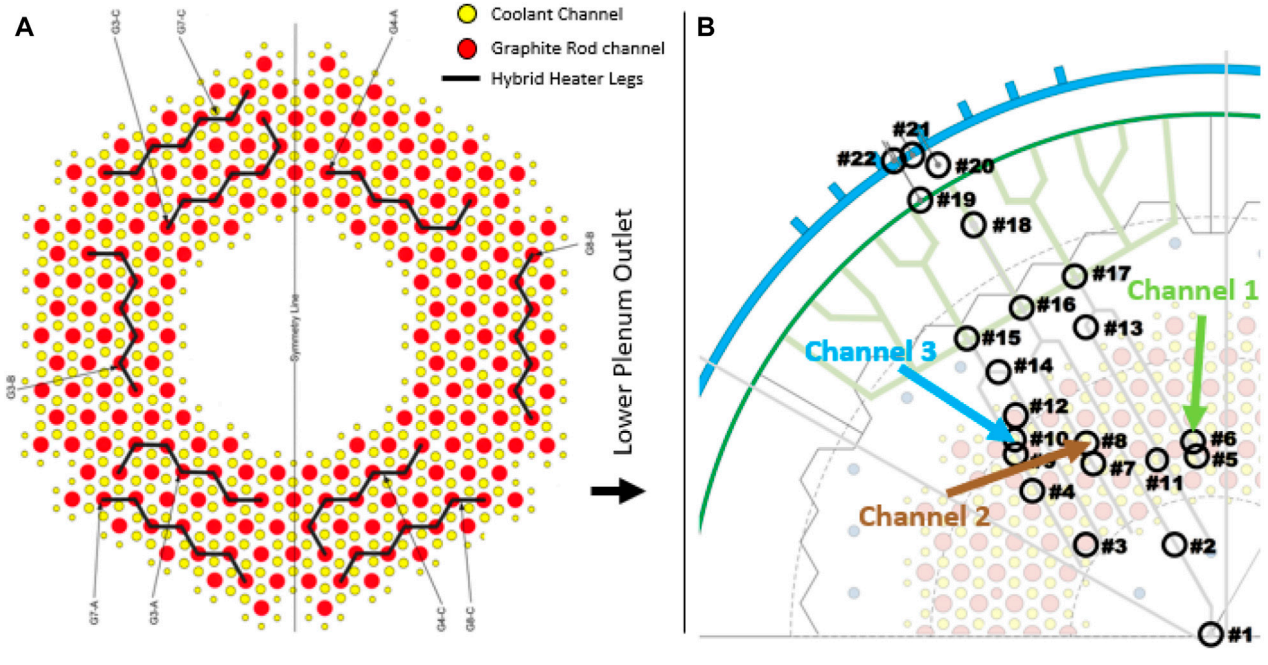

FIGURE 6
(A) PG-27 hybrid heater configuration; **(B)** Selected instrumented coolant channels for PG-27 experimental data assessment.

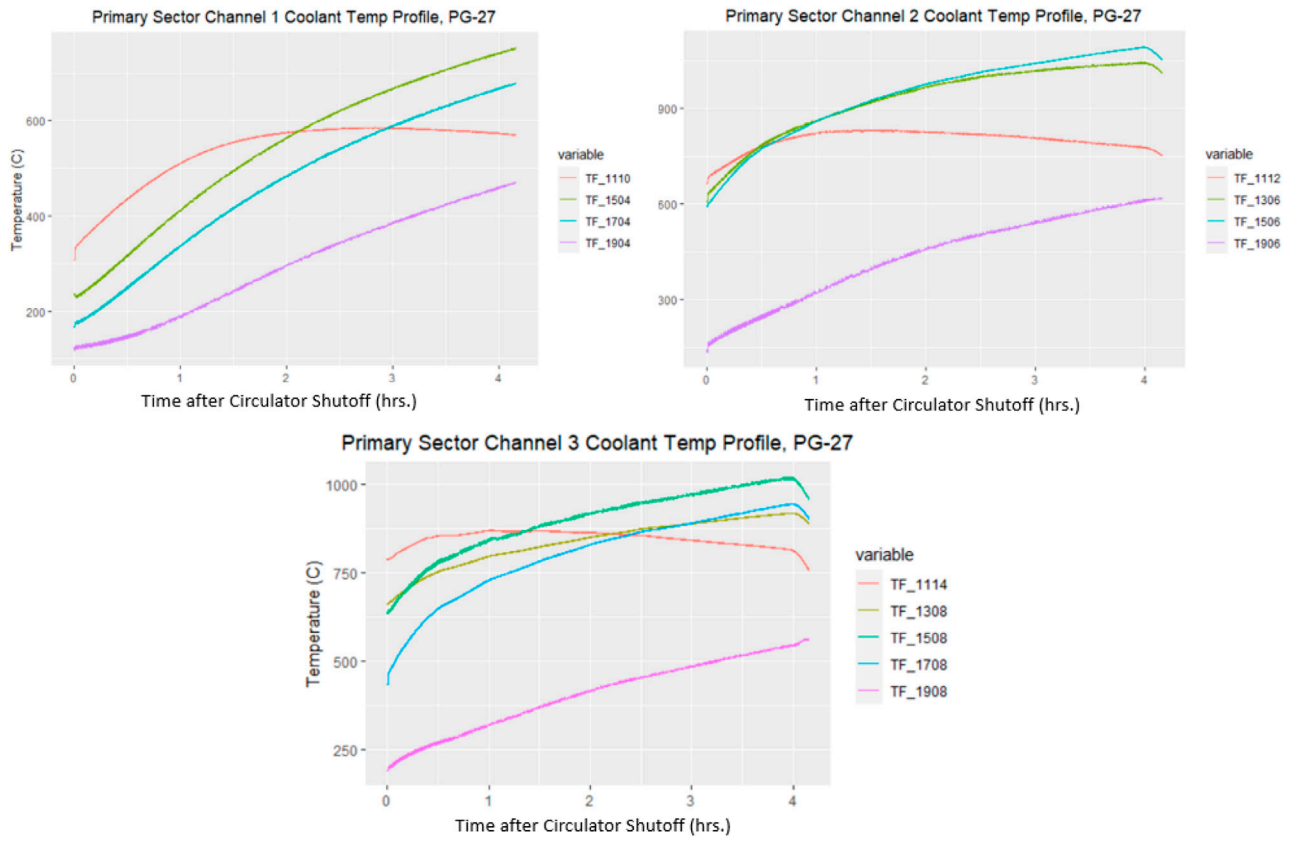

FIGURE 7
PG-27 Core primary sector, selected coolant channels temperature profiles (channels 1, 2, 3 representing inner, middle and outer core radial locations respectively).

temperatures at the channel midlevel (TF-1508, TF-1708), with relatively cooler temperatures at the top of the core (TF-1908). Some channels had the hottest temperatures towards the bottom of the core (indicating downflow), whereas no channels sampled had their hottest temperatures occur at the top of the core. In contrast, velocity data obtained from the pre-test RELAP5-3D simulation of the HTTF PCC test (simulation performed with different heat input) show that middle and outer core rings flow reverses almost immediately after transient initiation, followed closely by that in the inner core ring (Bayless, 2018a; Bayless, 2018b).

The upper plenum temperature profile resembles a similar trend to the PG-29 test: hot helium plumes enter the upper plenum and heat its structures. Based on Figure 8, it is shown that the two thermocouples registering temperatures for the upper plenum shroud indicate a substantial decrease, then increase, in temperatures. This provides some evidence that a thermosyphoning effect is taking place, although these hot jets do not align with or come from the coolant channels that were instrumented with fluid thermocouples. The minimum in both trendlines occurs at around the same time, and may formally indicate when stagnation ends as well as when buoyancy forces dominate. The initial decrease likely indicates a time when there was no coolant flow.

3.4 Mixing tests

The Phenomena Identification and Ranking Table (PIRT) report identifies a possible fragility of the HTGR due to hot streaking (temperature fluctuations due to imperfect mixing between hot and cold jets exiting from the core and bottom reflectors) (Chen et al., 2014). Temperature fluctuations on the structures downstream (on the lower plenum, then propagating to the hot gas duct walls and even to the steam generator or turbine blades) may induce prolonged exposure to thermal stresses (Landfried et al., 2019).

Two tests were conducted at the HTTF to provide data for the lower plenum mixing simulations validation: PG-28 and PG-30. The

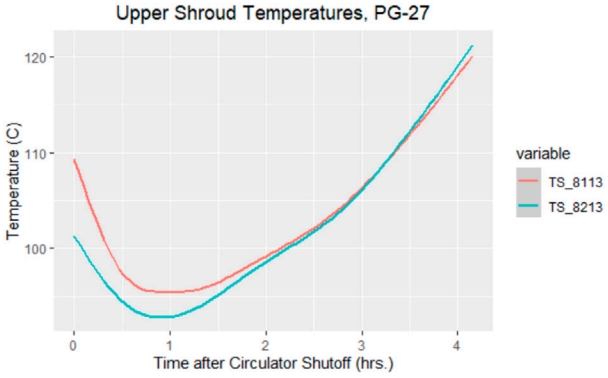

FIGURE 8
Upper plenum shroud temperatures during PG-27.

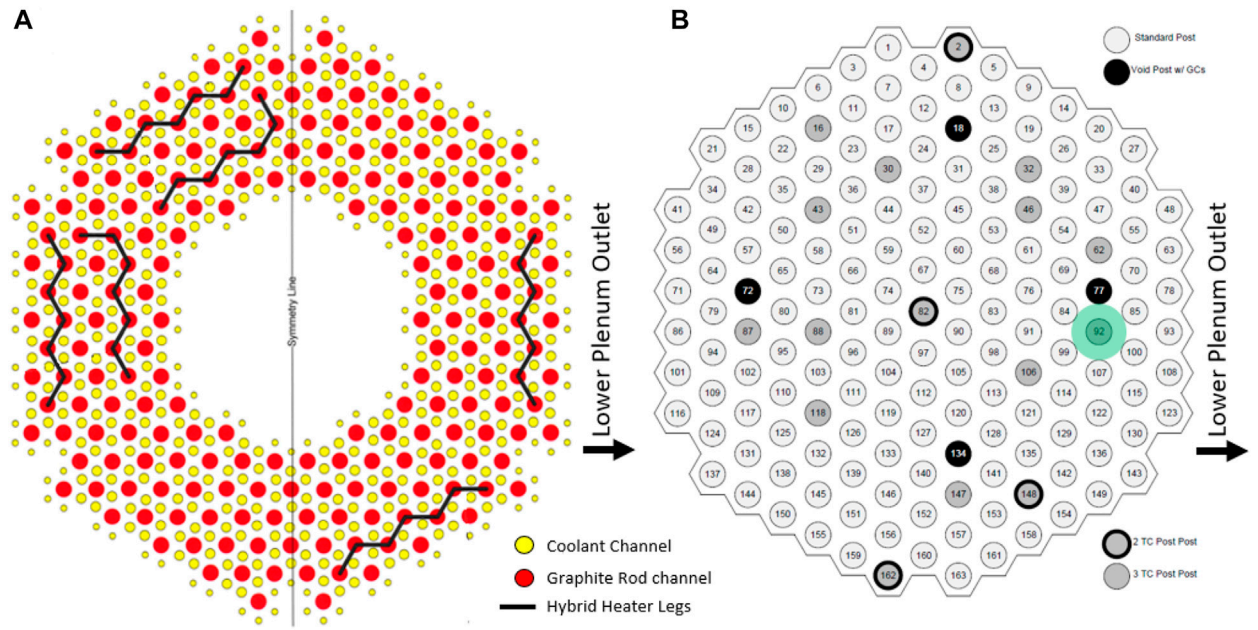

FIGURE 9
(A) Heater legs that were operated during the PG-28, PG-29 and PG-30 tests. **(B)** Lower plenum top view, with support and instrumented posts location (highlighted in green is the post 92 placement with thermocouples readings used to generate temperature plots in Figure 10).

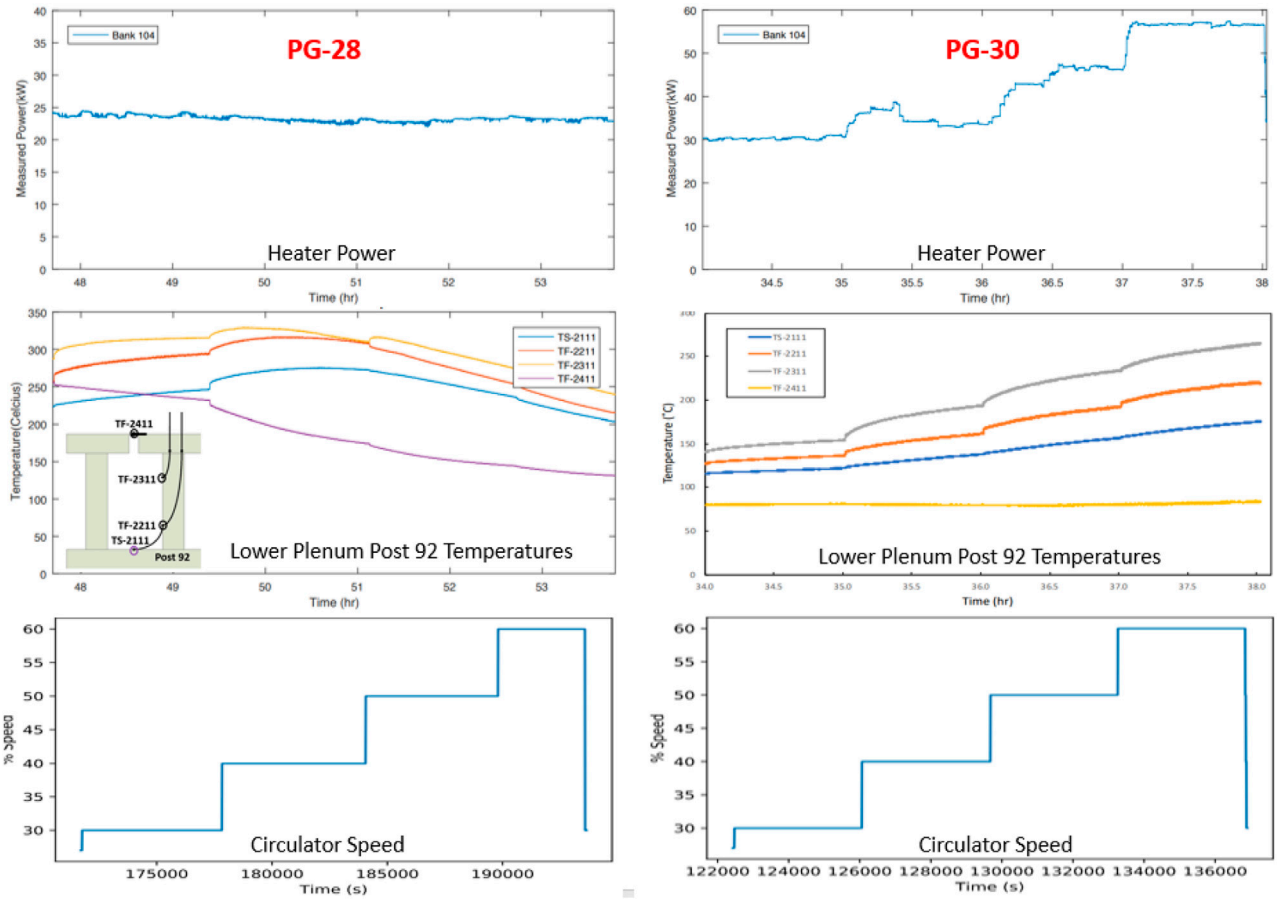

FIGURE 10
Power, lower plenum post #92 temperatures, and circulator speed distributions over the duration of the test PG-28 (left) and PG-30 (right).

purpose of these tests was to investigate the impact of changes in the system mass flow rate and core power on the lower plenum mixing and thermal profiles. The main difference between these two mixing tests was that PG-28 was executed at a constant power level of ~25 kW while PG-30 power input was gradually increased from 30 to 58 kW. The heaters distribution used during both tests is shown in Figure 9A. The top view of the lower plenum structure presenting lower plenum support posts and instrumented posts placement is given in Figure 9B. The following figure (Figure 10) presents power, lower plenum post #92 temperatures, and circulator speed distributions over both tests duration. In response to each gas flow rate change, there was a sudden temperature change (drop in the PG-28 test and increase in the PG-30 test, as expected). Validation analysis for the PG-28 test using RELAP5-3D and STAR-CCM + codes was performed by Halsted (2022) (Halsted, 2022).

3.5 Heat up tests

The heat up tests allow for addressing the phenomena of core flow distribution changes due to temperature gradients identified in the PIRT tables (Normal Operation, 20%–100% power) as a phenomenon characterized by medium knowledge level and of medium importance to plant safety. The purpose of the heat up tests (PG-32 and PG-34) was to examine the facility's thermal profile and the rate of change in the core temperatures under asymmetric heating conditions. The input power during PG-32 started at approximately 10 kW and was increased steadily during testing to a peak final power of 30 kW with a constant circulator speed (25% of the rated speed). While the power input was kept at a similar level during the PG-34 test, the circulator speed was set to 30% of the rated speed, therefore one can observe a slower heat up rate compared to PG-32 (Figure 11).

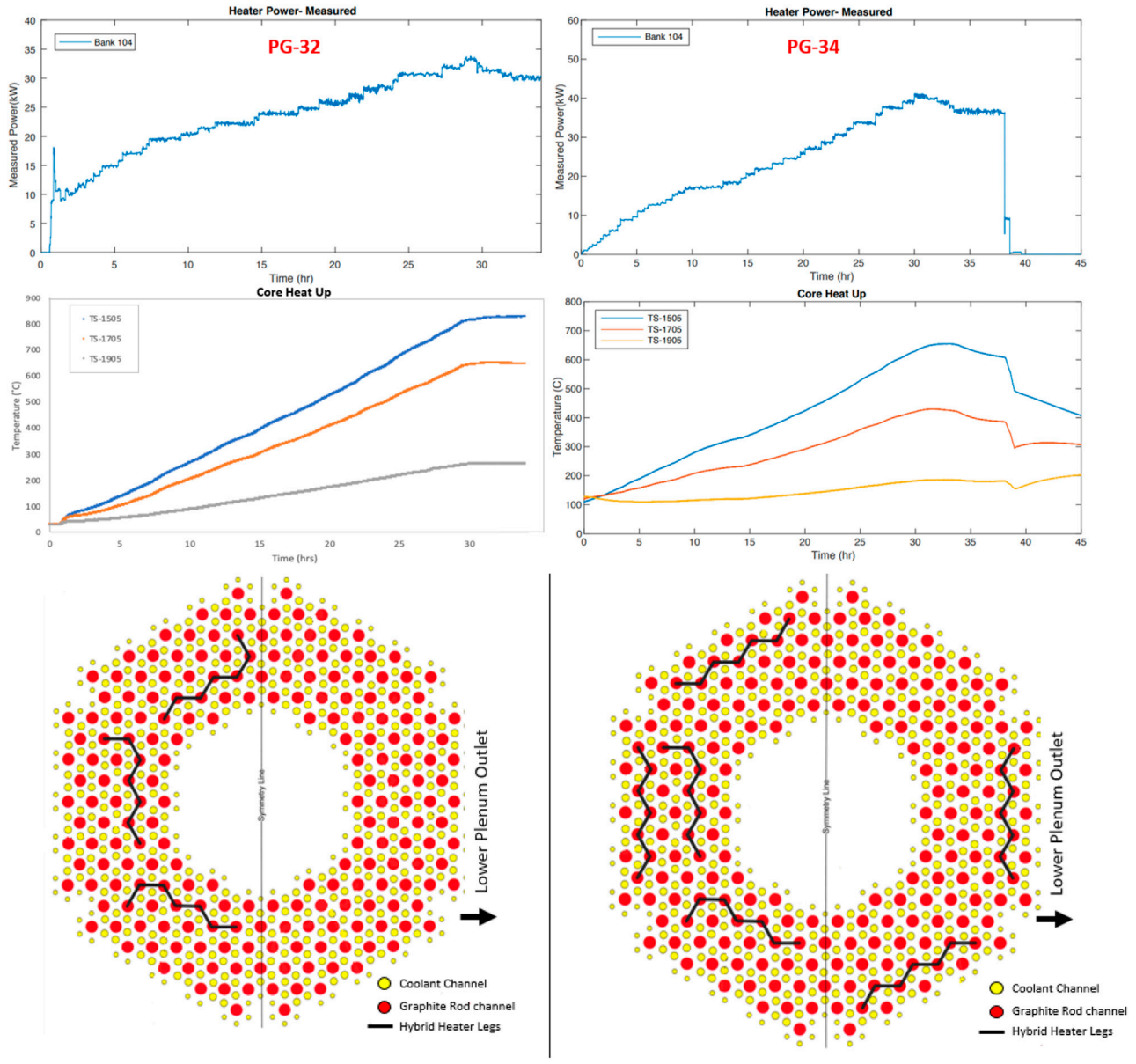

FIGURE 11
Heater Power, core heat up rate (temperature distribution) and operational heaters distribution during tests PG-32 (left) and PG-34 (right).

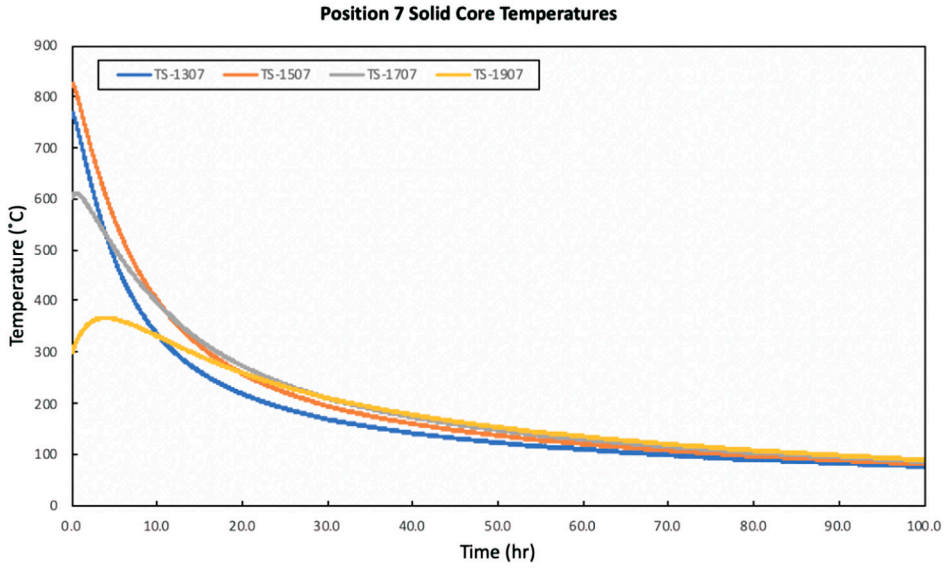

FIGURE 12
Core ceramic temperatures during PG-33 test.

Both heat up tests were executed without running the RCCS. Therefore useful data can be extracted from analyzing the facility heat up during the PG-28 test conditioning (when the RCCS pump motor speed was set to 30% range) and comparing with PG-32 and PG-34 (outside of the scope of this paper).

3.6 Cooldown tests

The purpose of the PG-33 test was to examine the long-term passive cooldown of the HTTF through conduction and convection within the vessel and radiation and convection outside of the vessel. The test was initiated after completion of the PG-31 and continued for 5 days as the core and system cooled down. Figure 12 shows the core ceramic temperature at 4 different axial locations. Throughout this test, exponential decrease in the core ceramic temperatures is observed.

3.7 Experimental data uncertainty and limitations

The selected instruments channels uncertainties (that includes both the systematic and random uncertainties) are shown in Table 5. Data were collected at 1.0 Hz sampling rate.

For the tests examined in this paper, none of the HTTF gas concentration sensors worked. This is problematic since understanding how the gas concentrations change during a DCC event is imperative for understanding how the lock exchange and diffusion mechanisms work during the gas-ingress phase. It is also challenging to find instruments that would operate at HTTF extreme temperature conditions and do not significantly affect the flow field distribution. Moreover, central to correctly quantifying the energy balance and core conditions before any transient within the HTTF is knowing the mass flow rate in the primary loop. The ability to quantify the mass flow rate directly permits the investigator to deduce important parameters such as frictional losses across the core and in plenums, where form factors are difficult to quantify. Although these data were also missing from the HTTF results, the helium mass flow rate during forced flow conditions can be indirectly derived from the circulator pump curve and system energy balance. There were multiple times through the HTTF tests where helium leaked out of the primary loop and additional helium had to be added. Most of these leaks occurred at valve fittings, flanges, and instrumentation bulkheads. Preventing helium leaks is not an easy task because of its small molecule size, but can be reduced if tests are conducted to find where leaks occur, and an adhesive is placed to seal the leak. These preventive actions were taken at the facility to the maximum possible extent. Another alternative is to find a surrogate gas that has a larger molecule size. Implementing this strategy requires a scaling analysis to track the distortions that may occur from using a different gas. The gas leakage along with administrative constraints prevented addressing

TABLE 5 HTTF Instruments uncertainty.

Instrument	Units	Uncertainty
Thermocouple Type K	°C	0°C–275°C: 4.284°C
		600°C–1,450°C: $2[1.538^2 + (0.4\%reading)^2]^{1/2}$
Thermocouple Type C	°C	0°C–600°C: 6.477°C
		600°C–1,450°C: $2[2.174^2 + (0.4\%reading)^2]^{1/2}$
Flow meter	% reading	2.946%
Voltage Transducer	V	Type 1–4.655 V
		Type 2–9.1255 V
Current Transducer	A	0.574 A

the HTTF's ability to generate similar results for multiple tests performed under the same operational conditions (data repeatability).

4 Conclusion

The OSU HTTF is first of a kind IET facility to deliver experimental data on depressurized and pressurized conduction events, heat up, cooldown and mixing phenomena during normal operations in gas-cooled reactors at prototypical temperatures. While the facility assembly and operation came with several challenges, gathered data and accumulated research experience create solid foundations for future gas-cooled reactors testing programs. The facility delivered data on 20 tests, out of which six were developed to characterize the facility operational features, eight modeled the DCC event, 1 was focused on the PCC transient, two aimed at simulating mixing scenario and the remaining experiments tested facility heat up and cooldown conditions. Obtained test data can be used for thermal hydralic codes validation. Data from tests PG-27, PG-28, and PG-29 will be used in the HTTF thermal-hydraulic benchmark exercise for gas cooled reactors applications organized by OECD and led by INL, OSU, CNL, ANL, NRG, and UTK. Test data are available at https://osti.gov.

The HTTF DCC test results provide data on the air ingress and natural circulation stages without depressurization. Data available are the thermocouples and power sensors readings. These results are addressing experimental data needs for some of the major phenomena or system characteristics identified in the VHTR PIRT D-LOFC chart, including:

- Core effective thermal conductivity,
- Cavity Gas stratification and mixing,
- Duct exchange flow.

The facility is further capable of addressing additional D-LOFC phenomena identified in the PIRT tables if the testing campaign is resumed and upgraded instrumentation (for instance gas concentration sensors) is available.

- RCCS spatial heat loadings,
- Coolant flow and thermal properties for mixed gases in the vessel,
- Heat transfer correlations for mixed gases in the core,
- Core and core support structures oxidation,
- Molecular diffusion (maximum core temperature, gas distribution, time scale).

The HTTF PCC test results are also addressing experimental data needs for some of the major phenomena or system characteristics identified in the VHTR PIRT P-LOFC chart, including:

- Inlet plenum stratification and plumes,
- Radiant heat transfer from the top of the core to upper vessel head,
- Core coolant flow distribution (addressed partially—some data can be derived from temperature readings).

Similarly to DCC testing capabilities, the facility is further capable of addressing additional P-LOFC phenomena identified in the PIRT tables, if the testing campaign is resumed, upgraded instrumentation is available and some design changes are introduced (if needed):

- RCCS spatial heat loadings,
- Core coolant (channel) bypass flow (if core blocks structure is redesigned),
- Coolant flow friction/viscosity effects.

The future work includes the execution of an experimental campaign that will address the PCC, DCC, and normal operation PIRT phenomena that have not yet been tested (listed above). The facility can be also accommodated for pebble-bed gas-cooled reactors PIRT testing and gas-cooled reactors components and subsystems testing at elevated temperatures and in a helium environment.

Data availability statement

The datasets presented in this article are readily available. Requests to access the datasets should be directed to US DOE.

Author contributions

IG and BW contributed to the design and implementation of the research, to the analysis of the results, to the writing of the manuscript, and were involved in executing the HTTF tests. JH contributed to assessing PG-27 and PG-29 results, and to the writing of the manuscript.

Conflict of interest

The authors declare that the research was conducted in the absence of any commercial or financial relationships that could be construed as a potential conflict of interest.

Publisher's note

References

ASME V&V 20-2009 (2016). *Standard for verification and validation in computational fluid dynamics and heat transfer"*. New York, NY, USA: American Society of Mechanical Engineers.

Ball, S., and Fisher, S. (2008). Next generation nuclear plant phenomena identification and ranking tables (PIRTs) (Rockville, MD, USA: Nuclear Regulatory Commission). NUREG/CR-6944.

Bayless, P. D. (2018). RELAP-3D pre-test prediction for high temperature test facility test PG-26. IIdaho Falls, ID, USA: Idaho National Laboratory. INL/EXT-18-45717.

Bayless, P. D. (2018)RELAP5-3D input model for the high temperature test facility IIdaho Falls, ID, USA: daho National Laboratory. INL/EXT-18- 45579.

Chen, F., Dong, Y., Zheng, Y., Shi, L., Li, F., and Zhang, Z. (2014). Progress of the HTR-10 measured data utilization. International conference on nuclear engineering. *Proc. ICONE* 3. doi:10.1115/ICONE22-30088

Glass, M. (2017). *Effect of initial conditions and depressurization on lock exchange flow after a depressurized conduction cool-down event in the high temperature test facility*. Corvallis, Oregon: Oregon State University.

Gutowska, I., and Woods Brian, G. (2019). "CFD assessment of LOFA intra core natural circulation in the high temperature test facility," in Proceedings of the NURETH-18, Portland, Oregon, Auguest 2018.

Halsted, J. K. (2022). *Validation analysis for the OSU HTTF PG-28 test using relap5-3D and star-ccm+*. Corvallis, Oregon: Oregon State University.

Hishida, M., Fumizawa, M., Takeda, T., Ogawa, M., and Tekenaka, S. (1993). Researches on air ingress accidents of the HTTR. *Nucl. Eng. Des.* 144, 317–325. doi:10.1016/0029-5493(93)90147-2

Landfried, D. T., Kristo, P., Clifford, C. E., and Kimber, M. (2019). Design of an experimental facility with a unit cell test section for studies of the lower plenum in prismatic high temperature gas reactors. *Ann. Nucl. Energy* 133, 236–247. doi:10.1016/j.anucene.2019.05.037

Maruyama, S., Fujimoto, N., Sudo, Y., Murakami, T., and Fujii, S. (1994). Evaluation of core thermal and hydraulic characteristics of HTTR. *Nucl. Eng. Des.* 152 (1-3), 183–196. Issues. doi:10.1016/0029-5493(94)90084-1

Qin, S., Song, M., Vietz, S. H., T Pham, C. B., Plummer, M., and Strydom, G. (2022). High-temperature gas-cooled reactor research Survey and Overview: Preliminary data Platform construction for the nuclear energy university Program. United StatesAvailable At https://www.osti.gov/servlets/purl/1887092. doi:10.2172/1887092

Rousseau, P. G., and van Staden, M. (2008). Introduction to the PBMR heat transfer test facility. *Nucl. Eng. Des.* 238 (11), 3060–3072. HTR-2006: 3rd International Topical Meeting on High Temperature Reactor TechnologyISSN: 0029-5493.

Schultz, R. R., Ougouag, A. M., Nigg, D. W., Gougar, H. D., Johnson, R. W., Terry, W. K., et al. (2008). Next generation nuclear plant methods research and development technical Program plan. United StatesAvailable At https://www.osti.gov/servlets/purl/950995.doi:10.2172/950995

Woods, B. G. (2019). *Integral system testing for prismatic block core design HTGR*. Washington, DC, USA: OSTI. United States. Web. doi:10.2172/1580081

Woods, B. G. (2018). OSU high temperature test facility design technical report. OSU-HTTF-TECH-003-R2available at: https://www.osti.gov/biblio/1599410-osu-high-temperature-test-facility-design-technical-report-revision.

Nomenclature

Abbreviations

ANL Argonne national laboratory
CNL Canadian national laboratories
DCC Depressurized conduction cooldown
DOE Department of energy
NEUP Nuclear energy university program
D-LOFC Depressurized loss of forced cooling
GA General atomics
GT-HTR Gas turbine high temperature reactor
HPTU High pressure test unit
HTGR High temperature gas cooled reactor
HTTF High temperature test facility
HTTR High temperature test reactor
HTTU High temperature test unit
HTR-PM High temperature pebble bed modular nuclear reactor
INL Idaho national laboratory
JAERI Japan atomic energy agency
MHTGR Modular high temperature gas cooled reactor
NGNP Next-generation nuclear power
NRG Nuclear research and consultancy group
PIRT Phenomena identification and ranking tables
PCC Pressurized conduction cooldown
PG Procedural guide
P-LOFC Pressurized loss of forced cooling
PPV Primary pressure vessel
RCCS Reactor cavity cooling system
RCST Reactor cavity storage tank
RELAP Reactor excursion and leak analysis program
RPV Reactor pressure vessel
OECD Organization for economic cooperation and development
OSU Oregon State University
TF Fluid thermocouple
TS Solid thermocouple
UTK University of Tennessee Knoxville
VHTR Very high temperature gas cooled reactor

frontiers | Frontiers in Energy Research

TYPE Review
PUBLISHED 25 January 2023
DOI 10.3389/fenrg.2023.1085264

OPEN ACCESS

EDITED BY
Michael Fleming,
Organisation For Economic Co-Operation and Development, France

REVIEWED BY
Jiankai Yu,
Massachusetts Institute of Technology, United States
Oliver Buss,
Organisation For Economic Co-Operation and Development, France
Thomas M. Miller,
Oak Ridge National Laboratory (DOE), United States

*CORRESPONDENCE
Yosuke Iwamoto,
iwamoto.yosuke@jaea.go.jp

SPECIALTY SECTION
This article was submitted to Nuclear Energy, a section of the journal Frontiers in Energy Research

RECEIVED 31 October 2022
ACCEPTED 16 January 2023
PUBLISHED 25 January 2023

CITATION
Iwamoto Y, Tsuda S and Ogawa T (2023), Benchmark shielding calculations for fusion and accelerator-driven sub-critical systems.
Front. Energy Res. 11:1085264.
doi: 10.3389/fenrg.2023.1085264

Benchmark shielding calculations for fusion and accelerator-driven sub-critical systems

Yosuke Iwamoto*, Shuichi Tsuda and Tatsuhiko Ogawa

Nuclear Science and Engineering Center, Japan Atomic Energy Agency, Ibaraki, Japan

We conducted benchmark calculations of neutron-shielding experiments for fusion applications such as (1) Neutron spectra in iron shields with 14 MeV neutrons; and (2) Leakage neutron spectra from various sphere piles by 14 MeV neutrons, and for Accelerator-Driven Sub-Critical system (ADS) such as (3) Neutron energy spectra after transmission through iron and concrete shields using a quasi-monochromatic neutron source, (4) Thick target neutron yield produced by high-energy heavy ion incidence on a thick target, and (5) Induced radio activity in concrete exposed to secondary particles produced by heavy-ion incident reaction on an iron target by using the Particle and Heavy Ion Transport code System (PHITS). For case (1), the calculated neutron energy spectra using the nuclear data libraries, JENDL-4.0, agreed with the experimental data in iron shields. For the cases (2) of Al, Ti, Cr, and As piles, the neutron energy spectra calculated with JENDL-4.0 agreed with the experimental results well. For the case (3), the neutron spectra calculated with JENDL-4.0/HE reproduced the experimental data because the proton data library of ^{7}Li can produce source neutrons for proton incident reactions. For the case (4), calculated results for thick target neutron spectra produced by a 400 MeV per nucleon carbon incident reaction on lead reproduced the experimental data well. For the case (5) with a neutron source produced by the 200–400 MeV per nucleon heavy-ion incident reaction, the calculated results of the reaction rate depth profiles of ^{197}Au (n, γ)^{198}Au reactions reproduced the experimental results within a factor of 2. Overall, PHITS with nuclear data libraries reproduced the experimental data sufficiently well. Thus, PHITS has a potential application in the design of advanced reactor systems, such as fusion and ADS facilities. This experimental data are also useful in validating nuclear reaction models in other Monte Carlo codes and evaluating nuclear data libraries for advanced reactor systems.

KEYWORDS

neutron, shielding, benchmark, fusion, ADS, PHITS

1 Introduction

A fusion nuclear facility is one of the most advanced reactor systems in the high-energy region. Nuclear fusion is a process to fuse two lighter nuclei to form one heavier nucleus, which releases a large amount of energy. Fusion reactions occur in a matter at a state called plasma, which is a hot mixture composed of positive ions and freely moving electrons. Plasma has unique properties different from those of solids, liquids, and gases. The reaction between two hydrogen isotopes, deuterium (D) and tritium (T), is the most efficient fusion reaction. The International Thermonuclear Experimental Reactor (ITER) is an international research project aimed at producing energy through fusion processes. It is the first fusion device to produce energy continuously by chain reactions; ITER will test the integrated technologies, materials, and physical regimes necessary to commercially produce electricity from fusion.

Fusion neutron engineering is one of the most important issues in the development of fusion reactors, which studies various nuclear parameters. D-T neutrons interact with steel materials as structural materials for blankets and diverters, SiC/SiC composites as functional materials, copper alloys as heat sink and cooling tube materials, and tungsten as counterpart materials for high load parts, causing nuclear heating and induced radioactivity production, along with tritium breeding. In particular, the tritium breeding ratio is the most important parameter in terms of fuel self-sufficiency. Fusion reactor design involves concerns such as radiation shielding, material heating, and displacement damage. Activation is also an important concern in terms of dose rate, heat generation, and radioactive waste management. These evaluations are essential to obtain approval for equipment construction in terms of radiation safety. Important parameters in activation are products of the interaction between neutrons and materials. On the other hand, the effects of gamma irradiation must be considered in radiation shielding design and material aging. Tritium treatment is also important from the viewpoint of radiation protection. The nuclear design of a fusion reactor relies on currently-available computational codes and data. These include Monte Carlo particle codes and related data libraries such as neutron cross sections and neutron activation cross sections. In order to accurately evaluate the above nuclear parameters, the codes and data applied to the design calculations need to be validated using experimental data. Fusion neutron engineering research began in Japan in the early 1980s. The high-intensity D-T neutron facilities, i.e., the Fusion Neutronics Source (FNS) at the Japan Atomic Energy Research Institute (JAERI, now the Japan Atomic Energy Agency) and the OKTAVIAN at Osaka University, are the world's leading facilities providing experimental data related to fusion research (Konno et al., 1991; Sub Working Group of Fusion Reactor Physics Subcommittee, 1994). Fundamental integral benchmark experiments were performed in these facilities for fusion applications. These integral experiments were performed using the D-T neutron source, with simple geometry and materials.

The Accelerator-Driven Sub-Critical system (ADS) is also one of the advanced reactor systems. In this system, the transmutation and separation of actinides and some long-lived fission products from nuclear production produced in a fission reactor can reduce the radio-toxicity of high-level waste to one-hundredth that of the current once-through fuel cycle (Mukaiyama et al., 2001). Only fission reactors and spallation sources are available in the medium term because of the high intensity required for transmutation. The concept of ADS combines a proton particle accelerator using an energy of around 1 GeV with a sub-critical core. Protons are incident on a spallation target made up of solid or liquid heavy metals, such as a lead bismuth eutectic alloy, that produces source neutrons to drive a subcritical reactor. The spallation reaction at the target produces dozens of neutrons per incident proton and introduces them into the subcritical core. It is similar to a critical reactor core, except that it is subcritical. In the design of an ADS facility, the behavior of spallation neutrons in the material and radiation shielding must be studied as well as those in fusion devices as described above. It should be noted that the maximum neutron energy is 14 MeV for fusion. The maximum neutron energy for ADS is around the energy of the maximum energy of the proton for a proton driven system. Therefore, experimental data on high-energy neutron shielding is required to validate nuclear reaction models in the Monte Carlo (MC) code and data libraries used for fusion and ADS design calculations. The nuclear reaction model of the intranuclear cascade model + evaporation model is used for energies above the table based cross sections. Shielding experiments for neutrons have been performed at the Takasaki Ion Accelerator for Advanced Radiation Application (TIARA) (Nakao et al., 1996; Nakashima et al., 1996) and the Heavy Ion Medical Accelerator in Chiba (HIMAC) at the National Institute of Radiological Science (NIRS) (Kurosawa et al., 1999; Satoh et al., 2007; Ogawa et al., 2011). These facilities have achieved results in fundamental benchmark experiments for accelerator applications. These neutron shielding experiments have been performed using a neutron source with a 40–70 MeV proton-lithium nuclear reaction, a neutron source with a 230–400 MeV/u helium, and various ions with 100–800 MeV/u incident nuclear reaction on a thick target.

The experimental data needs to be reviewed and then compared to the results calculated with nuclear reaction models and nuclear data libraries so as to validate nuclear reaction models and nuclear data in the design of advanced reactor systems in the high-energy region. Therefore, it is desirable for benchmark calculations to use the shielding integral benchmark archive and database (SINBAD) [9–11].

In this paper, our developing MC code, the Particle and Heavy Ion Transport code (PHITS) (Iwamoto et al., 2017; Sato et al., 2018), was validated with the experimental data included in the SINBAD database and our experimental data. This paper is organized as follows. Section 2 presents experimental and calculation conditions of two experiments related with fusion and three experiments related with accelerator-shielding, which were generated from (1) Integral experiment on iron cylindrical assembly with D-T neutron source at FNS (Konno et al., 1991; Sub Working Group of Fusion Reactor Physics Subcommittee, 1994), (2) Leakage neutron spectra from various sphere piles with D-T neutron source at OKTAVIAN, Osaka university (Sub Working Group of Fusion Reactor Physics Subcommittee, 1994), (3) Neutron energy spectra after transmission through shields using a quasi-monochromatic neutron source at TIARA (Nakao et al., 1996; Nakashima et al., 1996), (4) Thick target neutron yield produced by high-energy heavy-ion incident reaction at HIMAC (Kurosawa et al., 1999; Satoh et al., 2007), and (5) Induced activity in shield exposed to particles produced by heavy-ion on Fe at HIMAC (Ogawa et al., 2011). For the cases of (3), (4), and (5), the benchmark studies have been conducted in our previous paper and report (Ogawa et al., 2011; NEA, 2022b; Iwamoto et al., 2022). In this paper, we introduce a part of our benchmark study for these cases and present a new benchmark calculation with PHITS for the case of (1) and (2). Section 3 presents the benchmark results and discussion in all cases, and Section 4 shows the summary of this research work.

2 Experiments and calculation procedure

2.1 Overview of the PHITS code

PHITS (Iwamoto et al., 2017; Sato et al., 2018) is a general-purpose Monte Carlo particle transport code. It can deal with the transport of all particles over wide energy ranges, using several nuclear reaction models and nuclear data libraries. For the PHITS nuclear reaction models, the Liège intranuclear cascade model (INCL4.6) (Boudard et al., 2013) is used for neutrons above 20 MeV and protons above 1 MeV. The JAERI Quantum Molecular Dynamics (JQMD) model (Ogawa et al., 2015) is used for nucleus above 10 MeV/u. These models are coupled with the evaporation model GEM (Furihata, 2000), which handles the statistical decay of the spallation residues. The nuclear data

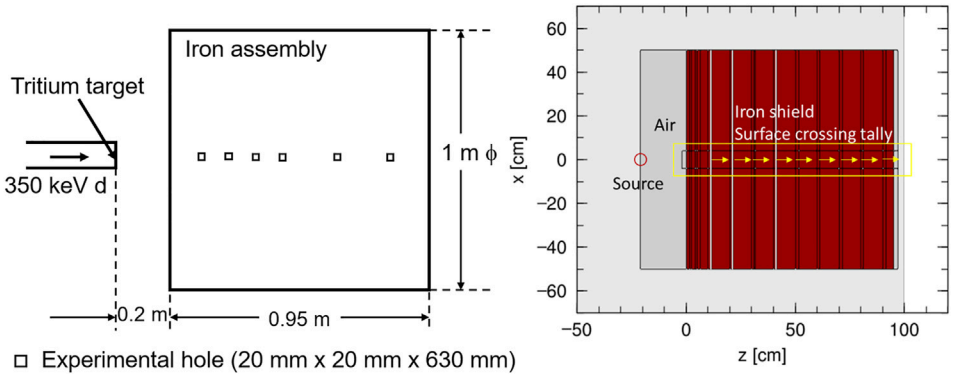

FIGURE 1
Experimental setup (left) and geometry in PHITS (right) for the FNS experiment (Konno et al., 1991; Sub Working Group of Fusion Reactor Physics Subcommittee, 1994). The neutron energy spectra produced by the D-T reaction compiled in the SINBAD (NEA, 2022b) was used as a source term.

library, JENDL-4.0 (Shibata et al., 2011), is used for neutrons below 20 MeV. For the case (3), the high-energy nuclear data library, JENDL-4.0/HE (Kunieda et al., 2016), is also used for protons and neutrons below 200 MeV.

The weight window variance reduction method in PHITS is similar to that in the MCNP code (Goorley et al., 2012). Particle weights are affected by importance, forced collisions, implicit capture, and the weight window function. If the weight is lower than a user-defined weight cutoff, a Russian roulette method is applied to determine if the particle should be killed. In PHITS, the weight window defined in the weight widow section is automatically determined by the weight window generator section.

2.2 Experimental conditions

This subsection describes the experimental condition of five experiments.

2.2.1 Integral experiment on iron cylindrical assembly at FNS

Figure 1 shows the experimental setup with a 0.95-m-thick-iron and calculation geometry for the FNS experiment. The experimental data and the calculation geometry of the integral experiment on the iron cylindrical assembly at the FNS were compiled in the SINBAD abstract NEA-1553/45 (Kodeli et al., 2006; NEA, 2022a; ORNL, 2022). The experiment was done in the first target room of the FNS facility of JAERI (Konno et al., 1991; Sub Working Group of Fusion Reactor Physics Subcommittee, 1994). Neutrons were produced by D-T nuclear reaction. A 350 keV deuteron beam with 0.5–150 μA current was incident on a water-cooled Tritium-Titanium (T-T) target. The activity of tritium was 3.7×10^{11} Bq. Neutron at the tritium target were measured by the alpha particle counting method with an accuracy of about 3%. The iron shield with 1 m diameter and 0.95 m thickness was placed 0.2 m from the T-T target. Impurities include 0.148 wt% S, 0.834 wt% Mn, and 0.185 wt% C. It has 6 holes (20 × 20 × 630 mm) in the radial direction. The proton recoil gas counter was placed into the 6 holes inside the iron assembly to measure neutron spectra with energies from a few keV to 1 MeV. The center locations of the holes were 0.11, 0.21, 0.31, 0.41, 0.61, and 0.81 m from the front of the iron shield. The number of incident neutrons was monitored at the front of the iron shield. Total neutron yields ranged from 9.4×10^{11}–2.8×10^{14}. The calculation geometry in PHITS was taken from the MCNP input in the SINBAD abstract NEA-1553/45. The neutron energy spectra of the D-T source compiled in the SINBAD abstract were employed as a source term in the PHITS calculation. Neutrons were emitted in isotropic direction. The nuclear data library, JENDL-4.0 (Shibata et al., 2011), was used for the transport calculation of neutrons in the iron assembly. Neutron energy spectra in the iron assembly were tallied at each depth with the [t-cross] tally, which is the surface crossing tally for neutrons. The flux tally is representative for the flux on the surface with 4 cm radius of the block.

2.2.2 Leakage neutron spectra from various sphere piles with D-T neutrons

The experimental data and the calculation geometry of the leakage neutron spectra from various sphere piles with D-T neutrons at OKTAVIAN were compiled in the SINBAD abstract NEA-1553/45 (Kodeli et al., 2006; NEA, 2022a; ORNL, 2022). The experiment was conducted at the beam line of OKTAVIAN (Sub Working Group of Fusion Reactor Physics Subcommittee, 1994). A 250 keV deuteron beam was incident on a 370 GBq tritium target to produce neutrons. Figure 2 shows the experimental set-up and calculation geometry. The 40-cm diameter sphere piles were used for the piles of aluminum, titanium, chromium, cobalt, arsenic, and tungsten. There is a layer of 0.2-cm thick stainless steel (JIS SUS-304) around the 40-cm diameter sphere pile. The pile has a 20 cm diameter void and an 11 cm diameter re-entrant hole through which the target beam duct can pass. A target was set at the center of the pile. This pile was replaced after each measurement. The neutron source spectra given in (Sub Working Group of Fusion Reactor Physics Subcommittee, 1994) were obtained with the time-of-flight (TOF) technique. Note that the references 1 and the SINBAD abstract NEA-1553/45 contain no information about the tritium target. The neutron energy spectrum listed in reference 1 was used as a source term and neutrons were emitted isotropically in the calculation.

The liquid organic scintillator NE-218 to measure neutrons was positioned at 55° to the beam direction and 10.5 m from the target.

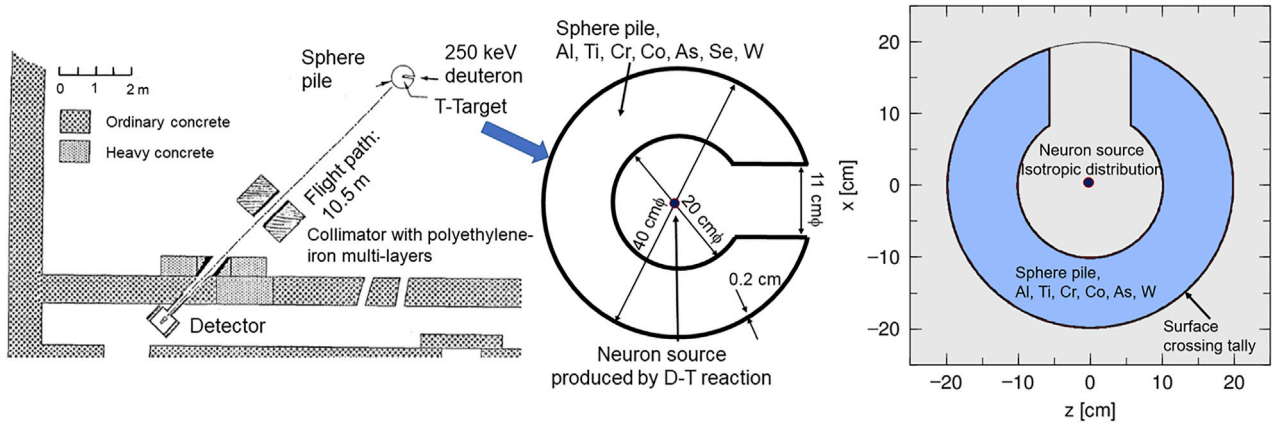

FIGURE 2
Arrangement of the experimental configuration and modeling geometries for the OKTAVIAN experiments.

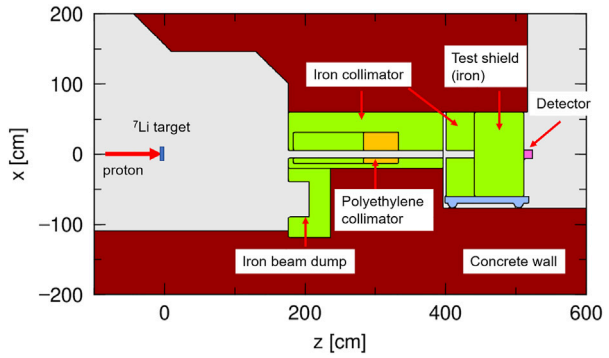

FIGURE 3
Geometry in PHITS calculations for the TIARA experiments. The test shield is either an iron shield or a concrete shield.

Detailed information on the collimator system is available in reference 1. A collimator with multi-layer polyethylene and iron was placed between the detector and the sphere pile to decrease the background events. The absolute value of the leakage neutron yield from the pile is obtained by the gamma-rays intensity of the induced radioactivity of ^{92m}Nb, a niobium foil in front of the target, and the number of the integrated source neutron spectrum (Sub Working Group of Fusion Reactor Physics Subcommittee, 1994).

The simplified calculation geometry in PHITS was taken from the MCNP input in the SINBAD abstract NEA-1553/45 (Kodeli et al., 2006; NEA, 2022a; ORNL, 2022). The neutron transport was calculated by using JENDL-4.0. The neutrons that penetrated through a pile were scored with the [t-cross] tally, and the neutron energy spectra of source compiled in the SINBAD were used as a source term in the PHITS calculation.

2.2.3 Transmuted neutron energy spectra through shields using a quasi-monoenergetic neutrons

The shielding experiments were performed for iron and concrete shields with quasi-monoenergetic neutron sources with energies of 41- and 65-MeV developed at TIARA. Quasi-monoenergetic neutrons were produced by the 43- and 68-MeV proton incident reaction on lithium. In this experiment, neutron energy spectra transmitted through 25- to 200-cm-thick concrete shields (Nakao et al., 1996) and through 10- to 130-cm-thick irons (Nakashima et al., 1996) were obtained by using Bonner ball sphere detectors and a liquid scintillator BC501A. The neutron spectrum in the energy region between a few MeV and a peak energy were obtained with a BC501A and thermal neutrons with energies below a few MeV were obtained from Bonner ball measurements.

Figure 3 shows the calculation geometry with PHITS for TIARA experiments (Kos and Kodeli, 2019).

The targets were 3.6-mm and 5.2-mm thick lithium (99.9% enriched ^{7}Li) for the 43- and 68-MeV proton, respectively. Neutrons went through an iron collimator with 10.9-cm-diameter and experimental assembly. The protons that penetrated the target were bent downward to the iron beam dump by the magnetic field. The 25–200 cm thick concrete shields were assembled with 120 × 120 × 25 cm thick plates and the 10–130 cm thick steel shields were assembled with 120 × 120 × 10 cm thick plates. The concrete density was 2.31 g/cm^3 and the iron density was 7.87 g/cm^3.

The contribution of the neutrons generated by the iron beam dump to the detector is negligible. The proton incident reaction on lithium was simulated with the physics model, INCL4.6 (Boudard et al., 2013), or the proton data library for JENDL-4.0/HE (Kunieda et al., 2016).

2.2.4 Thick target neutron yield produced by heavy-ion incident reaction

Secondary neutron yields from thick targets (Kurosawa et al., 1999; Satoh et al., 2007) of graphite, aluminum, copper, and lead irradiated with heavy-ions from helium to xenon with energies of 100–800 MeV/u were obtained at HIMAC of NIRS, compiled in the SINBAD abstract NEA-1552/35 (Kodeli et al., 2006; NEA, 2022a; ORNL, 2022). The neutron yields from materials produced by heavy-ion-induced reactions were used as the source term for the neutron shielding experiment at HIMAC (Kurosawa et al., 1999). The thicknesses of the materials varied depending on the ion energy so as to ensure that the ions come to a complete stop within the target.

The experiment was performed in the general-purpose irradiation room (PH2) beam line shown in Figure 4A. Room

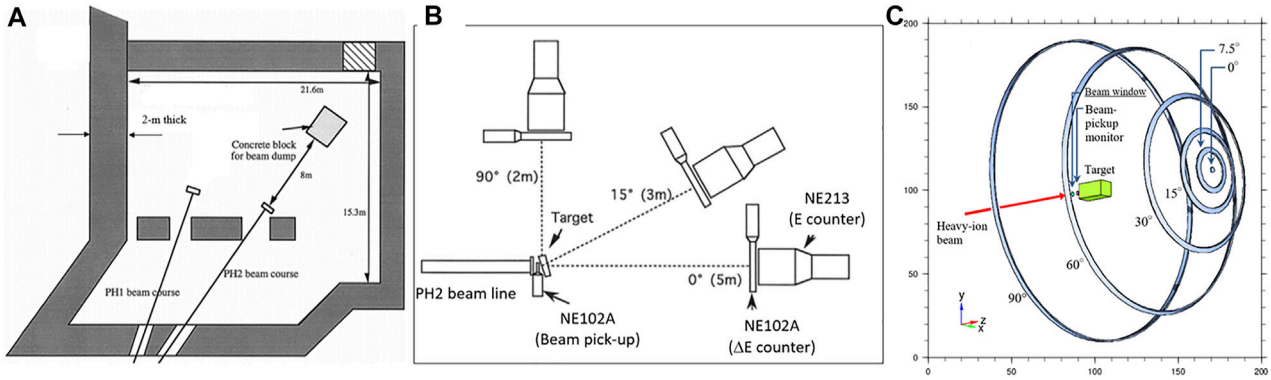

FIGURE 4
(A,B) Experimental setup for thick target neutron yield produced by heavy-ion incident reaction in HIMAC and **(C)** geometry in PHITS calculations.

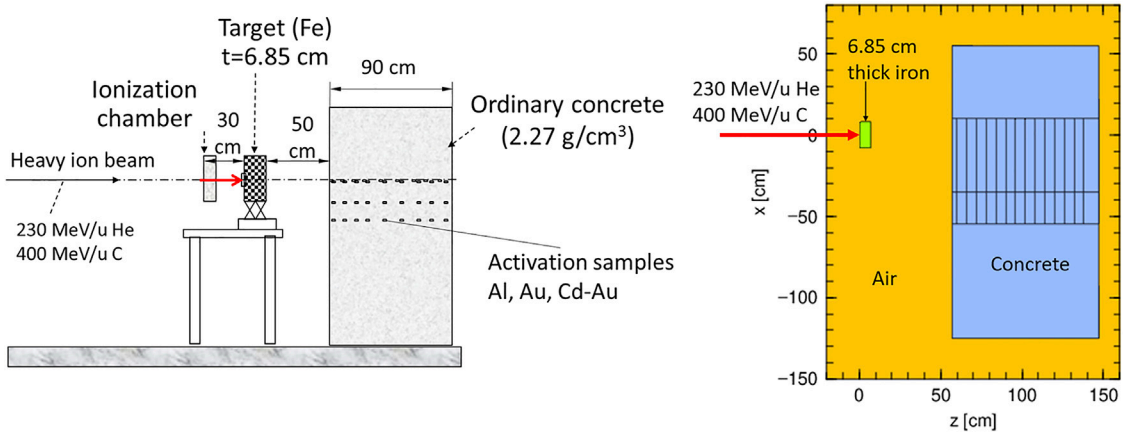

FIGURE 5
The experimental layout used in HIMAC and geometry in PHITS calculations. Heavy ion beam was incident on the iron target and secondary particles produced by nuclear reactions were injected into the concrete shield. The activation samples were set in parallel or lines along to the beam axis (Ogawa et al., 2011). A 90-cm-thick ordinary concrete shield was assembled from rectangular blocks measuring 60 × 15 × 15 cm.

walls, made of 2-m-thick concrete, were located at least 8 m away from the target in all directions, except for the pillars near the target. The concrete ceiling was located about 6 m above the target, and the floor was about 1.25 m below the target. The distance from the target to the beam dump surface was set to be 8.0 m.

Figure 4B shows a schematic view of the typical arrangement of target and detectors. Neutron energy produced in the target was obtained by TOF between the beam pick-up detector set in front of the target and a liquid organic scintillator (NE213, 12.7 cm in diameter, 12.7 cm long), located at 0°, 7.5°, 15°, 30°, 60°, and 90°. Figure 4C shows geometry in PHITS calculations for the experiment of thick target neutron yields.

Regarding the radiation transport calculation, the INCL4.6 model was employed for nucleons and light particles (proton, deuteron, triton, and alpha) and the JQMD model (Ogawa et al., 2015) was used for nucleus. JENDL-4.0 was applied for neutrons below 20 MeV.

2.2.5 Induced radioactivity in shield exposed to secondary particles produced by heavy ions on Fe

The experiments were performed at the PH1 of HIMAC at NIRS (Ogawa et al., 2011) where heavy ion beams of several 100 MeV/u are available. Figure 5 shows the experimental layout and the calculation geometry in HIMAC. The target was a stack of 16 × 16 cm iron plates. Its thickness, 6.85 cm was larger than the range of the projectiles. The center of the target was an independent stack of cylindrical iron plates with 0.15 cm thickness and 4 cm diameter used to verify the direction and positioning of the beam. The target center was positioned to agree with the beam axis with an accuracy of a few millimeters.

A 90-cm-thick ordinary concrete shield was assembled from rectangular blocks measuring 60 × 15 × 15 cm and having a density of 2.27 g/cm^3. The concrete shield, whose upstream surface had a roughness of less than 1 cm owing to the minor tilts of concrete blocks accumulated from the ground to the top, was located 50 cm downstream from the target.

TABLE 1 Chemical composition of the shielding concrete used for the shielding experiment (Ogawa et al., 2011). The unit is g/cm³.

Hydrogen	Oxygen	Sodium	Magnesium	Aluminum	Silicon	Potassium	Calcium	Iron
0.0237	1.08	0.049	0.02	0.138	0.641	0.0435	0.188	0.0438

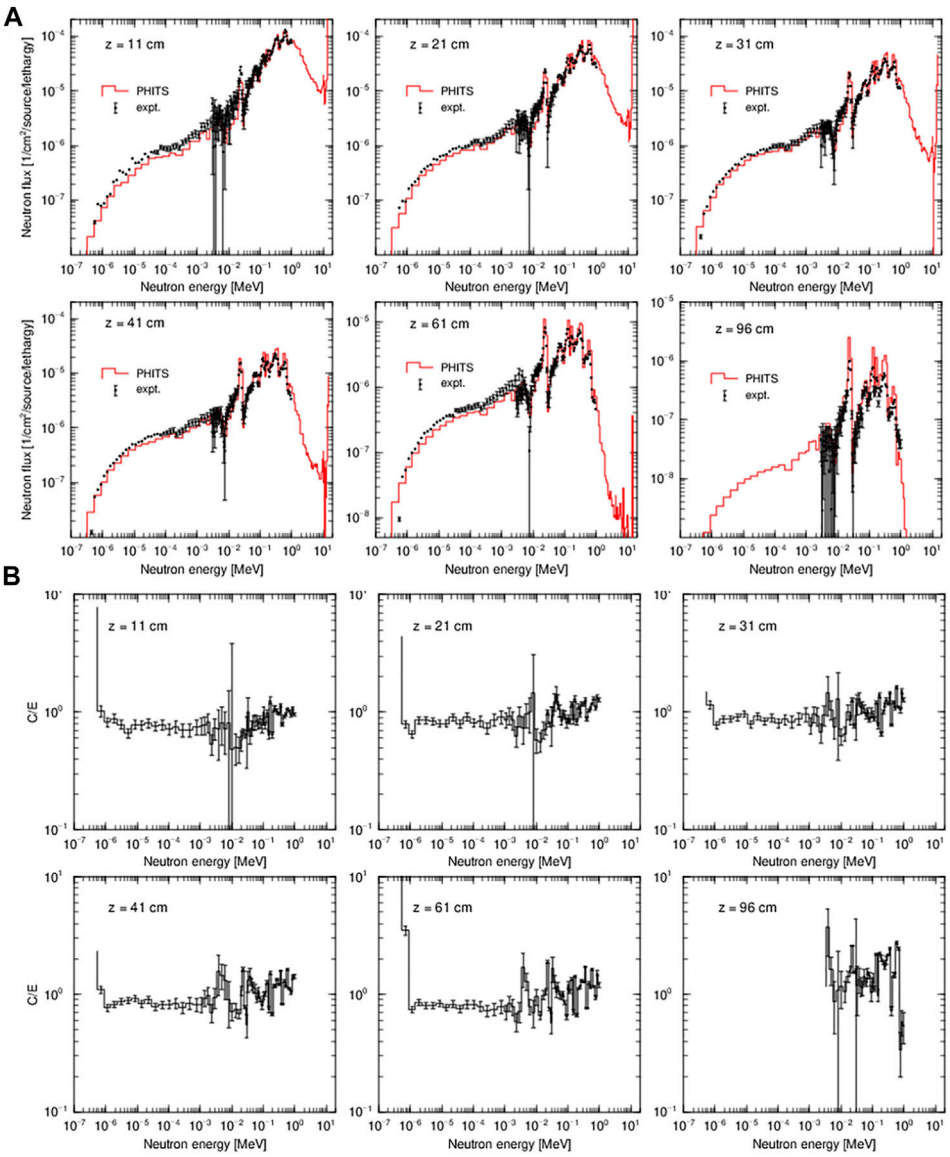

FIGURE 6
(A) Neutron energy spectra at each depth in the iron shield for a 350-keV D-T neutron source. The experimental data only includes uncertainty due to counting statistics. **(B)** The ratio of calculation results and experimental data to the neutron energy. Note that there are places where the energy bins in the experimental neutron flux plots are different from those in the calculated results.

Table 1 shows the chemical composition of the concrete blocks analyzed by using atomic emission spectrometry, atomic absorption spectrometry, and gravimetry. Moisture varies by aging and equilibration in environment but it is fair to assume that the moisture reached equilibrium because the blocks had been stored in the PH1 irradiation room, where the temperature and moisture were kept stable for the accelerator components, for more than 10 years. Owing to the difficulty in chemical composition analysis, carbon was not measured which is likely to be responsible for the discrepancy between the total density of 2.27 g/cm³ obtained by weighing actual concrete blocks and the sum of the partial densities (Ogawa et al., 2011) of Table 1.

The detectors for activation were set along four parallel lines, at 0, 15, 30, and 45 cm, in the vertical plane that included the beam axis and were shifted below the beam axis. At several depths, thin foils of gold (15 μm thickness), gold (15 μm thickness) covered with cadmium (500 μm thickness) on both sides, and aluminum (1–3 mm thickness)

10.3389/fenrg.2023.1085264

TABLE 2 *C/E* **with one standard deviation for the accumulated neutron yields in the neutron energy region from 0.003 MeV–10 MeV in the iron shield for a 350-keV D-T neutron source. The experimental data only includes uncertainty due to counting statistics.**

Depth (cm)	11	21	31	41	61	96
C/E	1.39 ± 0.01	1.31 ± 0.01	1.24 ± 0.01	1.21 ± 0.01	1.15 ± 0.01	1.78 ± 0.02

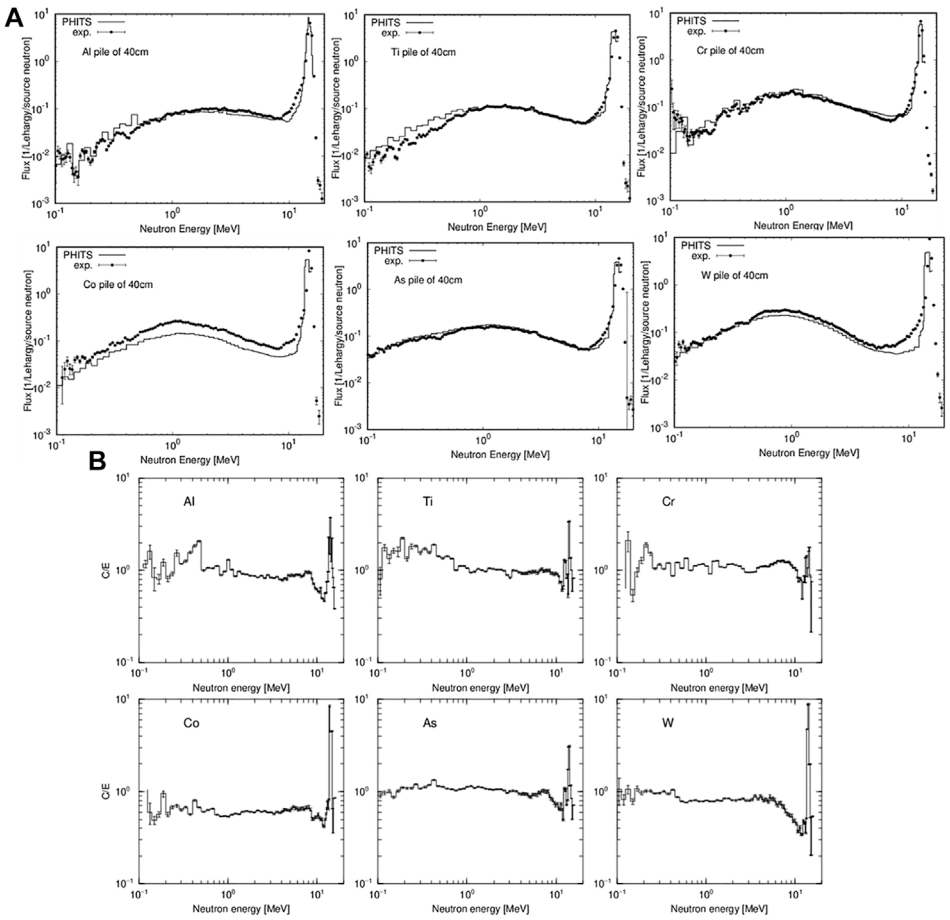

FIGURE 7
(A) Neutron energy spectra from Al, Ti, Cr, Co, As, and W piles for a 250-keV D-T neutron source. The experimental errors include only the statistical deviation of neutrons in the measurement. **(B)** The ratio of calculation results and experimental data to the neutron energy. Note that there are places where the energy bins in the experimental neutron flux plots are different from those in the calculated results.

activation detectors were placed to measure the activation depth profiles. The ion beams were extracted through an Al beam window with 100 μm thickness as pulses of 400–600-msec-long with 3.3 s repetition intervals. The beam was injected into the target surface and collimated to less than 1 cm in diameter. The iron plate stack, which constituted the central part of the target, was disassembled after irradiation and put on a BAS-MS Imaging Plate to confirm the beam collimation and positioning.

3 Results and discussion

All results are discussed in this section. Numerical data including computational and experimental uncertainties in the figures are provided as Supplementary Material. In the case of (1), (2), and (3), the ratios of calculated and experimental data and their uncertainties in figures are also included as Supplementary Material.

3.1 Integral experiment on iron cylindrical assembly at FNS

Figure 6A shows neutron energy spectra at 11, 21, 31, 41, 61, and 96 cm from the surface of the iron assembly (Konno et al., 1991; Sub Working Group of Fusion Reactor Physics Subcommittee, 1994). Figure 6B shows the ratio of calculation results and experimental data to the neutron energy. The experimental data only includes uncertainty due to counting statistics. At energies above 50 keV, the

TABLE 3 *C/E* with one standard deviation for the accumulated neutron yields in the neutron energy region from 0.1 MeV to 15 MeV from Al, Ti, Cr, Co, As, and W piles for a 250-keV D-T neutron source. The experimental data only includes uncertainty due to counting statistics.

Target	Al	Ti	Cr	Co	As	W
C/E	1.028 ± 0.001	1.118 ± 0.002	1.039 ± 0.001	0.804 ± 0.002	1.064 ± 0.002	0.866 ± 0.002

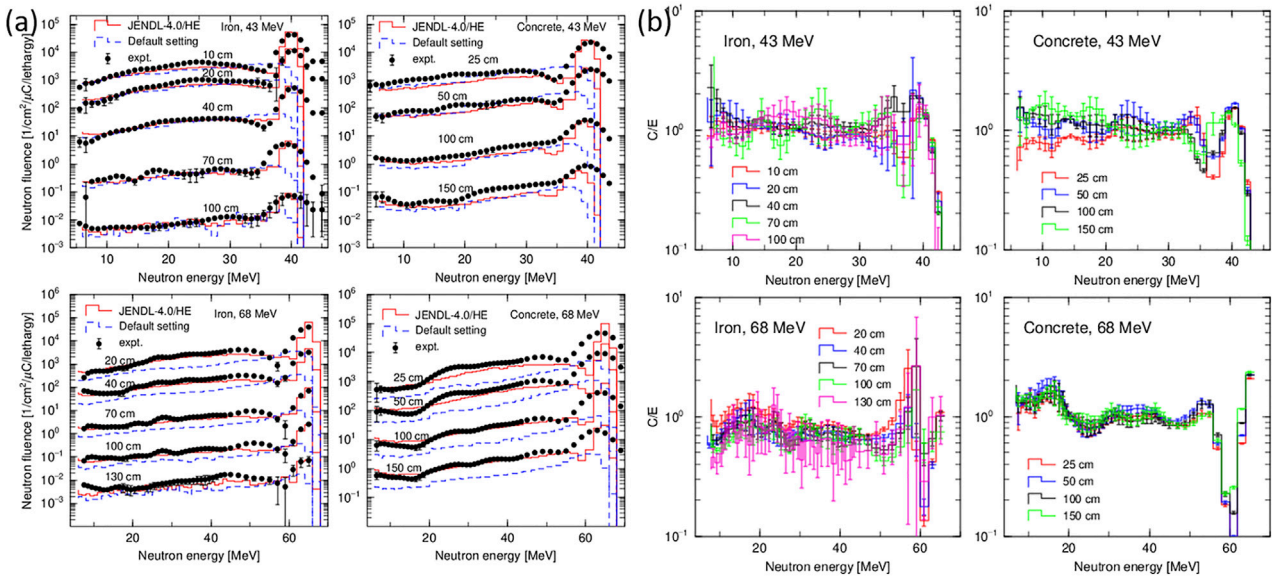

FIGURE 8
(A) Neutron energy spectra after transmission through iron and concrete shields for the TIARA experiments with the 43- and 68-MeV proton incident reactions on lithium target. The experimental errors include one standard deviation based on a full uncertainty analysis. **(B)** The ratio of calculation results with JENDL-4.0/HE and experimental data to the neutron energy.

total error of experiments was almost 10% or less. In these spectra, fine structures due to iron resonance were clearly observed around 10, 30, 100, 150, 200, 400, and 800 keV. Table 2 indicates *C/E* with one standard deviation for the accumulated neutron yields in the neutron energy region from 0.003 MeV–10 MeV in the iron shield for a 350-keV D-T neutron source.Overall, the PHITS calculation results agreed with the experimental data within a factor of 2 as shown in Table 2.

3.2 Leakage neutron spectra from various sphere piles with D-T neutrons

Figure 7A shows the leakage neutron energy spectra from sphere piles of aluminum, titanium, chromium, cobalt, arsenic, and tungsten with D-T neutrons. The experimental errors include only the statistical deviation of neutrons in the measurement. Figure 7B shows the ratio of calculation results and experimental data to the neutron energy. The relative error in measuring the niobium activation foils was less than 1%. The calculated results for Al, Ti, Cr, and As piles reproduce the experimental data within a factor of 1.5 over a wide neutron energy region for all energy bins. The calculated results for a W pile were lower than the experimental data by a factor of 2 at around 10 MeV due to the underestimation of peak neutrons by a factor of 2. The calculated results for a Co pile were lower than the experimental data by a factor of 1–2 below 10 MeV and by a factor of 1.5 at around 15 MeV. Table 3 lists *C/E* with one standard deviation for the accumulated neutron yields in the neutron energy region from 0.1 MeV–20 MeV from Al, Ti, Cr, Co, As, and W piles for a 250-keV D-T neutron source. The PHITS calculation results agreed with the experimental data within 20%.

3.3 Neutron energy spectra after transmission through concrete and iron shields using a quasi-monoenergetic neutron source

Figure 8A shows the neutron energy spectra after transmission through the iron and concrete shields for the TIARA experiment with the 43-and 68-MeV proton incident reactions on lithium target (NEA, 2022a). The experimental errors include one standard deviation based on a full uncertainty analysis. The solid line shows the results calculated with the proton and neutron data libraries, JENDL-4.0/HE, and the dashed line shows the results with the physics model, INCL4.6 (Boudard et al., 2013). These figures show that the JENDL-4.0/HE can simulate the peak neutron production. The peak indicates the discrete levels of excited nuclei generated by the proton-lithium reaction. JENDL-4.0/HE also reproduces the experimental data well in the continuum part of the energy spectrum. This is because the neutron data for nuclides in the shielding composition of JENDL-4.0/HE was correctly evaluated. Figure 8B shows the ratio of

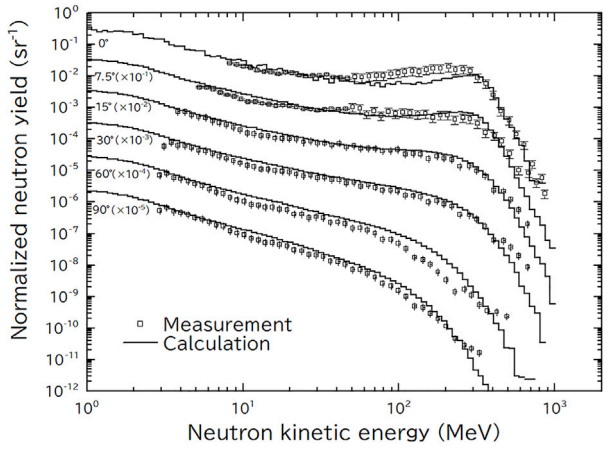

FIGURE 9
Normalized neutron yields for 400 MeV/u C-ion incidence on lead target. The experimental errors include one standard deviation based on an uncertainty analysis.

calculation results with JENDL-4.0/HE and experimental data to the neutron energy. For the 43-MeV proton incidence, the PHITS results agree with the experimental data within a factor of 2 except for the neutron energies below 10 MeV for iron. For the 68-MeV proton incidence, the PHITS results agree with the experimental data within a factor of 2 except for neutron energies around peak.

3.4 Thick target neutron yield produced by heavy-ion incident reaction at HIMAC

Figure 9 presents the measured normalized neutron yields for the lead target irradiated by 400 MeV/u C ions. The neutron detection efficiency of a BC501A was calculated by SCINFUL-QMD code (Satoh et al., 2006). The data were measured at various angles and then compared with the results of the calculation by PHITS. A broad peak was found in the yields in the forward direction, 0°. This peak was at the neutron energy equal to about 2/3 of the incident particle energy per ion. It would happen through the peripheral collisions between projectile and target nuclei. An ion strikes directly a neutron of the target nucleus, and transfers its momentum to the neutron. The broad peak energy was moved to a lower energy side and become broad due to the decrease of the incident particle energy in the target material.

Table 4 presents the comparisons between calculation and measurement in terms of accumulated neutron yield, based on a full uncertainty analysis (NEA, 2022b). Though the values of *C/E* depend on angles, they were found to be within a factor of 2. The evaluation report of these series of measurements using various targets and ion beams in HIMAC will be published in the International Criticality Safety Benchmark Evaluation Project Handbook (NEA, 2022b) by OECD/NEA.

Figure 10 shows the reaction rate distributions of ^{27}Al (x, α)^{24}Na, cadmium-covered ^{197}Au (n, γ)^{198}Au and bare ^{197}Au (n, γ)^{198}Au reactions. The experimental errors include one standard deviation based on an uncertainty analysis. As explained in the figure, the reaction rates along the 4 lines were scaled by 1,10,100 and 1,000.

Comparison of the measured and calculated reaction rates shows that the deviation is largest for ^{27}Al(x,X)^{24}Na reactions along the 15–45 cm axes in the 230 MeV/u He irradiation. This deviation probably came from the overestimation of source term neutrons because spallation induced by helium ions tends to be inaccurate owing to its cluster characteristics. A discrepancy of similar magnitude was observed for cadmium-covered ^{197}Au (n, γ) reactions at the depth from 0–20 cm for the 230 MeV/u He beam. Except for the systematic overestimation of ^{27}Al(x,X)^{24}Na reaction with 230 MeV/u He, the calculated and measured reaction rates at the depth of 60 cm agree within a factor of 2 as shown in Table 5. The reaction rates in the first 20 cm of depth are strongly dependent on the depth therefore a slight fluctuation of the depth leads to a large uncertainty of the ratios. To avoid this uncertainty, the ratios are calculated at 60 cm of depth where the reaction rate decline is exponential.

According to (Ogawa et al., 2011), the thick target neutron yield calculated by PHITS at the forward direction of 230 MeV/u He incident reaction is relatively high with neutron energies below 20 MeV and low with neutron energy above 20 MeV compared with FLUKA code (Ferrari et al., 2005; Battistoni et al., 2007). Moreover, in the first 20 cm of concrete, cadmium-covered ^{197}Au(n, γ) reactions are attributed to the source neutrons with energies below 20 MeV down-scattered in the concrete, while the reaction beyond a greater depth is attributed to the neutrons of higher energies. This explains why cadmium-covered ^{197}Au(n, γ) reaction rates are overestimated in the first 20 cm while the agreement is good in the deeper region (Ogawa et al., 2011). It means that source neutrons in a few MeV are important as the main contributor of the induced radioactivity maximum, which is found at 10–20 cm of depth.

4 Summary

In this study, we conducted benchmark studies of neutron shielding experiments for fusion, such as (1) Neutron spectra in iron shields with 14 MeV neutrons and (2) Leakage neutron spectra from various piles with D-T neutrons and for Accelerator-Driven Sub-Critical systems, such as (3) Neutron energy spectra after transmission through concrete and iron shields using a quasi-monochromatic neutron source (4) Thick target neutron yield produced by high-energy heavy ion incident reaction in a thick target and (5) Induced activity in shield exposed to particles produced by heavy ion irradiation in a target using the PHITS code.

The calculated neutron energy spectra in the case (1) using the nuclear data libraries, JENDL-4.0, agreed with the experimental data well in iron shields at various depths. For the Al, Ti, Cr, and As piles in the case (2), neutron energy spectra calculated using JENDL-4.0 agreed with the

TABLE 4 *C/E* with one standard deviation based on a full uncertainty analysis for the accumulated neutron yields for 400 MeV/u C-ion bombardment of lead target.

Angle	0°	7.5°	15°	30°	60°	90°
C/E	0.68 ± 0.16	1.16 ± 0.28	1.27 ± 0.30	1.36 ± 0.33	1.55 ± 0.37	1.35 ± 0.32

Induced activity in shield exposed to secondary particles produced by heavy ions on Fe.

10.3389/fenrg.2023.1085264

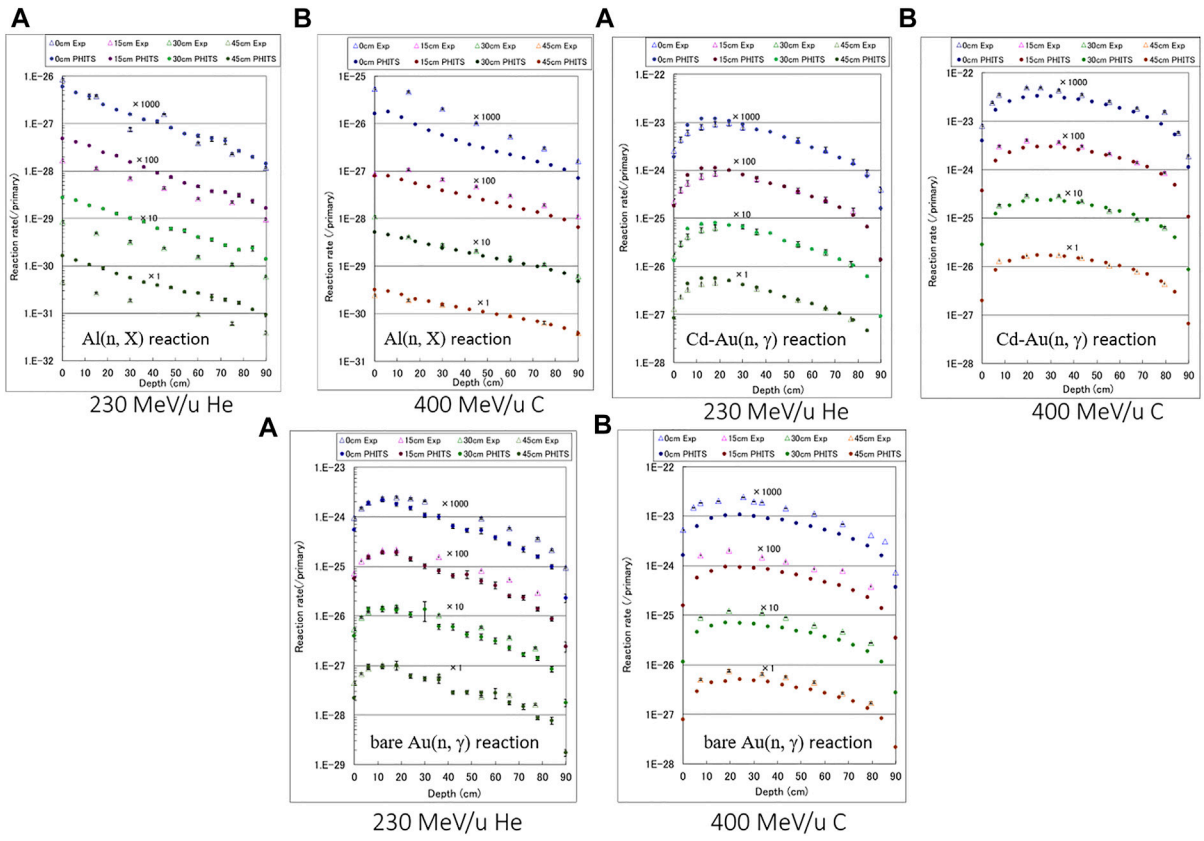

FIGURE 10
Reaction rate distributions of ^{27}Al (x, X)^{24}Na, ^{197}Au (n, γ)^{198}Au, and ^{197}Au (n, γ)^{198}Au reactions for **(A)** 230 MeV/u He reaction and **(B)** 400 MeV/u C reaction (Ogawa et al., 2011). The experimental errors include one standard deviation based on an uncertainty analysis.

TABLE 5 *C/E* **with one standard deviation for Al(n, X), Cd-Au(n, γ), and bare Au(n, γ) reaction rates at 60 cm of depth. The experimental errors include one standard deviation based on an uncertainty analysis.**

Al(n, X) reaction	Lateral coordinate			
	0 cm	15 cm	30 cm	45 cm
(a) 230 MeV/u He	2.30 ± 0.11	2.75 ± 0.14	2.83 ± 0.17	2.47 ± 0.13
(b) 400 MeV/u C	0.41 ± 0.02	0.59 ± 0.03	0.85 ± 0.04	0.95 ± 0.05
Cd-Au(n, γ)	Lateral coordinate			
	0 cm	15 cm	30 cm	45 cm
(a) 230 MeV/u He	0.71 ± 0.05	0.68 ± 0.05	0.68 ± 0.06	0.81 ± 0.05
(b) 400 MeV/u C	0.57 ± 0.03	0.56 ± 0.03	0.67 ± 0.03	0.74 ± 0.03
bare Au(n, γ)	Lateral coordinate			
	0 cm	15 cm	30 cm	45 cm
(a) 230 MeV/u He	1.22 ± 0.13	1.16 ± 0.13	1.03 ± 0.11	0.99 ± 0.11
(b) 400 MeV/u C	0.83 ± 0.03	0.94 ± 0.04	1.15 ± 0.04	1.11 ± 0.04

experimental values well. However, the calculated results for case (2) underestimate the experimental data for Co and W piles. The neutron energy spectra for case (3) using JENDL-4.0/HE reproduced the experimental data well because proton data library for lithium could simulated this reaction. The proton data library in JENDL-4.0/HE was essential for good reproduction of proton incident reactions. In case (4), the calculated results for a thick target neutron yield produced by 400 MeV per nucleon carbon incident reaction on lead showed good

agreements with the experimental data. For the case (5) with a neutron source produced by the 200–400 MeV per nucleon heavy-ion incident reaction, the calculated results of the reaction rate depth profiles of ^{197}Au (n, γ)^{198}Au reactions agreed with the experimental data within a factor of 2. Thus, the results of the PHITS calculations using the nuclear data library are in good agreement with the experimental data. Based on these findings, PHITS has been validated for usage in the domain in the design of advanced reactor systems such as fusion and ADS facilities. These experimental data are also useful in validating other Monte Carlo codes and evaluating nuclear data libraries for advanced reactor systems. The usage of the SINBAD database for fusion and ADS applications is also useful in benchmark shielding calculations with all Monte Carlo codes and evaluated nuclear data libraries.

Author contributions

YI, ST conceived the idea of the study. YI, ST, and TO contributed the review of shielding calculations. YI drafted the original manuscript. ST supervised the conduct of this study. YI, ST, and TO reviewed the manuscript draft and revised it critically on intellectual content. YI, ST, and TO approved the final version of the manuscript to be published.

Conflict of interest

The authors declare that the research was conducted in the absence of any commercial or financial relationships that could be construed as a potential conflict of interest.

Publisher's note

Supplementary material

The Supplementary Material for this article can be found online at: https://www.frontiersin.org/articles/10.3389/fenrg.2023.1085264/full#supplementary-material

References

Battistoni, G., Muraro, S., Sala, P. R., Cerutti, F., Ferrari, A., Roesler, S., et al. (2007). "The FLUKA code: Description and benchmarking," in *Proceedings of the hadronic shower simulation workshop 2006, batavia, ILL,6–8, september 2006*. Editors M. Albrow and R. Raja (Maryland: AIP), 31–49.

Boudard, A., Cugnon, J., David, J., Leray, S., and Mancusi, D. (2013). New potentialities of the Liege intranuclear cascade model for reactions induced by nucleons and light charged particles. *Phys. Rev. C* 87, 014606. doi:10.1103/PhysRevC.87.014606

Ferrari, A., Sala, P. R., Fasso, A., and Ranft, J. (2005). *Fluka: A multi-particle transport code*. Washington, D.C: United States. Department of Energy. CERN 2005-10, INFN TC 05/11, SLAC-R-773.

Furihata, S. (2000). Statistical analysis of light fragment production from medium energy proton-induced reactions. *Nucl. Instrum. Methods Phys. Res. B* 171 (3), 251–258. doi:10.1016/s0168-583x(00)00332-3

Goorley, T., James, M., Booth, T., Brown, F., Bull, J., Cox, L. J., et al. (2012). Initial MCNP6 release overview. *Nucl. Technol.* 180, 298–315. doi:10.13182/nt11-135

Iwamoto, Y., Hashimoto, S., Sato, T., Matsuda, N., Kunieda, S., Celik, Y., et al. (2022). Benchmark study of particle and heavy-ion transport code system using shielding integral benchmark archive and database for accelerator-shielding experiments. *J. Nucl. Sci. Technol.* 59, 665–675. doi:10.1080/00223131.2021.1993372

Iwamoto, Y., Sato, T., Hashimoto, S., Ogawa, T., Furuta, T., Abe, S., et al. (2017). Benchmark study of the recent version of the PHITS code. *J. Nucl. Sci. Technol.* 54, 617–635. doi:10.1080/00223131.2017.1297742

Kodeli, I., Sartori, E., and Kirk, B. (2006). "Sinbad - shielding Benchmark Experiments - status and planned activities," in Proceedings of the ANS 14th Biennial Topical Meeting of Radiation Protection and Shielding Division, Carlsbad, New Mexico, 2006 April 3–6.

Konno, C., Ikeda, Y., Kosako, Y., Oyama, Y., Maekawa, H., Nakamura, T., et al. (1991). Measurement and analysis of low energy neutron spectrum in a large cylindrical iron assembly bombarded by D-T neutrons. *Fusion Eng. Des.* 18, 297–303. doi:10.1016/0920-3796(91)90142-d

Kos, B., and Kodeli, I. (2019). *MCNP modelling of the TIARA SINBAD shielding benchmark, INDC(NDS)-0785*. Austria: IAEA.

Kunieda, S., Osamu, I., Nobuyuki, I., Tsutomu, O., Futoshi, M., Tatsuhiko, S., et al. (2016). "Overview of JENDL-4.0/HE and benchmark calculation," in JAEA-Conf 2016-004, Ibaraki, Japan, 19-20 Nov 2015, 41–46.

Kurosawa, T., Nakao, N., Nakamura, T., Uwamino, Y., Shibata, T., Nakanishi, N., et al. (1999). Measurements of secondary neutrons produced from thick targets bombarded by high-energy helium and carbon ions. *Nucl. Sci. Eng.* 132, 30–57. doi:10.13182/nse98-53

Mukaiyama, T., Takizuka, T., Mizumoto, M., Ikeda, Y., Ogawa, T., Hasegawa, A., et al. (2001). Review of research and development of accelerator-driven system in Japan for transmutation of long-lived nuclides. *Prog. Nucl. Energy* 38, 107–134. doi:10.1016/S0149-1970(00)00098-6

Nakao, N., Nakashima, H., Nakamura, T., Tanaka, S. i., Tanaka, S., Shin, K., et al. (1996). Transmission through shields of quasi-monoenergetic neutrons generated by 43- and 68-MeV protons —I: Concrete shielding experiment and calculation for practical application. *Nucl. Sci. Eng.* 124, 228–242. doi:10.13182/nse96-a28574

Nakashima, H., Nakao, N., Tanaka, S., Nakamura, T., Shin, K., Sakamoto, Y., et al. (1996). Transmission through shields of quasi-monoenergetic neutrons generated by 43- and 68-MeV protons —ii: Iron shielding experiment and analysis for investigating calculational method and cross-section data. *Nucl. Sci. Eng.* 124, 243–257. doi:10.13182/nse96-a28575

NEA (2022). International criticality safety benchmark evaluation project (ICSBEP) Handbook. Available at: https://www.oecd-nea.org/jcms/pl_20291/international-criticality-safety-benchmark-evaluation-project-icsbep-handbook (Accessed October 14, 2022).

NEA (2022). SINBAD website. Boulogne-billancourt. France: OECD/NEA. Available at: https://www.oecd-nea.org/jcms/pl_32139/shielding-integral-benchmark-archive-and-database-sinbad (Accessed October 14, 2022).

Ogawa, T., Morev, M., N., Iimoto, T., and Kosako, T. (2011). Measurements of induced activity in concrete by secondary particles at forward direction produced by intermediate energy heavy ions on an Fe target. *Nucl. Instrum. Methods B* 269, 1929–1939. doi:10.1016/j.nimb.2011.05.031

Ogawa, T., Sato, T., Hashimoto, S., Satoh, D., Tsuda, S., and Niita, K. (2015). Energy-dependent fragmentation cross sections of relativistic. *Phys. Rev. C* 92, 024614. doi:10.1103/PhysRevC.92.024614

ORNL (2022). RSICC website. Available at: https://www.ornl.gov/onramp/rsicc (Accessed October 14, 2022).

Sato, T., Iwamoto, Y., Hashimoto, S., Ogawa, T., Furuta, T., Abe, S., et al. (2018). Features of particle and heavy ion transport code system (PHITS) version 3.02. *J. Nucl. Sci. Technol.* 55, 684–690. doi:10.1080/00223131.2017.1419890

Satoh, D., Kurosawa, T., Sato, T., Endo, A., Takada, M., Iwase, H., et al. (2007). Reevaluation of secondary neutron spectra from thick targets upon heavy-ion bombardment. *Nucl. Instrum. Methods Phys. Res. A* 583, 507–515. doi:10.1016/j.nima.2007.09.023

Satoh, D., Sato, T., Shigyo, N., and Ishibashi, K. (2006). "SCINFUL-QMD:Monte Carlo Based Computer Code to calculate response function and detection efficiency of a liquid organic scintillator for neutron energies up to 3 GeV,". JAEA-Data/Code 2006-023. Available at: https://www.osti.gov/etdeweb/biblio/20890219.

Shibata, K., Iwamoto, O., Nakagawa, T., Iwamoto, N., Ichihara, A., Kunieda, S., et al. (2011). JENDL-4.0: A new library for nuclear science and engineering. *J. Nucl. Sci. Technol.* 48, 1–30. doi:10.1080/18811248.2011.9711675

Sub Working Group of Fusion Reactor Physics Subcommittee (1994). *Collection of experimental data for fusion Neutronics benchmark*. Tōkai, Ibaraki Prefecture: Japan Atomic Energy Research Institute.

frontiers | Frontiers in Energy Research

TYPE Original Research
PUBLISHED 08 February 2023
DOI 10.3389/fenrg.2023.1094285

OPEN ACCESS

EDITED BY
Mark David DeHart,
Idaho National Laboratory (DOE),
United States

REVIEWED BY
Di Yun,
Xi'an Jiaotong University, China
Luteng Zhang,
Chongqing University, China

*CORRESPONDENCE
Kyle M. Paaren,
kyle.paaren@inl.gov

SPECIALTY SECTION
This article was submitted to Nuclear Energy, a section of the journal Frontiers in Energy Research

RECEIVED 09 November 2022
ACCEPTED 11 January 2023
PUBLISHED 08 February 2023

CITATION
Paaren KM, Gale M, Medvedev P and Porter D (2023), Evaluation of BISON metallic fuel performance modeling against experimental measurements within FIPD and IMIS databases. *Front. Energy Res.* 11:1094285. doi: 10.3389/fenrg.2023.1094285

Evaluation of BISON metallic fuel performance modeling against experimental measurements within FIPD and IMIS databases

Kyle M. Paaren*, Micah Gale, Pavel Medvedev and Douglas Porter

Idaho National Laboratory, Idaho Falls, ID, United States

Simulations were conducted using the BISON fuel performance code on an automated process to read initial and operating conditions from two databases—the Fuels Irradiation and Physics Database (FIPD) and Integral Fast Reactor Materials Information System (IMIS) database. These databases contain metallic fuel data from the Experimental Breeder Reactor-II (EBR-II) and the Fast Flux Test Facility (FFTF). The work demonstrates use of an integrated framework to access EBR-II fuel pin data for evaluating fuel performance models contained within BISON to predict fuel performance of next-generation metallic fuel systems. Between IMIS and FIPD, there is enough information to conduct 1,977 unique EBR-II metallic fuel pin histories from 29 different experiments, and 338 pins from FFTF MFF-3 and MFF-5 with varying levels of details between the two databases. Each of these fuel performance histories includes a high-resolution power history, flux history, coolant channel flow rates, and coolant channel temperatures, and new model developments in BISON since the initial demonstration of this integrated framework. Fission gas release (FGR), cumulative damage fraction, fuel axial swelling, FCCI wastage thickness, cladding profilometry, and burnup were all simulated in BISON and compared to post-irradiation examination (PIE) results to evaluate BISON fuel performance modeling. Implementation of new fuel performance models into a generic BISON input file coupled with IMIS and FIPD yielded results with a better representation of physics than the initial evaluation of the integrated framework. Cladding profilometry, FGR, and fuel axial swelling were found to be in good agreement with PIE measurements for most of the pins simulated. The chosen mechanical contact solver was found to significantly impact the axial fuel swelling and cladding strain predictions when used in conjunction with the U-Pu-Zr hot-pressing model since it bound the fuel to prevent further swelling and increased hydrostatic stresses. This work suggests that fuel performance modeling in BISON under steady-state conditions represents the PIE data well and should be reassessed when new PIE data become available in IMIS and FIPD databases and when improved physical models to better capture fuel performance are added to BISON.

Abbreviations: ANL—argonne national laboratory; EBR-II—experimental breeder reactor-II; FCCI—fuel cladding chemical interaction; FCMI—fuel cladding mechanical interaction; FFTF—fast flux test facility; FGC—fission gas collected; FGP—fission gas produced; FGR—fission gas release; FIPD—fuels irradiation and physics database; GLASS—germanium-lithium argon-scanning system; HFEF—hot fuel examination facility; IMIS—integral fast reactor materials information system; INL—idaho national laboratory; LHGR—linear heat generation rate; MFF—mechanistic fuel failure; MOOSE—multiphysics object-orientated simulation environment; PIE—post-irradiation examination; SEE—Standard error of the estimate; SMR—small modular reactor; VTR—versatile test reactor.

KEYWORDS
BISON, metallic fuel, simulation, validation, assessment

Introduction

With the recent advances in development of Small Modular Reactors (SMRs) and the framework for their licensing, there is growing need to have a greater understanding of metallic fuels and associated fuel pin failure rates (Crawford et al., 2018; Williamson et al., 2021). The Versatile Test Reactor (VTR) will perform the necessary experiment scale tests to aid in acquisition of experimental data to provide insight for the development of next-generation nuclear reactors such as those being conceptualized by TerraPower and Oklo (Crawford et al., 2018). To prepare BISON to help the VTR and other next-generation reactor testing programs, BISON has been paired with the Fuels Irradiation and Physics Database (FIPD) and Integral Fast Reactor Materials Information System (IMIS), which supply post-irradiation examination (PIE) and fuel pin data from Experimental Breeder Reactor (EBR) II and Fast Flux Test Facility (FFTF) MFF-3 and 5 (Yacout et al., 2017; Oaks et al., 2019; Porter and Mariani, 2019). With the databases linked to BISON, proper assessment cases can be used to validate metallic fuel models within the BISON code (Paaren et al., 2021a). This work attempts to replicate the behavior and benchmark 29 EBR-II experiments with PIE data supplied through IMIS and FIPD, with an evaluation of BISON predicted burnup, axial fuel swelling, fission gas release (FGR), and cladding profilometry. Since the initial demonstration of the integrated framework, significant advances within BISON's metallic fuel performance modeling have been made, such as the inclusion of void swelling of cladding materials, integration of fuel cladding chemical interaction (FCCI) effects, capturing frictional contact, and integrating hot-pressing of U-Pu-Zr fuel to correct the overprediction of fuel swelling (Paaren et al., 2021b; Paaren et al., 2021c). These mechanics, with the exception of hot-pressing, were implemented in all 1,977 EBR-II BISON simulations so fuel performance for next-generation reactors can be evaluated.

Until relatively recently, Idaho National Laboratory (INL) and Argonne National Laboratory (ANL) have developed IMIS and FIPD to store EBR-II and FFTF MFF data for easy access in order to support model development and validation activities (Yacout and Billone, 2017; Yacout et al., 2017; Oaks et al., 2019; Porter and Mariani, 2019). Note that much of these data have yet to be qualified for use for fuel qualification. ANL is in the process of qualifying data to Nuclear Quality Assurance standards (Yacout and Billone, 2017). Each of these databases includes crucial reactor conditions needed to properly simulate a fuel pin within BISON. These reactor conditions include axial power and flux profiles for individual pins, average and the max linear heat generation rate (LHGR) for each operating cycle, reactor power, flux and fluence histories, and coolant boundary conditions. These reactor conditions from FIPD are read directly into the BISON fuel performance simulations for each fuel pin. Access to the reactor conditions used for each fuel pin in this work is controlled by Argonne National Laboratory (Yacout and Billone, 2017; Yacout et al., 2017; Oaks et al., 2019; Porter and Mariani, 2019). In addition to these reactor conditions, geometric dimensions and compositions of each pin are available, which will be used in this work for the inputs for the BISON fuel performance simulations (Yacout et al., 2017; Oaks et al., 2019; Porter and Mariani, 2019). PIE measurements available for BISON model comparison in this work includes 551 digitized cladding profilometry scans, 1,333 axial fuel swelling measurements, and 168 FGR measurements for EBR-II pins. Also available with this PIE collection from IMIS and FIPD are gamma scans, neutron radiograph, gas chemistry, irradiated pin weights, and laser profilometry measurements.

BISON, a finite element method code, is based off the Multiphysics Object-Orientated Simulation Environment (MOOSE). This allows users to create C++ objects for tightly coupled simulations, such as void swelling models (Williamson et al., 2016). BISON is capable of predicting fuel performance for a variety of fuel forms including light-water reactor fuel rods and metallic fuel (Medvedev, 2012; Hales et al., 2014). BISON solves the fully coupled thermomechanical equations and species diffusion for varying geometry. Fuel models within BISON include temperature, porosity, and burnup-dependent thermal properties, along with models that describe fuel behavior such as swelling from FGR (Galloway and Matthews, 2016). Mechanical and thermal contact were also modeled to allow for thermomechanical coupling and cladding profilometry comparisons with PIE data. The primary benefit of using BISON compared to other fuel performance codes is that BISON users can contribute their own C++ objects to the code and develop models BISON, such as void swelling correlations, FCCI correlations, and zirconium redistribution presented in prior works (Galloway, 2015; Matthews et al., 2017; Paaren et al., 2021b; Paaren et al., 2021c).

The irradiation-induced volumetric swelling models added into the BISON code were based off EBR-II and FFTF MFF fuel pins from the irradiation experiments. There have been multiple iterations and updates to these equations over the years, which were originally developed to predict the cladding strain and volumetric swelling of cladding while in a reactor system (Garner and Porter, 1988; Briggs et al., 1995; Garner, 2017; Hofman et al., 2019). Each of the volumetric swelling correlations depend on the volume change due to void formations and thermal precipitation-based densification, with SS316 having no thermal densification term (Garner and Porter, 1988; Briggs et al., 1995). Each correlation is dependent on temperature and fluence in the cladding material to predict the volumetric swelling. Time-dependent forms of these equations were utilized to allow users to integrate over the operating cycles of a reactor to capture time-dependent changes in-reactor operating conditions. These equations are shown in Eqs 1–11. Implementation of volumetric void swelling models for cladding materials was found to give BISON an improvement in cladding profilometry predictions for HT9, D9, and SS316 cladding for EBR-II experiments X421, X441, and X486 (Paaren et al., 2021b). These same equations were used in this work to evaluate all EBR-II pins available within the aforementioned databases. $\dot{S}_0$ is the fractional volume rate of change due to void swelling, and $\dot{D}$ is the fractional volume rate of change due to solid swelling. R is the swelling rate parameter, and varies for each cladding type, which is also true for the incubation parameter τ, and the curvature parameter α (Briggs

TABLE 1 Swelling constants and units.

Parameter	Constant and units	HT9	D9	SS316
Incubation Parameter	τ $10^{22}\frac{n}{cm^2 s}$	14.2	11.9	$6.58 - 0.566\beta$ $T < 848\ K$
				$4.3105 + 2.46\beta$ $T \geq 848\ K$
Curvature Parameter	α $10^{22}\frac{cm^2}{n}$	0.75	0.75	0.75

et al., 1995; Hofman et al., 2019; Paaren et al., 2021b). Temperature is in Kelvin, and neutron flux is in units of 10^{22}. Constant values and units for each cladding are available in Table 1.

$$\text{HT9}\ \frac{d\frac{\Delta V}{V_0}}{dt} = \dot{V} = \dot{S}_0 + \dot{D} \tag{1}$$

$$\text{D9}\ \frac{d\frac{\Delta V}{V_0}}{dt} = \dot{V} = \dot{S}_0 - \dot{D} \tag{2}$$

$$\text{SS316}\ \frac{d\frac{\Delta V}{V_0}}{dt} = \dot{V} = \frac{S_0}{(1 - S_0)^2} \tag{3}$$

$$\text{SS316}\ R = e^{\left(0.497 + 0.795\beta - 0.0948\beta^2 + 0.908\beta^3 - 1.49\beta^4\right)} + e^{\left(-8\left(\beta - 1.35\right)^2\right.} \tag{4}$$

$$\text{HT9}\ R = 0.085e^{\left(-0.0001\left(T - 673.15\right)^2\right)} \tag{5}$$

$$\text{D9}\ R = 2.76e^{\left(-0.00017\left(T - 773.15\right)^2\right)} \tag{6}$$

$$\text{SS316}\ \beta = \frac{T - 773}{100} \tag{7}$$

$$\text{All}\int \dot{V}dt = \sum \dot{V}dt = \frac{\Delta V}{V_0} \tag{8}$$

$$\text{All}\ \frac{dS_0}{dt} = \dot{S}_0 = \frac{0.01\phi Rt}{1 + e^{\alpha\left(\tau - \phi t\right)}} \tag{9}$$

$$\text{HT9}\ \frac{dD}{dt} = \dot{D} = 1.5 \cdot 10^{-4}\phi e^{-0.1\phi t} \tag{10}$$

$$\text{D9}\ \frac{dD}{dt} = \dot{D} = 0.3\phi e^{-30\phi t}\left(-1.7 \cdot 10^{-4}T + 0.241\right). \tag{11}$$

A model for FCCI from the LIFE-METAL fuel performance code has been previously implemented into BISON to estimate the wastage thickness formed on the interface between the metallic fuel and the cladding interior surface. It allows for the wastage to be calculated using time-at-temperature and either flux, burnup, or a combination of the two for HT9, D9, and SS316 cladding. These empirical correlations are seen in Eqs 12–14, with the coefficients fitted based on PIE data from EBR-II experiments. Within Eqs 12–14, ϕ is neutron flux, B is the at% burnup, R is the gas constant, T is temperature in Kelvin, and D_0, Q, k_0, and D_{i0} are empirical constants. Note that the burnup and flux-burnup empirical models are aonly available for HT9 cladding. Within this work, only the flux dependent model was used. These models and coefficients used may all be found within the BISON documentation and the work which they were derived in and in Table 2 (Hales et al., 2015; Paaren et al., 2021b). These same coefficients were also used in prior works (Galloway, 2015; Matthews et al., 2017; Paaren et al., 2021b; Paaren et al., 2021c). The flux mode was calibrated using a variety of EBR-II experiments where the burnup and flux-burnup modes were calibrated using only experiment X447 due to the high temperatures exhibited within the experiment (Carmack, 2012; Hales et al., 2015). To represent FCCI, these equations were used in conjunction with continuum damage mechanics to mimic the thinning of the cladding wall by applying an enhanced effective stress (Paaren et al., 2021c). The damage from FCCI results in a reduction in the effective stiffness of the material,

TABLE 2 Wastage constants and units.

Constant and units	HT9	D9	SS316
k_0 $\frac{m}{s^{0.5}}$	39.13	N/A	N/A
Q_b $\frac{J}{mol}$	252253	N/A	N/A
Q $\frac{J}{mol}$	201782	266102	266102
D_0 $\frac{m^2}{s}$	$1.122 \cdot 10^{-4}$	7.885	2.419
D_{10} m^4	$1.792 \cdot 10^{-39}$	$6.398 \cdot 10^{-38}$	$1.953 \cdot 10^{-38}$

and, in its simplest form, the fractional reduction in stiffness can be represented by a scalar damage index between 0 (undamaged state) and 1 (fully damaged) for a material. The implementation of continuum damage mechanics for FCCI in high temperature experiments such as EBR-II X447 allowed for significant improvement in cladding profilometry predictions for D9 and HT9 clad pins (Paaren et al., 2021c).

$$\text{FCCI Flux Dependent}\ \frac{\Delta w}{\Delta t} = \frac{1}{2}\left(D_0 e^{-\frac{Q}{RT}} + D_{i0}\phi\right)^{\frac{1}{2}} t^{\frac{-1}{2}} \tag{12}$$

$$\text{FCCI Burnup Dependent}\ \frac{\Delta w}{\Delta t} = 2B\left(k_0 e^{-\frac{Q_b}{RT}}\right) t^{\frac{-1}{2}} \tag{13}$$

$$\text{FCCI Flux} - \text{Burnup Dependent}\ \frac{\Delta w}{\Delta t} = 2B\left(D_0 e^{-\frac{Q}{RT}} + D_{i0}\phi\right)^{\frac{1}{2}} t^{\frac{-1}{2}}. \tag{14}$$

Within this work, it will be described how the data for 1,977 EBR-II experimental pins are compared to empirical fuel performance correlations from the databases to evaluate current metallic fuel performance models with advances in metallic fuel models from prior works. With the IMIS and FIPD databases, BISON models were created that encompassed a power and flux history, variable flowrates throughout each operating cycle, and as-fabricated dimensions. These models were compared to digitized PIE data for burnup, FGR, fuel axial swelling, and cladding profilometry. The 1,977 fuel pin models developed were compared with all PIE data available and were provided along with statistical assessment and discussion. To do this, the two databases were fed into a Python 3.8 script to create the BISON input files in order to compare the BISON simulation results to PIE data.

Methods

The integrated framework between BISON and the two databases demonstrated in prior work is utilized in combinations with advances in BISON metallic fuel performance models to simulate and evaluate 1,977 EBR-II fuel pins (Paaren et al., 2021a). Improvements to the

integrated framework include utilizing FIPD generated power, flux, and coolant flowrate histories similar to how reactor operating histories were parsed in the initial integrated framework (Paaren et al., 2021a). New material model advancements within the BISON code have been added to the integrated framework as well. The general BISON input file for an EBR-II pin fuel performance simulation is discussed, along with relevant EBR-II data available to be compared with simulation predictions. Methods for PIE comparison with simulation data are discussed.

General solution

All BISON simulations used in this work are based on an evolving EBR-II input file with the latest BISON fuel performance models, with FIPD data and reactor conditions written into the simulations for each individual pin. In total, the following process produced 1,977 BISON simulations for the current fuel pin data found within FIPD. Generic scripts were developed within Python to update and create new EBR-II simulations to compare fuel performance predictions to experimental measurements. Each BISON model consisted of 2D-RZ geometry to take advantage of axial symmetry. An aspect ratio of 25.18 was used to mesh the fuel and cladding in each BISON simulation due to fast convergence of each simulation with no artifacts in the results. The SmearedPelletMesh meshing scheme creates a mesh encompassing a fuel slug and cladding, with dimensions, axial elements, and horizontal elements being specified. This meshing scheme was used as it allows BISON to create the mesh directly. All reactor condition functions within the BISON simulations were supplied by FIPD using linear interpolation between timesteps to approximate power, flux, and flowrates. At the very end of each fuel pin irradiation, the modeled coolant temperature is set to 20°C for room temperature conditions, and the LHGR and neutron flux are set to zero to end power production and irradiation to mimic PIE measurement conditions. This is important as all PIE data were collected and measured under these conditions within the Hot Fuel Examination Facility (HFEF) facility at INL the volumetric heat source used in the EBR-II fuel pin simulations relies on coupling the fission reaction rate and LHGR history to calculate power generated in the fuel slug. The fission reaction rate is computed by applying the axial profile, dimensions, and LHGR profile of each fuel pin. These values were calculated from the Physics Analysis Database which is then fed into FIPD.

Mechanical and thermal contact were implemented in the BISON EBR-II fuel pin simulations to allow for gap conductance heat transfer and Fuel Cladding Mechanical Interaction (FCMI). Thermal contact was allowed from the outer surface of the fuel to the inside wall of the cladding to transfer heat, with a temperature-dependent thermal conductivity sodium gap between the outer fuel surfaces and inside the cladding (Fink and Leibowitz, 1995). As the fuel expands, swells, and contacts the cladding, sodium is forced out of the gap and heat is directly transferred to the cladding wall. GapHeatTransfer was used to account for this and to transfer heat between the fuel and the cladding wall. The gap conductance method displaces sodium into the plenum region to account for the expansion of the metallic fuel. Mechanical contact used Augmented Lagrange frictional contact for all simulations with a friction coefficient of $\mu = 0.2$ based off previous work (Paaren et al., 2021c). The contact solver chosen within BISON affects the forces exhibited on the fuel and cladding after FCMI occurs and the fuel continues to swell, which helps prevent excess axial fuel swelling by binding the fuel. The anisotropic factor used within the gaseous fuel swelling model, ranging from 0.24 to 0.9, is dependent on plutonium content (Karahan, 2010; Paaren et al., 2021c). Currently, this has little physical basis, but allows for a variable parameter to better fit the difference between radial and axial swelling.

Several boundary conditions were used for the BISON EBR-II fuel pins, which include fixing all surfaces on the axial line of symmetry with a Dirichlet condition. This sets the radial displacements to zero at those surfaces so no elongation or swelling occurred over the axial boundary line. The bottom of the cladding and fuel were given a Dirichlet condition, setting all axial displacements to zero at those surfaces. Doing so allows for a reference point to be established for swelling deformation. The pressure of the sodium coolant channel was set to a constant 0.151 MPa on the outside of the cladding (Galloway and Matthews, 2016). Initially, the internal plenum pressure of 0.086 MPa was applied to the fuel's outer surfaces and the inner surfaces of the cladding, and released fission gas was added as a function of fuel burnup to the plenum volume to create a new pressure (Galloway and Matthews, 2016). Material models used to describe material properties for the fuel and the cladding are listed in Table 3 with the corresponding BISON object. Documentation over blocks used within the BISON EBR-II fuel pin simulations may be found in the BISON documentation and BISON user's manual (Hales et al., 2015).

EBR-II pin information and post-irradiation examination data

The 1,977 pin simulations are spread across 29 experiments in EBR-II, with some fuel pins being involved in multiple irradiation cycles of experiments. Each of the EBR-II experiments performed was used to investigate various phenomena that occur within U-Pu-Zr fuel, such as FCCI in X447, FCMI with different smeared densities in X441, and EBR-II driver fuel qualifications in X448 and X486. Most of the experiments within EBR-II contained sub-experiments, such as X425 having subsequent irradiations labeled X425A, X425B, and X425C. During the operating cycles between each experiment, pins were pulled for axial growth and profilometry measurements, axial gamma scanning, and neutron radiography. These pins were then reloaded into new assembly hardware to be re-irradiated. This process allowed insight on time or burnup dependent fuel performance phenomena as irradiation progresses. In addition, multiple datapoints for a singular fuel pin allows for a larger dataset used in this evaluation of fuel performance models. A list of all available 29 EBR-II experiments detailing fuel and cladding types used is provided in Table 4.

Irradiation conditions, including pin-specific power and flux, axial power and flux profiles, coolant conditions, and as-designed and as-fabricated dimensions of each fuel slug and cladding within EBR-II is obtained from FIPD (Yacout and Billone, 2017; Yacout et al., 2017; Oaks et al., 2019; Porter and Mariani, 2019). These irradiation conditions are written into each BISON simulation and follow the reactor power history contained within the GLASS data. The fidelity of the GLASS data allows for the power and flux histories of EBR-II pins to change every 60 s and is used within these simulations. The irradiation conditions used within the

TABLE 3 BISON Objects used in BISON Simulations (Hales et al., 2015).

Phenomenon	Fuel	Cladding
Fuel Phase	PhaseUPuZr (Galloway et al., 2015)	N/A
Thermal Conductivity	ThermalUPuZr (Billone et al., 1968) (Savage, 1968)	ThermalHT9 (Hofman et al., 2019) (Yamanouchi et al., 1992)
		ThermalD9 (Hofman et al., 2019) (Banerjee et al., 2007) (Leibowitz and Blomquist, 1988)
		Thermal316 (Mills, 2002)
Density ($g{\cdot}cm^{-3}$)	15.8	7.8
Burnup	UPuZrBurnup (Olander, 1976)	N/A
Fission Rate	UPuZrFissionRate (Hales et al., 2015)	N/A
Elasticity Tensor	UPuZrElasticityTensor (Hofman et al., 2019)	HT9ElasticityTensor (Los Alamos National Laboratory, 2014)
		D9ElasticityTensor (Hofman et al., 2019)
		SS316ElasticityTensor
Creep	UPuZrCreepUpdate (Hofman et al., 2019)	HT9CreepUpdate (Hofman et al., 2019)
		D9CreepUpdate (Hofman et al., 2019)
		SS316CreepUpdate (Altenbach and Gorash, 2013) (Garner and Porter, 1988)
Thermal Expansion	UPuZrThermalExpansionEigenstrain (GeelHood and Porter, 2018)	HT9ThermalExpansionEigenstrain (Leibowitz and Blomquist, 1988)
		D9ThermalExpansionEigenstrain (Hofman et al., 2019) (Leibowitz and Blomquist, 1988)
		SS316ThermalExpansionEigenstrain (American Society of Mechanical Engineers, 2016) (Niffenegger and Reichlin, 2012)
Gaseous Swelling	UPuZrGaseousEigenstrain (Olander, 1976) (Karahan, 2010)	N/A
Fission Gas Release	UPuZrFissionGasRelease (Hofman et al., 1997)	N/A
Solid Swelling	BurnupDependentEigenstrain (Ogata and Takeshi, 1999)	N/A
Cladding Void Swelling	N/A	SS316VolumetricSwellingEigenstrain (Briggs et al., 1995)
		HT9VolumetricSwellingEigenstrain (Hofman et al., 2019)
		D9VolumetricSwellingEigenstrain (Hofman et al., 2019)
FCCI	N/A	MetallicFuelWastage (Hales et al., 2015)
		MetallicFuelWastageDamage (Hales et al., 2015)
CDF	N/A	FailureCladHT9 (Karahan and Buongiorno, 2010)
		FailureCladD9 (Briggs et al., 1995)

BISON simulations are available upon request and with access granted by ANL. Note that FIPD data is currently being merged into the BISON code, with plans to have dual BISON and FIPD users to have access to these irradiation conditions directly and simulate any of these assessment cases.

EBR-II PIE data within IMIS and FIPD used in this study included 1,337 axial swelling measurements, 551 cladding profilometry contact roller measurements, and 168 FGR measurements. In addition to this, FIPD provides calculated peak and average burnups, fuel temperatures, and cladding temperatures for each fuel pin during each operating cycle. These calculated parameters serve as a comparison for BISON predictions. The PIE data were usually measured within the HFEF facility at INL, with an internal temperature around 300 K. This is important, as the EBR-II fuel pins simulated in BISON need to be brought to 300 K for a direct comparison with PIE measurements. To do so, the LHGR history in BISON was set to zero after irradiation was completed, and the coolant channel temperature was set to 300 K. Uncertainty analyses for the BISON simulations and PIE data were not possible because uncertainties in the data and reactor conditions were not available. It is recognized that some models used in the conducted BISON simulations use empirical equations to describe phenomena, and occasionally expert bias may be present when performing measurements for PIE data, particularly axial fuel growth. This particularly refers to historical axial swelling measured by hand from neutron radiographs; however, new efforts have yielded implementation of image recognition software to determine axial swelling measurements from digitized radiographs (V Gribok et al., 2021).

TABLE 4 Pin information.

Experiment	Fuel Type(s)	Number of unique pins[a]	Cladding Type(s)	Peak linear power ($kW \cdot m^{-1}$)	Peak cladding temperature (K)	Peak fuel temperature (K)	Burnup (at%)	Fast fluence (10^{22} $n \cdot cm^2$)
X419	U-10Zr	89	D9	51.18	833.15	1007.15	12.41	12.01
	U-19Pu-10Zr							
	U-8Pu-10Zr							
X420	U-10Zr	80	D9	47.90	859.15	1003.65	18.13	18.54
	U-19Pu-10Zr							
	U-8Pu-10Zr							
X421	U-10Zr	80	D9	47.90	820.15	978.15	18.96	19.7
	U-19Pu-10Zr							
	U-8Pu-10Zr							
X423	U-10Zr	82	316SS	43.96	773.15	963.15	5.22	8.08
	U-19Pu-10Zr							
	U-22Pu-10Zr							
	U-26Pu-10Zr							
	U-3Pu-10Zr							
	U-8Pu-10Zr							
X425	U-10Zr	92	HT9	48.23	880.58	1000.58	19.9	20.67
	U-19Pu-10Zr							
	U-8Pu-10Zr							
X429	U-10Zr	65	316SS	45.93	843.58	986.15	14.18	13.86
	U-19Pu-10Zr		HT9					
	U-8Pu-10Zr							
X430	U-10Zr	52	HT9	50.85	864.58	1010.15	11.83	18.11
	U-19Pu-10Zr							
	U-22Pu-10Zr							
	U-26Pu-10Zr							
X431	U-10Zr	22	HT9	39.37	859.58	915.15	4.36	15.02
	U-2Zr							
	U-6Zr							
X432	U-10Zr	21	HT9	40.35	867.15	925.15	4.69	16.25
	U-2Zr							
	U-6Zr							
X435	U-10Zr	115	D9	47.90	803.15	918.15	20.21	22.28
X441	U-10Zr	72	D9	54.13	852.15	1039.15	12.91	10.11
	U-19Pu-10Zr							
	U-19Pu-14Zr							
	U-19Pu-6Zr							

(Continued on following page)

TABLE 4 (*Continued*) Pin information.

Experiment	Fuel Type(s)	Number of unique pins[a]	Cladding Type(s)	Peak linear power ($kW \cdot m^{-1}$)	Peak cladding temperature (K)	Peak fuel temperature (K)	Burnup (at%)	Fast fluence (10^{22} $n \cdot cm^2$)
X447	U-10Zr	53	D9	36.42	930.58	1000.15	9.99	9.18
			HT9					
X448	U-10Zr	68	HT9	46.59	807.15	918.15	14.79	14.89
X449	U-10Zr	61	HT9	32.81	846.58	911.58	11.44	10.55
X450	U-10Zr	61	HT9	36.09	869.15	940.15	10.25	9.51
X451	U-10Zr	65	HT9	35.43	916.58	983.15	12.92	12.06
X452	U-10Zr	61	D9	34.12	852.15	923.15	6.07	5.39
X453	U-10Zr	61	D9	34.12	845.58	917.15	9.35	8.46
X454	U-10Zr	61	D9	49.54	808.15	927.15	9.14	9.13
X455	U-10Zr	61	D9	50.20	810.15	933.15	9.18	9.17
X482	U-10Zr	123	316SS	40.68	890.58	967.15	14.92	14.73
	U-19Pu-10Zr		D9					
			HT9					
X483	U-10Zr	107	316SS	48.23	818.15	930.15	15.09	15.7
X484	U-10Zr	61	316SS	33.79	842.15	912.15	11.65	10.68
X485	U-10Zr	61	316SS	38.39	865.58	942.15	10.74	10.22
X486	U-10Zr	109	316SS	39.04	918.58	992.15	12.6	12.27
X489	U-10Zr	61	HT9	35.10	864.58	991.15	5.47	4.83
	U-19Pu-10Zr							
	U-28Pu-10Zr							
X492	U-10Zr	71	316SS	41.34	840.58	960.15	9.03	8.82
	U-19Pu-10Zr							
	ZR-U-10Zr							
	ZR-U-19Pu-10Zr							
X496	U-10Zr	37	HT9	61.68	794.15	982.15	5.95	4.15
X501	U-10Zr	61	316SS	46.46	790.58	955.15	4.72	4.24
	U-20.3Pu-1.3Np-2.1Am-10Zr		HT9					

[a]Includes replacement pins for those destructively examined during an interim experiment exam.

Simulation and post-irradiation examination comparison

For comparing BISON simulations to PIE data, BISON postprocessors and vector postprocessors were written to csv files to be read into Python. PIE profilometry data obtained from FIPD was read into Python from csv files as well. It is important to note that much of the EBR-II cladding contact profilometry PIE data was digitized by ANL from data directedly recorded to chart paper and is being qualified to Nuclear Quality Assurance quality standards. PIE measurements compared to BISON simulations include FGR, cladding profilometry, and fuel axial swelling, along with calculated burnup. These measurements and calculations were compared within Python, with statistical analysis performed. Standard deviations were provided for single value measurements, such as FGR, burnups, and axial fuel swelling. For cladding profilometry, the standard error of the estimate (SEE) was used as it takes into account the axial shift of the profiles by accounting for the differences between the two sets of data, as seen in Figure 1 and Eq. 11, with y being the BISON clad displacement, $\hat{y}$ being the PIE clad displacement, and n being the number of profilometry datapoints for each pin (Cohen, 1988; Everitt and Skrondal, 2010). For each axial height within the cladding

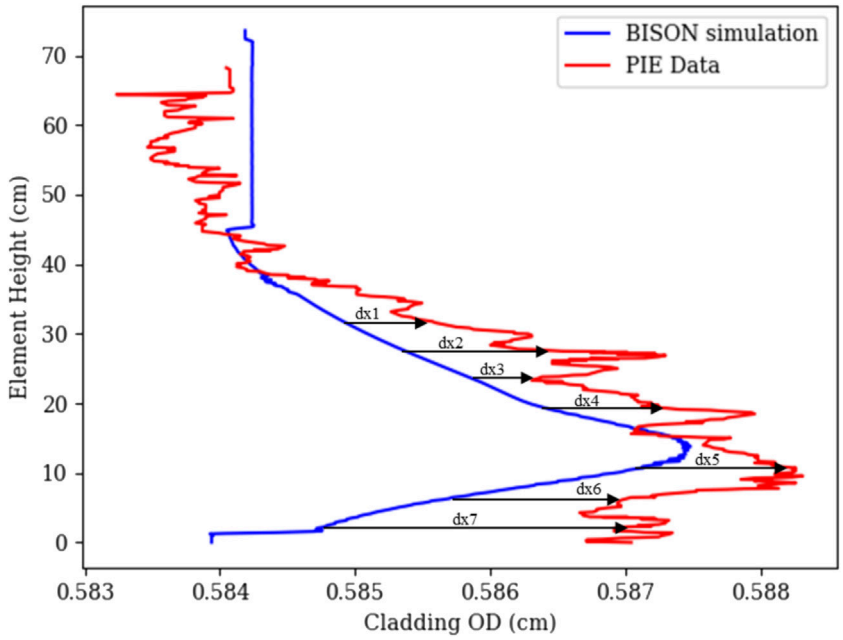

FIGURE 1
Profilometry profile statistical assessment with Standard Error of the Estimate (Paaren et al., 2021b; Paaren et al., 2021c).

profilometry PIE, the difference between the measured cladding diameter and BISON prediction was taken, then squared and summed, then divided by the number of axial positions for each pin to obtain the particular pin variance. For each pin's SEE value, the square root of the variance was taken.

$$SEE = \sqrt{\frac{\sum (y - \hat{y})^2}{n - 2}}. \tag{11a}$$

The cladding profilometry SEE, axial fuel swelling, calculated burnup, and FGR errors between the BISON simulations and PIE data were calculated for each pin among the 1,977 pins simulated in BISON. In addition to pin-wise statistics, the cladding profilometry SEE values for all 551 pins were reported to evaluate the cladding strain for various fuel and cladding types. A single value for SEE encompassing all 551 pins was reported along with the standard deviation. Creep is included in the cladding profilometry for both modeling and PIE data, the variability of which could affect the differences between the two in addition to differences caused from FCMI and FCCI. The oscillations seen within the experimental measurements is due to how contact profilometry is performed. Traditionally, mechanical rollers are used and roll along the outer diameter of the cladding. Small spikes and oscillations may occur due to dirt and debris being on the cladding wall during PIE measurements, or from manufacturing tolerances of EBR-II cladding, which was ±0.0005" (0.00127 cm) (Paaren et al., 2021b; Paaren et al., 2021c).

Results

To illustrate the capabilities developed, 1,977 pins were simulated within BISON from 29 different EBR-II experiments that applied operating conditions obtained from IMIS and FIPD for each pin. The pins discussed in the results below represent different smeared densities, irradiation lengths of time, cladding materials, fuel compositions, and linear heat rates to demonstrate how BISON and the databases can assess different metallic fuel pins that undergo different conditions. Burnup results obtained from BISON simulations were in agreement with IMIS and FIPD values. Cladding profilometry simulation results presented in this section were compared to PIE cladding profilometry, with SEE provided for each of the 551 pins. The highest SEE values observed were 85% smeared density pins, due to BISON overpredicting FCMI. FGR from BISON simulations were predicted around 70%, where 81 PIE FGR measurements did not exceed 73% on average. Implementation of frictional contact allowed for better BISON predictions for axial fuel elongation, with most for the 1,337 pins underpredicting PIE measurements by 1.2 cm. Overall, the development of new BISON material models and fitting of empirical coefficients has significantly improved the predictability of BISON to model metallic fuel performance.

Burnup

The average burnup values obtained from all BISON simulations were compared to FIPD, with the difference between the two values displayed in Figure 2. The difference in peak burnup values between the BISON simulations and FIPD are displayed in Figure 3. Because the reactor power history data were written into the BISON input files, excluding the short durations of power reduction and ascension at the beginning and end of the operating cycles (as explained earlier in this paper), burnup rate is fairly constant over time, with deviation form linearity at burnups exceeding 10 at%. This also contributes to BISON underpredicting

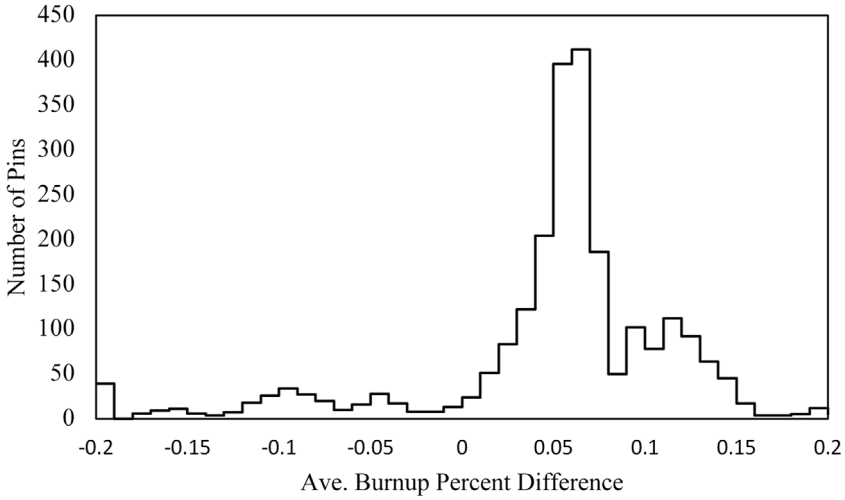

FIGURE 2
Difference in average burnup between BISON and Fuels Irradiation and Physics Database (BISON subtracted from FIPD).

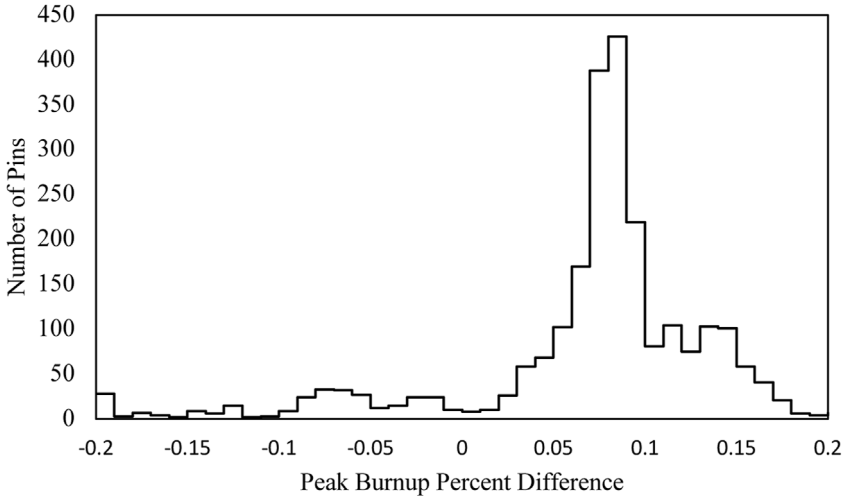

FIGURE 3
Difference in peak burnup between BISON and Fuels Irradiation and Physics Database (BISON subtracted from FIPD).

the burnup of most pins by 5%. The energy per fission assumed within the BISON simulations was 3.2×10^{-11} J. This assumption breaks down for non-plutonium bearing pins and higher enriched uranium fuel, both of which EBR-II are contained within EBR-II. This is due to the energy released per fission being unique to each isotope in the fuel. Accounting for plutonium production, isotopic enrichment, and decay in the BISON simulations would lead to better agreement between FIPD and the BISON simulations, as the increased energy per fission would lead to a higher burnup by ~5% due to the increased energy per fission (210 Mev for ^{239}Pu and 200 Mev for ^{235}U). Likewise, BISON peak burnup would increase from this as well, but at different rate due to plutonium bearing and non-plutonium bearing fuel. This is seen in Figure 4, with two distinct peaks formed.

Differences in peak burnup values between BISON and FIPD were larger than average burnup values due to not accounting for zirconium redistribution within the modeling efforts. Allowing zirconium to redistribute within the fuel matrix creates a zirconium depletion zone in the beta-phase of fuel, which is then filled with uranium migrating from the gamma and alpha phases. This creates a uranium rich zone leading to increased local fission rates and burnup. Overall, BISON is able to accurately predict average burnup results of metallic fuel with the current burnup material model in the BISON code after accounting for plutonium breeding and initial isotopic enrichment. Adding zirconium redistribution into BISON simulations would increase peak burnup, allowing for better agreement with FIPD burnup values. In each case, BISON simulations underpredicted peak burnup. This was expected due to zirconium redistribution

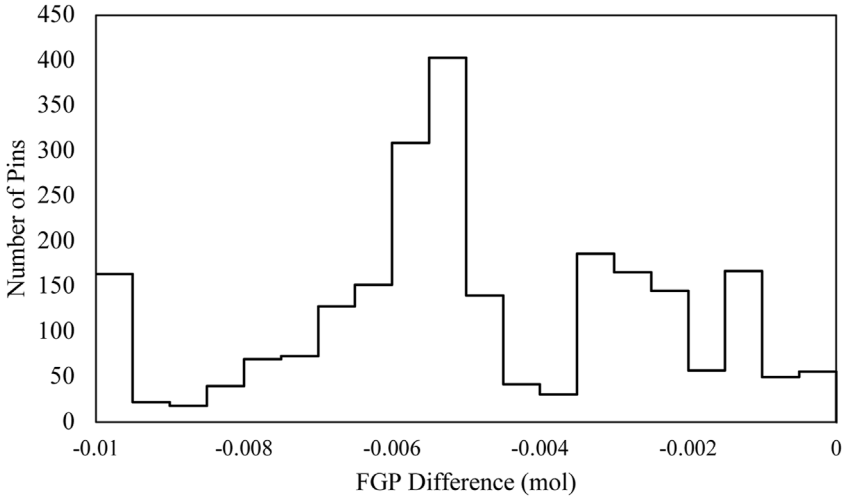

FIGURE 4
Fission gas produced comparison (BISON subtracted from FIPD).

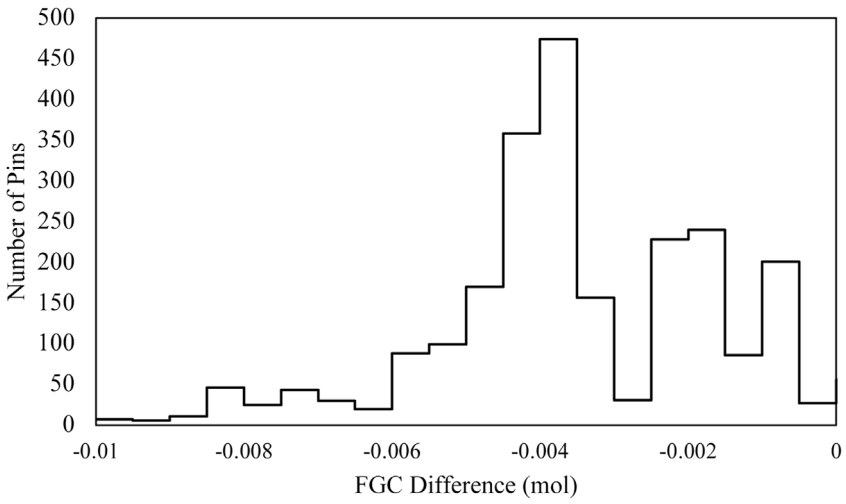

FIGURE 5
Fission gas collected comparison (BISON subtracted from FIPD).

not being enabled, not accounting for operating cycle disruptions, and fission energy from plutonium and plutonium production. FIPD use the average LHGRs recorded for a pin to calculate burnup, where BISON uses the average fission rate density of the current and previous timestep (Paaren et al., 2021a).

FISSION gas release

FGR predictions from the BISON simulations were compared to PIE measurements within the IMIS database for 81 of the fuel pins presented, with the other pins using a correlation developed in IMIS (Paaren et al., 2021a). Each of the fuel pins simulated in BISON predicted more FGR than was measured experimentally within the HFEF. Values for the fission gas produced (FGP), fission gas collected (FGC), and FGR fraction predicted from BISON results were compared to the 81 PIE measurements. Other pins used correlations within the IMIS database from these 81 measured pins to estimate FGP, FGC, and FGR percent for other EBR-II fuel pins not selected for measurements. Comparison of these parameters (IMIS estimated vs. BISON predictions) are shown in Figures 4–6. FGC is measured by puncturing the cladding and measuring the pressure differential in a controlled volume. Using the ideal gas law and the temperate of the hot cell, the total number of moles from fission gas production was calculated. Of the fission gas collected, the amount of fission gas produced (including gas still contained within the fuel), is determined by analyzing the number of krypton gas moles released into the controlled volume, and assuming 25% of the fission gas is

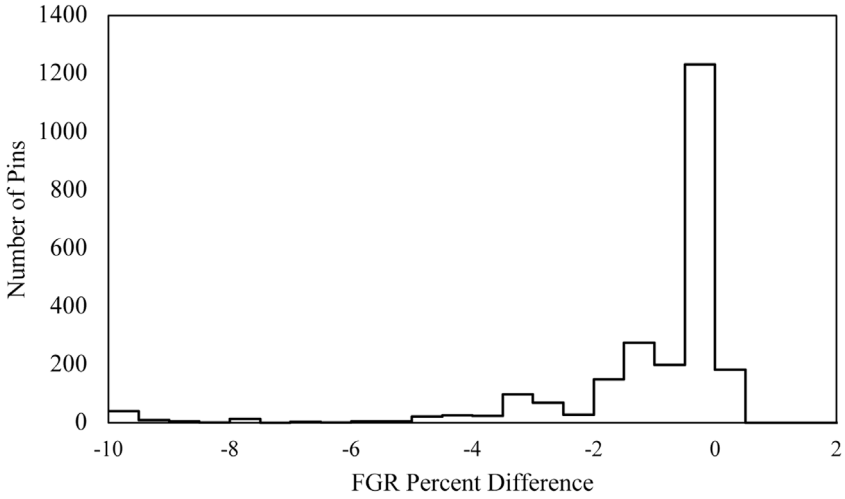

FIGURE 6
Fission gas release comparison (BISON subtracted from FIPD).

retained within the fuel, for both measurements and BISON simulations. Fission gas release percent is simply the ratio of FGC over FGP.

When comparing the values of FGR fraction, FGP, and FGC, between BISON and PIE measurements, FGR values found to be in agreement with BISON underpredicting FGP and FGC. BISON calculates FGP by incorporating porosity and the average fission rate in each element in the U-Pu-Zr FGR material model, but IMIS multiplies the burnup by the number of moles of fissile material in each fuel pin and the fission gas yield fraction to determine the amount of moles from FGP (Hofman et al., 1997). The maximum FGR fraction that BISON simulations can reach is 73.5% and is based on IMIS data. The data itself have considerable scatter and has a non-linear regression R^2 value of 0.67. The BISON simulations represent the IMIS FGR data fairly well, with subtle differences in the FGR fraction. Pins simulated in BISON that differed by more than 2% for FGR had an average burnup less than 1 at %. This is important, as the BISON model does not allow for fission gas to be released from the fuel until terminating porosity is reached, which is speculated to occur between 1-2 at % burnup. Allowing for terminating porosity to occur sooner in BISON would have led to better predictions of FGR for low burnup pins. To increase the accuracy of the BISON model, more FGR experimental measurements need to be performed for both low and high burnup pins to generate a better correlation, such as the data gathered for legacy pins from the FFTF MFF experiments.

Cladding profilometry and fuel axial swelling

Within 29 different experiments simulated, 551 of the pins had cladding profilometry measurements available for BISON comparison, with Figure 7 highlighting BISON's ability to predict cladding strain. For pins with CW316 SS cladding, BISON was able to predict the cladding strain with good agreement, with the highest SEE being 26.5 μm for a CW316 SS pin (J630). This is due to the cladding profilometry being highly dependent on the CW316 SS void swelling and creep models, with FCMI contributing a minimum amount. Both the shape and magnitude of the cladding strain for CW316 SS pins were in agreement. Most of the strain is created by void swelling in the cladding and not entirely dependent upon stresses induced on the cladding by fuel swelling or fission gas pressure. The same cannot be said with D9 cladding pins, with void swelling over and underpredicting cladding strain data. This may be due to lower-numbered experiment (X419—X421) pins not utilizing Germanium-Lithium Argon-Scanning System (GLASS) power history data before operating cycle 139A as it was not available. This allowed for pins irradiated in early operation cycles to utilize effective full power days within the BISON simulations to achieve FIPD fluence values. Although this simulates the FIPD fluence, the temperature history within the fuel and the cladding are averaged over the operating cycle duration, creating lower than expected operating temperatures and discounting important phenomena at higher temperatures, such as creep.

Within Figures 7D, F, the size and profile of the main bulge at fuel centerline (~17 cm) are dependent on the cladding material, cladding temperature, irradiation-induced creep, and the amount of force the fuel is exerting on the cladding at each element. The amount of irradiation creep is indirectly controlled by the axial flux profile used in the BISON simulations and the magnitude of the fast neutron flux. The neutron flux also affects the amount of void swelling in cladding materials in conjunction with temperature. In addition to this, higher burnup pins impart more stress on the cladding though FCMI, allowing for more irradiation and potentially thermal creep. These three effects, when modeled simultaneously, compound and overpredict cladding strain. For the pins in Figures 7D, F, pin T069 and T709 contained plutonium and exceeded burnups of 12 at %. This high burnup and plutonium content simulated increased fuel swelling and anisotropic proportionality constant, leading to the overprediction of cladding strain. The strain seen over the entire cladding wall is due to plenum pressure created from FGR and irradiation-induced creep. For most pins, this is neglected, as the digitized PIE cladding profilometry does not extend for the whole fuel element length, such as T325.

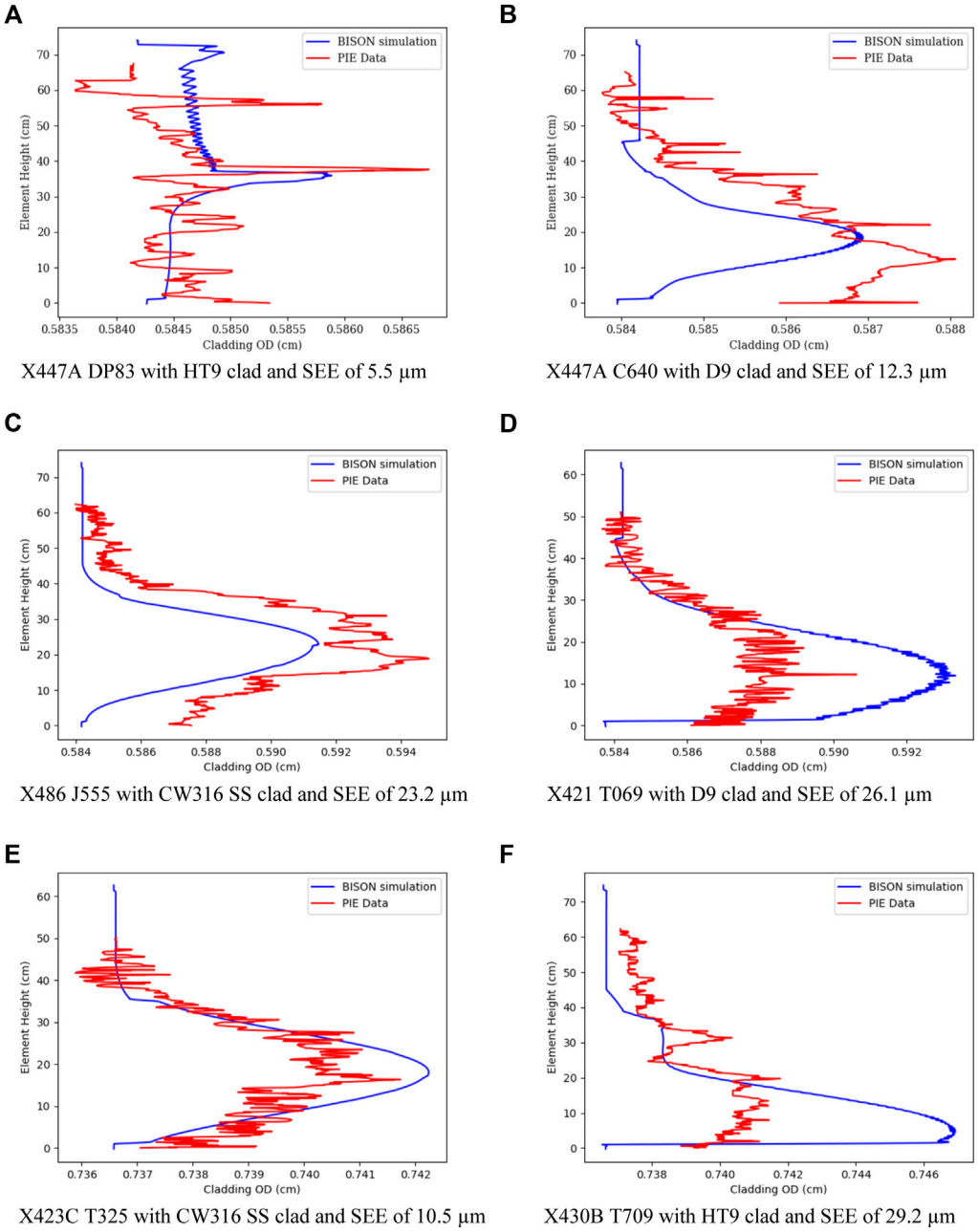

FIGURE 7
Profilometry comparisons of EBR-II fuel pins with various fuel compositions and claddings.

Two examples of cladding profilometry for each cladding type are provided within Figure 7 to show the impact irradiation conditions and different fuel compositions impact fuel performance and profilometry predictions. For the case of HT9 cladding in Figures 7A, F, and upper peak within both PIE measurements and BISON predictions are seen near the top of the fuel (~35–39 cm), which is due to thermal creep. In the case of Figure 7A, pin DP83 underwent a moderate LHGR (~35 kW·m^{-1}) with a reduced flowrate to increase cladding temperatures. These increased cladding temperatures accelerated FCCI, thermal creep, and increased cladding strain. Pin T709 in Figure 7F had a similar LHGR to DP83 but had plutonium within the fuel in addition to a higher coolant flowrate, larger fuel diameter, and higher burnup. These lower cladding temperatures simulated in Figure 7F allowed for less FCCI and thermal creep, resulting in lower cladding strain near the top of the fuel. In the case of the two SS316 profilometry examples shown in Figures 7C, E, differences between the BISON profilometry predictions are contributed to different irradiation conditions, fuel composition, and fuel diameter.

One fuel performance phenomenon not considered within this modeling scope, due to simulation time, was the addition of a hot-pressing model developed for U-Pu-Zr fuel. This model allows for pore collapse reducing the overall amount of volumetric swelling in the fuel. This would significantly aid pins simulated with SEE values

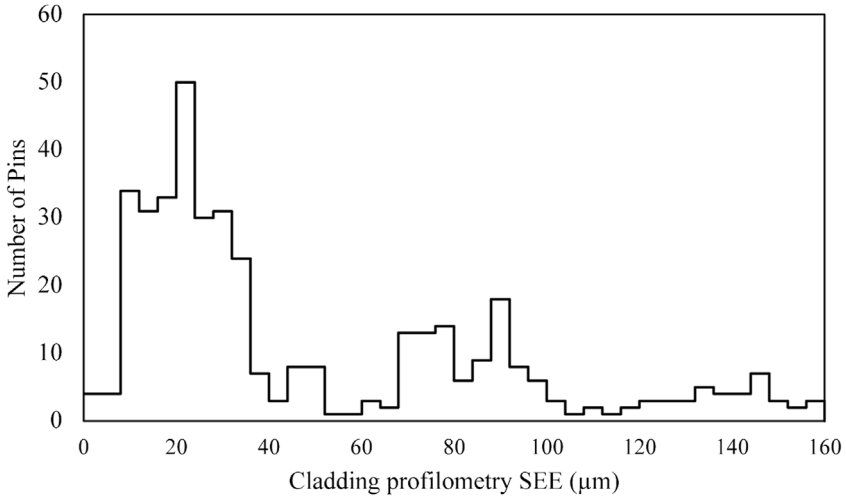

FIGURE 8
Cladding profilometry Standard Error of the Estimate values.

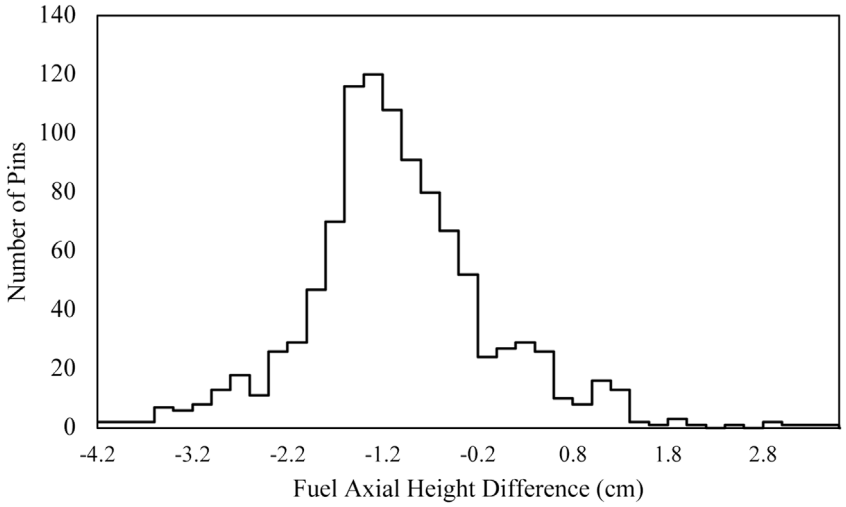

FIGURE 9
Difference in axial fuel swelling length between BISON and Fuels Irradiation and Physics Database (FIPD subtracted from BISON).

greater than 30 μm in Figure 8 (Paaren et al., 2022). Within Figure 8, there are a significant number of pins with SEE values greater than 60 μm, with all being either 85% smeared density, plutonium bearing fuel, or both in the case of DP45 from X441. The high SEE values suggest that the anisotropic swelling proportionality constant is not plutonium dependent, as all plutonium bearing pins overpredicted cladding strain. Removing the anisotropic swelling proportionality constant would decrease SEE values for plutonium bearing pins and increase the axial fuel swelling height, reducing the difference between BISON and PIE measurements in Figure 9.

The friction coefficient used in the simulations also affects the fuel axial swelling, with a friction coefficient greater than 0.2 resisting the axial growth of the fuel (Medvedev, 2012; Hales et al., 2014). The difference in axial fuel height between BISON and PIE measurements is displayed in Figure 9, underpredicting the axial growth of most of the pins by 1.2 cm. In all cases, BISON underpredicts axial fuel lengths of irradiated pins. Implementation of a hot-pressing model for U-Pu-Zr fuel and removal of the anisotropic proportionality constant, in conjunction with zirconium redistribution, would allow for the modulus of elasticity and Poisson's ratio to decrease, allowing for more swelling and creep in the radial direction while limiting overprediction of cladding strain. Efforts are currently being implemented to see how these material models used in conjunction will affect the results produced from a smaller set of BISON EBR-II fuel pin simulations.

Within FIPD, there are unique axial fuel swelling lengths that BISON simulation results may be compared to. Of the unique axial fuel swelling lengths available, some pins contain multiple measurements after each sub-experiment. An example of this is pin T707 containing axial fuel swelling lengths for X430, X430A, and

X430B, each with BISON simulation results to compare to. The axial fuel swelling measurements were subtracted from the corresponding BISON simulations to generate the histogram presented in Figure 9. Note that the histogram contains EBR-II fuel pins with different dimensions, cladding materials, fuel compositions, and irradiation histories although the majority of fuel meat in EBR-II pins had a fabrication height of ~13.5 in. Figure 9 shows in the majority of fuel pins simulated, axial fuel swelling height for the majority of pins was underpredicted, largely due to the direction of swelling controlled by the plutonium-dependent anisotropic proportionality constant. Although only 356 pins within this evaluation contained plutonium, this shows that the fuel swelling material model used in conjunction with the anisotropic proportionality constant does not adequately predict axial fuel swelling. Although the average axial fuel swelling height in BISON simulations is underpredicted by 1.2 cm, this a significant improvement compared to 7 cm overprediction of previous simulations (Medvedev, 2012; Hales et al., 2014).

Discussion

This automated BISON analysis shows it is possible for EBR-II pin information to be supplied in a BISON input file, and simulation results compared to PIE measurements from IMIS and FIPD. This capability serves as the initial benchmark in validating metallic fuel models on a large scale, as well as benchmarking material models in development. The databases used contain the pin dimensions, power history, flux history, axial profiles for power and neutron flux, calculated temperature profiles, coolant channel boundary conditions, burnup calculations, FGR measurements, fuel axial swelling, cladding profilometry, fission product concentrations, and other pin-associated data. The biggest challenge with this work was having discrepancies between fuel pins that utilize the same material and geometric dimensions but contain different resultant PIE measurements. The discrepancies between the BISON simulations and PIE measurements were discussed, along with possible sources of uncertainty within BISON material models, and reactor conditions within IMIS and FIPD.

Since the initial demonstration of linking BISON to IMIS and FIPD for generating EBR-II fuel performance simulations, several new material models have been implemented to enhance BISON's prediction capabilities by describing fuel performance phenomenon using empirical models, such as void swelling of cladding materials, FCCI coupled with damage mechanics for HT9 and D9 cladding, and hot-pressing of the U-Pu-Zr fuel matrix. Each of these, when appended to the BISON general input file, has increased predictions against PIE measurements including cladding strain and axial fuel swelling (Paaren et al., 2021b; Paaren et al., 2021c). However, both the U-Pu-Zr hot-pressing model and the UPuZrGaseousEigenstrain model use an anisotropic proportionality constant to describe the anisotropic swelling nature that is exhibited in Pu-bearing metallic fuels. However, these phenomena can be replicated without the use of this proportionality constant, by including zirconium redistribution into the modeling efforts. This is due to the Young's modulus decreasing with increased plutonium and zirconium content within the fuel matrix, allowing for more creep and deformation in the axial direction when gravity is included in the simulations. The zirconium depletion layer would create a stiff beta-phase matrix relative to the soft gamma and alpha-phase uranium surrounding it. This is represented by correlations in Eqs 15–24 (Hofman et al., 2019).

$$\text{Young's modulus (Pa) } E = E_U{}^*E_T{}^*E_p{}^*E_w \tag{15}$$

$$\text{Pure Uranium at 588 K } E_U = 1.6{}^*10^{11} \tag{16}$$

$$\text{Porosity correction } E_p = 1 - 1.2p \tag{17}$$

$$\text{Weight percent correction } E_w = \frac{1 + 0.17W_{Zr}}{1 + 1.34W_{Zr}} - W_{Pu} \tag{18}$$

$$\text{Temperature correction } E_T = \left(1 - 1.03\left(\frac{T - 588}{T_{mu}}\right)\right) - 0.3f\left(1 - 1.06\left(\frac{T^a_{end} - 588}{T_{mu}}\right)\right). \tag{19}$$

E_U is the Young's modulus for pure uranium at 588 K, E_p is the porosity correction factor, with p being porosity, W_{Zr} and W_{Pu} being zirconium and plutonium weight fractions, p being porosity, and T^a_{end} being the end transition temperature of alpha-phase uranium. The Poisson's ration is adjusted in a similar manner for the fuel matrix, with T_{mu} being the meting temperature of uranium.

$$\text{Poisson's Ratio } V = V_U{}^*V_T{}^*V_p{}^*V_w \tag{20}$$

$$\text{Pure Uranium at 588 K } V_U = 0.24 \tag{21}$$

$$\text{Porosity correction } V_p = 1 - 0.8p \tag{22}$$

$$\text{Weight percent correction } V_w = \frac{1 + 3.4W_{Zr}}{1 + 1.9W_{Zr}} \tag{23}$$

$$\text{Temperature correction } V_T = 1 + 1.2\left(\frac{T - 588}{T_{mu}}\right) \tag{24}$$

In addition to the anisotropic proportionality constant being plutonium dpendent and controlling the direction of the swelling, the total swelling of the fuel, which is modeled being burnup dependent, plays a significant role in FCMI, stresses, and cladding strain. Using a burnup dependent swelling model for 75% smeared density pins leads to overprediction of cladding strain at higher burnups above 8.6 at. %, and underprediction at lower burnups below 8.6 at. %. When simulating higher smeared density pins, such as 85% smeared density pins from X441, simulated cladding strain was overpredicited at lower and higher burups (4 at % and 8.6 at. %). This shows the need to implement a porosity collapse model based off FCMI stress and creep rate used in previous work (Paaren et al., 2021b; Paaren et al., 2021c).

Other modeling characteristics that may cause discrepancies between the BISON simulations and the PIE measurements is the uncertainty of the reactor operating conditions, including reactor power, fluence, and flowrate conditions. As shown in previous work, a fluctuation in base power can significantly affect fuel performance predictions (Galloway et al., 2015; Paaren et al., 2021c). In addition to the uncertainty within reactor power, EBR-II reactor power history is not available for operating cycles before 139A and after 167A. This leads to relying on the FIPD average LHGR values for each of those operating cycles, leaving out important temperature-dependent fuel performance phenomenon that would otherwise be captured if power oscillations were included. This simplification only impacts low and high numbered EBR-II experiments, such as X421 and X496.

While this paper is intended to demonstrate the direct connection of high-fidelity fuel performance modeling using BISON with a large experimentally obtained database to evaluate fuel performance models

for metallic fuel, this study revealed sophisticated interplay of the different phenomena previously described in the literature, but never coupled together. Specifically, that the implementation of U-Pu-Zr hot-pressing and zirconium redistribution need to be coupled together in general metallic fuel modeling and evaluated against the IMIS and FIPD databases to assess the improvement.

The BISON results presented in evaluating metallic fuel models used input conditions from FIPD to produce fuel performance predictions and compared them to PIE measurements. Each PIE parameter acted as a validation check for the BISON simulation results, where the BISON results are highly dependent on modeling parameters chosen in the input files and the reactor conditions supplied by the database. This large comparison shows that uncertainty analysis is needed in addition to incorporating new material models for a better benchmark with the EBR-II data. This would remove the need for proportionality constants such as anisotropic proportionality constant from the code. Depending on the proportionality constants used within BISON, different BISON input files can be statistically fitted to PIE measurements. This shows the need to have defined input parameters for various metallic fuel models to yield the best quantitative results. This is difficult to evaluate because the BISON code is constantly changing due to new material models being committed.

Conclusion

The purpose of this work was to evaluate metallic fuel performance predictions from the BISON code against experimental data contained within the IMIS and FIPD databases, measured from pins out of in-reactor experiments. Here, all 1,977 unique pins within FIPD were modeled within BISON to produce simulation results validated with PIE comparisons. The BISON simulations coupled with IMIS and FIPD have proven successful in predicting average burnup for metallic fuel pins irradiated in EBR-II, but underpredict peak burnup values compared to the data in IMIS and FIPD. Cladding profilometry, fission gas behavior (FGR, FGP, and FGC), and axial fuel swelling were examined as well then compared to PIE measurements within the databases. Cladding profilometry was evaluated using SEE to determine the fitment of BISON-predicted profilometry to the PIE profilometry measurements. Agreement was seen between CW316 SS clad pins, with D9 and HT9 clad pins both overpredicting and underpredicting FCMI and cladding strain at higher burnups. The FGR for the BISON simulations were in agreement with PIE measurements, but more experimental measurements for both very low and high-burnup metallic fuel pins need to be performed to further optimize the BISON model for FGR in U-Pu-Zr fuel. Axial fuel swelling predicted by BISON underrepresented the PIE measurements by ~1.2 cm for most pins. With BISON overpredicting cladding strain and underpredicting axial fuel swelling, a combination of models influencing fuel swelling should be explored. Additionally, the uncertainty of in-reactor operating conditions and empirical material models should be considered when evaluating metallic fuel performance. This modeling work shows that BISON simulations may be created and evaluated using IMIS and FIPD data to compare corresponding PIE measurements for benchmarking and validating advances in metallic fuels and changes to the BISON code. As models become more advanced and the BISON code evolves by using this process for inspection, this tool will be adapted to validate new metallic fuel models.

Data availability statement

The original contributions presented in the study are included in the article/supplementary material, further inquiries can be directed to the corresponding author.

Author contributions

KP: Conceptualization, Methodology, Software, Validation, Formal analysis, Investigation, Resources, Data Curation, Writing—Original Draft, Preparation, Writing—Review and Editing, Visualization MG: Writing—Review and Editing, Supervision, Project administration, Funding acquisition Pavel Medvedev: Writing—Review and Editing, Supervision, Project administration, Funding acquisition DP: Resources, Writing—Review and Editing, Supervision, Project administration, Funding acquisition.

Funding

This research made use of the resources of the High Performance Computing Center at Idaho National Laboratory, which is supported by the Office of Nuclear Energy of the U.S. Department of Energy and the Nuclear Science User Facilities under Contract No. DE-AC07-05ID14517.

Acknowledgments

The authors acknowledge Adam X. Zabriskie, Stephen R. Novascone, Nancy J. Lybeck, Aaron Oaks, Kun Mo, and Abdellatif Yacout for providing review input, knowledge, and experimental data.

Conflict of interest

The authors declare that the research was conducted in the absence of any commercial or financial relationships that could be construed as a potential conflict of interest.

The handling Editor declared a shared affiliation with the authors at the time of review.

Publisher's note

References

Altenbach, H., and Gorash, Y. (2013). *Advanced materials modelling for structures*. 1st. Verlag Berlin Heidelberg: Springer.

American Society of Mechanical Engineers (2016). *ASME boiler and pressure vessel code*. New York, NY: Boiler and Pressure Vessel Committee

Banerjee, A., Raju, S., Divakar, R., and Mohandas, E. (2007). High temperature heat capacity of alloy D9 using drop calorimetry based enthalpy increment measurements. *International Journal of Thermophysics*, 28, 1, 97–108. doi:10.1007/s10765-006-0136-0

Billone, M. C., Liu, Y. Y., Gruber, E. E., Hughes, T. H., and Kramer, J. M. (1968). "Status of fuel element modeling codes for metallic fuels," in Proceedings American Nuclear Society Internaionl Conference on Reliable Fuels for Liquid Metal Reactors. Beijing China

Briggs, L. L., Il Chang, Y., and Hill, D. J. (1995). *Safety analysis and technical basis for establing an interim burnup limit for mark-V and mark-VA fueled subassemblies in EBR-II*. Argonne National Lab. ANL, Argonne, IL

Carmack, W. J. (2012). *Temperature and burnup correlated fuel-cladding chemical interaction in U-10Zr metallic fuel*. University of Idaho. Moscow, ID, USA

Cohen, J. (1988). *Statistical power analysis for the behavioral sciences*. Department of Psychology University NY China 2nd.

Crawford, D. C., Steven, L., and Powers, J. J. (2018). A proposed startup fuel for the versatile test reactor. *Trans. Am. Nucl. Soc.* 118.

Everitt, B. S., and Skrondal, A. (2010). *The cambridge dictionary of statistics*. 4th. New York: Cambridge University Press.

Fink, J. K., and Leibowitz, L. (1995). *Thermodynamic and transport properties of sodium liquid and vapor*. Argonne, Illinois.

Galloway, J. D. (2015). Fully-coupled metallic fuel performance simulations using BISON. *LA-UR* 15-26773.

Galloway, J. D., and Matthews, C. (2016). Enhancements to BISON U-Zr metallic fuel X447 example problem. https://www.osti.gov/biblio/1329651

Galloway, J., Unal, C., Carlson, N., Porter, D., and Hayes, S. (2015). Modeling constituent redistribution in U-Pu-Zr metallic fuel using the advanced fuel performance code BISON. *Nucl. Eng. Des.* 286, 1–17. doi:10.1016/j.nucengdes.2015.01.014

Garner, F. A., and Porter, D. L. (1988). Irradiation creep and swelling of AISI 316 to exposures of 130 dpa at 385-400 C. *J. Nucl. Mat.* 155, 1006–1013. doi:10.1016/0022-3115(88)90458-8

Garner, F. A. (2017). Swelling, creep and embrittlement of D9 stainless steel cladding and duct irradiated in three FFTF driver fuel assemblies to high neutron exposures. *Twelfth Int. Ural. Semin. Radiat. Damage Phys. Mater. alloy. Abstr.* 109.

GeelHood, K. J., and Porter, I. E. (2018). Modeling and assessment of EBR-II fuel with the US NRC's fast fuel performance code. *Proc. Top Fuel* 12.

Hales, J. D., and Zhao, M. (2015). BISON users manual - BISON release 1. *Ida. Falls* 2.

Hales, J. D., Novascone, S. R., Spencer, B. W., Williamson, R. L., Pastore, G., and Perez, D. M. (2014). Verification of the BISON fuel performance code. *Ann. Nucl. Energy* 71, 81–90. doi:10.1016/j.anucene.2014.03.027

Hofman, G. L., Billone, M. C., Koenig, J. F., and Kramer, J. M. (2019). *Metallic fuels handbook*. NY China

Hofman, G. L., Walters, L. C., and Bauer, T. H. (1997). Metallic fast reactor fuels. *Prog. Nucl. Energy* 31 (1), 83–110. doi:10.1016/0149-1970(96)00005-4

Karahan, A., and Buongiorno, J. (2010). A new code for predicting the thermo-mechanical and irradiation behavior of metallic fuels in sodium fast reactors. *J. Nucl. Mat.* 396, 283–293. doi:10.1016/j.jnucmat.2009.11.022

Karahan, A. (2010). *Modeling of thermo-mechanical and irradiation behavior of mixed oxide fuel for sodium fast reactors*. Massachusetts Institute of Technology. Cambridge, MA

Leibowitz, L., and Blomquist, R. A. (1988). Thermal conductivity and thermal expansion of stainless steels D9 and HT9. *Int. J. Thermophys.* 9, 873–883. doi:10.1007/bf00503252

Los Alamos National Laboratory (2014). AFCI materials handbook, materials data for particle accelerator applications, chapter 18 - Design properties of HT9 and Russian ferritic/martensitic steels. *Rev* 6.

Matthews, C., Galloway, J., Unal, C., Novascone, S., and Williamson, R. (2017). BISON for metallic fuels modelling, https://inis.iaea.org/collection/NCLCollectionStore/_Public/48/088/48088059.pdf, IAEA-CN245-366

Mills, Kenneth C. (2002). *Recommended values of thermophysical properties for selected commercial alloys*. Woodhead Publishing. Sawston, Cambridge

Niffenegger, M., and Reichlin, K. (2012). The proper use of thermal expansion coefficients in finite element calculations. *Nucl. Eng. Des.* 243, 356–359. doi:10.1016/j.nucengdes.2011.12.006

Oaks, A., Mo, K., Mohamed, W., and Yacout, A. (2019). "Development of FIPD: The EBR-II fuels irradiation and physics database," in Proceedings of the Top Fuel 2019: IIght Water Reactor Fuel Performance Conference, Beijing China.

Ogata, T., and Takeshi, Y. (1999). Development and validation of ALFUS: An irradiation behavior analysis code for metallic fast reactor fuels. *Nucl. Technol.* 128, 113–124. doi:10.13182/nt99-1

Olander, D. R. (1976). *Fundamental aspects of nuclear reactor fuel elements*. Technical Information Center, Energy Research and Development Administration. Souel Korea

Paaren, K. M., and Chen, L. (2021). BISON fuel performance modeling optimization for experiment X447 and X447A using axial swelling and cladding strain measurements. *Nucl. Eng. Des.* 10.

Paaren, K. M., Gale, M. D., Medvedev, P. G., and Porter, D. L., "Fuel performance analysis of fast flux test facility MFF-3 and -5 fuel pins using BISON with post irradiation examination data," *J. Nucl. Mat.*, vol. TBD, no. TBD, p. 16, 2022.

Paaren, K. M., Gale, M., Kerr, M. J., Medvedev, P. G., and Porter, D. L. (2021). Initial demonstration of Automated fuel performance modeling with 1,977 EBR-II metallic fuel pins using BISON code with FIPD and IMIS databases. *Nucl. Eng. Des.* 37, 1,

Paaren, K. M., Lybeck, N., Mo, K., Medvedev, P. G., and Porter, D. L. (2021). Cladding profilometry analysis of experimental breeder reactor-II metallic fuel pins with HT9, D9, and SS316 cladding. *Energies* 14, 515. doi:10.3390/en14020515

Medvedev, P. G., "Fuel performance modeling results for representative FCRD irradiation experiments: Projected deformation in the annular AFC-3A U-10Zr fuel pins and comparison to alternative designs," *Ida. Natl. Lab. Rep.*,) 13 no. September, p. INL/EXT-12-27183, 2012, doi:10.2172/1091354

Porter, D., and Mariani, R. D. (2019). *Archiving EBR-II metallic fuel test data using NDMAS to accelerate fast reactor fuel qualification*. United States: Idaho National Lab.

Savage, H. (1968). The heat content and specific heat of some metallic fast-reactor fuels containing plutonium. *J. Nucl. Mat.* 25 (3), 249–259. doi:10.1016/0022-3115(68)90168-2

V Gribok, A., Porter, D. L., Paaren, K. M., Gale, M. D., Middlemas, S. C., and Lybeck, N. J. (2021). Automatic information extraction from neutron radiography imaging to estimate axial fuel expansion in EBR-II. *J. Nucl. Mat.* 557–153250. doi:10.1016/j.jnucmat.2021.153250

Williamson, R. L., Gamble, K., Perez, D., Novascone, S., Pastore, G., Gardner, R., et al. (2016). Validating the BISON fuel performance code to integral LWR experiments. *Nucl. Eng. Des.* 301, 232–244. doi:10.1016/j.nucengdes.2016.02.020

Williamson, R. L., Hales, J. D., Novascone, S. R., Pastore, G., Gamble, K. A., Spencer, B. W., et al. (2021). BISON: A flexible code for advanced simulation of the performance of multiple nuclear fuel forms. *Nucl. Technol.* 207, 954–980. doi:10.1080/00295450.2020.1836940

Yacout, A. M., Oaks, A., Mohamed, W., and Mo, K. (2017). Fipd: EBR-II fuels irradiation and physics database. https://www.osti.gov/biblio/1480520

Yacout, B. A. M., and Billone, M. C. (2017). Pre-licensing evaluation of legacy SFR metallic fuel data. *ANL-ART* 76.

Yamanouchi, N., Tamura, M., Hayakawa, H., and Kondo, T. (1992). Accumulation of engineering data for practical use of reduced activation ferritic steel: 8%Cr-2%W-0.2%V-0.04%Ta-Fe. *J. Nucl. Mat.* 191–194, 822–826. doi:10.1016/0022-3115(92)90587-b

frontiers | Frontiers in Energy Research

TYPE Methods
PUBLISHED 14 February 2023
DOI 10.3389/fenrg.2023.1085857

OPEN ACCESS

EDITED BY
John Darrell Bess,
JFoster & Associates, LLC (JFA),
United States

REVIEWED BY
Larry Greenwood,
Pacific Northwest National Laboratory (DOE), United States
David Brown,
Brookhaven National Laboratory (DOE), United States
Mark Stoyer,
Lawrence Livermore National Laboratory (DOE), United States

*CORRESPONDENCE
Steven van der Marck,
✉ vandermarck@nrg.eu

SPECIALTY SECTION
This article was submitted to Nuclear Energy, a section of the journal Frontiers in Energy Research

RECEIVED 31 October 2022
ACCEPTED 03 February 2023
PUBLISHED 14 February 2023

CITATION
van der Marck S and Koning A (2023), STEK: A potential fast spectrum benchmark for fission product cross sections.
Front. Energy Res. 11:1085857.
doi: 10.3389/fenrg.2023.1085857

STEK: A potential fast spectrum benchmark for fission product cross sections

Steven van der Marck[1]* and Arjan Koning[2]

[1]Nuclear Research and consultancy Group (NRG), Petten, Netherlands, [2]International Atomic Energy Agency (IAEA), Vienna International Centre, Vienna, Austria

The reactivity worth of many fission product samples was measured in fast spectrum conditions in the STEK facility during the early 1970s. These results were then used to improve and validate nuclear data evaluations for fission products, but in the last 2 decades STEK has not been used: the nuclear data evaluations for fission products in the current versions of libraries like ENDF/B or JEFF have not been tested against STEK results. Here we argue that the STEK data are still valuable, because there is no other data set that can replace them, and the interest in fast spectrum conditions is picking up strongly of late. It should be considered to evaluate whether a benchmark can be defined for the International Reactor Physics Experiments Handbook.

KEYWORDS

fast spectrum, cross section, fission product, benchmark, reactor

1 Introduction

There is an increasing effort underway to design new nuclear reactors (IAEA 2022). While many initiatives involve designs that are evolutionary in that they are largely based on the designs of the currently operational reactor fleet, it is noticeable that there are serious developments towards fast spectrum reactors. Some of these are developed in the Generation-IV framework, while more recently a strong push towards small modular reactors (SMR) has given rise to new fast spectrum designs (IAEA 2020; OECD 2021).

This leads to a situation where there is a need for experimental data to support such designs. Given that the defining feature of these designs is their fast neutron spectrum, the cross section data in this spectrum warrant special attention. The last period during which there was a similar need was, arguably, the 1970s–1980s, when fast breeder reactors were under design.

In that period the STEK experiment was performed in Petten, the Netherlands. The experiments were performed with a reactor that consisted of a thermal spectrum outer 'driver' zone, coupled to a fast spectrum inner zone. In the middle of the inner zone was an experimental facility in which a sample could be moved into and out of the reactor core. In this way the reactivity worth was measured for many samples, among which many fission product samples, in five different spectrum conditions.

The STEK results were used for the development of various nuclear data library versions at the time: JEF-1 (Janssen et al., 1986), JEF-2.2 (Dietze et al., 2001) and JENDL-3.2 (NEA 2001) are examples of this. Since then several newer versions of the same libraries were released, but the use of the STEK experiments during library development was discontinued without other integral data being used instead.

Because of the recent developments in fast reactor designs, we argue that the results of the STEK experiments are still (or again) valuable today, together with other measurement

data of the same period such as RRR/SEG (Rossendorf, Germany). In 2003 all available information on the STEK experiments, including more than 25 technical reports, was sent to the OECD/NEA Databank, where it was digitized and archived under the name NEA-1714 IRPhE/STEK (OECD/NEA, 2022). In the current way of working in the international reactor physics field, the measurements should be evaluated in the framework of the International Reactor Physics Experiments Handbook. Once that is done the experimental results would become more easily available to whoever needs them to support their fast spectrum reactor design. Such benchmark definitions of past measurement campaigns would allow progress in the field before new integral experiments are performed.

In this paper a high level description is given of the STEK facility (Section 2), together with an overview of the measurements results that were obtained (Section 3). The role that these results have played in the past in nuclear data developments is reviewed (Section 4), to clarify the potential of this set of measurements to improve the quality of future nuclear data for fission products, especially for fast spectrum conditions.

2 The STEK facility

The STEK facility was built around 1970 in the framework of the cooperation on fast breeder reactor development between (then Western) Germany and the Benelux countries (Belgium, Netherlands and Luxemburg). The main objective was to perform integral measurements of fission product cross sections. These cross sections were determined from central reactivity worth measurements, using an oscillator technique. The zero power reactor consisted of a thermal spectrum driver zone on the outside and a fast spectrum inner center of the core.

The central fast zone, in a cylindrical inner tank of 1,060 mm diameter and 1,275 mm height, had fuel elements on a rectangular grid surrounded by rows of lead and graphite assemblies, acting as reflector and buffer zones. The fast fuel assemblies were stacks of high enriched (90 wt%) uranium and graphite platelets, held together by aluminum boxes. The uranium platelets had areas of 50.63×50.63 mm^2 or 43.0×43.0 mm^2, thickness of 1.4 mm or 0.7 mm, and a 15 μm nickel coating.

Depending on the number and type of the platelets, different levels of spectrum hardness could be realized by changing the ratio of carbon atoms to ^{235}U atoms (C/U). The fuel elements with high C/U ratio contained less fissile material than the ones with low C/U, and therefore, for the higher C/U cases, more fuel elements were needed to achieve criticality. In total five different cores were built, with C/U ratios ranging from C/U = 11 for the fastest spectrum to C/U = 72 for the least fast spectrum. The number of fuel elements varied from 49 for the fastest spectrum core to 129 for the core with the least fast spectrum. The number of graphite and lead elements varied accordingly, from 88 lead elements and 104 graphite elements for the fastest spectrum core to 56 and 56 elements for the core with the least fast spectrum.

Surrounding the inner, fast spectrum zone was an annular tank, made of aluminum, with an outer diameter of 2,140 mm and a height of 1,360 mm. The ring is subdivided in four equal sectors, each comprising of about 80° of the annulus. These four sectors were separated by four graphite blocks, through which beam tubes gave access to the central part. In each of the four sectors 10 plate type fuel elements were placed, moderated by water. These elements, with a cross section of 77×150 mm^2, consisted of boxes in which 5 to 16 fuel plates were placed. The plates were made of high enriched (90 wt%) UAl_4 with Al cladding. The number of plates per elements depended on the composition of the fast, central zone. The radial reflector outside the annular tank consisted of water.

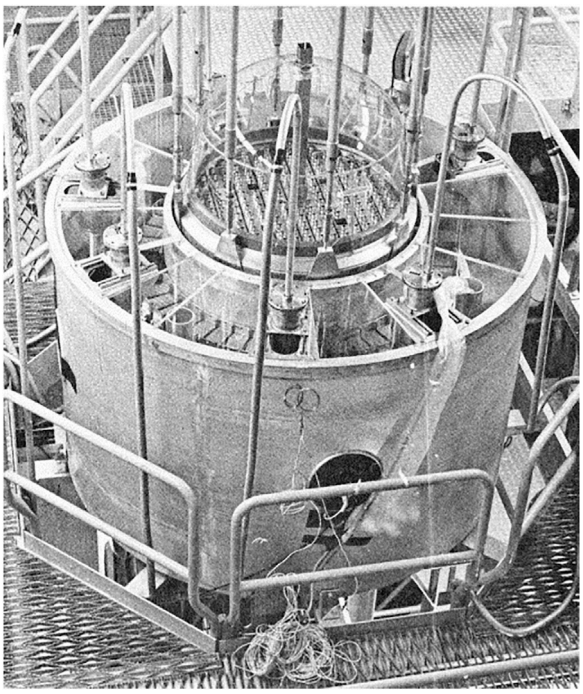

FIGURE 1
The STEK facility.

In the center of the fast zone a normal fuel element could be replaced by a square guide tube, in which a special oscillator element was placed, connected to a driving system to move the element with a velocity in the range of 1–10 m/min. The effective length of the guide tube was 1,200 mm, penetrating the core from top to bottom. In this guide tube the 2,600 mm long oscillator element could be moved up and down. The oscillator element was subdivided into 53 compartments by stainless steel-304 partitions. Most of the compartments were filled with fast fuel material, except for compartments 15 and 41, which were alternately in the center of the core during oscillation measurements. One of the two compartments contained a sample, whereas the other compartment was empty. In order to reduce the (small) effect of the reactor and the oscillation element not being fully symmetric in the axial direction, two measurements were performed for each sample: one with the sample in compartment 15, and the other measurement with the sample in compartment 41. Also, measurements for a dummy reference sample were performed, with the reference sample having the same composition and weight as the packing of the original sample. The distance between compartments 15 and 41 was 1,248 mm.

A photo of STEK is shown in Figure 1. The annular tank with the thermal spectrum driver zone can be seen clearly, as well as the cylindrical, fast spectrum inner zone containing a rectangular grid with fuel elements. Also visible, in the center of the facility, sticking

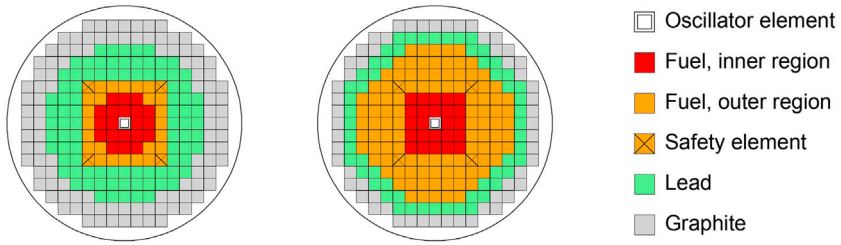

FIGURE 2
A schematic core map of the inner core regions of STEK-500 (left) and STEK-4000 (right). The outside "driver" fuel zone with a thermal spectrum is not visible in this picture, beyond the outer ring.

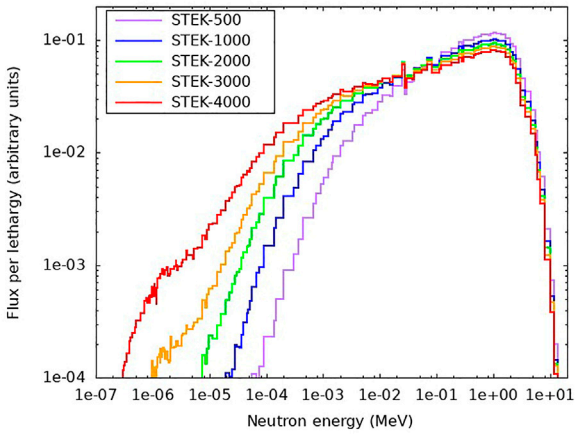

FIGURE 3
The neutron spectrum in the sample position in the five core configurations of STEK.

out at the top, is the rectangular guide tube for the oscillator element. More detailed (schematic) core maps of the inner core region of the STEK-500 and STEK-4000 configurations are shown in Figure 2.

The neutron spectrum in the center of the five different core configurations was recently calculated using MCNP models made by Da Cruz et al. (2013). The results are shown in Figure 3. The fastest spectrum, for the configuration labeled STEK-500, the neutron flux starts to drop precipitously below approximately 10 keV, with virtually no flux left below 0.1 keV. For the most thermal spectrum, STEK-4000, the flux drops significantly only below 1 keV, and the spectrum extends down to thermal energies, around 0.3 eV. It is this wide range of neutron spectra that makes the STEK measurements almost unique.

3 Measurement data

3.1 Measurements and analysis

Fission reaction rate measurements were performed in all five core configurations, in a location very close to the center of the core. These reactions were measured with fission chambers for the nuclides ^{233}U, ^{238}U, ^{232}Th, ^{237}Np, ^{239}Pu, ^{240}Pu, and ^{242}Pu. The results were reported as reaction rate ratios relative to the ^{235}U fission reaction rate. For ^{235}U and ^{238}U also reaction rate traverses were measured, both in the axial and radial directions. These measurements enabled a characterization of the neutron spectrum, as well as a determination of the ^{235}U fission rate as part of the normalization of the reactivity worths to be measured.

For the reactivity worth measurements, the neutron flux level was measured by one or more compensated ionization chambers located in the region around the thermal core, either in the water reflector or in one of the beam tubes. Another chamber, used for verification of the validity of point reactor kinetics, was located in the fast zone. The output voltages were converted to pulse trains, which were counted in a buffer register in time intervals adjustable from 0.25 to 4 s. The total number of pulses per time interval and the position of the measuring element were stored.

The inverse kinetic method was used to calculate the reactivity for each time interval. The reactivity was calculated on-line as a function of time by solving the inverse kinetics equations, based on the measured neutron flux time history. The movement of the oscillator element was analyzed in different phases of the movement. After a number of sample oscillations the program performed a final calculation to determine the average reactivity difference, including statistical uncertainty, between the positions "IN" (the sample in the center of the core) and "OUT" (the sample completely out of the core). A correction was performed for the linear component of a possible reactor drift.

Normalization of the measured reactivity worths was done by measuring reactivity effect of 'standard materials'. These materials were selected based on the requirements that their cross sections must be known accurately, and the energy dependence of their cross sections should be relatively similar to the energy dependence of the cross sections of the samples. The materials used were ^{235}U, boron, and ^{252}Cf.

The measurement errors were reported to be, in general, composed of a systematic error ≤2.1% and a statistical error ≤2.0%.

3.2 Reported results for reactivity worth.

Results were reported for a large collection of samples, with masses typically in the order of 1–10 g of the element of interest. The majority of the samples contained a fission product, either as a natural element or in enriched form. Many samples were highly hygroscopic and had to be dried and packed carefully since any water contamination would have given a large reactivity disturbance in the STEK cores.

The fission product samples in the form of natural elements were Zr, Nb, Mo, Rh, Pd, I, Cs, La, Ce, Pr, Nd, Eu, and Tb.

The fission product samples in enriched form were samples with high content of ^{90}Zr, ^{91}Zr, ^{92}Zr, ^{96}Zr, ^{92}Mo, ^{94}Mo, ^{95}Mo, ^{96}Mo, ^{97}Mo, ^{98}Mo, ^{100}Mo, ^{99}Tc, ^{101}Ru, ^{102}Ru, ^{104}Ru, ^{104}Pd, ^{105}Pd, ^{106}Pd, ^{107}Pd, ^{108}Pd, ^{110}Pd, ^{109}Ag, ^{111}Cd, ^{128}Te, ^{130}Te, ^{129}I, ^{131}Xe, ^{135}Cs, ^{142}Ce, ^{142}Nd, ^{143}Nd, ^{144}Nd, ^{145}Nd, ^{146}Nd, ^{148}Nd, ^{150}Nd, ^{147}P.m., ^{147}Sm, ^{148}Sm, ^{149}Sm, ^{150}Sm, ^{151}Sm, ^{152}Sm, ^{154}Sm, ^{153}Eu, ^{156}Gd, and ^{157}Gd.

A special sample was zirconium with 20% ^{93}Zr, produced by irradiation in the High Flux Reactor (also in Petten). Various other samples were measured, sometimes to correct for the chemical composition of the samples with fission products. A typical example was cesium, which was available as $CsCl_2$. A correction for the reactivity effect due to chlorine could be obtained *via* separate measurements of the effects of Pb and $PbCl_2$.

For example, various samples of ^{103}Rh in the mass range of 1–10 g were measured (for reference: the amount of ^{103}Rh in spent fuel is typically of the order of 0.5 g per kg of fuel). The reactivity effect of a sample of 1.1 g was reported to decrease from −1.46 pcm/g in STEK-4000 (the least hard spectrum) to −0.30 pcm/g in STEK-500 (the hardest spectrum). These values were reported as a fraction relative to a reference sample, and the value for the reference sample was given in units of 10^{-4} β_{eff}/g. The values were translated here to units of pcm/g for convenience of reading, but the uncertainty of the converted values has not been evaluated and is therefore not stated here.

4 Use in nuclear data evaluation

The STEK measurements are particularly important for validation, and improvement, of fission product nuclear data evaluations in the fast range. The main difference with nuclear reactions in thermal spectra is that the peak of the spectra of Figure 3, say between 100 keV and 2 MeV is in the region where inelastic neutron scattering plays an important role, as it is a competing channel for neutron capture. Hence, *via* inelastic scattering the neutrons will lose energy in a different way than they would do in a thermal spectrum. The importance of this effect was recognized by the nuclear data community, and the Working Party on Evaluation Coordination (WPEC) launched a special subgroup (SG10) for this (NEA 2001).

Validation using the STEK data showed the calculated sample reactivity worths are in reasonable to good agreement (20%) with those measured at STEK for strong absorbers but that for weak absorbers some anomalous results were obtained. It was considered that these problems probably came from poor inelastic scattering data. After this validation exercise, OECD/NEA launched two other international nuclear data efforts: WPEC SG17 (NEA 1998), which assessed the status of pseudo-fission products cross sections for fast spectra, and SG-21 (NEA 2004), on a comparison between, and SG-23 (NEA 2009) for the evaluation of, neutron data files for fission products. The latter data files have found their way in several international nuclear data libraries like ENDF/B, JEFF and JENDL, but a proper validation with integral data in the fast neutron range has not been carried out since then, to our knowledge.

Moreover, in the past 2 decades the evaluation methods for fission products have been improved considerably, leading to better founded nuclear data libraries and a more routinely use of powerful optical models for scattering and non-approximate coupled-channels methods for inelastic reactions, mainly thanks to a significant increase in computer power and automation of evaluation software. Current nuclear data evaluators are confident that improved nuclear data files, and this time with covariance information, can be produced to answer new requests from fast reactor technology. Nuclear data evaluations and the associated covariance adjustment could repeated with a perturbation method (Dragt et al., 1977) or with modern Total Monte Carlo techniques. An issue is which type of simulation will be used given the small reactivity worth per sample, which makes validation by a Monte Carlo code tedious.

The definition of a high-quality integral benchmark for fast neutrons would surely motivate the nuclear data file projects that reside under WPEC to invest effort into new fission product evaluations. The construction of the integral benchmark and new nuclear data libraries could progress in parallel in the coming years.

5 Discussion

The STEK measurement results provide an interesting opportunity for checking nuclear data evaluations of fission products. Yet to our knowledge this has not been done for evaluations in the current versions of libraries like ENDF/B or JEFF, most probably because the measurement results are not in a form that makes it easy to perform such a check. Therefore, if there is sufficient interest in fission product worths in fast spectrum conditions, it should be evaluated whether the STEK measurements can be converted into a benchmark for the International Reactor Physics Experiments (IRPhE) Handbook.

An important part of such an evaluation is the availability of information on the measurements, and the accuracy of the results. In the case of STEK, it should also be discussed how the complex geometry can be dealt with, because the geometrical complexity of the facility does not lend itself easily to deterministic calculations. Yet on the other hand, many the measured fission product worths were of the order of a couple of pcm ('pour-cent-mille', 10^{-5}), which is very hard to calculate with Monte Carlo techniques.

Data availability statement

Publicly available datasets were analyzed in this study. This data can be found here: OECD/NEA Data Bank, www.oecd-nea.org/tools/abstract/detail/nea-1714.

Author contributions

All authors listed have made a substantial, direct, and intellectual contribution to the work and approved it for publication.

Conflict of interest

SM is currently employed by NRG and AK was employed by NRG until 2015.

Publisher's note

References

Da Cruz, D. F., Sciolla, C. M., and Rochman, D. A. (2013). STEK experiment – opportunity for validation of fission products nuclear data. *Trans. ANS* 108, 701–703.

Dietze, K., Ishikawa, M., and Rimpault, G. (2001). *Integral test of neutron data and comparison of codes by Re-analysis of the SEG and STEK experiments.* JEFF/DOC-861.

Dragt, J. B., Dekker, J. W. M., Gruppelaar, H., and Janssen, A. J. (1977). Methods of adjustment and error evaluation of neutron capture cross sections; application to fission product nuclides. *Nucl. Sci. Eng.* 62, 117–129. doi:10.13182/nse77-3

IAEA (2022). Advanced reactors information system (ARIS). Available at: https://aris.iaea.org/(Accessed October 6, 2022).

IAEA (2020). *Advances in small modular reactor technology developments - a supplement to: IAEA advanced reactors information system.* (ARIS) - 2020 Edition, IAEA Report.

Janssen, A. J., Gruppelaar, H., Heijboer, R. J., Karouby-Cohen, N., Martin-Deidier, L., Rimpault, G., et al. (1986). Integral-data test of JEF-1 fission product cross sections. *Jef. Rep.* 5. ECN-176.

NEA (2004). Assessment of neutron cross sections for the bulk of fission products, OECD/NEA Report NEA/WPEC-21.

NEA (2009). Evaluated data library for the bulk of fission products, OECD/NEA Report NEA/WPEC-23.

NEA (2001). Evaluation method of inelastic scattering cross-sections for weakly absorbing fission-product nuclides, OECD/NEA Report NEA/WPEC-10.

NEA (1998). Status of pseudo-fission-product cross-sections for fast reactors, OECD/NEA Report NEA/WPEC-17.

OECD (2021), Small modular reactors: Challenges and opportunities, OECD/NEA Report No, 7560.

OECD/NEA (2022). IRPhE/STEK, reactor physics experiments from fast-thermal coupled facility. Available at: www.oecd-nea.org/tools/abstract/detail/nea-1714 (Accessed October 6, 2022).

frontiers | Frontiers in Energy Research

TYPE Original Research
PUBLISHED 28 February 2023
DOI 10.3389/fenrg.2023.1085788

OPEN ACCESS

EDITED BY
Hitesh Bindra,
Kansas State University, United States

REVIEWED BY
Liangzhi Cao,
Xi'an Jiaotong University, China
Jesson Hutchinson,
Los Alamos National Laboratory (DOE), United States

*CORRESPONDENCE
John D. Bess,
john.bess@jfaidaho.com

SPECIALTY SECTION
This article was submitted to Nuclear Energy, a section of the journal Frontiers in Energy Research

RECEIVED 31 October 2022
ACCEPTED 09 February 2023
PUBLISHED 28 February 2023

CITATION
Bess JD, Ivanova T, Hill I, Martin J-F, Briggs JB, Scott L, DeHart MD, Percher C, Marshall BJ and Blaise P (2023), Intrinsic value of the international benchmark projects, ICSBEP and IRPhEP, for advanced reactor development. *Front. Energy Res.* 11:1085788. doi: 10.3389/fenrg.2023.1085788

Intrinsic value of the international benchmark projects, ICSBEP and IRPhEP, for advanced reactor development

John D. Bess[1]*, Tatiana Ivanova[2], Ian Hill[2], Julie-Fiona Martin[2], J. Blair Briggs[3], Lori Scott[3], Mark D. DeHart[3], Catherine Percher[4], B. J. Marshall[5] and Patrick Blaise[6]

[1]JFoster & Associates, LLC, Idaho Falls, ID, United States, [2]Organisation for Economic Co-operation and Development, Nuclear Energy Agency, Paris, France, [3]Idaho National Laboratory, Nuclear Science and Technology, Idaho Falls, ID, United States, [4]Lawrence Livermore National Laboratory, Nuclear Criticality Safety Division, Livermore, CA, United States, [5]Oak Ridge National Laboratory, Nuclear Energy and Fuel Cycle Division, Oak Ridge, TN, United States, [6]Commissariat à l'Energie Atomique et aux Energies Alternatives, Scientific Division of Energies, Paris, France

The International Criticality Safety Benchmark Evaluation Project, a sanctioned program under the auspices of the Nuclear Energy Agency of the Organisation for Economic Co-operation and Development, has been a highly successful and productive collaboration, now encompassing over 5,000 evaluated experimental benchmarks trusted and relied upon throughout the international nuclear communities. The success of this project led to the development of the International Reactor Physics Experiment Evaluation Project, which is dedicated to the evaluation of benchmark experiment data to sustain current and future reactor physics validation needs. These exemplary programs, and their widely utilized handbooks, serve as gold standards to which other databases strive to emulate. The purpose of the two projects is to preserve modern and legacy experimental data and evaluate it in a standardized handbook format to provide quality benchmarks to support modern and future criticality safety and reactor physics validation. These two projects have often served as the mechanism through which historic and modern neutronics experiments are evaluated and shared across international borders, to best provide unique, high-quality peer-reviewed, and often otherwise unavailable, benchmark data. The contents of these handbooks are utilized not only in validating criticality safety, reactor physics, and advanced reactor calculations, but are used to validate neutronics calculations and nuclear data for most other nuclear applications. This manuscript discusses both international programs and available content to enable advanced reactor design validation.

KEYWORDS

advanced reactors, benchmark, criticality safety, experiment, handbook, nuclear data, reactor physics, validation

1 Introduction

What began as an emblematic effort to bolster best practices in the 1990s for nuclear criticality safety validation has evolved into the backbone testing suite for contemporary neutronics methodologies, simulation, and nuclear data (Palmiotti, et al., 2014). The International Criticality Safety Benchmark Evaluation Project (ICSBEP) (Briggs, et al.,

2003), a sanctioned program under the auspices of the Nuclear Energy Agency (NEA) of the Organisation for Economic Co-operation and Development (OECD), has been a highly successful and productive collaboration, now encompassing over 5,000 evaluated experimental benchmarks trusted and relied upon throughout the international nuclear communities. The success of the ICSBEP led to the development of the International Reactor Physics Experiment Evaluation Project (IRPhEP) (Briggs and Gulliford, 2014), which is dedicated to the evaluation of benchmark experiment data to sustain current and future reactor physics validation needs. The benchmark experiments, covering a wide range of applications, from thermal light water reactors (LWRs) and high temperature reactors (HTRs) to fast reactors of various designs or even special applications, are most often obtained *via* zero power reactors, many of which have been shut down or are nearing the end of their expected lifetimes. These two exemplary benchmark programs, and their widely utilized handbooks, serve as gold standards to which other databases strive to emulate, such as the OECD NEA Spent Fuel Composition (SFCOMPO) database (Michel-Sendis, et al., 2017), the OECD/IAEA (International Atomic Energy Agency) co-sponsored International Fuel Performance (IFPE) collection (Menut, et al., 2000), the International Experimental Thermal Hydraulics Systems (TIETHYS) database (Rohatgi, et al., 2018), the collection of multi-physics experiments being created by the NEA Expert Group on Reactor Systems Multi-Physics (EGMUP) (Valentine, et al., 2018), and the OECD-NEA/RSICC (Radiation Safety Information Computational Center) co-sponsored Shielding Integral Benchmark Archive and Database (SINBAD) (Kodeli and Sartori, 2021).

From the inception of the ICSBEP until very recently, both the ICSBEP and IRPhEP have been managed by a single chair, nominated and endorsed by the technical review group (TRG), whom has historically been from the United States (US). Most recently, the management of these projects has been divided into two separate chair and vice chair positions and expanded to include non-US representatives. The purpose of the two projects is to preserve both legacy and current generation experiment data and evaluate it in a standardized handbook format to provide quality benchmarks to support modern and future criticality safety and reactor physics validation. These two projects have often served as the mechanism through which historic and modern neutronics experiments are evaluated and shared across international borders, to best provide unique, high-quality peer-reviewed, and often otherwise unavailable, benchmark data. The handbooks provide a consolidated, maintained repository for benchmark data, instead of a landscape of fragmented information spread throughout various scientific journals, laboratory reports, and conference proceedings (Bess and Ivanova, 2020). Furthermore, detailed neutron spectral characteristics are calculated and provided in the handbook for most benchmark configuration to enable users to clearly understand the range of their applicability (Rozhikhin, 1999).

A key fact to note is that these benchmarks preserve and evaluate experiments performed to support past, current, and future nuclear research needs. There is constant variability in programmatic needs amongst and between various international entities. The contents of these handbooks have enabled the development of nuclear data and codes now used to design the next-generation of nuclear reactors. Various numerous benchmarks can assist in the advanced reactor development, although no doubt additional benchmarks will be needed.

A historic summary of investment costs with conservative estimates of the monetary and intrinsic values of these two programs has been independently assessed:

> "The total cost of the IRPhEP and ICSBEP over the past 2 decades is approximately $50 million, while the data obtained from those two programs can easily be valued at over $1.5 billion (estimate conservatively based on 5,000 experiments at $300,000 per experiment). If one new reactor or reprocessing facility is designed and built using advanced simulation methods validated only by legacy data without the construction of a separate critical facility, the entire cost of the two programs will be offset by many times. Furthermore, the IRPhEP and ICSBEP activities have helped pass knowledge from those involved in these legacy experiments to future generations and have influenced the development of future experimental programs." (Palmiotti, et al., 2014)

Although benchmarks represent a cost investment, they very nearly always cost significantly less than the costs associated with construction and performance of the actual experiments themselves. The benchmarking process not just ensures that all data are collated, but more importantly, the quality of the experimental data are evaluated and preserved.

2 History and background

The Criticality Safety Benchmark Evaluation Project (CSBEP) was initiated in 1992 by the US Department of Energy (US DOE) under the Idaho National Engineering and Environmental Laboratory (INEEL). In 1995, the CSBEP became an official activity of the NEA Nuclear Science Committee at which time the name was changed to the ICSBEP. Historically, the management of the projects was funded in the US *via* the Nuclear Criticality Safety Program (NCSP) under the National Nuclear Security Administration (NNSA), but for approximately the past decade the management has been funded under the Nuclear Engineering Advanced Modeling and Simulation (NEAMS) program within the US Department of Energy, Office of Nuclear Energy (DOE-NE). Initial funding to support the establishment of the IRPhEP within the OECD NEA was graciously provided by the Japan Atomic Energy Agency (JAEA). Management of these projects includes coordination of benchmark evaluation and reviews, organizing TRG meetings, publication of the handbooks, and user engagement *via* international conferences and meetings, in close cooperation with NEA. Typically, additional funding has been provided to universities in the US *via* annual Nuclear Energy University Program (NEUP) MS-NE-1 awards to contribute to the handbooks. Funding for the evaluation and review of benchmarks, worldwide, has often been contributed *via* government, corporate, or even individual entities from 28 countries and OECD NEA seeking to improve upon the available content found within these handbooks.

DOE-NE has previously utilized the MS-NE-1 award to direct US reactor physics benchmark development. Prioritization and funding of criticality safety benchmarks in the US are currently managed by the NCSP. Prioritization of other reactor physics benchmarks in the US are provided by individual projects, organizations, and/or companies. A historic example includes Next-Generation Nuclear Plant (NGNP) funding of eight benchmark evaluations of graphite-moderated reactor systems with tristructural-isotropic (TRISO) fuel. International entities fund and prioritize their own benchmark development depending upon their respective needs, international collaborative activities, and/or university-driven research interests. However, through the ICSBEP and IRPhEP, independent technical review is coordinated and provided to ensure the utmost quality in modern benchmark development for these handbooks, at a peer-review standard greater than most, if not all, published scientific and engineering journals.

The *International Handbook of Evaluated Criticality Safety Benchmark Experiments* (ICSBEP Handbook) (NEA, 2022a) is primarily utilized in criticality safety, neutronics code validation, and nuclear data validation. We would not have, nor continue to maintain, the quality of neutronics codes implemented today without this handbook, as many of the ICSBEP evaluations are established key benchmarks in neutronics software validation suites. The *International Handbook of Evaluated Reactor Physics Benchmark Experiments* (IRPhEP Handbook) (NEA, 2022b) is used by reactor physicists that need further validation for specific reactor design and experiment characterization; it also supports specific nuclear data validation needs that cannot be provided *via* eigenvalue benchmark evaluations alone. International nuclear regulatory agencies, government facilities, industrial, and commercial entities utilize these handbooks to validate their codes and data to support neutronics modeling and simulation of the current power and research reactor fleets. Universities use them primarily for training and education purposes world-wide. These benchmark handbooks are known as the quality standard for international benchmarking activities. They are implemented internationally in advanced modeling and simulation; analytical and computational methods development, validation, and verification; reactor design and licensing; training; criticality and reactor safety analyses; fuel cycle and related activities; range of applicability and experiment design; and nuclear data refinement. Without modern integral benchmarks, we would be unable to reduce uncertainties in nuclear data, which are fundamental in sustaining practical, reliable, and realistic computational analyses.

The 2022 edition of the ICSBEP Handbook, when published, will include 592 evaluations containing acceptable benchmark specifications for 5,144 critical, subcritical, or near-critical configurations, representing contributions from 26 countries. An additional 838 configurations deemed unacceptable to support criticality safety requirements, yet present historical and legacy value, are also preserved within the handbook. There are eight criticality alarm placement/shielding evaluations containing a total of 46 benchmark configurations, and 11 fundamental physics evaluations containing a total of 246 measurements relevant to criticality safety applications. A summary of the ICSBEP Handbook contents in provided in Table 1. The 2022 edition of the IRPhEP Handbook will include data for 57 unique nuclear facilities with evaluations containing benchmark specifications for 170 experimental series, of which four are draft benchmark specifications yet to be formally adopted, with contributions from 25 countries. A summary of the IRPhEP Handbook contents is shown in Table 2. Many reactor physics benchmark evaluations include additional data besides criticality measurements, e.g., buckling and extrapolation length, spectral characteristics, reactivity effects, reactivity coefficients, kinetics measurements, reaction-rate distributions, power distributions, isotopic composition, and other miscellaneous types of measurements. Full technical details can be found for the various benchmark evaluations within the latest editions of these handbooks. The following countries have contributed towards the success of these two benchmark projects: Argentina, Austria, Belarus, Belgium, Brazil, Canada, the People's Republic of China, the Czech Republic, Denmark, France, Germany, Hungary, India, Israel, Italy, Japan, Kazakhstan, Poland, Republic of Korea, the Russian Federation, Serbia, Slovenia, South Africa, Spain, Sweden, Switzerland, United Kingdom, and United States of America.

3 Enhanced handbook database tools

The already extensive and yearly increasing handbooks' content required development of an evolving database structure to collate, organize, and better facilitate their use. The Database for the International Handbook of Evaluated Criticality Safety Benchmark Experiments (DICE) (Nouri, et al., 2003) was developed specifically for the ICSBEP Handbook. This relational database is loaded with pre-selected information from each of the benchmark evaluations. A users' interface enables querying for specific parameters to identify benchmarks suitable for their respective needs. DICE also includes the ability to plot and compare neutron spectra and sensitivity coefficients for many evaluations. The IRPhEP Database and Analysis Tool (IDAT) (Hill, et al., 2014) was similarly developed for use with the IRPhEP Handbook. This database tool dramatically simplifies the identification of validation cases from the various reactor types and their respective benchmark measurements. The database also contains calculated quantities of the reactor systems such as neutron flux, capture, and fission spectrum data; neutron balance data; and sensitivity data. The ability to visualize these datasets is also included in IDAT.

4 Uncertainty guides

The benchmark and experiment design community benefits from the development of uncertainty guides for both criticality safety and reactor physics measurements. Participants in these international projects contribute their expertise to enable the preservation of best practices, both historically and at present, for the benefit of current and future benchmark evaluation. Characterization and quantification of the typical uncertainties encountered for the varying measurements in criticality safety and reactor physics systems further contributes towards activities extended beyond typical benchmark evaluation and validation such as training, licensing, and design.

The *ICSBEP Guide to the Expression of Uncertainties* (Dean and Blackwood, 2008) was developed primarily to address uncertainties in

TABLE 1 Contents summary for the 2022 edition of the ICSBEP handbook.

801 Plutonium Experiments	**244 ^{233}U Experiments**
• 36 Compound	• 6 Compound
• 136 Metal	• 11 Metal
• 629 Solution	• 227 Solution
1443 Highly Enriched Uranium Experiments	**536 Mixed Plutonium-Uranium Experiments**
• 291 Compound	• 301 Compound
• 618 Metal	• 52 Metal
• 527 Solution	• 86 Solution
• 2 Mixed Compound/Solution	• 76 Mixed Compound/Solution
• 5 Mixed Metal/Solution	• 21 Mixed Metal/Compound
278 Intermediate- and Mixed-Enrichment Uranium Experiments	**20 Special Isotope Experiments**
• 156 Compound	• Metal
• 57 Metal	• ^{237}Np,^{238}Pu,^{242}Pu,^{244}Cm
• 65 Solution	
1822 Low Enriched Uranium Experiments	**8 Criticality-Alarm-Placement/Shielding Experiments**
• 1,560 Compound	• 46 Unique Configurations with Numerous Dose Points
• 82 Metal	**11 Fundamental Physics Experiments**
• 120 Solution	• 246 Unique Measurements
• 60 Mixed Compound/Solution	• Fissions Rates
	• Transmission Measurements
	• Subcritical Neutron Multiplication
Contents Summary	
• 5,144 critical, subcritical, or near-critical configurations	
• Additional 838 configurations are unacceptable to support criticality safety requirements	
• Contributions from 26 countries	

the evaluation and characterization of critical experiments, i.e., measurement of k_{eff}. The *International Reactor Physics Experiments Evaluation Project (IRPhEP) Guide to the Expression of Uncertainty* (Dos Santos, et al., 2018) was more recently developed to support evaluation of uncertainties in the evaluation and characterization of other types of measurements aside from criticality, such as, buckling, spectral characteristics, reactivity effects/coefficients, kinetics, and reaction-rate/power distributions. These uncertainty guides are included in the ICSBEP and IRPhEP Handbooks and publicly available on-line.

5 Example evaluations enabling advanced systems design

The fundamentally cross-cutting nature of the handbooks serves to enable neutronics simulation to support nuclear safety and design through all aspects of the nuclear fuel cycle. Furthermore, the framework is established such that new benchmark evaluation data can be prepared, reviewed, and published for current and future handbook users. An overview of the benchmark evaluation process for these two international programs is shown in Figure 1. Brief examples of benchmarks relevant to contemporary research and development needs are provided in the subsections below. Explanations regarding the nomenclature for the report identifiers are located within the ICSBEP and IRPhEP Handbooks; some benchmark evaluations are cross listed within both handbooks.

5.1 Advanced reactor designs

5.1.1 Sodium-cooled and lead-cooled fast reactor (SFR and LFR) designs

5.1.1.1 BFS-61 assemblies: Experimental model of lead-cooled fast reactor with core of metal plutonium-depleted uranium fuel and different reflectors

The BFS-1 critical facility (shown in Figure 2) of the Institute of Physics and Power Engineering (IPPE) in Obninsk, Russia, was

TABLE 2 Contents summary for the 2022 edition of the IRPhEP handbook.[b]

PWR (7)	SERIES (14)
BEAVRS	1 Draft
DIMPLE	2
DUKE	1
EOLE	2
OTTOHAHN	1
SSCR	2
VENUS	3 + 2 Drafts
VVER (3)	**SERIES (5)**
LR-0	3
P-Facility	1
ZR-6	1
BWR (0)	**SERIES (0)**
LMFR (10)	**SERIES (26)**
BFS-1	2
BFS-2	1
BR2	1
EBR2	1
FFTF	1
JOYO	1
SNEAK	1
ZEBRA	3
ZPPR	11
ZPR	4

GCR (5)	SERIES (10)
ASTRA	1
HTR10	1
HTTR	3
PROTEUS	4
VHTRC	1
GCFR (2)	**SERIES (4)**
PROTEUS†	3
ZPR†	1
LWR (5)	**SERIES (31)**
CROCUS	1
DIMPLE†	2 + 1 Draft
IPEN(MB01)	21
KRITZ	4
TCA	3
HWR (3)	**SERIES (5)**
DCA	1
ETA	2
ZED2	2
MSR (1)	**SERIES (1)**
MSRE	1
RBMK (1)	**SERIES (1)**
RBMK(CF)	1
Total Facilities	**Total Series**
57	170

SPACE (7)	SERIES (13)
ORCEF	1
KRUSTY	1
SCCA	3
TOPAZ	2
UKS1M	1
ZPPR†	4
ZPR†	1
FUND (23)	**SERIES (59)**
ATR	1
BFS-1†	4
BFS-2†	1
CORAL(1)	1
FCA	1
FR0	3
HECTOR	2
IGR	1
KUCA	1
LAMPRE	1
LR-0†	1
MINERVE	1
NRAD	2
ORCEF	1
ORSPHERE	1
PBF	1
RA-6	1
RB	10
RHF	1
TREAT	3
TRIGA	2
ZEBRA†	1
ZPR†	18

[a]Duplicate Facility.

[b]PWR, pressurized water reactor; LWR, light water moderated reactor; VVER, Vodo-Vodynaoi Energetichesky Reactor; HWR, heavy water moderated reactor; BWR, boiling water reactor; MSR, molten salt reactor; LMFR, liquid metal fast reactor; RBMK, reaktor bolshoy moshchnosti kanalniy; GCR, Gas Cooled (Thermal) Reactor; SPACE, space reactor; GCFR, Gas Cooled (FAST) reactor; FUND, fundamental physics measurements.

utilized to provide full-scale mockups of fast reactor cores including additional neutron physics measurements. The BFS-61 experiments included three core designs with lateral reflectors of depleted UO_2, lead, and steel pellets contained within stainless steel tubes. The core itself contained Pu metal fuel with additional pellets of Pb, depleted U metal, and graphite. Additional spectral and reaction rate measurements have also been evaluated. Benchmark identifiers: BFS1-LMFR-EXP-002 (IRPhEP)/MIX-MET-FAST-006 (ICSBEP).

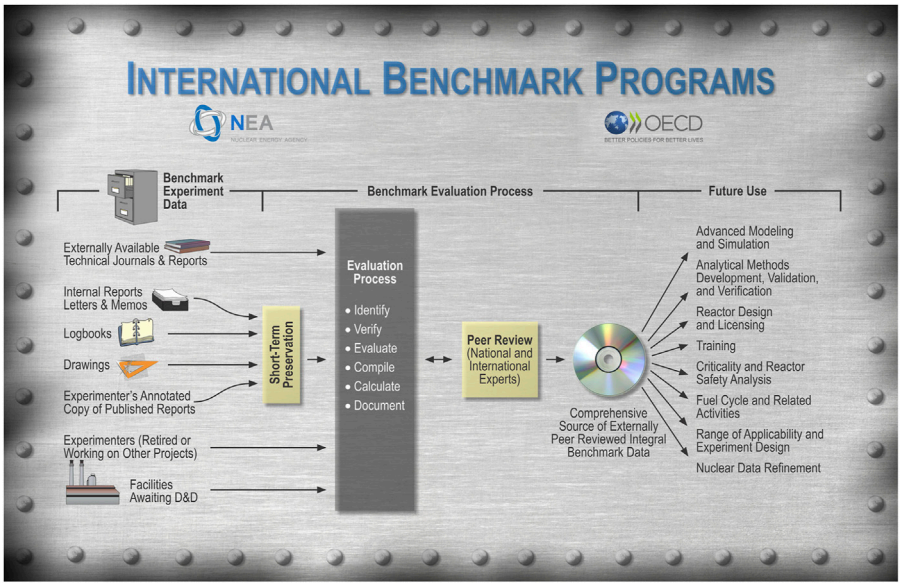

FIGURE 1
Overview of benchmark evaluation process for ICSBEP and IRPhEP.

5.1.1.2 Evaluation of run 138B at experimental breeder reactor II, a prototypic liquid metal fast breeder reactor

The Experimental Breeder Reactor-II (EBR-II) was a 62.5 MW_{th} test reactor operated by Argonne National Laboratory (ANL) between 1964 and 1994, and initially used to demonstrate operability of a SFR, but later to support a myriad of testing needs. One of the most important experiments was the Shutdown Heat Removal Tests (SHRT) to test a liquid metal reactor during catastrophic failures of heat removal at full power. The critical configuration for the most extreme of these tests, SHRT 45, was evaluated. Benchmark identifier: EBR2-LMFR-RESR-001 (IRPhEP).

5.1.1.3 Japan's experimental fast reactor JOYO MK-I core: Sodium-cooled uranium-plutonium mixed oxide fueled fast core surrounded by UO_2 blanket

JOYO is Japan's first experimental fast reactor and was constructed at the Oarai Engineering Center. Its purpose was to acquire data for fast reactor performance including nuclear characteristics, thermal hydraulics, and safety-related features. This benchmark includes evaluation of the first and second critical core loadings, six control rod worth measurements, six sodium void reactivities, six fuel replacement reactivities, one isothermal temperature coefficient, and five burnup reactivity coefficients. Benchmark identifier: JOYO-LMFR-RESR-001 (IRPhEP).

5.1.1.4 ZPR-3 assembly 59: A cylindrical assembly of plutonium metal and graphite with a thick lead reflector

ZPR-3 (Zero Power Reactor) was the first of four fast critical facilities constructed by ANL. While constructed to support fast reactor development, data from some of the ZPR assemblies were also well suited for nuclear data validation needs. Assemblies 58 and 59 were constructed to test the worth of replacing a depleted U reflector with Pb. Benchmark identifier: PU-MET-INTER-004 (ICSBEP).

5.1.1.5 ZPPR-12: Mockup of the 400 MW_e sodium-cooled Clinch River Breeder Reactor

The Zero Power Physics Reactor (ZPPR) was the last fast critical facility constructed by ANL. ZPPR-11, -12, and -13 were constructed to perform engineering mockup tests for the Clinch River Breeder Reactor (CRBR). The measurements in ZPPR-12 were designed specifically to address sodium void worth, cell heterogeneity, and the effects of changes in neutron streaming upon reactivity worth. Benchmark identifier: ZPPR-LMFR-EXP-010 (IRPhEP).

5.1.2 Molten salt and fluoride-salt-cooled high-temperature reactor (MSR and FHR) designs

5.1.2.1 VVER-1000 physics experiments hexagonal lattices (1.275 cm pitch) of low enriched U (3.3 wt% $^{235}U)O_2$ fuel assemblies in light water with graphite and fluoride salt insertions in central assembly

The zero-power reactor LR-0 at Research Centre Řež in the Czech Republic is utilized to mockup various tests for material testing and vodo-vodyanoi enyergeticheskiy reactors (VVERs). Tests were performed in 2014–2015 to support MSR and FHR development with material insertions in the center of the reactor containing various quantities of graphite, FLINA (LiF and NaF mixture), or FLIBE (LiF and BeF_2 mixture), as shown in Figure 3. Benchmark identifier: LR (0)-VVER-RESR-003 (IRPhEP).

5.1.2.2 Molten-salt reactor experiment (MSRE) zero-power first critical experiment with ^{235}U

The MSRE was built and operated at Oak Ridge National Laboratory from 1965 to 1969 with the explicit purpose to

FIGURE 2
BFS-1 critical facility (Top) and example fuel pellet loading (Bottom).

demonstrate key features of MSR technology. The initial zero-power nuclear experiments were to establish the basic nuclear characteristics as a baseline for evaluating system performance. The initial critical core has been evaluated. There are a total of seventeen critical configurations with neutron spectra measurements for three cores: void center, graphite center, and FLINA center. Benchmark identifier: MSRE-MSR-RESR-001 (IRPhEP).

5.1.2.3 HTR-PROTEUS pebble bed experimental program core 4: Random packing with a 1:1 moderator-to-fuel pebble ratio

The versatile *PROTEUS* facility from the Paul Scherrer Institute (PSI) in Villigen, Switzerland was utilized to support measurements for various reactor concepts. The modular HTR series investigated 11 core loadings with TRISO-laden graphite pebbles from 1992 to 1996. Core four represented a randomly packed core of moderator and fuel pebbles with a 1:1 ratio (as demonstrated in Figure 4). The critical configuration and control rod worths are evaluated as benchmark experiment data. Benchmark identifier: PROTEUS-GCR-EXP-002 (IRPhEP).

5.1.3 Gas-cooled fast reactor (GCFR)

5.1.3.1 GCFR-PROTEUS experimental program core 11: Homogeneous MOX fuel test region

The aforementioned *PROTEUS* facility also supported GCFR research from 1972 to 1979. Core 11 served as a reference configuration to test reproducibility and evaluate infinitely dilute cross sections of ^{232}Th, ^{233}U, and ^{237}Np with a Pu-fueled core driven by a UO_2-fueled annulus within a D_2O shield annular tank and radial graphite reflector. Nine spectral indices were evaluated for this configuration. Benchmark identifier: PROTEUS-GCFR-EXP-001 (IRPhEP).

5.1.3.2 ZPR-9/29: Gas Cooled fast reactor critical experiments–Phase II

On the third fast critical facility by ANL, loadings 28 through 30 on ZPR-9 represented three phases supporting GCFR research in

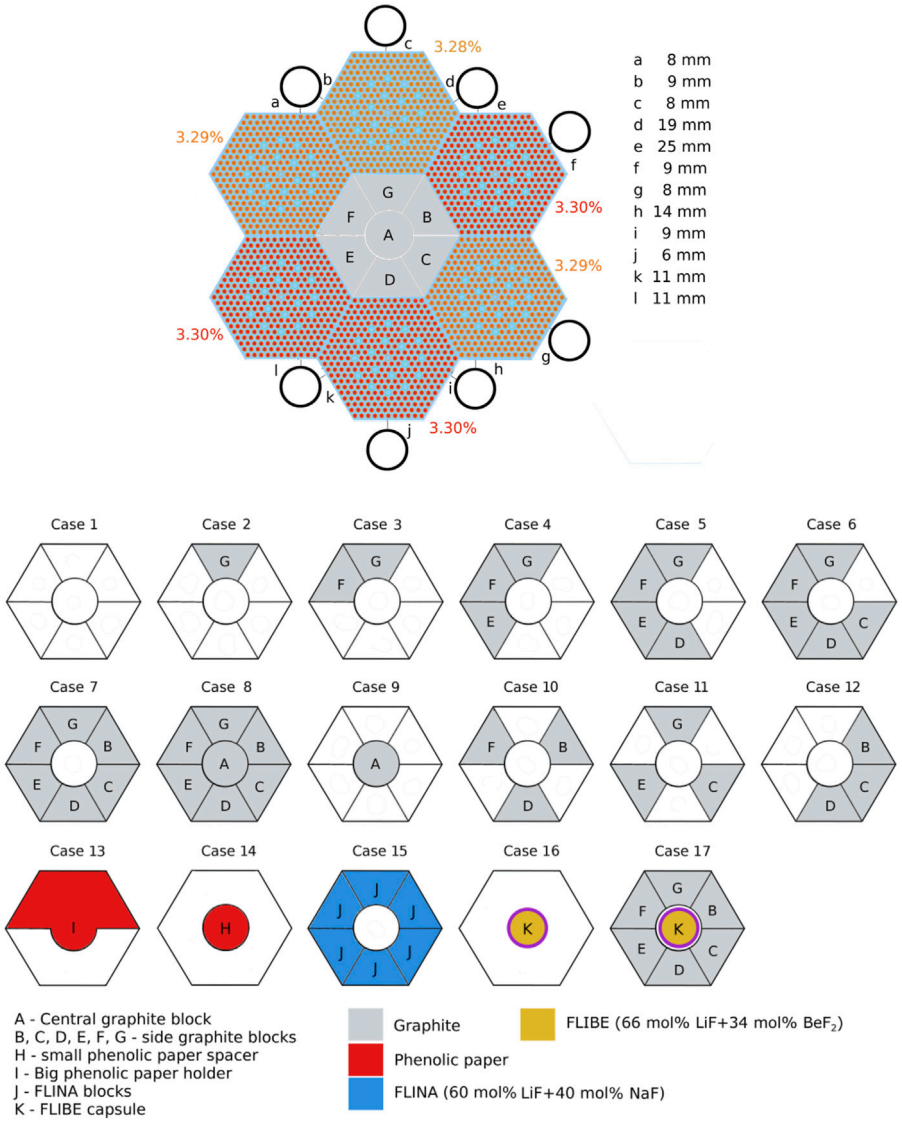

FIGURE 3
Schematic of the VVER core loading (Top) with various arrangements of central module testing materials (Bottom).

the US in 1975–1976. Criticality, spectral measurements, and reactivity measurements were evaluated for Phase II of this series, which was an unreflected core with ~43% void/gas fraction. Benchmark identifier: ZPR-GCFR-EXP-001 (IRPhEP).

5.2 Small modular reactor (SMR), microreactor, and space reactor designs

5.2.1 TRISO-based designs

5.2.1.1 Evaluation of the start-up core physics tests at Japan's high temperature engineering test reactor (fully-loaded core)

The High Temperature Engineering Test Reactor (HTTR) of the Japan Atomic Energy Agency (JAEA) is a 30 MW_{th}, graphite-moderated, helium-cooled reactor constructed to establish and upgrade the technological bases for advanced high-temperature gas-cooled reactors (HTGRs). It is fueled with TRISO within graphite blocks. The fully loaded start-up core was operated in 1998 and evaluated as a benchmark. Evaluated measurements include a critical and subcritical core, excess reactivity, shutdown margin, and an axial reaction-rate distribution. Benchmark identifier: HTTR-GCFR-RESR-001 (IRPhEP).

5.1.2.2 HTR-PROTEUS pebble bed experimental program cores 9 and 10: Columnar hexagonal point-on-point packing with a 1:1 moderator-to-fuel pebble ratio

Cores 9 and 10 from the HTR-PROTEUS experimental program contained hand-stacked TRISO-fueled pebbles with columnar hexagonal point-on-point packing and a moderator-to-fuel pebble ratio of 1:1. Criticality and rod worth measurements were evaluated for each core. These two cores are nearly identical, with

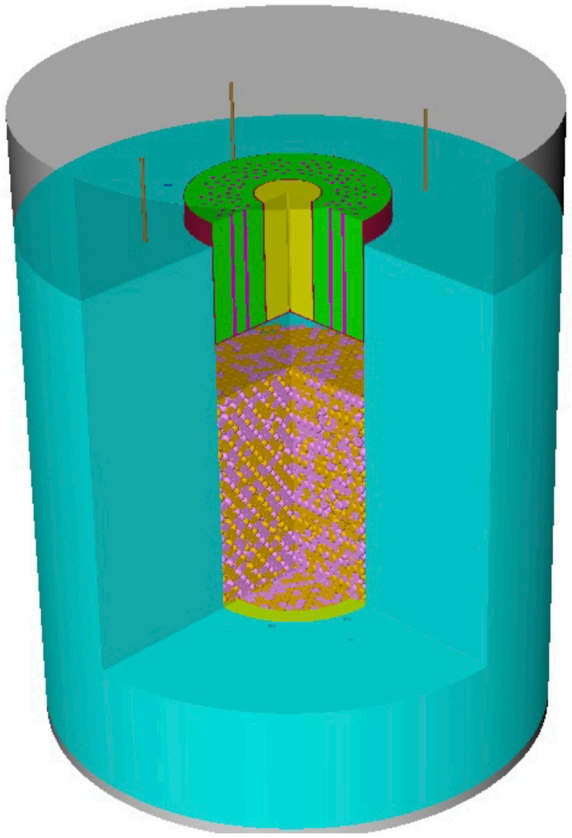

FIGURE 4
MONK10 model of HTR-PROTEUS core 4 with random pebble loading.

Core 10 containing a shorter stack of pebbles and 654 polyethylene rods to simulate water ingress. Benchmark identifier: PROTEUS-GCR-EXP-004 (IRPhEP).

5.2.1.3 Temperature effect on reactivity in VHTRC-1 core

The Very High Temperature Reactor Critical Assembly (VHTRC), as shown in Figure 5, is another JAEA facility dedicated to the verification of calculation accuracy to support neutronic design of the HTTR. Seven critical configurations and ten temperature coefficients were evaluated for this BISO-fueled graphite reactor mockup facility. Benchmark identifier: VHTRC-GCR-EXP-001 (IRPhEP).

5.2.2 Space reactors

5.2.2.1 KRUSTY: Beryllium-oxide and stainless-steel reflected cylinder of HEU metal

The Kilopower Reactor Using Stirling Technology (KRUSTY) demonstration was performed in 2017–2018 at the National Criticality Experiments Research Center (NCERC) in the US. Five of the sixty critical configurations were evaluated for this 93.1 wt% ^{235}U U-Mo annular fuel reflected by BeO and shielded by stainless steel. The entire series was designed to test power generation from a nuclear reactor *via* heat pipes connected to Stirling engines. Benchmark identifiers: KRUSTY-SPACE-EXP-001 (IRPhEP)/HEU-MET-FAST-101 (ICSBEP).

5.2.2.2 Intermediate heterogeneous assembly with highly enriched uranium dioxide (96% ^{235}U) and zirconium hydride moderator

During 1992 to 1993, an experiment was performed at the Kurchatov Institute in Russia to investigate accidental water immersion of a TOPAZ space reactor. Six configurations were evaluated representing various stages of water ingress and complete water immersion. Benchmark identifiers: TOPAZ-SPACE-RESR-001 (IRPhEP)/HEU-COMP-MIXED-003 (ICSBEP).

5.2.2.3 ZPPR-20 phase C: A cylindrical assembly of U metal reflected by beryllium oxide

The ZPPR-20 experimental series provided data for development of the SP-100 nuclear power source for space applications. Phase C represents the reference flight configuration. Phases D and E represented water immersion and earth burial accidents and are also available as benchmarks. Benchmark identifiers: ZPPR-SPACE-EXP-001 (IRPhEP)/HEU-MET-FAST-075 (ICSBEP).

5.2.3 Other SMR-Relevant benchmarks

5.2.3.1 PWR type UO_2 fuel rods with enrichments of 3.5 and 6.6 wt% with burnable absorber ("Otto Hahn" nuclear ship program, second core)

Before installation of a second core into the German nuclear-powered merchant ship, Otto Hahn, a series of zero-power experiments were performed to test the fuel loading, start up, and subcriticality safety issues such as a stuck control rod. These experiments validated theoretical calculations before the core was successfully installed and operated. Currently only the critical configuration (see Figure 6) of the zero-power tests has been evaluated as a benchmark. Benchmark identifiers: OTTOHAHN-PWR-RESR-001 (IRPhEP)/LEU-COMP-THERM-081 (ICSBEP).

5.2.3.2 Critical configuration and physics measurements for beryllium reflected assemblies of U (93.15)O_2 fuel rods (1.506-cm pitch and 7-tube clusters)

A series of small, compact critical assembly (SCCA) experiments were performed at Oak Ridge National Laboratory (ORNL) in the US from 1962 to 1965 to support the Medium-Power Reactor Experiments (MPRE) program, which was a stainless-steel system with 1 MW_{th} boiling potassium, or 140 kW_e. Initial SCCA experiments were graphite reflected. The third benchmark in this series was Be-reflected; two critical configurations, nine cadmium ratio measurements, and various fuel and material reactivity measurements were evaluated. Benchmark identifiers: SCCA-SPACE-EXP-003 (IRPhEP)/HEU-COMP-FAST-004 (ICSBEP).

5.3 Irradiation and testing facility development

5.3.1 Versatile test reactor (VTR) design

5.3.1.1 Evaluation of the initial isothermal physics measurements at the fast flux Test Facility, a prototypic liquid metal fast breeder reactor

The initial isothermal physics tests of the Fast Flux Test Facility (FFTF) have been evaluated: criticality, spectral,

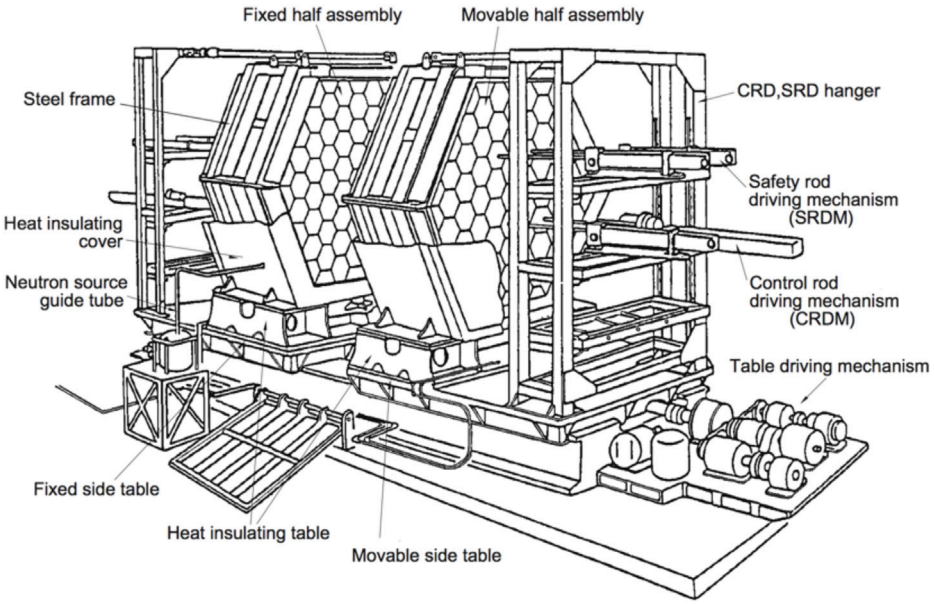

FIGURE 5
Schematic of VHTRC facility.

reactivity worth, reactivity coefficient, and additional miscellaneous measurements. The FFTF was a 400 MW_{th} SFR located at the Hanford Site near Richland, Washington. This reactor was operated from 1982 to 1992 as a prototype liquid metal fast breeder reactor and a fast test reactor for mixed oxide (MOX) and metal fuels. Benchmark identifier: FFTF-LMFR-RESR-001 (IRPhEP).

5.3.1.2 ZPR-3 assembly 56B: A cylindrical assembly of mixed (Pu,U) oxide and sodium with a nickel-sodium reflector

This ZPR assembly was a part of a series of critical experiments performed to support design of the FFTF. The simplistic geometry of this experiment consisted of primarily Pu-U-Mo alloy fuel, sodium, iron, and nickel components. Benchmark identifiers: ZPR-LMFR-EXP-004 (IRPhEP)/MIX-COMP-FAST-004 (ICSBEP).

5.3.2 High flux irradiation testing facilities

5.3.2.1 Advanced test reactor: Serpentine arrangement of highly enriched water-moderated uranium-aluminide fuel plates reflected by beryllium

The Advanced Test Reactor (ATR) is a 250 MW_{th} high flux test reactor located at Idaho National Laboratory (INL) in the US. This reactor is currently in operation. The fresh core internals changeout (CIC) from 1994 (Cycle 103A-2) critical loading is evaluated as a benchmark to support irradiation testing and experiment design, including tests necessary for advanced reactor development. Benchmark identifiers: ATR-FUND-RESR-001 (IRPhEP)/HEU-MET-THERM-022 (ICSBEP).

5.3.2.2 Evaluation of measurements performed on the French high flux reactor (RHF)

The French RHF is 58.3 MW_{th}, located in Grenoble, and was refurbished in 1993–1995. It consists of a single fuel element with curved plates, very similar to the High Flux Isotope Reactor (HFIR) at ORNL. Currently only the critical configuration is evaluated. Benchmark identifier: RHF-FUND-RESR-001 (IRPhEP).

5.3.3 Transient testing facilities

5.3.3.1 IGR reactor–Uranium-graphite blocks reflected by graphite

The Impulse Graphite Reactor (IGR) is located at the Atomic Energy Institute of the National Nuclear Center of Kazakhstan Republic. It is a large graphite stack with very low ^{235}U content to support high-temperature transient testing (the core loading is provided in Figure 7). Benchmark identifiers: IGR-FUND-RESR-001 (IRPhEP)/HEU-COMP-THERM-016 (ICSBEP).

5.3.3.2 Transient reactor test (TREAT) facility M8 calibration (M8CAL) core test

The TREAT facility at INL also serves to provide transient testing capabilities for a variety of fuels, materials, and instrumentation needs. The historic critical core loading from 1994 is evaluated and is most representative of the core loading currently in operation. Many modern experiments are proposed to enable advanced reactor development. Figure 8 shows a model of a more modern experiment test. Benchmark identifier: TREAT-FUND-RESR-002 (IRPhEP).

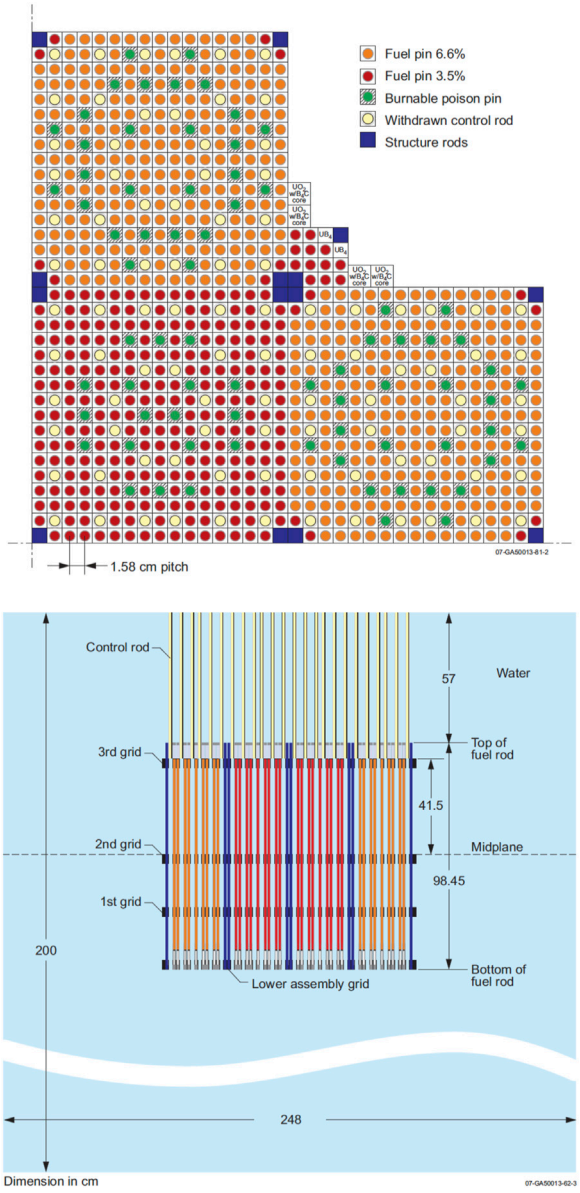

FIGURE 6
Quarter-core Top view (Top) and side view (Bottom) of otto hahn reactor core benchmark model.

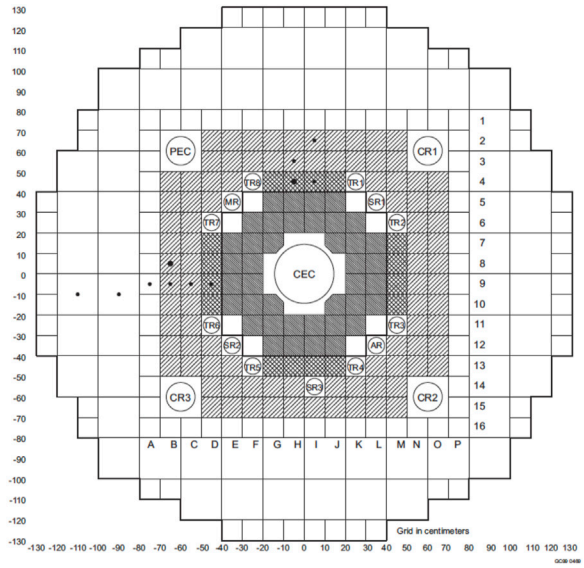

FIGURE 7
Cross-Sectional View of IGR Core and Reflector (the three fuel regions are shaded).

5.4 Enhancing the nuclear fuel cycle

5.4.1 LEU + fuel for power reactors

There are ~50 ICSBEP evaluations containing fissile material with ^{235}U enrichments between 5% and 10%.

5.4.1.1 Evaluation of the Kyoto University Critical Assembly erbium oxide experiments

Five core loadings are evaluated for the Kyoto University Critical Assembly (KUCA) in Japan. The goal of these experiments was to assess the basic neutronic properties of erbia-loaded, low-enriched thermal spectrum cores. Three of the cores had an average U enrichment of 5.4 wt% ^{235}U, and the other two cores 9.6 wt%. Erbia content was increased from 0 wt % up to 1.12 wt%. These experiments support development of higher burnup fuel, which is a necessity with the increase in fuel enrichment above ~5 wt%. Benchmark identifiers: KUCA-FUND-RESR-001 (IRPhEP)/LEU-MET-THERM-005 (ICSBEP).

5.4.1.2 Titanium and/or aluminum rod-replacement experiments in fully-reflected water-moderated square-pitched U (6.90)O_2 fuel rod lattices with 0.67 fuel to water volume ratio (0.800 cm pitch)

The Seven Percent Critical Experiment (7uPCX) is located at Sandia National Laboratories (SNL) in Albuquerque, New Mexico. It was designed to investigate critical systems with fuel for light water reactors in the enrichment range above 5 wt% ^{235}U. The current fuel is 6.90 wt% enriched. Twenty-four different critical core arrangements are evaluated implementing fuel rods, some with empty grid positions, titanium, and/or aluminum interstitial rods. Benchmark identifier: LEU-COMP-THERM-097 (ICSBEP).

5.4.1.3 Partially-reflected water-moderated square-pitched U (6.90)O_2 fuel rod lattices with 0.52 fuel to water volume ratio (0.855 cm pitch)

There are currently several benchmarks using the 7uPCX facility. This benchmark evaluates 22 critical configurations of varying designs: rectangular, cylindrical, and split rectangular arrays. Benchmark identifier: LEU-COMP-THERM-101 (ICSBEP).

5.4.2 High assay low enriched uranium (HALEU) validation

There are ~20 ICSBEP evaluations containing fissile material with ^{235}U enrichments between 10% and 20%.

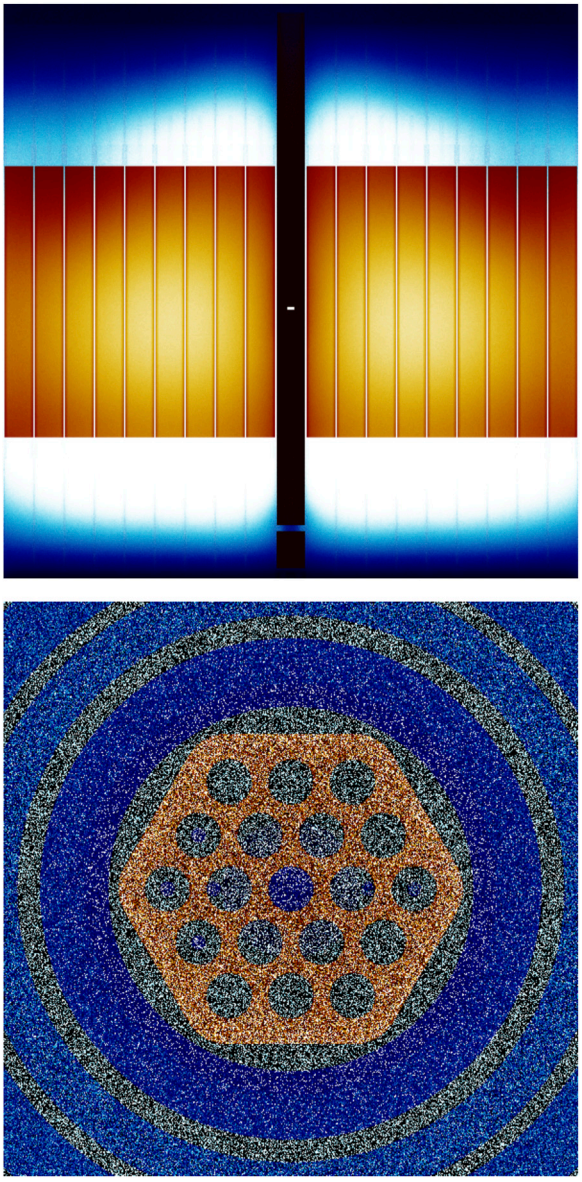

FIGURE 8
Serpent model of TREAT for SIRIUS calibration experiment: Vertical view of core (Top) and horizontal view of test fuel (Bottom).

5.4.2.1 Critical loading configurations of the IPEN/MB-01 reactor composed of fuel rods and U-Mo plates in its core center

The IPEN/MB-01 research reactor center is located in São Paulo, Brazil. Of the numerous contributed benchmarks from this reactor facility, this series of experiments performed in 2016 investigates the reactivity worth of HALEU U-Mo plates placed within the core center (see Figure 9). Benchmark identifiers: IPEN (MB01)-LWR-RESR-020 (IRPhEP)/LEU-COMP-THERM-103 (ICSBEP).

5.4.2.2 Neutron radiography (NRAD) reactor 64-element core upgrade

The neutron radiography (NRAD) reactor is a 250 kWt TRIGA® (Training, Research, Isotopes, General Atomics) Mark II tank-type research reactor located at INL. This reactor was converted to HALEU UErZrH fuel in 2010 and upgraded to include more fuel in 2013. Two critical loadings and rod worth measurements are evaluated in this benchmark. Benchmark identifier: NRAD-FUND-RESR-002 (IRPhEP).

5.4.2.3 Power burst facility: U (18)O_2-CaO-ZrO_2 fuel rods in water

The Power Burst Facility (PBF) operated at INL from 1972 to 1985. It was designed to provide experimental data to define failure thresholds under postulated LWR accident conditions. This transient test facility used HALEU "inert-matrix" ternary oxide fuel. Two similar critical loadings from the startup tests were evaluated. Benchmark identifiers: PBF-FUND-RESR-001 (IRPhEP)/IEU-COMP-THERM-009 (ICSBEP).

5.4.3 Mixed oxide (MOX) fuel cycle

5.4.3.1 Undermoderated MOX (11 wt% PuO_2) lattice in the EOLE reactor

The ERASME/S undermoderated MOX experiment was performed in 1985 as part of a 3-year program dedicated to high conversion PWRs. The experiment was performed in the EOLE facility at Cadarache in France. A single critical configuration was evaluated. Benchmark identifiers: EOLE-PWR-EXP-001 (IRPhEP)/MIX-COMP-INTER-005 (ICSBEP).

5.4.3.2 VENUS-PRP configurations No. 9 and 9/1

The Vulcain Experimental Nuclear Study (VENUS) zero power reactor has been used for a variety of experiments at the SCK-CEN complex in Mol, Belgium. The Plutonium Recycle Programme (PRP) was between 1967 and 1975. Configurations 9 and 9/1, the core loading of the latter provided in Figure 10, were performed to study boundary effects between zones with different plutonium content and the effective influence of perturbations at the boundary. Power distribution measurements were evaluated as benchmark experiment data. Benchmark identifier: VENUS-PWR-EXP-005 (IRPhEP).

5.4.4 Thorium Fuel cycle

5.4.4.1 *PROTEUS* experimental program core 12: Homogeneous MOX and thorium oxide fuel test region

Core 12 of the GCFR-PROTEUS experimental program contained a homogeneous mixed arrangement of (U-Pu)O_2 and ThO_2 fuel pins in a similar core design as the previously described Core 11. Six spectral indices were evaluated for this configuration to enable evaluation of the ^{232}Th/^{233}U fuel cycle. Benchmark identifier: PROTEUS-GCFR-EXP-002 (IRPhEP).

5.4.4.2 B&W spectral shift reactor lattice experiments: A 2188 uranium-thorium rods critical experiment moderated by heavy-light water mixture

The benchmark summarizes a 1960 study by Babcock and Wilcox (B&W) for a Spectral Shift Control Reactor (SSCR) concept using rod lattices moderated by D_2O-H_2O mixtures. This evaluation includes a critical eigenvalue and thermal disadvantage factor. Benchmark identifier: SSCR-PWR-EXP-002 (IRPhEP).

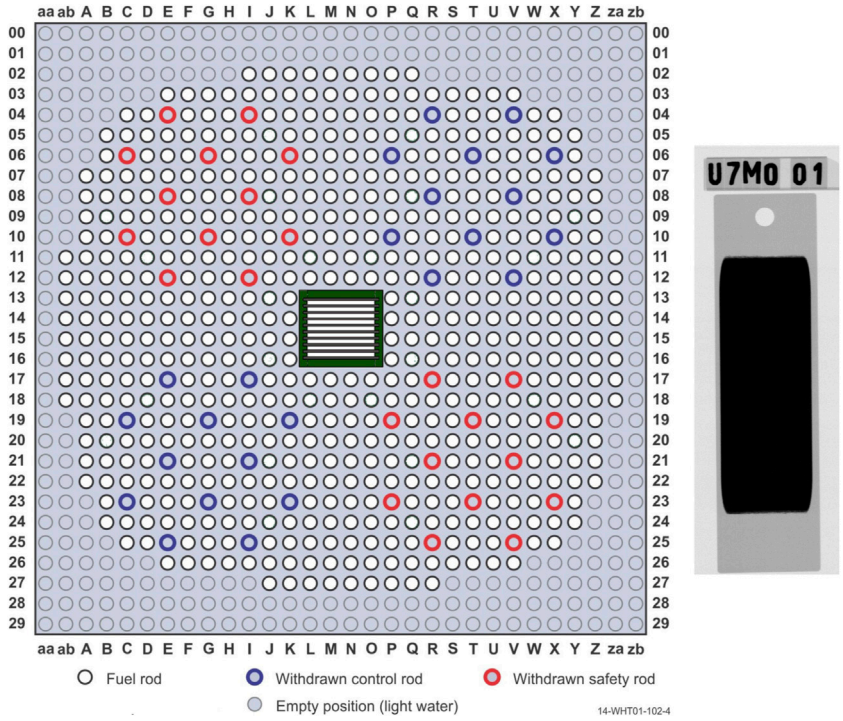

FIGURE 9
Schematic of IPEN MB-01 reactor core loading (Left) and X-Ray of a UMo fuel plate (Right).

5.4.4.3 LWBR SB core experiments

Critical experiments were conducted at the High Temperature Test Facility of the Bettis Atomic Power Laboratory (BAPL) in West Mifflin, Pennsylvania, US to support a Light Water Breeder Reactor (LWBR) program. Benchmark identifier: U233-COMP-THERM-001 (ICSBEP).

5.4.4.4 Kalpakkam mini (KAMINI) reactor: Beryllium-oxide-reflected water-moderated ^{233}U-Fueled reactor

The KAMINI reactor (see Figure 11) is a zero-power reactor with ^{233}U fuel, light water moderation, and BeO reflector. It is located at the Indira Gandhi Centre for Atomic Research in Kalpakkam, India. A single critical configuration from 1996 has been evaluated as a benchmark. Benchmark identifier: U233-MET-THERM-001 (ICSBEP).

5.4.5 Minor actinide management (NEA, 2015)

5.4.5.1 BFS-97, -99, -101 assemblies: Experimental program on critical assemblies with heterogeneous compositions on plutonium, depleted-uranium dioxide, and polyethylene

Another series of experiments with BFS-1 include MOX fast-neutron critical assemblies simulating damp MOX powders. The spectral characteristics were measured *via* fission chambers to obtain fission ratios for ^{238}U, ^{237}Np, ^{239}Pu, ^{240}Pu, ^{241}Am, ^{243}Am, ^{244}Cm, and ^{245}Cm relative to ^{235}U and/or ^{239}Pu, and the capture-to-fission ratio of ^{238}U–^{235}U. Benchmark identifiers: BFS1-FUND-EXP-001 (IRPhEP)/MIX-MISC-MIXED-001 (ICSBEP).

5.4.5.2 BFS-73–1 assembly: Experimental model of sodium-cooled fast reactor with core of metal uranium fuel of 18.5% enrichment and depleted uranium dioxide blanket

Another BFS-1 critical experiment of a sodium-cooled fast reactor included spectral and reactivity worth measurements for isotopes of Np, Pu, and Am. Benchmark Identifier: BFS1-LMFR-EXP-001 (IRPhEP).

5.4.5.3 Replacement measurements performed with Curium-244, Plutonium-239, and HEU using jezebel

A high-purity sample worth for ^{244}Cm was evaluated for a replacement measurement performed with the Jezebel plutonium-240 sphere (PU-MET-FAST-002 in ICSBEP). Benchmark identifier: SPEC-MET-FAST-001 (ICSBEP).

5.4.5.4 Neptunium-237 and highly enriched uranium replacement measurements performed using flattop

A high-purity sample worth for ^{237}Np was evaluated for a replacement measurement performed with the Flattop uranium sphere (MIX-MET-FAST-002 in ICSBEP). Benchmark identifier: SPEC-MET-FAST-003 (ICSBEP).

5.4.5.5 Neptunium-237 sphere surrounded by hemispherical shells of highly enriched uranium

A neptunium sphere was encased within matching pairs of HEU shells to decrease the uncertainty in the critical mass of ^{237}Np for criticality safety and non-proliferation issues (see Figure 12). Benchmark identifier: SPEC-MET-FAST-008 (ICSBEP).

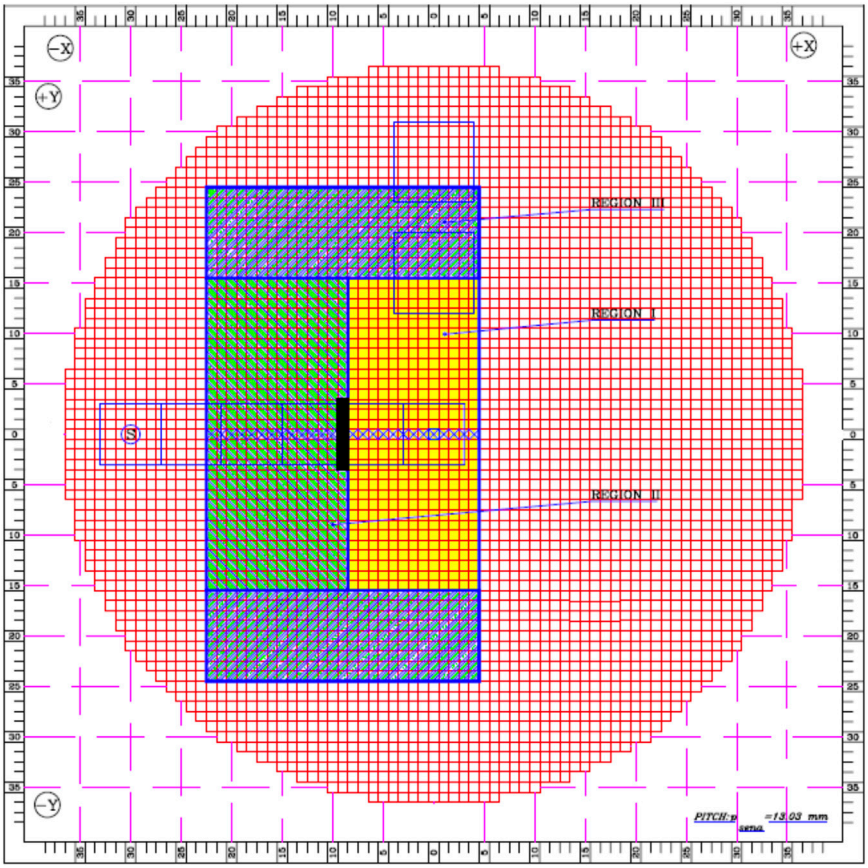

FIGURE 10
Horizontal Historical Schematic of Configuration 9/1 Core Loading from VENUS-PRP (Region I represents MOX fuel pins; Regions II and III represent UO_2 fuel pins).

5.5 Improvements in modeling, simulation, and nuclear data

5.5.1 Pressurized Water Reactor (PWR) characterization

5.5.1.1 BEAVRS–A multi-cyle full core commercial PWR depletion benchmark

The Benchmark for Evaluation And Validation of Reactor Simulations (BEAVRS) is a multi-cycle full-core PWR depletion benchmark based upon measurement data from two operational cycles of a commercial nuclear plant. This benchmark is excellent for testing computational capabilities. However, it remains as a draft evaluation on the IRPhEP Handbook as much of the original data is proprietary, significantly limiting bias and uncertainty analyses requisite of a high-quality benchmark experiment. Benchmark identifier: BEAVRS-PWR-POWER-001 (IRPhEP).

5.5.1.2 PWR fuel assembly depletion reactivity determination using PWR fission rate measurements

Core-wide fission rate distribution measurements from 44 cycles of PWR operation at Duke Power Company's McGuire and Catawba nuclear power plants were utilized to infer fuel assembly reactivity due to nuclide burnup. The results are then used to create benchmarks for core-averaged fuel assembly depletion up to 60 GW d/t. Benchmark identifier: DUKE-PWR-POWER-001 (IRPhEP).

5.5.1.3 Reactivity worth measurements of major fission products in MINERVE LWR-Lattice experiment

The reactivity worth of major fission products was measured in the MINERVE reactor in Cadarache, France as part of the CERES program between France and the United Kingdom to validate LWR fuel reactivity loss with burnup. The CERES Phase II measurements performed in MINERVE are evaluated in this benchmark for various isotopes including Sm, Nd, Gd, Eu, Rh, Cs, Mo, and Tc. Benchmark identifier: MINERVE-FUND-RESR-001 (IRPhEP).

5.5.2 Expanding neutron spectra coverage

5.5.2.1 TEX-HEU baseline assemblies highly enriched uranium plates with polyethylene moderator and polyethylene reflector

The Thermal/Epithermal eXperiments (TEX) program was designed to provide a platform of similar experiments for testing materials and fuels across the neutron spectra. Historically experiments have focused upon neutron behavior in thermal or fast regimes. The TEX program includes experiments for testing fuels and materials across the intermediate neutron energy spectra. The TEX-HEU experiments evaluated in this benchmark provide

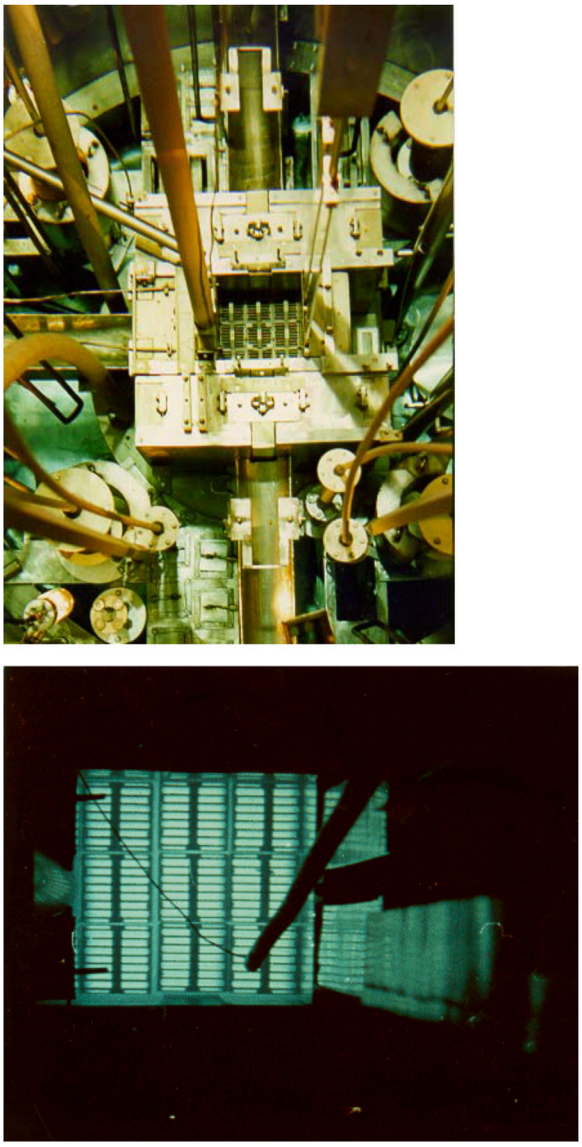

FIGURE 11
Photo of KAMINI reactor (Top) and cherenkov radiation (Bottom).

five baseline cases. Benchmark identifier: HEU-MET-MIXED-021 (ICSBEP).

5.5.2.2 TEX plutonium baseline assemblies: Plutonium/aluminum metal alloy plates with varying thicknesses of polyethylene moderator and a thin polyethylene reflector

This benchmark contains the TEX baseline cases for plutonium experiments across the neutron spectra. Benchmark identifier: PU-MET-MIXED-002 (ICSBEP).

5.5.3 Selected examples of benchmarks testing nuclear data

It is impossible to summarize the plethora of benchmarks available to support testing and validation of the nuclear data utilized in nuclear codes, methods, design, and applications worldwide. Only a snippet of examples is provided below, and many more examples can be found within the handbooks using the tools presented in Section 3.

FIGURE 12
Np sphere with highly enriched uranium shells mounted in the planet assembly.

5.5.3.1 Static critical experiments for the sorgente rapida (SORA) reactor mockup

A series of critical experiments were performed at ORNL in 1965–1966 to support the design of SORA, which was to be a U-Mo burst facility. Fifteen mockup critical configurations were evaluated for U-metal rod arrays reflected by high-purity (99.5 wt%) Fe and Be. Benchmark identifier: HEU-MET-FAST-096 (ICSBEP).

5.5.3.2 Reactor physics experiments in the IPEN/MB-01 reactor with heavy reflectors composed of carbon steel and nickel

Thirty-five critical loadings were evaluated for the IPEN/MB-01 reactor. The core was reflected on the west side by increasing cumulative thicknesses of carbon steel or nickel laminates. This experiment tests neutron absorption and scattering in the reflecting material as the spectra hardens from thermal neutron absorption to fast neutron reflection. Benchmark identifiers: IPEN (MB01)-LWR-RESR-015 (IRPhEP)/LEU-COMP-THERM-088 (ICSBEP).

5.5.3.3 4.738-wt.%-enriched-uranium-dioxide-fuel-rod arrays in water, reflected or separated by various structural materials (aluminum, concrete, copper, glass, iron, lead, nickel, titanium, zirconium)

The Matériaux Interaction Réflexion Toutes Epaisseurs (MIRTE) program was carried out from 2008 to 2013 at the Commissariat à l'Energie Atomique (CEA) Valduc center in France. The purpose of this program was to measure integral reactivity characteristics of various structural materials, as demonstrated in Figure 13, to support validation of computer

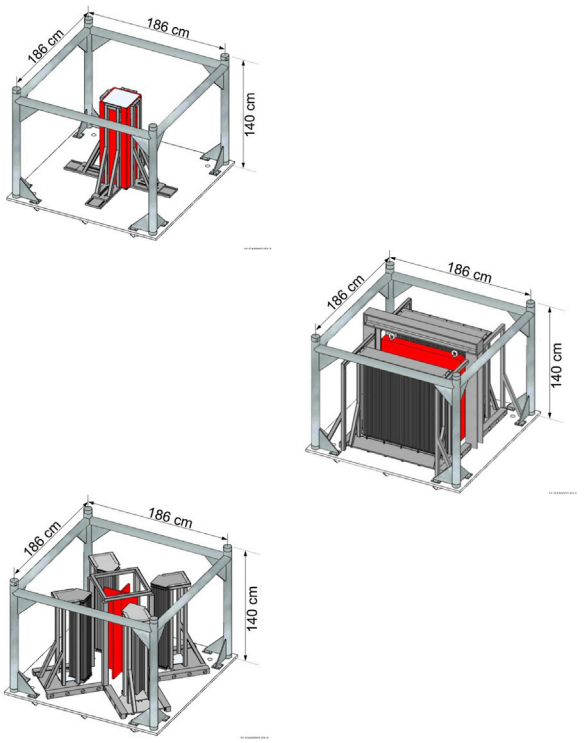

FIGURE 13
Configurations of screens in MIRTE experiments: Reflected (Top), interacting with Thick screen (middle), and interacting with Thin cruciform screens (Bottom).

codes and nuclear data. A total of 28 benchmark configurations were evaluated from this experimental series. The experiments consisted of LEU rod arrays reflected or separated by screens of the test materials. Benchmark identifier: LEU-COMP-THERM-074 (ICSBEP).

6 Conclusion

The ICSBEP and IRPhEP actively provide international preservation, evaluation, and dissemination of integral benchmark data to support computational validation of models, simulations, and nuclear data in support of criticality safety and reactor physics applications. Annual contributions to their respective handbooks provide an ever-growing resource of evaluated benchmark experiment data that has been assessed qualitatively and quantitatively to provide uncertainties, biases, and established benchmark models within a standardized handbook format. All benchmark evaluations undergo an intensive peer-review process with participants and contributions representing over 20 countries. Experiments were performed historically to support reactor operations, measurements, design, and nuclear safety. The extensive investments in infrastructure, expertise, and cost are not cheaply reproduced should the information from these legacy experiments become lost. The preservation and evaluation activities of the ICSBEP and IRPhEP provide a means to provide quality nuclear data for current and future needs in computational tools and nuclear data testing.

The needs of the nuclear modeling and simulation community continues to expand and evolve. The ICSBEP and IRPhEP provide well-established frameworks to continue to provide high-quality, peer-reviewed benchmark data to serve as the intrinsic backbone of contemporary neutronics methodologies, simulation, and nuclear data. The true value of their handbooks is priceless considering the impact they have in supporting, sustaining, and enabling modern nuclear safety, design, modeling, and simulation.

Future endeavors in advancement of nuclear reactor designs builds upon contemporary and historic efforts to understand and characterize our nuclear world *via* experimentation. The ICSBEP and IRPhEP serve as an international omnibus of curated and evaluated experimental data from around the world. The benchmarks contained within their handbooks serve as the backbone for validation testing of contemporary neutronics methodologies, simulation, and nuclear data. This manuscript serves as only a snapshot of the current culmination of international collaborations to utilize our nuclear heritage to enable our nuclear future. It does not include numerous evaluations that are currently being considered or that are in the initial phases of the evaluation process.

Data availability statement

The data analyzed in this study is subject to the following licenses/restrictions: Data available to OECD NEA member countries and participating organizations. Requests to access these datasets should be directed to Julie-Fiona Martin (Julie-Fiona.MARTIN@oecd-nea.org) and Ian Hill (Ian.HILL@oecd-nea.org).

Author contributions

All authors listed have made a substantial, direct, and intellectual contribution to the work and approved it for publication.

Funding

Contributions, financial and otherwise, towards the success of the OECD NEA international benchmark projects have come from a myriad of national and international sources.

Acknowledgments

The ICSBEP and IRPhEP are collaborative efforts that involve numerous scientists, engineers, and administrative support personnel from 28 different countries. The authors would like to acknowledge the efforts of all these dedicated individuals without whom these technical working groups would not be possible. A listing of all contributors can be found in the introductory material of both ICSBEP and IRPhEP Handbooks.

Conflict of interest

JB is employed by JFoster & Associates, LLC.

The remaining authors declare that the research was conducted in the absence of any commercial or financial relationships that could be construed as a potential conflict of interest.

Publisher's note

References

Bess, J. D., and Ivanova, T. (2020). Current overview of ICSBEP and IRPhEP benchmark evaluation practices. *EPJ Web Conf.* 239, 18002. doi:10.1051/epjconf/202023918002

Briggs, J. B., and Gulliford, J. (2014). An overview of the international reactor physics experiment evaluation project. *Nucl. Sci. Eng.* 178 (3), 269–279. doi:10.13182/NSE14-27

Briggs, J. B., Scott, L., and Nouri, A. (2003). The international criticality safety benchmark evaluation project. *Nucl. Sci. Eng.* 145 (1), 1–10. doi:10.13182/NSE03-14

Dean, V. F., and Blackwood, L. G. (2008). *ICSBEP guide to the expression of uncertainties*. Paris, France: OECD Nuclear Energy Agency.

Dos Santos, A., Briggs, J. B., Tsiboulia, A. M., Hill, I., Szatmary, Z., Snoj, L., et al. (2018). "Overview of the international reactor physics experiments evaluation project (IRPhEP) guide to the expression of uncertainty," in Proceedings of International Conference on Physics of Reactors (PHYSOR 2018), Cancun, Mexico, April 22-26 2018.

Hill, I., Soppera, N., and Bossant, M. (2014). Idat: The international handbook of evaluated reactor physics benchmark experiments database and Analysis tool. *Nucl. Sci. Eng.* 178 (3), 280–294. doi:10.13182/NSE14-37

Kodeli, I. A., and Sartori, E. (2021). Sinbad – radiation shielding benchmark experiments. *Ann. Nucl. Energy* 159, 108254. doi:10.1016/j.anucene.2021.108254

Menut, P., Sartori, E., and Turnbull, J. A. (2000). "The public domain database on nuclear fuel performance experiments (IFPE) for the purpose of code development and validation," in Proceedings of the 2000 International Topical Meeting on Light Water Reactor Fuel Performance, Park City, Utah, April 10-13 2000.

Michel-Sendis, F., Gauld, I., Martinez, J., Alejano, C., Bossant, M., Boulanger, D., et al. (2017). SFCOMPO-2.0: An OECD NEA database of spent nuclear fuel isotopic assays, reactor design specifications, and operating data. *Ann. Nucl. Energy* 110, 779–788. doi:10.1016/j.anucene.2017.07.022

NEA (2022a). *International handbook of evaluated criticality safety benchmark experiments*. Paris, France: OECD Nuclear Energy Agency.

NEA (2022b). *International handbook of evaluated reactor physics benchmark experiments*. Paris, France: OECD Nuclear Energy Agency.

NEA (2015). *Review of integral experiments for minor actinide management. NEA No. 7222*. Paris, France: OECD Nuclear Energy Agency.

Nouri, A., Nagel, P., Briggs, J. B., and Ivanova, T. (2003). Dice: Database for the international criticality safety benchmark evaluation program handbook. *Nucl. Sci. Eng.* 145 (1), 11–19. doi:10.13182/NSE03-15

Palmiotti, G., Briggs, J. B., Kugo, T., Trumble, E. F., Kahler, A. C. S., and Lancaster, D. (2014). Applications of integral benchmark data. *Nucl. Sci. Eng.* 178 (3), 295–310. doi:10.13182/nse14-33

Rohatgi, U., Dyrda, J., and Soppera, N. (2018). "The international experimental thermal hydraulic systems database (TIETHYS): A new NEA validation tool," in Proceedings of the 26th International Conference on Nuclear Engineering, London, England, July 22-26 2018. doi:10.1115/ICONE26-82631

Rozhikhin, Y. (1999). "Detailed spectra data for the international handbook of evaluated criticality safety benchmark experiments," in Proceedings of International Conference on Nuclear Criticality Safety (ICNC 1999), Versailles, France, Sept. 20-24 1999, 1167–1172. Volume III.

Valentine, T., Avramova, M., Fleming, M., Hursin, M., Ivanov, K., Petruzzi, A., et al. (2018). "OECD-NEA Expert group on multi-physics experimental data, benchmarks and validation," in Proceedings of the 26th International Conference on Nuclear Engineering, London, England, July 22-26 2018. doi:10.1115/ICONE26-81571

frontiers | Frontiers in Energy Research

TYPE Original Research
PUBLISHED 16 March 2023
DOI 10.3389/fenrg.2023.1085764

OPEN ACCESS

EDITED BY
Mingjun Wang,
Xi'an Jiaotong University, China

REVIEWED BY
Pierre Ruyer,
Institut de Radioprotection et de Sûreté Nucléaire, France
Stephan Kelm,
Forschungszentrum Juelich GmbH, Germany
Luteng Zhang,
Chongqing University, China

*CORRESPONDENCE
John D. Bess,
john.bess@jfaidaho.com

SPECIALTY SECTION
This article was submitted to Nuclear Energy,
a section of the journal
Frontiers in Energy Research

RECEIVED 31 October 2022
ACCEPTED 07 March 2023
PUBLISHED 16 March 2023

CITATION
Bess JD, Blaise P, Buss O, DeHart M, Fleming M, Hill I, Ilas G, Ivanova T, Ivanov E, Marshall WJ, Martin J-F, Miller T, Percher C, Petruzzi A, Rohatgi US and Valentine TE (2023), Engagement opportunities in OECD NEA benchmark development.
Front. Energy Res. 11:1085764.
doi: 10.3389/fenrg.2023.1085764

Engagement opportunities in OECD NEA benchmark development

John D. Bess[1]*, Patrick Blaise[2], Oliver Buss[3], Mark DeHart[4], Michael Fleming[3], Ian Hill[3], Germina Ilas[5], Tatiana Ivanova[3], Evgeny Ivanov[6], William J. Marshall[5], Julie-Fiona Martin[3], Thomas Miller[5], Catherine Percher[7], Alessandro Petruzzi[8], Upendra S. Rohatgi[9] and Timothy E. Valentine[10]

[1]JFoster & Associates, LLC, Idaho Falls, ID, United States, [2]Commissariat à L'énergie Atomique et Aux Energies Alternatives, Scientific Division of Energies, Gif-sur-Yvette, France, [3]Organisation for Economic Co-operation and Development, Nuclear Energy Agency, Paris, France, [4]Idaho National Laboratory, Nuclear Science and Technology Division, Idaho Falls, ID, United States, [5]Oak Ridge National Laboratory, Nuclear Energy and Fuel Cycle Division, Oak Ridge, TN, United States, [6]Institut de Radioprotection et de Sûreté Nucléaire (IRSN), Fontenay-aux-Roses, France, [7]Lawrence Livermore National Laboratory, Nuclear Criticality Safety Division, Livermore, CA, United States, [8]Nuclear and INdustrial Engineering, Lucca, Italy, [9]Brookhaven National Laboratory, Nonproliferation and National Security Department, Upton, NY, United States, [10]Oak Ridge National Laboratory, Radiation Safety Information Computational Center, Oak Ridge, TN, United States

A myriad of opportunities is available to collaborate *via* international benchmark exercises and experimental data preservation activities. Many such opportunities abound under the auspices of the Nuclear Science Committee of the Organisation for Economic Co-operation and Development Nuclear Energy Agency (NEA). Key projects and activities of relevance to the development of advanced reactors design include the International Criticality Safety Benchmark Evaluation Project (ICSBEP), the International Reactor Physics Experiment Evaluation Project (IRPhEP), the International Assay Data of Spent Nuclear Fuel Database (SFCOMPO), the Shielding Integral Benchmark and Archive Database (SINBAD), and The International Experimental Thermal HYdraulicS Database (TIETHYS), and various cooperative benchmark exercises. Interested participants are encouraged to contact the leadership and secretariat of the various Technical Working Groups and Working Parties to become more engaged. This paper provides a summary of the current benchmark exercises and experimental databases available for international participation.

KEYWORDS

benchmark, database, nuclear, validation, working groups

1 Introduction

The Organisation for Economic Co-operation and Development (OECD) Nuclear Energy Agency (NEA) is an intergovernmental agency that fosters and facilitates international collaboration to advance nuclear technology infrastructures enabling excellence in nuclear safety, technology, science, environment, and law. The objective of the NEA is to assist its member countries in maintaining and developing the scientific, technological, and legal foundation requisite for safe, environmentally sound, and economical use of nuclear energy for peaceful purposes. It also provides authoritative assessments and forges common understandings on key issues as input to government

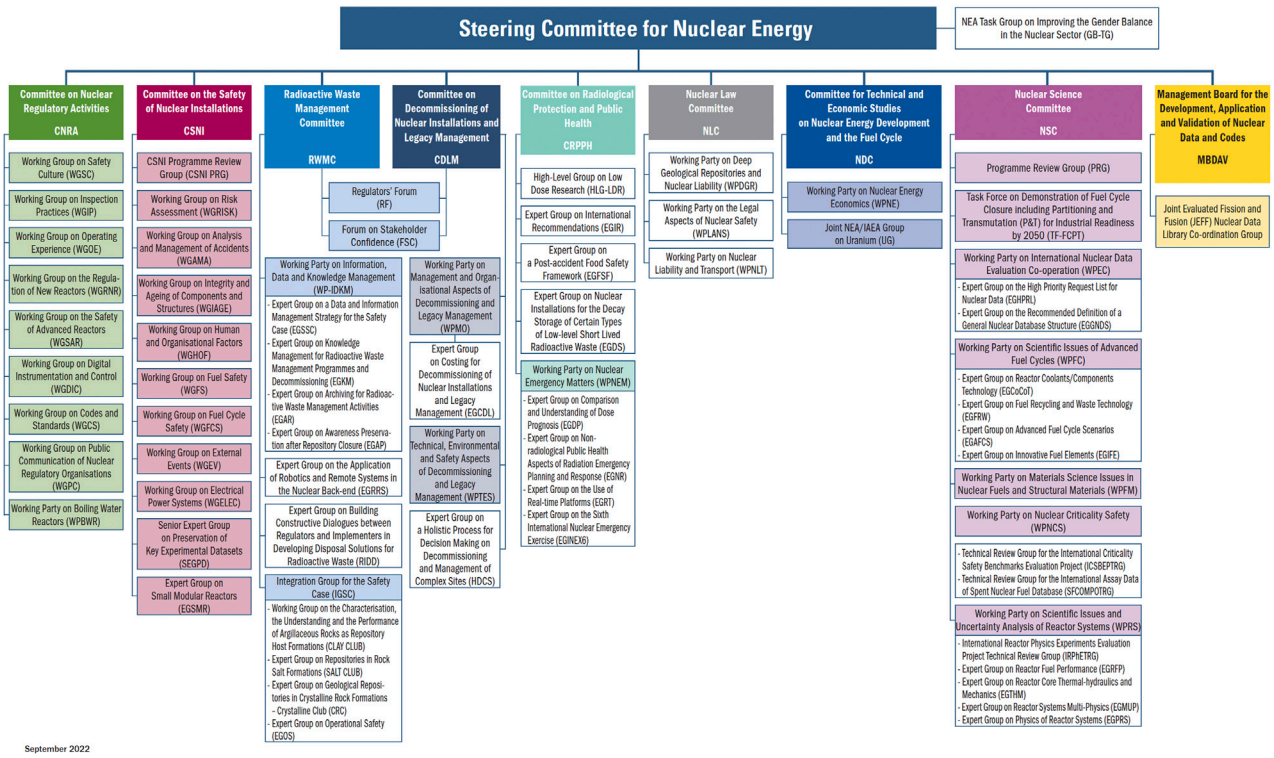

FIGURE 1
Structure of the Nuclear Energy Agency Committees and Subsidiary Bodies.

decisions on nuclear energy policy and to broader OECD analyses in areas such as energy and the sustainable development of low-carbon economies. However, the NEA is not a policy-making agency; policy decisions related to the use of information provided by NEA activities are made on a national or, as applicable, a regional level. This nuclear foundation is relevant to today's nuclear facilities as well as future advanced reactor systems.

The NEA oversees a broad range of activities organized within standing technical committees, including the Committee on Nuclear Regulatory Activities (CNRA), Committee on the Safety of Nuclear Installations (CSNI), the Radioactive Waste Management Committee (RWMC) and the Nuclear Science Committee (NSC) Some of the standing committees have established up discipline-oriented Working Parties which report directly to them, or expert groups in charge of specific tasks, reporting either to the working parties or directly to the standing technical committees. The Agency's nuclear science program is led by the NSC, while the CSNI is responsible for maintaining and advancing the scientific and technical knowledge base of the safety of nuclear installations. Both are comprised of high-level international scientific experts, and within each, various Working Parties and Technical Working Groups exist and operate to promote the co-ordination of work in different member countries that serve to maintain and enhance competence in nuclear safety matters, including the establishment of joint undertakings and assist in the distribution of the work to participating organisations. We will give a very abbreviated overview of CSNI and NSC activities to provide and understanding of activities that are relevant for the study of advanced reactor systems.

Within the CSNI, the Working Group on Fuel Safety (WGFS) is tasked with advancing the understanding of nuclear fuel safety issues by assessing the technical basis for current safety criteria and their applicability to high burnup and to new fuel designs and materials. WGFS aims to facilitate international convergence in this area, including as regards experimental approaches and interpretation and the use of experimental data relevant for fuel safety. One of the key areas in fuel safety is the analysis of fuel behavior under reactivity-initiated accident (RIA) conditions for which the WGFS has led major fuel performance codes benchmarking activities over the last decade. CSNI also oversees a number of International Standard Problems (ISPs) exercises, which are comparative exercises in which predictions or recalculations of a given physical problem with different best-estimate computer code that are compared with each other and above all with the results of a carefully specified experimental study.

Within the NSC, the WPFC Expert Group on Innovative Fuel Elements (EGIFE) is coordinating a benchmark related to fuel performance of fast reactor fuel. Among its constituent Expert Groups, the Expert Group on Innovative Fuels (EGIF) was

created with the objective of conducting joint and comparative studies to support the development of innovative fuels such as homogeneous and heterogeneous fuels, accelerator driven system (ADS) fuels, and oxide, metal, nitride and carbide fuels, all of which can be implemented in advanced nuclear fuel cycles with fast reactors. The Working Party on Nuclear Criticality Safety (WPNCS) deals with technical and scientific issues relevant to criticality safety. Specific areas of interest include (but are not limited to) investigations of static and transient configurations encountered in the nuclear fuel cycle. These include fuel fabrication, transport, and storage. The Working Party on Scientific Issues and Uncertainty Analysis of Reactor Systems (WPRS) studies the reactor physics, fuel performance, and radiation transport and shielding in present and future nuclear power systems. The Working Party also studies the uncertainties associated with the modelling of these phenomena, particularly the modelling of reactor transient events. The current structure of the NEA committees and subsidiary bodies is shown in Figure 1, and can also be found online at the following weblink: https://www.oecd-nea.org/jcms/pl_36698/structure-of-nuclear-energy-agency-committees-and-subsidiary-bodies.

The purpose of this paper is to present a synopsis of a subset of the myriad of opportunities available *via* the NEA that serve to preserve and evaluate experimental data, to establish reliable benchmark cases, and to challenge state-of-the-art tools in cooperative benchmark exercises of relevance to the development of advanced reactors. In the context of this paper, advanced reactors, refers to essentially any reactor outside the water reactor arena, including, but not limited to, molten salt reactors, high-temperature gas reactors (HTGRs) using graphite as a moderator and helium as a coolant, sodium-, lead-, and gas-cooled fast as well as small modular reactors (SMRs) and micro-reactors that are designed using non-water coolant. We make this distinction as data on water cooled reactors is more readily available. The activities described herein originate within and report on various Working Parties and Expert Groups established by the NSC. Interested participants are encouraged to become engaged in these groups by contacting their respective leadership and NEA secretariats which are summarized in Section 3.

2 International collaborative efforts within the NEA nuclear science committee

2.1 International criticality safety benchmark evaluation project (ICSBEP)

The International Criticality Safety Benchmark Evaluation Project (ICSBEP) (Briggs, Scott, and Nouri, 2003), a sanctioned program under the auspices of the OECD NEA since 1995, is considered the gold standard for experimental benchmarking within the nuclear community. Its main purpose is to preserve and evaluate new and legacy integral experiment data and publish it in a standardized handbook format to provide quality benchmarks for modern and future criticality safety and nuclear data validation. Many neutronics codes around the world use ICSBEP benchmarks in their test suites and nuclear data libraries use the benchmark predictions as a main indicator of library fidelity. The ICSBEP and the International Reactor Physics Experiment Evaluation Project (see Section 2.3) have been invaluable sources of benchmark data from many countries, allowing access to experimental benchmarks that are unique, otherwise unavailable, and would be cost-prohibitive to replicate.

The 2022 edition of the ICSBEP Handbook (NEA, 2022a) includes 592 evaluations containing acceptable benchmark specifications for 5,144 critical, subcritical, or near-critical configurations, representing contributions from 26 countries. An additional 838 configurations deemed unacceptable to support criticality safety requirements yet are valuable to the community are also preserved within the handbook. Additionally, there are 10 criticality alarm placement/shielding evaluations containing a total of 46 benchmark configurations, and 11 fundamental physics evaluations containing a total of 238 measurements relevant to criticality safety applications.

Many advanced reactor design concepts fall well outside of the established validation coverage used for traditional light water reactors, involving novel materials (molten salts, liquid metals, new fuel alloys, increased enrichments) and harder neutron spectra. Integral benchmarks to test neutronics codes and their underlying nuclear data are vital to assessing the fidelity of code predictions, and the ICSBEP benchmarks represent a significant breadth of experiments with fissile and non-fissile materials with various energy spectra. Validation gaps exist for advanced reactors and their fuel cycles, but a thorough review of the ICSBEP Handbook should identify existing applicable, evaluated benchmarks to reduce the number of new experiments that must be performed and evaluated in support of the deployment of these novel reactor systems.

2.2 International reactor physics experiment evaluation project (IRPhEP)

The OECD-NEA International Reactor Physics Experiment Evaluation Project (IRPhEP) (Briggs and Gulliford, 2014) seeks to preserve and evaluate integral reactor physics experiment data to support nuclear energy and technology needs. International contributions are collated within the IRPhEP Handbook (NEA, 2022b). Measurements found in the Handbook include criticality, buckling and extrapolation length, spectral characteristics, reactivity effects, reactivity coefficients, kinetics, reaction rate distributions, power distributions, isotopic compositions, and/or other miscellaneous types of measurements for various types of reactor systems. Distributed with the IRPhEP Handbook and available online is the IRPhEP Database and Analysis Tool (IDAT) (Hill et al., 2014), allowing users to search and interrogate the data.

A total of 26 countries have contributed to the past and continued success of these projects as benchmark evaluations, technical reviews, and experimental data using their own time and resources. Contributing countries include Argentina, Austria, Belarus, Belgium, Brazil, Canada, People's Republic of China, Czech Republic, Denmark, France, Germany, Hungary, India, Italy, Japan, Kazakhstan, Republic of Korea, Russian Federation, Serbia, Slovenia, South Africa, Spain, Sweden, Switzerland, United Kingdom, and the United States of America.

The IRPhE project is patterned after and closely coordinated with the International Criticality Safety Benchmark Evaluation Project (ICSBEP) (Briggs et al., 2003; NEA, 2020b) in order to avoid duplication of effort and publication of conflicting information. Some benchmark data are applicable to both nuclear criticality safety and reactor physics technology. Some have already been evaluated and published by the ICSBEP. However, the ICSBEP has focused primarily on critical and subcritical configurations and radiation transport measurements that are relevant to determining the need for and placement of criticality alarm systems.

The value of the IRPhEP is demonstrated by use of the benchmarks themselves. In (Palmiotti, et al., 2014) it is stated that the benchmark projects "have and will continue to make, vast amounts of valuable legacy and new data available to current and future nuclear energy–related programs." This includes advanced reactor designs, including systems for which traditional physics experiments cannot be easily performed. For example, the Versatile Test Reactor (VTR) project has used two relevant benchmarks for validation of their calculational methods:

- *Evaluation of the Initial Isothermal Physics Measurements at the Fast Flux Test Facility, a Prototypic Liquid Metal Fast Breeder Reactor*, FFTF-LMFR-RESR-001, and
- *ZPR-3 Assembly 56B: A Cylindrical Assembly of Mixed (Pu,U) Oxide and Sodium with a Nickel-Sodium Reflector*, ZPR-LMFR-EXP-004.

The DOE/NNSA Material Management and Minimization (M3) program has made extensive use of the IRPhEP benchmark Advanced Test Reactor: Serpentine Arrangement of Highly Enriched Water-Moderated Uranium-Aluminide Fuel Plates Reflected by Beryllium, HEU-MET-THERM-022.

A number of benchmarks will be of value to the DOE Advanced Reactor Technologies and the Department of Defense TRISO-Based Microreactor Design programs:

- *Evaluation of the Start-Up Core Physics Tests at Japan's High Temperature Engineering Test Reactor (Fully-Loaded Core)*, HTTR-GCFR-RESR-001,
- *HTR-PROTEUS Pebble Bed Experimental Program Cores 9 10: Columnar Hexagonal Point-On-Point Packing with a 1: 1 Moderator-To-Fuel Pebble Ratio*, PROTEUS-GCR-EXP-004, and
- *Temperature Effect on Reactivity in VHTRC-1 Core*, VHTRC-GCR-EXP-001.

Under the US Department of Energy's (DOE) Nuclear Engineering University Programs (NEUP), a number of benchmarks for advanced reactors are being developed, including:

- *Development and Evaluation of Neutron Thermalization Integral Benchmarks for Advanced Reactor Applications*, PI: Ayman I. Hawari, North Carolina State University (2019),
- *Regenerating Missing Experimental Parameters with Data-Assimilation Methods for MSRE Transient Benchmark Development and Evaluation*, PI: Zeyun Wu, Virginia Commonwealth University (2021), and
- *Separate and Mulitphysics Effects IRPhEP Benchmark Evaluation using SNAP Experiments*, PI: Dan Kotlyar, Georgia Institute of Technology (2021).

In general, individuals and organizations solicit funding from their companies or other avenues of research and development support to develop a benchmark. And as mentioned earlier, development of IRPhEP benchmarks is often supported under DOE NEUP. Benchmarks evaluations are prepared based upon historic or recently performed experimental data using guides and example evaluations provided in the IRPhEP Handbook. One or more evaluators provide the primary assessment of a benchmark experiment, which is followed by an in-house verification of the analyses, including adherence to the handbook guidance and procedures performed by internal reviewer(s). Independent review is coordinated *via* the IRPhEP and NEA to verify the analysis; independent reviewers typically are external, often foreign, participants. In the event that insufficient personnel are available to support internal review for a given evaluation, then at least two independent reviewers are assigned to ensure sufficient peer-review prior to submission to the IRPhE TRG. Reviewers often serve on a voluntary basis or are supported by their own research programs. Individuals interested in participating as TRG reviewers should contact IRPhE leadership. Regardless of experience, many would benefit from the experience gained when reviewing these benchmarks (DeHart, et al., 2022).

2.3 International assay data of spent nuclear fuel database (SFCOMPO)

SFCOMPO is the largest international database of open experimental assay data for spent nuclear fuel, publicly available online at https://www.oecd-nea.org/jcms/pl_21515/sfcompo-2-0-spent-fuel-isotopic-composition. The database is hosted by the NEA and managed by the SFCOMPO Technical Review Group (TRG) under the NEA Nuclear Science Committee - Working Party on Nuclear Criticality Safety (NEA/NSC/WPNCS). Assay data in the SFCOMPO database consists of datasets of measured nuclide concentrations of well characterized irradiated nuclear fuel samples, with description of samples' characteristics and operation histories being provided with adequate detail for potential use in benchmark models. Assay data are provided for 750 samples selected from fuel irradiated in 44 reactors, with 8 reactor types and over 24,000 measurement entries, and cover measurement data for 91 nuclides.

SFCOMPO originates from the database compiled in the 1990s by the Japan Atomic Energy Research Institute (JAERI), which consisted of a series of webpages with tables of measured data for fuel samples from 7 pressurized water reactors (PWRs) and 7 boiling water reactors (BWRs). This database was transferred from JAERI to NEA in 2001, has been hosted by NEA since and has been expanded significantly through the international community's concerted effort led by the NEA Expert Group of Assay Data of Spent Nuclear Fuel (EGADSNF) during 2001–2013. Development of a new, modern functionality database with a standardized format and improved accessibility was initiated in 2013 and culminated

with the release in 2016 of the SFCOMPO 2.0 new graphical user interface (Michel-Sendis et, al. 2017). This interface enables user-friendly content browsing and data visualization, and easy access to the primary references.

The SFCOMPO TRG has been mandated by the NEA/NSC/WPNCS to maintain and further coordinate the development of the SFCOMPO database. The TRG's members and contributors are science and engineering experts from academia, industry, and research institutions worldwide. The SFCOMPO TRG's mission is complementary to the efforts of IRPhEP and ICSBEP TRGs, to extend the applications beyond nuclear criticality safety or steady-state in-core analyses and support a broad range of fuel cycle needs, including radiological safety, source terms, shielding, and repository analyses. The primary missions of the SFCOMPO TRG are: 1) preservation of data (preserve and capture legacy data as well as new data as they become available); 2) accessibility of data (*ad hoc* formatting of the data, and continuous adaptation of the SFCOMPO database and its interface tools to address current and future needs); 3) evaluation of data (perform international peer-reviewed assessments to produce qualified benchmarks suitable for code validation); and 4) knowledge transfer (develop guidance for qualification of data evaluations and train new generations of experts through the evaluation/review process).

Evaluation of data for developing benchmarks is the current focus (Ilas, et al., 2020) of the TRG. Since 2019, two evaluations have been approved for release and are pending publication ("Evaluation of Three Mile Island Unit 1 Fuel Samples—Assemblies NJ05YU and NJ070G (Type 15 × 15)" by Georgeta Radulescu, and "Evaluation of Fukushima-Daini-1 Samples—Assemblies 2F1ZN2 and 2F1ZN3 (Type 9×9–9)" by Ugur Mertyurek). A further set of three draft evaluations are pending finalization of the independent review and approval by the TRG. To address community's great interest in decay heat data addition as a new key spent fuel metric to the SFCOMPO database, a task force was established in January 2022 to prepare, review, and curate full-assembly decay heat experimental data for addition as new entry datasets in the SFCOMPO database. The requirements that are being developed for decay heat addition will be consolidated with previous enhancements of the database and its interface.

SFCOMPO is an invaluable asset serving the needs of the international community. Validity of safety assessments for handling irradiated nuclear fuel including transportation, storage, processing and recycling, and repository applications is largely based on capabilities to accurately predict the evolution of nuclides during and after irradiation in fuel and structural materials. Experimental assay data are essential for evaluating bias and uncertainties in spent nuclear fuel safety analyses and provide one means for determining uncertainties in integral quantities important to safety, such as decay heat or spent fuel reactivity, and to validate nuclear data. The importance of experimental assay data for code and associated nuclear data validation goes well beyond the back end of the fuel cycle applications, to impact any area where accurate estimation of nuclide inventories is impactful. Most of the experimental data in SFCOMPO applies to light-water reactor fuel. However, data are available from previous MAGNOX and advanced gas-cooled reactor (AGR) fuel experiments and the database can be easily expanded to include any advanced reactor fuel assay data once they would become available. The current database and the evaluations being developed provide great support in assessing the abilities of the underlying methods and nuclear data for advanced reactors of accurately predicting the nuclear transmutation and decay physics.

2.4 Shielding integral benchmark and archive database (SINBAD)

An international shielding benchmark was first proposed in 1988 at the 7th International Conference on Radiation Shielding (ICRS-7), which resulted in the Shielding Integral Benchmark Archive Database (SINBAD) being established in 1996 as a joint effort between the Nuclear Energy Agency (NEA) and the Radiation Safety Information Computational Center (RSICC) (https://www.oecd-nea.org/jcms/pl_32139/shielding-integral-benchmark-archive-and-database-sinbad) (Kodeli, Sartori, and Kirk, 2006; Kodeli, et al., 2014). The goal of this type of database is to provide the community a way to validate their shielding or fixed source simulations and evaluated nuclear data. Today SINBAD continues under the auspices of the Expert Group on Physics of Reactor Systems (EGPRS), which is a subgroup of the NEA's Working Party on Scientific Issues and Uncertainty Analysis of Reactor Systems (WPRS). The current release of SINBAD, which is available from the NEA Data Bank and RSICC, contains evaluations of 102 benchmark experiments. These experiments are broken into three broad categories, fission systems, fusion systems, and accelerator systems, which have 31, 48, and 23 benchmarks, respectively.

In February 2021 the EGPRS established the SINBAD Task Force (TF) to oversee the future development of SINBAD, which is consistent with the strategy of the NEA to continuously improve data available from their data bank. The TF will operate for 3 years, and then the EGPRS will evaluate the performance and determine how SINBAD development should continue in the future. The proposed aim of the SINBAD TF is to maintain and begin modernizing SINBAD. There are two major factors that led to the EGPRS establishing the TF. First, is the reduction in new benchmarks being added to the database. The second motivating factor is to modernize the database while building upon previous work. This previous work includes all entries currently in SINBAD, but also the quality reviews (Kodeli and Sartori, 2021). The goals prescribed by the EGPRS for the SINBAD TF are to provide new database entries and to improve the quality of the existing database entries. Providing new database entries is self-explanatory. The goal of improving the quality of the existing database entries is a very broad goal. Discussions with the EGPRS and TF participants have led to specific deliverables that achieve this goal, which are:

- when updating current evaluations or producing new evaluations, have a single summary document following the SINBAD evaluation guide approved in 2019 (NEA, 2022c),
- perform sensitivity and uncertainty quantification,
- provide accurate models of the geometry (CAD or some code agnostic format), materials, sources, and detector response parameters, and
- provide supplemental resources like sample code inputs and outputs, variance reduction parameters, tools to convert data to code input, and tools to post process code output.

TABLE 1 Contact and leadership information for OECD NEA international benchmark exercises.

Activity	Chair/Co-chair/Coordinator	Secretariat	Email contact
ICSBEP	Mrs. Catherine Percher, Lawrence Livermore National Laboratory, United States	Dr. Julie-Fiona Martin	wpncs@oecd-nea.org
	Dr. William J. Marshall, Oak Ridge National Laboratory, United States		
SFCOMPO	Dr. Germina Ilas, Oak Ridge National Laboratory, United States of America		
EGMUP	Dr. Timothy E. Valentine, Oak Ridge National Laboratory, United States	Dr. Oliver Buss	wprs@oecd-nea.org
	Dr. Evgeny Ivanov, Institut de Radioprotection et de Sûreté Nucléaire (IRSN), France		
SINBAD	Dr. Thomas M. Miller, Oak Ridge National Laboratory, United States		
TIETHYS	Dr. Upendra Rohatgi, Brookhaven National Laboratory, United States		
	Dr. Alessandro Petruzzi, Nuclear and iNdustrial Engineering (NINE), Italy		
IRPhEP	Dr. Mark DeHart, Idaho National Laboratory, United States	Ian Hill	ian.hill@oecd-nea.org
	Dr. Patrick Blaise, Atomic Energy and Alternative Energies Commission in France (CEA), France		

The TF participants have also defined the following additional goals:

- do not lose or remove any existing information from the database,
- involve the nuclear data community, and
- capture the output of the Working Party on International Nuclear Data Evaluation Cooperation (WPEC) Subgroup 47, which was focused on the use of SINBAD for nuclear data validation (Kodeli, et al., 2022).

From the perspective of advance reactor design, like with criticality, thermal hydraulics, and other topics mention herein, many concepts are outside the domain of current benchmark experiments used for validation. Different fuel types, moderators, and coolants have been proposed that do not have benchmark quality experimental data. This becomes a shielding concern for biological dose around advanced reactors and their spent fuel, but also for radiation damage of reactor and fuel components. There is certainly a need for additional SINBAD benchmarks to help address these gaps in validation for advanced reactor designs.

2.5 The international experimental thermal Hydraulics database (TIETHYS)

Nuclear reactor design and accident analyses are generally multi-physics simulation problems. Validation of relevant multi-physics codes requires that the individual physics models are also validated in order to avoid compensating effects. One important component of multi-physics simulation is thermal-hydraulic (TH) physics and requires relevant TH data. Some of the TH codes are at a system level and others such as CFD (computational fluid dynamics) address more details of local thermal hydraulic phenomenon such as at sub-channel level. These system TH analytical tools have balance equations and many hundreds of correlations to provide information or model parameters about interactions between different phases at the interfaces. The shape and size of the interfaces determines the phasic transfer terms. In order to assess that capability of the codes and fidelity of the predictions, these codes must be validated with tests that represent phenomena in the plant for the specific scenario. The Element 2 in the US Nuclear Regulatory Commission (USNRC) suggested approach in Regulatory guide 1.203 (USNRC, 2005) for transient and accident analysis indicates that any analyses for licensing will require a validation matrix consisting of separate effects and integral effect tests. All advanced reactors will need design certification from USNRC. Similarly, other relevant guides exist for the UK (ONR, 2019), France (ASN, 2017), and Japan (AESJ, 2015).

The TH data is scattered in different locations and in different formats. Some of the data is in danger of being lost. The Nuclear Science Committee (NSC) of the NEA has developed a user-friendly GUI (graphical user interface) and a relational database, The International Experimental Thermal Hydraulic Systems database (TIETHYS) (Rohatgi, Dyrda, and Soppera, 2018), to organize and preserve the international TH test data for various reactor concepts and different scenarios. The database has an expandable platform with place holders for molten salt reactors, high temperature gas cooled reactors, CANDU, and liquid metal reactors. TIETHYS provides better access to and preserves this valuable information. In addition, the database will also expand as more information becomes available for given tests such as application, instrumentation uncertainty, and user guidelines. For TH code validation, it is important to provide accurate descriptions of geometry and initial conditions.

The validation of a code for a given application requires tests that cover the conditions expected in that application. The TIETHYS development has two parallel paths. One path includes a database for tests with searchable attributes. The second part is linking of these tests to applications through possible phenomena identification table, part of PIRT (Phenomena Identification and Ranking Table) process. The current database platform includes scenarios for PWRs, BWRs, vodo-vodyanoi enyergeticheskiy reactors (VVERs), and corresponding SETs (separate effects tests) and IETs (integral effects tests) along with specific benchmarks for CFD modelling. Currently, the database includes 45 integral facilities and 223 separate effects tests (which have been mostly derived from previous efforts carried-out by the OECD-NEA in the framework of the Computer Code Validation Matrix (CCVM) (NEA, 1994; NEA, 1996; NEA, 1997; NEA, 2001; NEA, 2017), and nine CFD-relevant tests (NEA, 2015). Numerous others have been identified for later inclusion for LWRs. This will meet some of the needs for the multi-physics development programs around the world. These tests are currently for LWRs, spanning PWR, BWR, and VVER designs.

It is important to note that it is difficult to define benchmarks for TH codes as they do not undergo rigorous nodalization studies as prediction can change with nodalization due to flow regime map definition, and related interfacial transfer of heat, mass, and momentum. The goal of this database is to provide descriptions of tests, geometry, initial conditions and transient test data, and examples of application. The code user can apply their own code guidelines to create nodalization.

The initial version of relational database TIETHYS and GUI software are freely open to public and available for testing *via* the NEA website (https://www.oecd-nea.org/tiethysweb/). Going forward the database will be extended to include additional links and data as they become available. The organizations conducting TH tests are encouraged to submit their test data to NEA for inclusion in database for wider exposure and for preservation.

Another initiative which is linked to TIETHYS and is worth mentioning is the OECD/NEA THEMPo (Harmonization of Methodologies for System Thermal-Hydraulics Experimental Meta-Data Preservation, Collection and Qualification) which will commence in 2023. The objective is to develop and/or to improve and then harmonize existing methodologies (Petruzzi and D'Auria, 2016) for collection, preservation, qualification, organization and then use of an exhaustive "Set of Experimental Information" (SEI). The derived methodology will provide the guide for the creation of a relational database of experimental meta-data with a standardization of the procedures by which the SEI are collected, qualified, and organized into a consolidated database which finally allows the code analysists for a faster and more accurate development of computational simulation models of experimental tests to be exploited for code validation purposes.

2.6 Challenging state-of-the-art tools in cooperative benchmark exercises

Benchmark exercises at OECD NEA challenge our current state-of-the-art tools and provide international best practice guidance on simulation methods and tools. Benchmarks are typically either based on existing experimental benchmark cases in the NEA databases or lead to the development of new benchmark cases which then become part of the databases.

Key activities with relevance to the development of advanced reactors design include the multi-physics benchmark exercises in the Expert Group on Reactor Systems Multi-Physics (EGMUP), which is here presented as a showcase. EGMUP originates from the Expert Group on Multi-Physics Experimental Data, Benchmarks and Validation (EGMPEBV) which was established in 2014 by the NEA to establish processes for certification of experimental data and development of benchmark models for validation of multi-physics computational methods (Finck, et al., 2016; Avramova, et al., 2017). This Expert Group was reorganized as the Expert Group on Reactor Systems Multi-Physics (EGMUP) and placed under the direction of the NEA Working Party on Scientific Issues and Uncertainty Analysis of Reactor Systems (WPRS) (Valentine, et al., 2021). The EGMUP seeks to advance the state-of-the-art in establishing processes and procedures for certifying experimental data and benchmarking multi-physics multi-scale modelling and simulation (M&S). The term multi-physics implies computationally coupled interaction of two or more of the following physical phenomena (physics) that include, but are not limited to, reactor physics, thermal-hydraulics, fuel performance, structural mechanics, materials chemistry, and heat transfer.

While single-physics benchmarks have significant value, in real-world systems all physics are coupled to one degree or another. In recognition of this truth, multi-physics methods have evolved internationally over the last 2 decades with varying degrees of fidelity (DeHart, et al., 2017). It has also been recognized that few measurements have been performed in which simultaneous measurements of coupled phenomena have been performed. Hence, this Expert Group is focused on the coupled physics aspects of both steady-state and transient simulations for both existing and advanced nuclear systems, along with uncertainty quantification and propagation through different scales (multi-scale M&S) and different physics phenomena (multi-physics M&S).

The expert group provides recommendations to the WPRS and the nuclear community on scientific development needs, e.g., data and methods, validation experiments, scenario studies, etc., for multi-physics and multi-scale M&S, including sensitivity and uncertainty methodologies for analysis of different reactor systems and scenarios. The Expert Group aims to develop guidance and recommendations for verification of experimental data for multi-physics multi-scale M&S and to apply this data to the benchmarking of models. To this end, the Expert Group will work to provide:

1. Standardized benchmark models with detailed uncertainty evaluations and uncertainty methodology guidelines;
2. Guidance on best practices to combine high fidelity and low fidelity simulation tools;
3. A framework and consensus recommendations for validating multi-physics simulations;
4. Sensitivity and uncertainty methods to facilitate quantification and ranking of coupled physics;
5. Evaluation methods for uncertainty quantification of the following parameters on multi-physics simulations:

a. Data (e.g., geometry, physical properties),
b. Numerical methods, and
c. Physical models.

6. Training opportunities to demonstrate validation principles and practices; and
7. Demonstrations of the validation recommendations for specific applications.

To support its activities, the group will collect and evaluate multi-physics data from available integral facilities, test and research reactor and nuclear power plant experimental data; analytical and numerical benchmarking will also be used to fulfil the objectives.

All nuclear reactor systems operate in a multi-physics domain. Simulations of many advanced reactor systems have demonstrated tightly coupled behavior between different physical aspects of the core, including micro-reactors, molten salt and fast reactor systems and nuclear thermal propulsion concepts. With these generally reactors still in early design phases and prototypes being developed for testing, multi-physics data from such systems may become available in the next few years. However, multi-physics data to support such design is in short supply. This need drives the importance of this Expert Group to strive to fill this gap.

Other similar benchmark exercise activities exist for all domains within the scientific portfolio covered by the OECD NEA Nuclear Science Committee. For more information, interested parties should reach out to the Secretariats of the OECD-NEA Nuclear Science Committee (see Section 3).

3 Active engagements within the NEA benchmark activities

The various activities rely on international participation, typically coordinated through in-person meetings once or twice a year, typically but not always held the NEA headquarters in Paris. In-person meeting were replaced by virtual meetings during COVID travel restrictions between 2020 and 2022, and future meetings will likely include virtual participation. However, time zone differences limit virtual meetings to short time windows. Nevertheless, each of the benchmark activities will move forward beyond 2023 with continued international coordination meetings.

Both the ICSBEP and IRPhEP Technical Review Groups (TRG) have traditionally been very active since their inceptions, meeting together once or twice a year to review new experimental benchmarks for inclusion into new respective handbook editions. Experiments are independently evaluated by scientists and engineers at institutions around the world, undergoing an extensive internal and external review process. The final step in this process is a final review by the TRG for potential inclusion into the handbook during the in-person meeting.

A pilot SFCOMPO TRG meeting was hosted by NEA in March 2019. Since then, more participants have joined the effort and are actively contributing. In 2021, a task force was formed under the TRG to review the existing evaluation guidance (NEA, 2016) and provide feedback on how to further improve it and address the uncertainty evaluation challenge, based on recent lessons learned and drawing from similar IRPhEP and ICSBEP experience.

Before WPRS's EGPRS established the SINBAD Task Force in 2021, SINBAD meetings were often held in tandem with IRPhEP/ICSBEP meetings. At the time of this writing, the schedule for future meetings of the SINBAD Task Force has not been determined, but the Task Force may continue to hold meetings in tandem with IRPhEP/ICSBEP meetings.

The first workshop on preservation of Thermal-Hydraulics experimental data workshop (TH-1) was conducted under the auspices of new Expert Group on Reactor Core Thermal Hydraulics (EGRCTH) within the WPRS. The meeting was hosted by Gesellschaft für Anlagen-und Reaktorsicherheit (GRS) gGmbH, in Garching, Germany in June, 2019. This workshop elected to endorse the effort to provide for preservation of experimental data for model development and validation in the form of the existing TIETHYS database. Since this time updates to TIETHYS are reported to EGRCTH, but workshops have held independently of WPRS meetings.

As was noted earlier, the EGMUP originated from the earlier EGMPEBV, which met twice a year, usually at NEA headquarters, beginning in 2014. After reformed as the EGMUP, this Expert Group has met in tandem with the WPRS since 2021 at NEA Headquarters.

Each of these benchmark projects continues to expand and improve through the concerted contributions of the international community, and each is actively and continuously soliciting new participants from NEA member countries; the nature of the participation (e.g., evaluators, reviewers, observers, etc.) varies by benchmark activity. International expertise and enthusiasm are needed to build the future of each project. There is ongoing work that practically all experts in various aspects of the nuclear energy community will find interesting and applicable to their daily work. Some of the projects currently do not have enough available volunteers to wholly fulfill their charters.

4 Conclusion

The OECD NEA enables international collaboration in advanced nuclear technology in support of nuclear safety, technology, science, environment, and law to ensure safe, economical, and environmentally sound use of peaceful nuclear energy. There are numerous ongoing activities relevant in support of modern nuclear facilities and future advanced reactor systems. International participants serving in the various efforts such as ICSBEP, IRPhEP, SFCOMPO, SINBAD, TIETHYS, and other cooperative benchmark exercises contribute their time and expertise to ensure continued success. The continued success of these projects has concatenated priceless information into utile resources supporting various aspects of modeling, design, simulation, and validation. This paper provides a summary of current ongoing work in these activities, and interested participants are encouraged to become engaged in these groups by contacting their respective leadership and NEA secretariat (Table 1).

To get more information on other benchmark exercises, please contact the following Secretariats within the NEA Division of Nuclear Science and Education:

- Working Party on Scientific Issues of Advanced Fuel Cycles (WPFC): wpfc@oecd-nea.org
- Working Party on Nuclear Criticality Safety (WPNCS): wpncs@oecd-nea.org

- Working Party on International Nuclear Data Evaluation Co-operation (WPEC): wpec@oecd-nea.org
- Working Party on Scientific Issues and Uncertainty Analysis of Reactor Systems (WPRS): wprs@oecd-nea.org

Data availability statement

The data analyzed in this study is subject to the following licenses/restrictions: The data from these working groups are available to OECD NEA member countries and participating scientists/organizations. Requests to access these datasets should be directed to the NEA Secretariats.

Author contributions

All authors listed have made a substantial, direct, and intellectual contribution to the work and approved it for publication.

Funding

Contributions, financial and otherwise, towards the success of the OECD NEA international benchmark projects have come from a myriad of international sources.

Acknowledgments

The OECD NEA activities are collaborative efforts that involve numerous scientists, engineers, and administrative support personnel across the world. The authors would like to acknowledge the efforts of all these dedicated individuals without whom these efforts would not be possible.

Conflict of interest

JB is employed by JFoster & Associates. AP is employed by Nuclear and INdustrial Engineering.

The remaining authors declare that the research was conducted in the absence of any commercial or financial relationships that could be construed as a potential conflict of interest.

The reviewer PR declared a shared affiliation with the author EI to the handling editor at the time of review.

Publisher's note

All claims expressed in this article are solely those of the authors and do not necessarily represent those of their affiliated organizations, or those of the publisher, the editors and the reviewers. Any product that may be evaluated in this article, or claim that may be made by its manufacturer, is not guaranteed or endorsed by the publisher.

References

AESJ (2015). *AESJ guide for the assessment of nuclear simulation credibility: 2015. AESJ-SC-A008E: 2015*. Tokyo, Japan: Atomic Energy Society of Japan. Available at: https://www.aesj.net/publish-1722.

ASN (2017). Qualification of scientific computing tools used in the nuclear safety case – 1st barrier. guide No. 28, autorité de Sûreté Nucléaire, montrouge, France. Available at: https://www.french-nuclear-safety.fr/asn-regulates/asn-guides/asn-guide-no.-28.

Avramova, M., Ivanov, K., DeHart, M., Dyrda, J., Hudelot, J-P., Petruzzi, A., et al. (2017). OECD/NEA EGMPEBV activities in multi-physics verification and validation. *Trans. Am. Nucl. Soc.* 116 (1), 1297–1300. Available at: https://epubs.ans.org/?p=trans.

Briggs, J. B., and Gulliford, J. (2014). An overview of the international reactor physics experiment evaluation project. *Nucl. Sci. Eng.* 178 (3), 269–279. doi:10.13182/NSE14-27

Briggs, J. B., Scott, L., and Nouri, A. (2003). The international criticality safety benchmark evaluation project. *Nucl. Sci. Eng.* 145 (1), 1–10. doi:10.13182/NSE03-14

DeHart, M. D., Bess, J. D., Ivanova, T., and Hill, I. (2022). *A Review of the Status of the Evaluated Reactor Physics Benchmark Experiments Project*, 127. Transactions of the American Nuclear Society. Available from: https://www.ans.org/pubs/transactions/.

DeHart, M. D., Le Pallec, J.-C., and Hudelot, J.-P. (2017). *Multinational efforts for development of novel multi-physics modelling and simulation tools*. Paris, France: OECD Nuclear Energy Agency. NEA/NSC/DOC(2017)12.

Finck, P., Valentine, T., Dyrda, J., Gulliford, J., Hudelot, J.-P., and Rohatgi, U. (2016). "OECD-NEA expert group on multi-physics experimental data, benchmarks and validation," in Proceedings of PHYSOR 2016: Unifying Theory and Experiments in the 21st Century, Sun Valley, Idaho, May 1–5. Available from: https://www.ans.org/store/item-700403/.

Hill, I., Soppera, N., and Bossant, M. (2014). Idat: The international handbook of evaluated reactor physics benchmark experiments database and analysis tool. *Nucl. Sci. Eng.* 178 (3), 280–294. doi:10.13182/NSE14-37

Ilas, G., Gauld, I., Ortego, P., and Tsuda, S. (2020). "SFCOMPO database of spent nuclear fuel assay data - the next frontier," in Proceedings of PHYSOR 2020 – International Conference on Physics of Reactors: Transition to a Scalable Nuclear Future, Cambridge, UK. doi:10.1051/epjconf/202124710019

Kodeli, I., Fleming, M., Cabellos, O., Leal, L., Çelik, Y., Ding, Y., et al. (2022). "Outcomes of WPEC SG47 on use of shielding integral benchmark archive and database for nuclear data validation," in Proceedings 15th International Conference on Nuclear Data for Science and Technology (ND2022), Virtual Meeting, July 25-29.

Kodeli, I., Milocco, A., Ortego, P., and Sartori, E. (2014). 20 Years of SINBAD (shielding integral benchmark archive and database). *Prog. Nucl. Sci. Technol.*, 4, pp. 308–311. doi:10.15669/pnst.4.308

Kodeli, I., Sartori, E., and Kirk, B. (2006). "SINBAD shielding benchmark experiments status and planned activities," in Proceedings of the 14th Topical Meeting of the Radiation Protection and Shielding Division (RPSD 2006), Carlsbad, New Mexico, April 3-6.

Kodeli, I., and Sartori, E. (2021). Sinbad – radiation shielding benchmark experiments. *Ann. Nucl. Energy* 159, 108254. doi:10.1016/j.anucene.2021.108254

Michel-Sendis, F, Gauld, I., Martinez, J., Alejano, C., Bossant, M., Boulanger, D., et al. (2017). SFCOMPO-2.0: An OECD NEA database of spent nuclear fuel isotopic assays, reactor design specifications, and operating data. *Ann. Nucl. Energy*, 110, 779–788. doi:10.1016/j.anucene.2017.07.022

NEA (2017). *A state-of-the-art report on scaling in system thermal-hydraulics applications to nuclear reactor safety and design*. NEA/CSNI/R(2016)14. Paris, France: OECD Nuclear Energy Agency. Available from: https://www.oecd-nea.org/jcms/pl_19744/scaling-in-system-thermal-hydraulics-applications-to-nuclear-reactor-safety-and-design-a-state-of-the-art-report.

NEA (2015). *Assessment of CFD codes for nuclear reactor safety problems – revision 2*. NEA/CSNI/R(2014)12. Paris, France: OECD Nuclear Energy Agency. Available from: https://www.oecd-nea.org/jcms/pl_19550/assessment-of-cfd-codes-for-nuclear-reactor-safety-problems-revision-2.

NEA (1996). *CSNI integral test facility validation matrix for the assessment of thermal-hydraulic codes for LWR LOCA and transients*. NEA/CSNI/R(1996)17. Paris, France: OECD Nuclear Energy Agency. Available from: https://www.oecd-nea.org/jcms/pl_16134/csni-integral-test-facility-validation-matrix-for-the-assessment-of-thermal-hydraulic-codes-for-lwr-loca-and-transients.

NEA (2016). *Evaluation guide for the evaluated spent nuclear fuel assay database (SFCOMPO)*. NEA/NSC/R(2015)8. France: OECD Nuclear Energy Agency. Available from: https://www.oecd-nea.org/jcms/pl_19678/evaluation-guide-for-the-evaluated-spent-nuclear-fuel-assay-database-sfcompo.

NEA (1997). *Evaluation of the separate effects tests (SET) validation matrix*. NEA/CSNI/R(1996)16. Paris, France: OECD Nuclear Energy Agency. Available from: https://www.oecd-nea.org/jcms/pl_16132/evaluation-of-the-separate-effects-tests-set-validation-matrix-1997.

NEA (2022a). *International handbook of evaluated criticality safety benchmark experiments*. Paris, France: OECD Nuclear Energy Agency. Available from: https://www.oecd-nea.org/jcms/pl_20291/icsbep-handbook.

NEA (2020b). *International handbook of evaluated reactor physics benchmark experiments*. Paris, France: OECD Nuclear Energy Agency. Available from: https://www.oecd-nea.org/jcms/pl_20279/international-handbook-of-evaluated-reactor-physics-benchmark-experiments-irphe.

NEA (1994). *Separate effects test matrix for thermal-hydraulic code validation, vol. 1 and 2. NEA/CSNI/R(1993)4*. Paris, France: OECD Nuclear Energy Agency. Available from: https://www.oecd-nea.org/jcms/pl_15968/separate-effects-test-matrix-for-thermal-hydraulic-code-validation-vol-1-and-2-1994.

NEA (2022c). *SINBAD project format/content guide*. NEA/NSC/WPRS/DOC(2022)5. Paris, France: OECD Nuclear Energy Agency.

NEA (2001). *Validation matrix for the assessment of thermal-hydraulic codes for VVER LOCA and transients*. NEA/CSNI/R(2001)4. Paris, France: OECD Nuclear Energy Agency. Available from: https://www.oecd-nea.org/jcms/pl_17492/validation-matrix-for-the-assessment-of-thermal-hydraulic-codes-for-vver-loca-and-transients.

ONR (2019). Validation of computer Codes and calculation methods. *NS-TAST-GD-042 rev. 5, office for nuclear regulation*. Bootle, UK. Available from: www.onr.org.uk/operational/tech_asst_guides/ns-tast-gd-042.pdf.

Palmiotti, G., Briggs, J. B., Kugo, T., Trumble, E. F., Kahler, A. C. S., and Lancaster, D. (2014). Applications of integral benchmark data. *Nucl. Sci. Eng.* 178 (3), 295–310. doi:10.13182/nse14-33

Petruzzi, A., and D'Auria, F. (2016). Standardized consolidated calculated and reference experimental database (sccred): A supporting tool for V&V and uncertainty evaluation of best-estimate system codes for licensing applications. *Nucl. Sci. Eng.* 182 (1), 13–53. doi:10.13182/NSE15-79

Rohatgi, U., Dyrda, J., and Soppera, N. (2018). "The international experimental thermal hydraulic systems database (TIETHYS): A new NEA validation tool," in Proceedings of the 26th International Conference on Nuclear Engineering, July 22-26 (London, England. doi:10.1115/ICONE26-82631

USNRC (2005). *Regulatory guide 1.203: Transient and accident analysis methods*. Washington, D.C: US Nuclear Regulatory Commission. Available from: https://www.nrc.gov/docs/ML0535/ML053500170.pdf.

Valentine, T., Avramova, M., Fleming, M., Hursin, M., Ivanov, K., Petruzzi, A., et al. (2021). Overview of the OECD-NEA expert group on multi-physics experimental data, benchmarks and validation. *EPJ Web Conf.* 247, 06048. doi:10.1051/epjconf/202124706048

frontiers | Frontiers in Energy Research

TYPE Original Research
PUBLISHED 17 March 2023
DOI 10.3389/fenrg.2023.1106601

OPEN ACCESS

EDITED BY
Germina Ilas,
Oak Ridge National Laboratory (DOE),
United States

REVIEWED BY
Pavel Tsvetkov,
Texas A&M University, United States
Jason Harp,
Oak Ridge National Laboratory (DOE),
United States

*CORRESPONDENCE
Dennis Keiser Jr.,
dennis.keiser@inl.gov

SPECIALTY SECTION
This article was submitted to
Nuclear Energy,
a section of the journal
Frontiers in Energy Research

RECEIVED 23 November 2022
ACCEPTED 09 March 2023
PUBLISHED 17 March 2023

CITATION
Keiser D Jr., Jue J-F, Rice F and Woolstenhulme E (2023), Post irradiation examination of a uranium-zirconium hydride TRIGA fuel element.
Front. Energy Res. 11:1106601.
doi: 10.3389/fenrg.2023.1106601

Post irradiation examination of a uranium-zirconium hydride TRIGA fuel element

Dennis Keiser Jr.*, Jan-Fong Jue, Francine Rice and Eric Woolstenhulme

Nuclear Fuels and Materials Division, Idaho National Laboratory, Idaho Falls, ID, United States

Low-enriched (LEU) U-ZrH fuel, with a ^{235}U content less than 20% of the total uranium, is being evaluated for possible use in different types of reactors, including space nuclear systems, light water reactors (LWRs) and micro-reactors. As a result, it is beneficial to better understand the macrostructural and microstructural changes that occur in this fuel during irradiation. This paper reports the results of the post irradiation examination of an LEU U-ZrH fuel element (30 wt.% U, <20% ^{235}U) using neutron radiography, precision gamma scanning, chemical analysis, optical metallography and scanning electron microscopy combined with energy dispersive spectroscopy and wavelength dispersive spectroscopy, where the fuel element was irradiated in a Training, Research, Isotope, General Atomics (TRIGA) reactor. Results of microstructural characterization indicated some dehydriding and cracking of the U-ZrH fuel occurred during irradiation; an axial and radial burnup gradient existed in the fuel during irradiation, as measured by gamma scanning and chemical analysis; negligible microstructural changes transpired during irradiation, based on comparison of irradiated and as-fabricated U-ZrH fuel microstructures; and, negligible, fission product-rich, phases could be resolved in a U-ZrH fuel that was irradiated to a calculated 20% depletion of ^{235}U.

KEYWORDS

TRIGA reactor, U-ZrH, micro-reactors, characterization, post irradiation examination

1 Introduction

TRIGA (Training, Research, Isotope, General Atomics) reactors were developed in the 1950s to act as safe reactors that could be constructed around the world (Fouquet et al., 2003). A U-ZrH fuel was developed as the fuel for these reactors, and its chemical formula is $U_{0.31}ZrH_{1.6}$, which corresponds to a nominal Zr/U atom ratio of 3.2 and a nominal H/Zr atom ratio of 1.6 (Olander and Ng, 2005). The cladding for a TRIGA fuel element is typically Type 304 stainless steel (SS) with a graphite reflector slug at each end. A Mo diffusion disc is present at the bottom. The fuel pellets have a concentric hole in the center where a solid zirconium rod is inserted in each fuel meat during assembly. Erbium can be added to the fuel as a burnable absorber to increase the core lifetime in a high-power reactor (Simand et al., 1976). The first exported TRIGA reactor was designed for the U.S. exhibit at the Second Geneva Conference on the Peaceful Uses of Atomic Energy in 1958. Over 6,000 fuel elements of seven distinct types were fabricated for use in the first 60 TRIGA research reactors. Some of the unique safety features for this reactor type include a prompt negative temperature coefficient of reactivity, high fission product retention, chemical stability when quenched from high temperatures in water, and dimensional stability over large swings of temperature (GA Technologies, 1992).

FIGURE 1
Thermal neutron radiographs for Fuel Rods 10172 and 10172 for the 0, 60- and 120-degree rotations.

U-ZrH fuel has been evaluated for use in different types of reactors, including space nuclear systems (Zinkle et al., 2002), light water reactors (LWRs) (Olander and Ng, 2005; Olander, 2009; Olander et al., 2012; Terrani et al., 2017), and micro-reactors such as the Microreactor Applications Research Validation and EvaLuation (MARVEL) reactor (American Nuclear Society, 2021). An evaluation of the literature shows that information from detailed microstructural characterization using techniques like electron microscopy of as-irradiated U-ZrH fuel is lacking. A few images from scanning electron microscopy (SEM) analysis are available in (Terrani et al., 2017; Meyer et al., 2020). The goal of this paper is to report the results of detailed characterization of U-ZrH fuel in an as-irradiated TRIGA fuel element using neutron radiography (NR), precision gamma scanning (PGS), optical metallography (OM), and scanning electron microscopy (SEM) combined with energy dispersive spectroscopy (EDS) and wavelength dispersive spectroscopy (WDS). Comparisons will be made to results from the microstructural characterization of an as-fabricated U-ZrH fuel element reported in another paper (Keiser et al.).

2 Experimental

Two irradiated TRIGA fuel rods (Rod 10170 and Rod 10172) (30 wt.% U and <20% ^{235}U) were selected for characterization. These came from a batch of fuel rods that were shipped to the Idaho National Laboratory (INL) from General Atomics in San Diego, California. The fuel rods were recovered from their storage location at the Irradiated Spent Fuel Storage facility and transported to the Hot Fuels Examination Facility (HFEF). Non-destructive visual examinations performed on both fuel rods did not indicate any evidence of any defects in the cladding.

For NR, a collimated neutron beam from a TRIGA reactor housed in HFEF, was employed to penetrate the fuel (McClellan et al., 1983; Craft et al., 2015). The beam was attenuated by the uranium-zirconium hydride fuel in the rods. Attenuation is dependent on uranium density, thickness, and local neutron cross section; the remaining beam passed onto a foil made of a high-neutron cross-section material, which became activated. The activated foil was placed on industrial x-ray radiography film in a vacuum cassette and allowed to decay for a minimum of five half-lives. The activated foil subsequently decayed by beta emission, and the beta particles exposed the radiography film, thus transferring a latent image of the fuel rod from the foil to the film. The film was developed using an automatic film processor to obtain a finished neutron-radiography image.

PGS was performed to verify the burnup profile and relative burnup using the ^{137}Cs spectra throughout the selected TRIGA rods prior to sectioning into specimens. PGS is a non-destructive examination method that records the gamma spectra emitted by irradiated items and is commonly used in post-irradiation characterization examinations (Barnes et al., 1979; Harp et al., 2014). Typical application of PGS involves recording a gamma spectrum to determine relative axial and radial fuel-burnup profiles, identifying radionuclide location, and generating other data to aid in evaluating the performance of irradiated fuels. In conducting a PGS assay on the TRIGA fuel rods, gamma rays from the irradiated fuel rod were passed through a narrow variable slit and collimator so that photons from only a small and identifiable part of the rod were counted over a particular time interval. The gamma rays struck the high-purity germanium detector, which emitted a pulse of electric charge proportional to the energy of each individual event. The pulses, after shaping and amplification, were counted. The collected data were analyzed to provide information about the isotopic composition of the area analyzed.

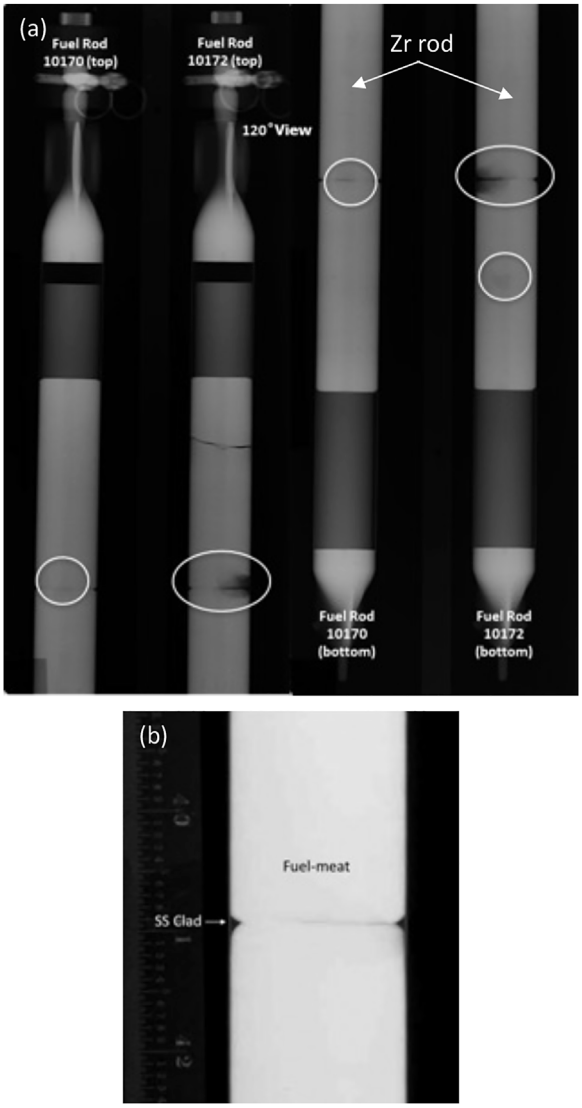

FIGURE 2
Fuel Rods 10170 and 10172 shown for the 120-degree view **(A)**. The circled regions are possible dehydride locations in the fuel meat. In **(B)** is shown the fuel meat to cladding interface for a local region of fuel rod 10172.

Additionally, a source scan of known isotopes spanning the energy range of the isotopes of interest was performed prior to each PGS measurement campaign on each TRIGA rod. To reduce uncertainty while performing assays with the smallest step size, the fuel rod was oriented such that it was centered as closely as possible in front of the collimator. This was accomplished by incrementally moving the fuel rod horizontally across the slit of the collimator, thereby determining the relative edge locations (right and left) of the sample by observing the count rate and spectra collected; by this method, the center-line coordinate of the fuel rod was determined.

Gamma scanning tomography (Parker and Joyce, 2015; Steven Hansen) was performed on cross sections taken from a fuel pellet. The scans were centered over the centerline of a cross section and were taken in 0.2 mm steps at nine different angles. Since decay counts were not high due to the long decay period of the fuel rod, improvement of the resolution of the plots and statistical noise for ^{137}Cs and ^{60}Co were reduced, by summing data from two step locations. Even lower counts for ^{154}Eu necessitated summing data from five step locations.

For destructive examinations, samples were cut from an irradiated fuel rod and used for analytical chemistry in order to benchmark the PGS data by establishing the local fission-product inventories for selected test specimens. The fission-product inventory was coupled with the PGS data to determine the fission density, burnup, and fission-product inventories at specific locstions of the fuel meats. Other samples from the highest burnup region of the highest burnup fuel rod were used for OM and SEM/EDS/WDS analysis. In the SEM, both backscattered electron (BSE) and secondary electron (SE) images were collected, and EDS and WDS were employed for poin-to-point and linescan analyses, and x-ray maps were also generated.

3 Results

3.1 Neutron radiography

NR is a non-destructive characterization method used to evaluate mechanical integrity and geometric stability prior to performing destructive examinations. A loss of integrity or geometric stability would be indicated by evidence of fuel

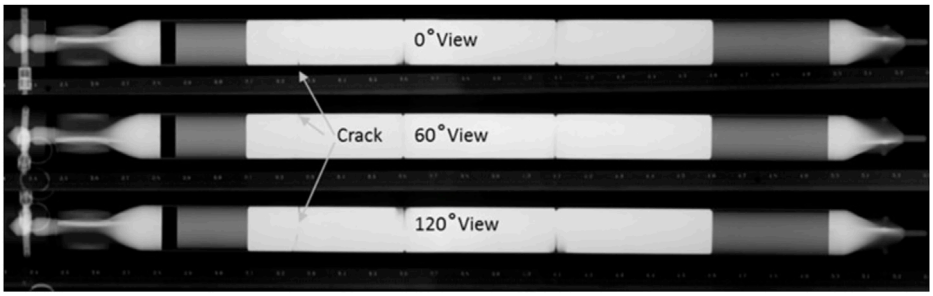

FIGURE 3
Fuel Rod 10172 showing crack in top fuel meat.

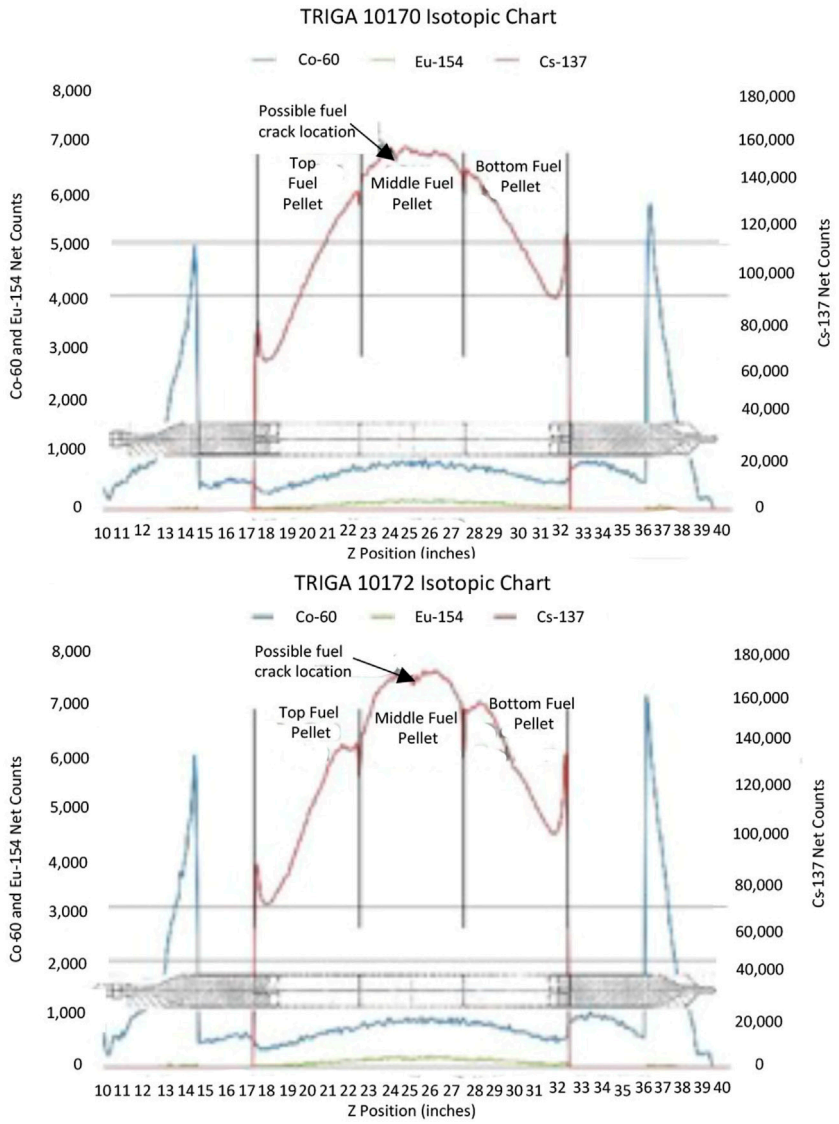

FIGURE 4
Isotopic gamma-scan profile for TRIGA fuel rods 10170 (top) and 10172 (bottom). To the right of each profile, the Y-axis is in ^{137}Cs counts, and the red profile is for ^{137}Cs. To the left, the Y-axis is in ^{60}Co and ^{154}Eu counts, and the blue and yellow profiles are for ^{60}Co and ^{154}Eu, respectively.

cracking, fuel relocation, or significant fuel density variations throughout the element and rod. NR images showed areas in the fuel meats that may have dehydrided or cracked.

The NR imaging of TRIGA Rods 10170 and 10172 was successful in providing data with which to assess the general condition of the fuel region of both rods. Thermal neutron and epithermal radiographs were generated, and the thermal neutron radiographs are shown in Figure 1.

Regions of possible dehydriding (or hydrogen depleted regions due to hydrogen transport) are observed in both rods (most pronounced in the 120-degree view) and are primarily located in the regions between the fuel meats. These areas were characterized by the circled darker regions on the fuel meats in the radiographs shown in Figure 2 for Fuel Rod 10170 and 10172. It is hypothesized that these were areas of higher temperatures during the operation of the reactor and the hydrogen diffused from these areas to cooler areas. The Zr rod at the center of the fuel pellets can also be seen in Figure 2A.

Due to irradiation-induced fuel swelling (with some possible contribution of thermal expansion), the fuel meat expanded. Of interest was if this resulted in good contact between the fuel and the cladding such that chemical interaction transpired between the fuel and cladding during irradiation. Fuel cladding mechanical interaction is also of interest. Figure 2B shows that there may be good fuel pellet contact with the cladding for the higher burnup rod, Fuel Rod 10172, excluding the regions between the fuel pellets where the fuel pellet ends are chamfered and do not contact the cladding. Fuel Rod 10172 was selected for destructive examination because it potentially had good fuel and cladding contact, was the highest-burnup rod, and contained the highest inventory of lanthanide fission products.

All views shown in Figure 3 for Fuel Rod 10172 (higher burnup than Fuel Rod 10170) show a crack (labelled) in the top fuel meat with some potentially dehydrided regions also visible. There was no

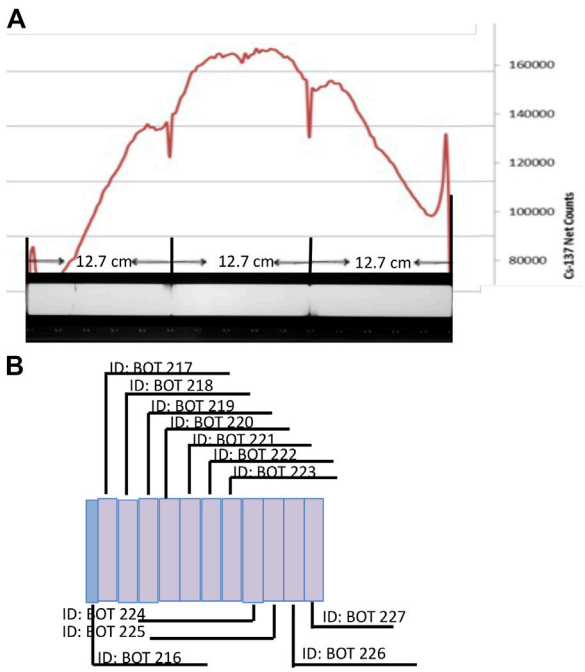

FIGURE 5
Neutron radiography image **(A)** showing fuel pellets in fuel rod 10172 and a gamma scanning profile for ^{137}Cs along the length of the fuel rod, which shows how the middle fuel pellet received the highest burnup during irradiation. The schematic diagram in **(B)** shows how the middle fuel pellet was sectioned to produce samples for analytical chemistry, gamma scanning tomography, and microstructural characterization.

indication in the gamma-scan data or during the visual inspection of the exterior of the rods that would have indicated damage to the fuel in this region. An explanation for the crack in the fuel is not currently available. Subsequent sectioning of Fuel Rod 10172 revealed radial cracking in most regions of the fuel pellet that were not resolvable in radiography. It is conceivable that cracking could have occurred during specimen sectioning. Sectioning is performed using a slow-speed saw with water cooling. A slightly smudged region just off-center in the middle fuel meat of Fuel Rod 10172 also indicates a dehydriding location. Based on radiography results, the cracked fuel and possibly dehydrided regions of the fuel were avoided during sectioning of samples for destructive analysis.

3.2 Precision gamma scanning

3.2.1 Axial gamma scanning

Gamma-scanning results are shown in Figure 4, and ^{137}Cs, which is a longer-lived fission product (half-life of 30.07 years), was selected to indicate burnup levels for the rods relative to each other. Spectral profiles of ^{137}Cs for both rods indicate the peak burnup location within each rod to be in the middle (center fuel meat) region of the rods. Also indicated in the ^{137}Cs spectra is a dip between each of the fuel meats (see Figure 4). While both Fuel Rods 10170 and 10172 have a slight dip in the ^{137}Cs spectra located in the center fuel-meat region, neutron radiography of the fuel rods indicates that the fuel is intact. Also, the uncertainty in the data indicates that the dips were not statistically significant relative to other data points in this region. ^{60}Co (half-life 5.27 years) is an activation product from the SS cladding of the fuel rod and end fittings. ^{154}Eu (half-life 8.59 years) is another gamma-emitting fission product by which burnup can be benchmarked.

The top of the rods in the overlay on the plots are oriented toward the left side (10,0) of the x and y-axes. While absolute position on the plots is arbitrary, the relative position from point to point is absolute. As shown in Figure 4, Fuel Rod 10170 has a relatively flat profile in the center region as compared to the areas to the left and the right of the middle fuel pellet. The peak net count for Fuel Rod 10170 is 152,602, based on a 240-s count time for each 0.254 cm step down the length of the rod. The center fuel-pellet region for Fuel Rod 10172, shown in Figure 4, has a less flat profile as compared to Fuel Rod 10170s profile in this location. The peak net count for Fuel Rod 10172 is 166,745 for the same count parameters. Therefore, Fuel Rod 10172 was selected for sectioning due to its higher relative burnup, as indicated by the higher gamma activity level for ^{137}Cs. These data also confirm the calculated physics estimates for which of the two rods had a higher burnup. Additionally, because of its higher burnup, the middle fuel-pellet region for fuel rod 10172 offers the highest fission-product inventories. Figure 5 shows the spectral profile of ^{137}Cs

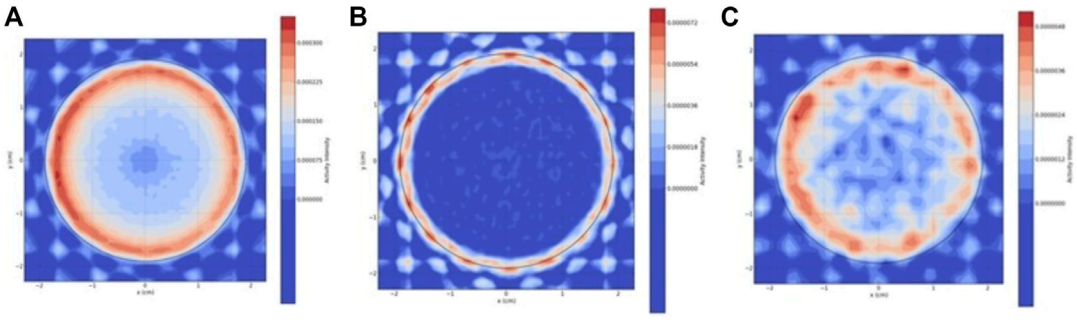

FIGURE 6
For sample BOT217, ^{137}Cs **(A)**, ^{60}Co **(B)**, and ^{154}Eu **(C)** tomographic maps. The black circle is the circumference of the sample. The y-axis to the right is in counts, where the highest counts are in red.

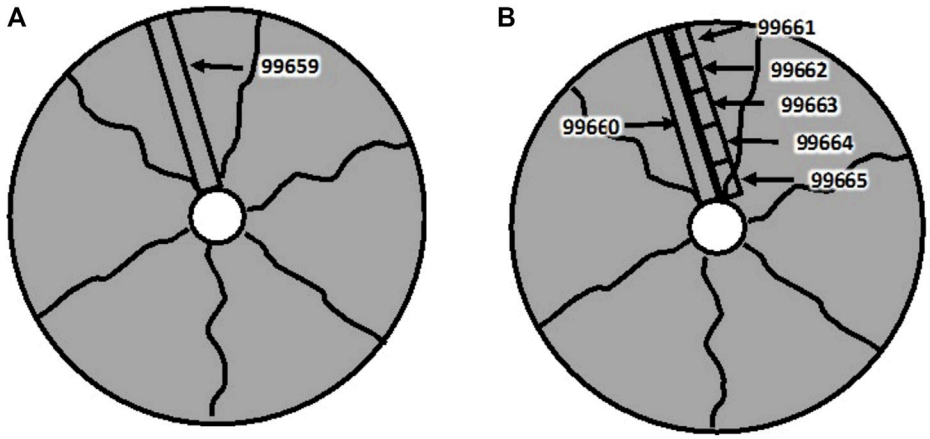

FIGURE 7
Chemistry sample-sectioning diagrams from cross-sections taken from Fuel Rod 10,172, fuel cross sections –1 **(A)** and –2 **(B)**.

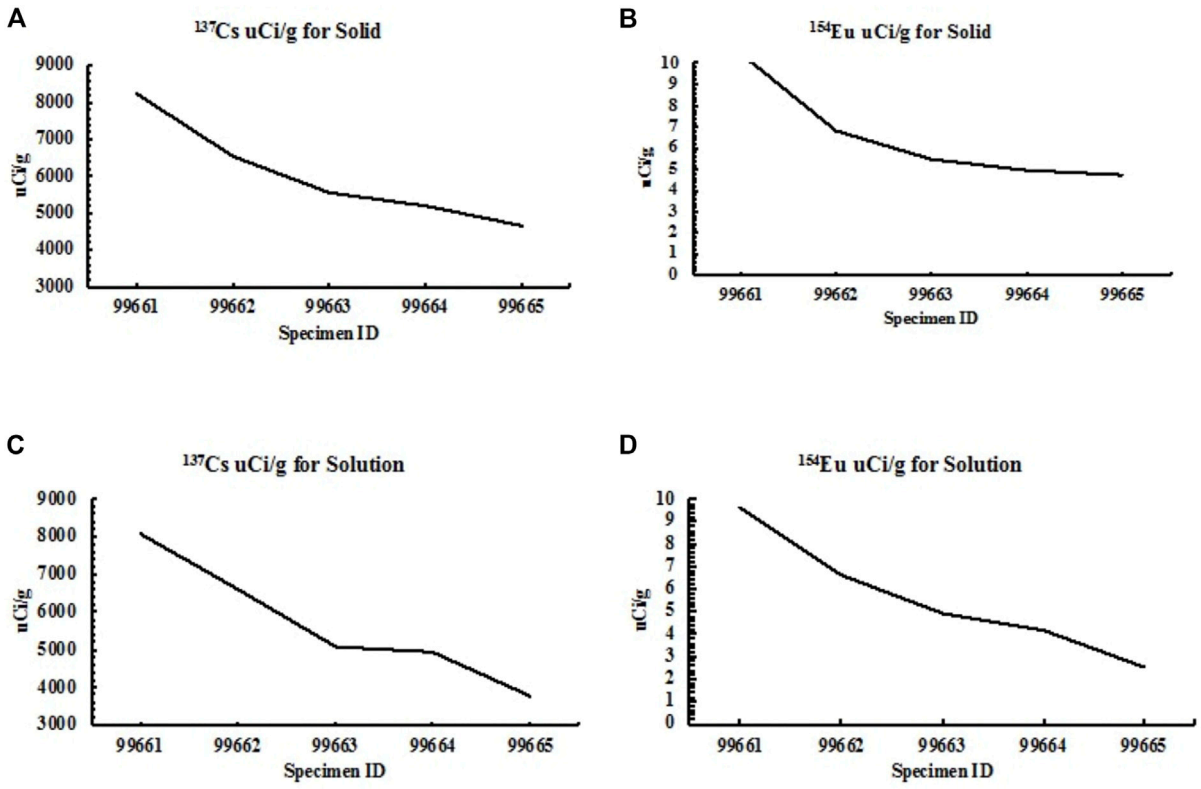

FIGURE 8
Results for ^{134}Cs **(A)** and ^{154}Eu **(B)** gamma spectroscopy as measured as a solid, and ^{134}Cs **(C)** and ^{154}Eu **(D)** as measured in solution.

for the 10,172 fuel pellets in more detail, along with a schematic cutting diagram for the middle fuel-pellet.

3.2.2 Gamma scanning tomography

Gamma scanning tomography was performed on three cross sections that were adjacent to the chemistry sample taken from the middle fuel pellet. The tomographic images of ^{137}Cs, ^{60}Co, and ^{154}Eu from these data are shown in Figure 6 for the BOT217 specimen. Results from the tomographic reconstruction of the circumferential count locations indicate a radial gradient in the burnup in the fuel meat. The higher ^{137}Cs count data at the perimeter indicate greater burnup

TABLE 1 Burnup percent determined from select fission-product inventories.

Depletion of ^{235}U calculated from generation of fission product				
Specimen ID	^{139}La	^{141}Pr	^{99}Tc	Comments
99659	18.3%	18.3%	17.9%	From highest-burnup, middle section of Fuel Rod 10,172 (Figure 7a)
99660	8.7%	8.7%	8.7%	From lower burnup section (Figure 7B)
99661	12.0%	12.1%	12.2%	Subsectioned radial strip piece (Figure 7B)
99662	9.1%	9.4%	9.5%	
99,663	7.7%	8.0%	8.0%	
99664	7.1%	7.6%	7.8%	
99665	7.8%	7.9%	7.5%	

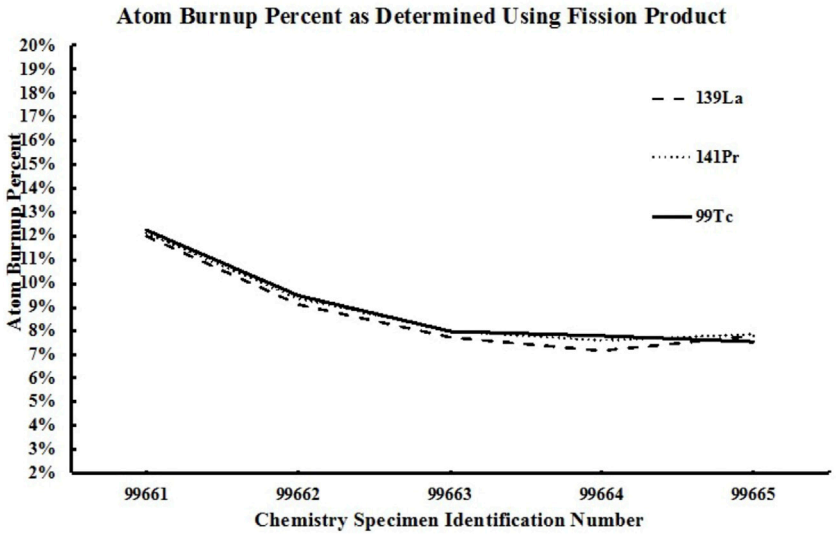

FIGURE 9
Plotted burnup values calculated *via* fission product measured using chemistry and ICP-MS.

relative to the center of the fuel pellet. Data for ^{60}Co are where they would be expected, at the fuel-perimeter and cladding region. The shape of the cobalt data is an artifact of the scanning method.

3.2.3 Gamma spectroscopy

Cross-sections were taken from the left fuel pellet (see Figure 7), and then smaller samples were produced from these cross-sections to confirm the radial burnup profile of the tomographic data compiled from the PGS both chemically and using gamma spectroscopy. Sample IDs are ordered left to right relative to the outside edge of the cross section, moving into the center of the cross section (see Figure 7). Results from gamma spectroscopy are shown in Figure 8 for ^{137}Cs (a) and ^{154}Eu (b), measured in solid form and as measured in solution for Cs and Eu (c and d, respectively). Qualitatively, the four plots illustrate a radial burnup gradient and are consistent with the PGS tomographic scan data.

3.3 Chemical analysis

Chemical analysis was performed to establish the burnup level and fission-product inventories for the different specimens. These data were coupled with the gamma-scan data to determine the fission-product density, burnup, and fission-product inventories for each specimen. Specimens were cut from each of the fuel-pellet sections to determine the fuel-rod axial burnup levels relative to gamma-scan data. Specimens had the SS cladding removed prior to chemical analysis.

The burnup results are found in Table 1 for the radial specimens that received chemical analysis. The specimen-sectioning diagram (see Figure 7) shows where a cross-section was taken from the left fuel pellet, specimen ID 99659 (a) and the specimens taken frrom a cross-section from the middle fuel pellet, specimen IDs 99660–99665 (b). Data obtained from chemical analysis and inductively coupled mass spectrometry

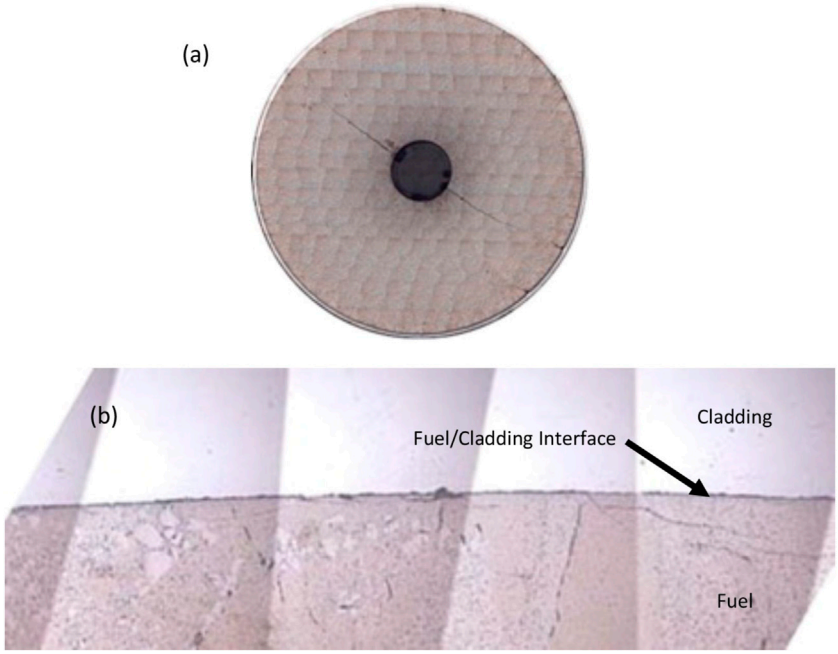

FIGURE 10
OM image montage **(A)** at ×31.5 magnification of the as-irradiated TRIGA fuel microstructure, and OM image **(B)** at ×200 magnification, showing a fuel to cladding region with the best signs of potential fuel and cladding contact.

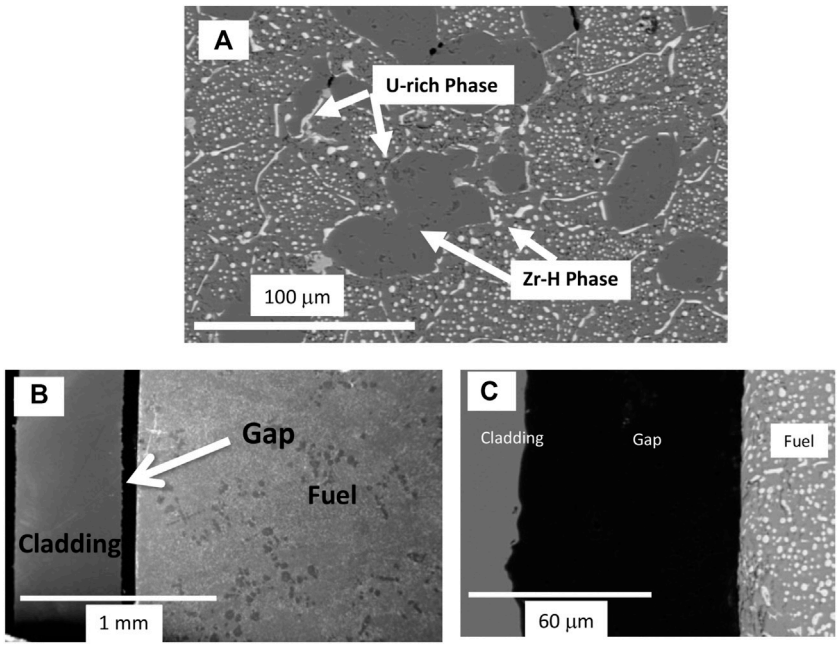

FIGURE 11
Backscattered electron images **(A–C)** showing the as-irradiated TRIGA fuel microstructure **(A)** and a gap **(B,C)** that was observed at the fuel and cladding interface.

(ICP-MS) are plotted in Figure 9 for the radial mini-sections. These results indicate a radial gradient burnup profile in the ^{235}U, which is consistent with the tomographic gamma-scan data. The burnup value for specimen 99659 of 18% is in reasonable agreement with the results for a physics burnup calculation of 20%.

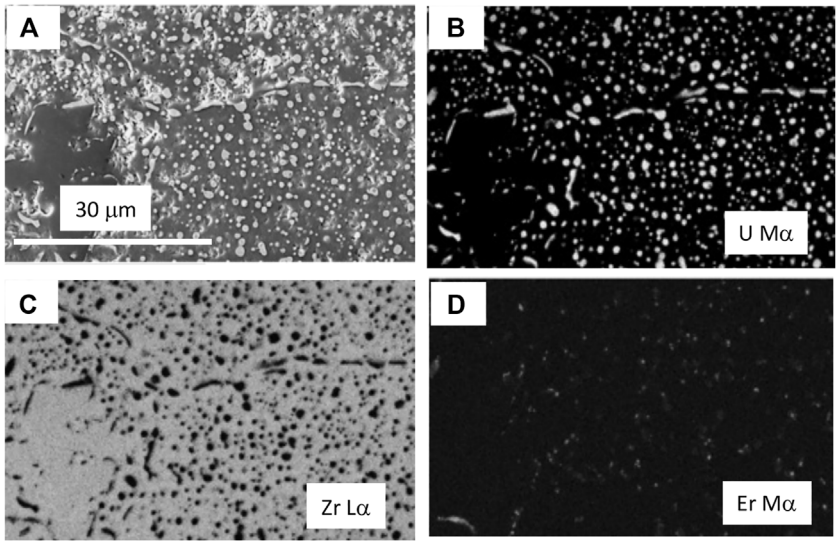

FIGURE 12
A BSE image **(A)** of the irradiated fuel specimen microstructure and WDS x-ray maps for **(B)** U, **(C)** Zr, and **(D)** Er. Hydrogen cannot be detected using WDS. Xe and Cs WDS x-ray maps did not show any enriched phases.

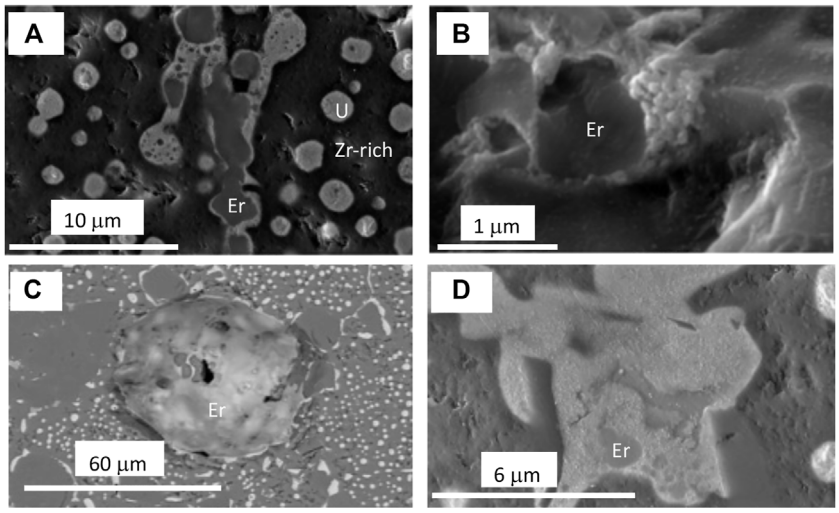

FIGURE 13
BSE images **(A–D)** showing examples of fuel meat phases that contain Er. The image in **(B)** is from a location where a fracture surface was found in the sample.

3.4 Optical metallography

NR (see Figure 5A) showed that the middle and right fuel pellets did not have obvious cracks, and the gamma scanning profile for ^{137}Cs showed the middle fuel pellet had received the highest burnup, but the left-side of the right fuel pellet also had received significant burnup. A cross-section from the left-side of the right fuel pellet was selected for microstructural characterization, and this sample was labeled as BOT229.

A montage of ×31.5 magnification optical images of the as-irradiated TRIGA fuel in this sample is shown in Figure 10A and a ×200 magnification image of the fuel and cladding interface in the specimen is presented in Figure 10B. It is not obvious from the image in Figure 10B whether the fuel pellet in this region had locations where the fuel and cladding were in contact with each other, but the gap between the fuel and cladding in this region was relatively small.

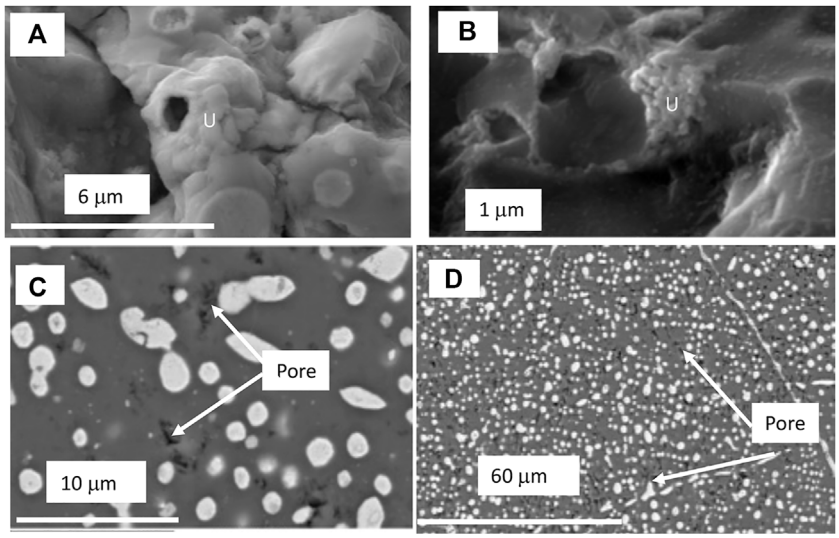

FIGURE 14
BSE images **(A,B)** showing fracture surfaces in the fuel pellet that expose the U-rich fuel phase that appears to be fine-grained with evidence of porosity. Porosity in the ZrH matrix can be seen in the images presented in **(C)** and **(D)**.

3.5 Scanning electron microscopy

For SEM analysis, samples were produced from a cross-section taken from the left-side of the right fuel pellet in Figure 5A. This cross-section looked like the one shown in Figure 10A. Sample reduction was necessary to keep radiation levels low so that the samples could be handled in the available SEM. The samples contained the cladding, fuel/cladding interface and fuel. BSE images of the as-irradiated fuel, cladding, and fuel/cladding interface microstructures are presented in Figure 11. As depicted in Figure 11A, the as-irradiated TRIGA fuel specimen is a multiphase material that is comprised of a U-rich precipitate phase and a Zr-H matrix phase as the major phases. Figure 11B and Figure 11C show that the specimen exhibited a gap at the fuel and cladding interface, and after careful inspection of the inner surface of the cladding and fuel meat using images and compositional linescans, no evidence of any FCCI zones could be observed that may have suggested there was fuel and cladding contact at some time during irradiation so that interaction between the fuel and cladding could have transpired. This type of information is important because U-ZrH fuel has a thermal expansion coefficient that is larger than that of the Type 304SS cladding (Kim, 1975; Olander et al., 2009), making fuel-cladding contact possible during irradiation even though they are not in contact at room temperature. WDS x-ray maps were produced (see Figure 12) to confirm the partitioning behavior for the U and Zr in the TRIGA fuel. Hydrogen cannot be detected using WDS and so is not shown.

Point-to-point and linescan analysis were performed on the sample, but no fission-product enriched phases could be found. Fission products present in the material appeared to be in concentrations below the resolution of the EDS detector that was employed. As shown in Figure 12D, Er-enriched phases could be resolved in the fuel meat. Figure 13 shows BSE images of different locations where such phases were present in the fuel meat.

The U-rich phase appeared mostly featureless on the as-polished surface of the fuel meat sample. Fission gas porosity could not be readily observed. However, when looking at different locations that had fracture surfaces (see Figures 14A, B) the U-rich phase appeared to be fine-grained and to contain porosity. Porosity could also be found in the Zr-H matrix of the fuel pellet (see Figures 14C, D). The nature of these pores can impact the mechanical propeties, thermal conductivity and fission gas retention in the fuel pellet. Overall, the submicron pores seemed well distributed and did not appear to coalesce into large voids during irradiation.

4 Discussion

Based on the results of non-destructive characterization of irradiated U-ZrH fuel for two as-irradiated TRIGA fuel elements (up to around 20% ^{235}U depletion) using NR, only limited cracking and dehydriding of the fuel pellet was observed. The dehydriding occurred in very localized regions of the fuel, where hydrogen may have migrated from these regions to lower temperature regions. The results of gamma scanning tomography and chemical analysis showed that the irradiated TRIGA fuel had a radial burnup gradient. The results of precision gamma scanning (PGS) showed that there was a burnup gradient along the length of the fuel rods, and the center fuel meat achieved the highest burnup. The effect of any diffusion of the measured constituents along any temperature gradients in the fuel must also be considered when interpreting these results and will need some investigation.

The results of OM and SEM analysis showed that a gas gap was present in the irradiated TRIGA fuel at room temperature. A gap was also observed for a sample from an as-fabricated TRIGA fuel element (Keiser et al.). As discussed in (Simand et al., 1976), there are three swelling mechanisms that could have contributed to gap closure during the irradiation of U-ZrH fuel: the accommodation of solid fission products, the agglomeration of fission gases, and a

saturable cavity nucleation phenomenon due to the nucleation and growth of irradiation-formed vacancies into voids. Thermal expansion differences between the fuel and the cladding could have also contributed. As-fabricated TRIGA fuel reportedly has a cold gap of around 25 or 50 microns between the fuel and cladding, after slip fitting the fuel into the cladding tube (Simand et al., 1976), and based on the characterization results reported in this paper, this gap did not close completely during irradiation. With respect to the ZrH matrix, the current analysis showed that very small pores/voids were present, and they did not appear to agglomerate to form large voids. This porosity could be as-fabricated porosity and/or pores that developed during irradiation. Similar porosity has been observed in as-fabricated fuel (Keiser et al.). For the Er-containing phases observed in the as-irradiated fuel, they are very similar to what has been observed in as-fabricated fuel, where it was observed that Er_2O_3 was present (Keiser et al.). Overall, the microstructure of the irradiated U-ZrH fuel was very similar to that of the original as-fabricated fuel (Keiser et al.). This agrees with what has been reported by Simnad (Simnad, 1981).

The presence of fission product-rich phases was not found in this fuel using SEM/EDS/WDS. However, gamma scanning and chemical analysis did confirm some of the fission products that were present in the fuel. Based on the SEM analysis, the concentration of the various constituents appeared to be low and homogeneously distributed in the fuel. Based on calculations using the Thermo-Calc computer code, yttrium, alkaline earth metals, and most lanthanides prefer to form binary hydrides. Oxide phases that can form include Y_2O_3, Pr_2O_3, Sm_2O_3, and Ce_2O_3. Uranium and noble metals prefer to remain in their elemental state, except for the formation of URu_3, URh_3, and UPd_3. CsI and SmTe can also form. Gaseous phases include H_2, Cs, Rb, CsRb and CsI. There is little consumption of hydrogen by fission products. Solid fission products form as a function of burnup, where for 45 wt.% U fuel with $ZrH_{1.6}$ matrix, it is estimated that the formation of solid fission product phases will be about 0.45% at 10,000 Mega-Watt-days-per-ton U (Huang et al., 2001).

5 Conclusion

Based on the non-destructive examination of two irradiated TRIGA fuel elements, using NR and PGS, and the destructive examination of one irradiated TRIGA fuel element, using OM and SEM, combined with EDS and WDS, the following conclusions can be drawn.

1. Some cracking and dehydriding of U-ZrH fuel was observed for a fuel rod irradiated in a TRIGA reactor where a burnup up to 20% ^{235}U depletion was calculated, with limited closure of the original gap between the fuel and the cladding due to fuel swelling.
2. The axial and radial burnup gradient present in a TRIGA fuel element can be identified using gamma scanning and chemical analysis.
3. Negligible microstructural changes can be identified in an irradiated U-ZrH fuel when comparisons are made with as-fabricated fuel.
4. Isolated fission product-rich phases are not prevalent in the microstructure of an irradiated U-ZrH fuel, where a maximum of 20% depletion of ^{235}U was calculated.

6 U.S. department of energy disclaimer

This information was prepared as an account of work sponsored by an agency of the U.S. Government. Neither the U.S. Government nor any agency thereof, nor any of their employees, makes any warranty, express or implied, or assumes any legal liability or responsibility for the accuracy, completeness, or usefulness of any information, apparatus, product, or process disclosed, or represents that its use would not infringe privately owned rights. References herein to any specific commercial product, process, or service by trade name, trademark, manufacturer, or otherwise, does not necessarily constitute or imply its endorsement, recommendation, or favoring by the U.S. Government or any agency thereof. The views and opinions of authors expressed herein do not necessarily state or reflect those of the U.S. Government or any agency thereof.

Data availability statement

The original contributions presented in the study are included in the article/supplementary material, further inquiries can be directed to the corresponding author.

Author contributions

DK: drafting of paper, data analysis, and work direction. FR: Paper drafting, conducted work, and data analysis. J-FJ: conducted work and data analysis. EW: Work direction, oversaw funding, and interacted with project sponsor.

Funding

This work is supported by the U.S. Department of Energy, under DOE Idaho Operations Office Contract DE-AC07-05ID14517.

Acknowledgments

This manuscript was authored by Battelle Energy Alliance, LLC, under Contract No. DE-AC07-05ID14517 with the U.S. Department of Energy. The U.S. Government retains and the publisher, by accepting the article for publication, acknowledges that the U.S. Government retains a non-exclusive, paid-up, irrevocable, worldwide license to publish or reproduce the published form of this manuscript, or allow others to do so, for U.S. Government purposes. Personnel at HFEF are recognized for completion of the neutron radiography and precision gamma scanning. Personnel at the Analytical Laboratory are recognized for completion of chemical analysis on provided samples.

Conflict of interest

The authors declare that the research was conducted in the absence of any commercial or financial relationships that could be construed as a potential conflict of interest.

Publisher's note

References

American Nuclear Society (2021). DOE touts a MARVEL of a micro-reactor project. *Nucl. News*. April 15, 2021. Available at: https://www.ans.org/news/article-2809/doe-touts-a-marvel-of-a-microreactor-project/.

Barnes, B. K., Phillips, J. R., Waterbury, G. R., Quintana, J. N., Netuschil, J. R., and Murray, A. S. (1979). Characterization of irradiated nuclear fuels by precision gamma scanning. *J. Nucl. Mater.* 81, 177–184. doi:10.1016/0022-3115(79)90076-x

Craft, A. E., Wachs, D. M., Okuniewski, M. A., Chichester, D. L., Williams, W. J., Papaioannou, G. C., et al. (2015). Neutron radiography of irradiated nuclear fuel at Idaho national laboratory. *Phys. Procedia.* 69, 483–490. doi:10.1016/J.PHPRO.2015.07.068

Fouquet, D. M., Razvi, J., and Whittemore, W. L. (2003). TRIGA research reactors: A pathway to the peaceful applications of nuclear energy. *Nucl. News* 46 (12), 46–56.

GA Technologies (1992). "Uranium-zirconium hydride TRIGA-LEU fuel," in *Research reactor core conversion guidebook, international atomic energy agency report IAEA-TECDOC-643*, 161–185.

Harp, J. M., Demkowicz, P. A., Winston, P. L., and Sterbentz, J. W. (2014). An analysis of nuclear fuel burnup in the AGR-1 TRISO fuel experiment using gamma spectrometry, mass spectrometry, and computational simulation techniques. *Nucl. Eng. Des.* 278, 395–405. doi:10.1016/J.NUCENGDES.2014.07.041

Huang, J., Tsuchiya, B., Konashi, K., and Yamawaki, M. (2001). Thermodynamic analysis of chemical states of fission products in uranium-zirconium hydride fuel. *J. Nucl. Mater.* 294, 154–159. doi:10.1016/s0022-3115(01)00446-9

Keiser, D., Jr., Perez, E., Jue, J. F., Rice, F., and Woolstenhule, E. Microstructural characterization of uranium-zirconium hydride fuel in an as-fabricated TRIGA fuel element. *J. Nucl. Mater. Energy*. submitted for publication.

Kim, C. S. (1975). *Thermophysical properties of stainless steel*. Argonne National Laboratory Report. ANL-75-55 (September 1975).

McClellan, G. C., and Richards, W. J. (1983). "Neutron radiography applications and techniques at the Hot fuel examination facility," in *Neutron radiography*. Editors J. P. Barton and P. von der Hardt (Dordrecht: Springer). doi:10.1007/978-94-009-7043-4_54

Meyer, M. K., Keiser, D. D., Jr., Jue, J.-F., and Shaber, E. (2020). "Research reactor fuels," in *Advances in nuclear fuel chemistry*. Editor M. H. A. Piro (Edinburgh, United Kingdom: Elsevier), 273–312.

Olander, D., Greenspan, E., Garkisch, H. D., and Petrovic, B. (2009). Uranium–zirconium hydride fuel properties. *Nucl. Engr. Des.* 239, 1406–1424. doi:10.1016/j.nucengdes.2009.04.001

Olander, D., Konashi, K., and Yamawaki, M. (2012). "Uranium-zirconium hydride fuel," in *Comprehensive nuclear materials*. Editor R. J. M. Konings (Amsterdam, Netherlands: Elsevier), 3, 314–345.

Olander, D. (2009). Nuclear fuels: Present and future. *J. Nucl. Mater.* 389, 1–22. doi:10.1016/j.jnucmat.2009.01.297

Olander, D. R., and Ng, M. (2005). Hydride fuel behavior in LWRs. *J. Nucl. Mater.* 346, 98–108. doi:10.1016/j.jnucmat.2005.05.017

Parker, H. M. O'D., and Joyce, M. J. (2015). The use of ionising radiation to image nuclear fuel: A review. *Prog. Nucl. Energy* 85, 297–318. doi:10.1016/j.pnucene.2015.06.006

Simand, M. T., Foushee, F. C., and West, G. B. (1976). Fuel elements for pulsed TRIGA research reactors. *Nucl. Tech.* 28 (1), 31–56. doi:10.13182/NT76-A31537

Simnad, M. T. (1981). The U-ZrHx alloy: Its properties and use in TRIGA fuel. *Nucl. Eng. Des.* 64, 403–422. doi:10.1016/0029-5493(81)90135-7

Steven Hansen, J. *Application guide to tomographic gamma scanning*. Los Alamos National Laboratory Report. LA-UR-04-7014.

Terrani, K., Balooch, M., Carpenter, D., Kohse, G., Keiser, D., Jr., Meyer, M., et al. (2017). Irradiation effects on thermal properties of LWR hydride fuel. *J. Nucl. Mater.* 486, 381–390. doi:10.1016/j.jnucmat.2017.01.030

Zinkle, S. J., Ott, L. J., Ingersoll, D. T., Ellis, R. J., and Grossbeck, M. L. (2002) "Overview of materials technologies for space nuclear power and propulsion," in *Space technology and applications international forum–STAIF 2002*. Editor M. S. El-Genk, 608, 1063–1073. 3–6 February 2002, Albuquerque, NM, USA. (Melville, NY, USA: American Institute of Physics).

frontiers | Frontiers in Energy Research

TYPE Brief Research Report
PUBLISHED 20 April 2023
DOI 10.3389/fenrg.2023.1159478

OPEN ACCESS

EDITED BY
Xiaojing Liu,
Shanghai Jiao Tong University, China

REVIEWED BY
Tengfei Zhang,
Shanghai Jiao Tong University, China
Mohammad Alrwashdeh,
Khalifa University, United Arab Emirates

*CORRESPONDENCE
Friederike Bostelmann,
bostelmannf@ornl.gov

RECEIVED 06 February 2023
ACCEPTED 10 April 2023
PUBLISHED 20 April 2023

CITATION
Bostelmann F, Ilas G and Wieselquist WA (2023), Key nuclear data for non-LWR reactivity analysis.
Front. Energy Res. 11:1159478.
doi: 10.3389/fenrg.2023.1159478

Key nuclear data for non-LWR reactivity analysis

Friederike Bostelmann*, Germina Ilas and William A. Wieselquist

Oak Ridge National Laboratory, Oak Ridge, TN, United States

An assessment of nuclear data performance for non-light-water reactor (non-LWR) reactivity calculations was performed at Oak Ridge National Laboratory that involved a thorough literature review to collect related observations made across different research institutions, an interrogation of the latest ENDF/B evaluated nuclear data libraries, and propagation of nuclear data uncertainties to key figures of merit associated with reactor safety for six non-LWR benchmarks. The outcome of this comprehensive study was published in a technical report issued by the US Nuclear Regulatory Commission. This paper provides a summary of the study's key observations and conclusions and demonstrates with two examples how the various methods available in the SCALE code system were used to identify key cross section uncertainties for non-LWR reactivity analyses.

KEYWORDS

nuclear data, non-LWR, reactivity, scale, uncertainty analysis, sensitivity analysis

1 Introduction

Uncertainty analyses are an essential component in the design and computational analysis of advanced reactors, especially due to the growing interest in new reactor concepts for which scant operational data are available[1]. The advanced reactor concepts currently being developed throughout the industry (US, 2022) are significantly different from light-water reactor (LWR) designs with respect to geometry, materials, and operating conditions—and, consequently, with respect to their reactor physics behavior. An overview of different advanced reactor concepts is provided by the Gen IV International Forum (NEA, 2014), and the different technologies along with considerations around their fuel cycle are thoroughly discussed in a recent publication by the Academy of Sciences (National Academies of Sciences Engineering, and Medicine, 2023). Given the limited operating experience with non-LWRs, the accurate simulation of reactor physics and the quantification of associated uncertainties are critical for ensuring that advanced reactor concepts operate within the appropriate safety margins.

While nuclear data provide the fundamental basis for reactor physics calculations, they also provide the major source of input uncertainty. The nuclear interaction cross sections, fission yields, and decay data used in these calculations have uncertainty resulting from measurements and subsequent data evaluations. Nuclear data used with reactor physics codes result from extensive data evaluations, including validation studies performed with

1 This manuscript has been authored by UT-Battelle LLC, under contract DE-AC05-00OR22725 with the US Department of Energy (DOE). The US government retains and the publisher, by accepting the article for publication, acknowledges that the US government retains a nonexclusive, paid-up, irrevocable, worldwide license to publish or reproduce the published form of this manuscript, or allow others to do so, for US government purposes. DOE will provide public access to these results of federally sponsored research in accordance with the DOE Public Access Plan (http://energy.gov/downloads/doe-public-access-plan).

criticality experiments. The evaluated nuclear data libraries, such as the US Evaluated Nuclear Data File/B (ENDF/B) (Brown et al., 2018), undergo continuous modifications based on additional measurements or improved evaluations, and new revisions are being released on a regular basis to capture these additional improvements.

To improve understanding of the uncertainties that result from nuclear data in the calculation of safety-relevant output quantities and to determine where additional efforts should focus to reduce relevant nuclear data uncertainties, these uncertainties must be propagated to key figures of merit that impact nuclear safety. Furthermore, it must be considered that uncertainty information is not available for all nuclear data used in the simulation. Missing uncertainty data must be identified and, where possible, the impact of these gaps must be assessed to inform recommendations for further evaluations.

Although many studies assessing the impact of nuclear data uncertainties are available in the public literature, a comprehensive overview of the impact of nuclear data uncertainties for reactivity in the most relevant non-LWRs designs (in terms of reactor concepts for which license applications are expected in the near future in the United States) based on the same set of evaluated nuclear data libraries and using the same simulation approaches did not exist until recently. A recently concluded project at Oak Ridge National Laboratory (ORNL) sponsored by the US Nuclear Regulatory Commission (NRC) addressed this need by performing a thorough literature study to collect the observations made across different research institutions and by using SCALE [Wieselquist, W. A., Lefebvre, R. A., and Jessee, M. A. (Eds.), 2020] to systematically propagate nuclear data uncertainties to key figures of merit associated with reactor safety for five non-LWR types: high-temperature gas-cooled reactor (HTGR), molten salt reactor (MSR), fluoride salt–cooled high-temperature reactor (FHR), heat pipe reactor (HPR), and sodium-cooled fast reactors (SFRs). As part of this study, missing nominal nuclear data and nuclear data uncertainties were identified for reactivity analyses as well as for further fuel depletion analysis. This paper provides a summary of key observations and conclusions obtained during this study, while providing just two examples to demonstrate how the computational analyses were performed. Detailed analysis results are available in a comprehensive technical report (Bostelmann et al., 2021b) issued by the NRC. It is noted that the study focused on systems with ^{235}U enriched or mixed uranium/plutonium fuel based on spent LWR fuel; ^{233}U-fueled systems were not considered here.

After introducing the selected non-LWRs in **Section 2**, the applied approach used for the uncertainty analyses is briefly summarized (**Section 3**). As examples of the performed computational analyses, the propagation of nuclear data uncertainties is presented and discussed for reactivity assessments of the HPR and the FHR concepts (**Section 4**). Afterwards, an overview of key observations for all considered systems based on both the literature research and the SCALE analyses is given (**Section 5**).

2 Benchmarks

The benchmarks for uncertainty analyses with SCALE were identified by selecting reactors with available detailed specifications for which the geometry, materials, and neutron energy spectra are similar to those of the advanced reactor technologies of interest. Given the limited availability of measured data for advanced reactor systems, only theoretical or simplified descriptions were found for some reactor technologies. However, as long as the models include representative geometric dimensions and representative materials, uncertainty analyses of these models can serve well to provide an understanding of the impact of nuclear data uncertainties and to identify relevant nuclide reactions. **Table 1** gives an overview of the selected benchmarks, and **Figure 1** illustrates the developed SCALE models. Details of the models can be found in the references provided in **Table 1**.

Many of the considered reactors share certain characteristics. Each of the thermal spectrum systems—HTR-10, the University of California Berkeley (UCB) PB-FHR, the Molten-Salt Reactor Experiment (MSRE)—rely on graphite as neutron moderator and reflector. Both the HTR-10 and the UCB PB-FHR are pebble-bed reactors that use graphite pebbles (of different size) in which tristructural isotropic (TRISO) fuel particles are distributed. The UCB PB-FHR uses molten salt FLiBe as coolant, which is a mixture of LiF and BeF_2. Fluoride-based salt is also used in the MSRE for both the carrier salt and the fuel salt. The fast spectrum systems (INL Design A, EBR-II, ABR1000) operate in the absence of a moderator. EBR-II and ABR1000 include irradiated fuel: EBR-II includes high enriched uranium fuel assemblies at various burnups, and ABR1000 uses spent LWR fuel, i.e., uranium/transuranic (U/TRU) fuel, in its equilibrium core. Both these SFRs are cooled by sodium. The INL Design A is an HPR operated with high-assay low-enriched uranium (HALEU) and uses potassium as its working fluid. An overview of key characteristics of the selected benchmarks is provided in **Table 2**.

3 Uncertainty and sensitivity analysis approach

Uncertainty and sensitivity analyses of eigenvalues and reactivity coefficients were performed using two approaches: linear perturbation theory and random sampling approach. Both approaches relied on neutron transport calculations with SCALE's Monte Carlo code KENO-VI in either multigroup (MG) or continuous-energy (CE) mode. Both approaches provided insights into the uncertainty of key metrics as well as the top-contributing nuclear data to the observed uncertainty. All analyses were performed using codes and nuclear data libraries from a pre-release version of SCALE 6.3.

3.1 Linear perturbation theory

Sensitivity analyses were performed for the eigenvalue and the reactivity effects using the perturbation theory–based approach implemented in SCALE's TSUNAMI code (Broadhead et al., 2004). TSUNAMI calculates sensitivity coefficients for all nuclides included in the model of interest with all reactions in all energy groups (Williams, 1986; Williams et al., 2001). TSUNAMI was applied to calculate eigenvalue sensitivities. For reactivity differences such as temperature feedback and control rod worth, TSUNAMI

TABLE 1 Overview of selected advanced reactor technology benchmarks.

Reactor technology	Selected benchmark	Reference	Type
Pebble-bed HTGR	HTR-10	Terry et al. (2007)	Experiment
FHR	UCB Mark 1 PB-FHR	Andreades et al. (2014)	Computational benchmark
Graphite- moderated MSR	MSRE	Shen et al. (2019)	Experiment
HPR	INL Design A*	Sterbentz et al. (2018)	Computational Benchmark
SFR	EBR-II	Lum et al. (2018)	Experiment
SFR	ABR-1000	Buiron et al. (2019)	Computational benchmark

*The original design contains oxide fuel. However, this study used a slightly modified version with metallic fuel consisting of 18.1%^{235}U enriched with a 10% weight fraction of zirconium (U-10Zr) (Hu et al., 2019).

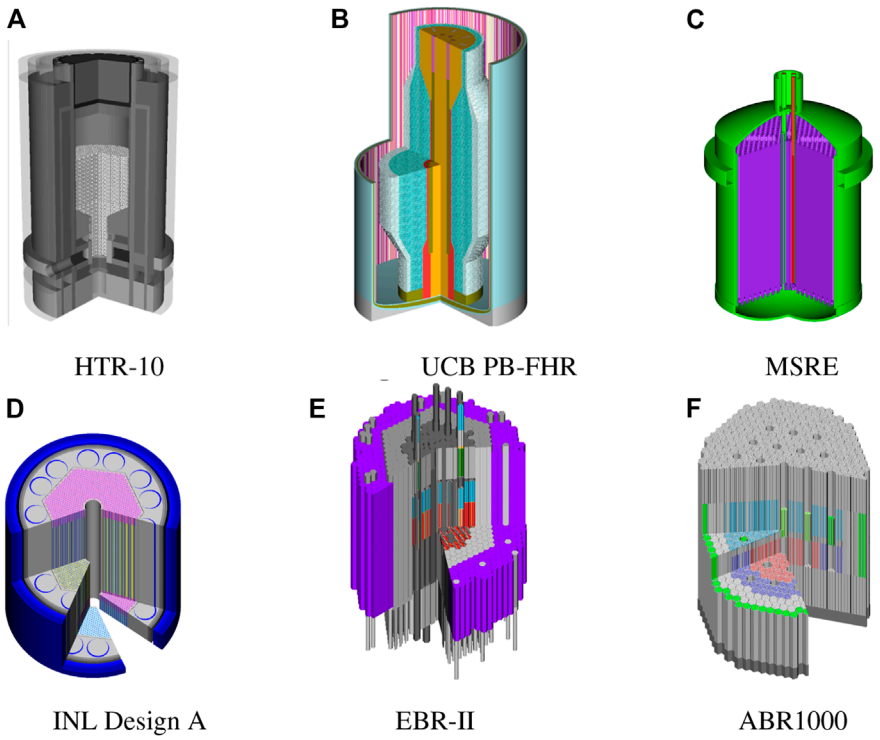

FIGURE 1
3D visualizations of the non-LWR SCALE models. **(A)** HTR-10, **(B)** UCB PB-FHR, **(C)** MSRE, **(D)** INL Design A, **(E)** EBR-II and **(F)** ABR 1000.

calculations were performed at two different states, and SCALE's module TSAR (Williams, 2007) was used to combine the two sets of sensitivity coefficients to obtain sensitivity coefficients for the reactivity difference.

The nuclear data uncertainties are given in energy-dependent covariance matrices for each nuclide reaction and for correlations between different nuclide reactions. The multiplication of these covariance matrices with the corresponding sensitivity coefficients determined using TSUNAMI in the so-called *sandwich formula* leads to the total output variance (Rearden et al., 2011). In addition to the total output uncertainty, TSUNAMI provides a list of the individual contributions of all relevant covariance matrices so that the top contributors to the output uncertainty can be identified.

Note that the output uncertainty is usually shown as the 1-sigma standard deviation of a normal distribution, due to the input nuclear data covariances being normal distributions.

3.2 Random sampling

For some reactor concepts, the random sampling approach as implemented in SCALE's Sampler sequence (Williams et al., 2013) was used to study uncertainties resulting from nuclear data. The nuclear data are perturbed based on covariance data as provided in the ENDF/B nuclear data files. Sampler performs calculations multiple times based on the perturbed dataset. A statistical analysis of the output of interest yields the output's uncertainty. To identify

TABLE 2 Key design characteristics of the selected benchmarks.

Characteristic	HTR-10 (HTGR)	UCB mark 1 (FHR)	MSRE (MSR)	INL design a (HPR)	EBR-II (SFR)	ABR-1000 (SFR)
Fuel Type	UO_2 (TRISO)	UCO (TRISO)	FLiBe salt	UO_2	Metal	Metal
Enrichment (wt%)	17.0	19.9	34.5	19.75	66.72	17–22*
Coolant	He (gas)	FLiBe salt	FLiBe salt	K (liq.)	Na (liq.)	Na (liq.)
Primary Moderator	Graphite	Graphite	Graphite	—	—	—
Neutron Energy Spectrum	thermal	thermal	thermal	fast	fast	fast
Core Thermal Power (MW)	10	236	10	5	62.5	1,000
Active Fuel Height (m)	0.27	5.3	1.70	1.50	0.34	0.86
Average Fuel Temp. (K)	293	1,003	932	1,061	616	807
Average Coolant Temp. (K)	293	923	845	950	616	705.65
Initial Heavy Metal Loading (tHM)	0.049	0.702	0.233	4.57	9.57	11.66

*Pu/TRU, content.

the top-contributing nuclide reactions to the output uncertainty, Sampler calculates the sensitivity index R^2 (Bostelmann et al., 2022) of all reactions of all nuclides relevant for the model. On a level from 0 to 1, R^2 provides a measure of the importance of an individual nuclear reaction to the observed output uncertainty.

Note that the output uncertainty is usually shown as the 1-sigma standard deviation using sample statistics. Although SCALE/Sampler can draw from many distributions, the fundamental nuclear data is specified as a normal distribution. To avoid generating non-physical nuclear data (such as negative cross sections), the normal distribution is truncated.

3.3 Applied nuclear data

Neutron transport calculations were performed using ENDF/B-VII.0 (Chadwick et al., 2006), ENDF/B-VII.1 (Chadwick et al., 2011), and ENDF/B-VIII.0 cross section libraries (Brown et al., 2018). For the uncertainty quantification, TSUNAMI applied the corresponding ENDF/B-VII.0–based, ENDF/B-VII.1–based, and ENDF/B-VIII.0–based covariance libraries, respectively. Sampler calculations were performed using perturbation factors that were generated based on these covariance libraries. More details on these libraries can be found in the SCALE manual (Wieselquist et al., 2020).

4 Nuclear data uncertainty propagation

Only the reactivity analysis of the INL Design A HPR and the FHR are presented here to demonstrate how the uncertainty and sensitivity analyses were performed. When considering the presented results, it is useful to keep in mind results usually obtained for the same quantities in LWR analysis. A k_{eff} uncertainty between 0.5% for fresh fuel and 0.8% for depleted fuel, and a fuel Doppler coefficient uncertainty between 1.2% and 1.8% is usually obtained

TABLE 3 INL Design A HPR uncertainties† in quantities of interest due to nuclear data uncertainty, for different ENDF/B library versions.

Quantity	VII.0 (%)	VII.1 (%)	VIII.0 (%)	$\frac{\text{VII.1}}{\text{VII.0}} - 1$	$\frac{\text{VIII.0}}{\text{VII.1}} - 1$
k_{eff}	2.01	2.08	0.98	3.4%	−53.0%
$\Delta\rho$ fuel temperature	8.77	6.59	4.34	−24.9%	−34.1%
$\Delta\rho$ grid radial expansion	1.40	1.68	1.49	19.9%	−11.3%
$\Delta\rho$ fuel axial expansion	2.92	2.69	2.00	−8.0%	−25.7%

†1-σ relative standard deviation of normal distribution.

(Aures et al., 2017; Delipei et al., 2021). Key contributors to these uncertainties are ^{238}U and ^{239}Pu radiative capture, as well as ^{235}U and ^{239}Pu neutron multiplicity.

4.1 INL design A

Based on a SCALE full core model initially developed for a different project (Walker et al., 2022), the sensitivity and uncertainty analyses for the fresh core of the INL Design A (**Figure 1D**) were performed with CE TSUNAMI for the following quantities of interest.

1 k_{eff}
2 $\Delta\rho$ fuel temperature: reactivity change from increasing fuel temperature by 500 K
3 $\Delta\rho$ grid radial expansion: reactivity change from radial expansion of the fuel element grid 0.08% into the surrounding gap
4 $\Delta\rho$ fuel axial expansion: reactivity change from axial expansion of the fuel by 0.5% into the lower gas plenum

The temperature increase and the relative expansions were chosen to obtain statistically distinguishable results with the Monte Carlo approach, but they do not correspond to actual changes during reactor operation. While the relative uncertainties obtained with the ENDF/B-VII.0 and ENDF/B-VII.1 libraries

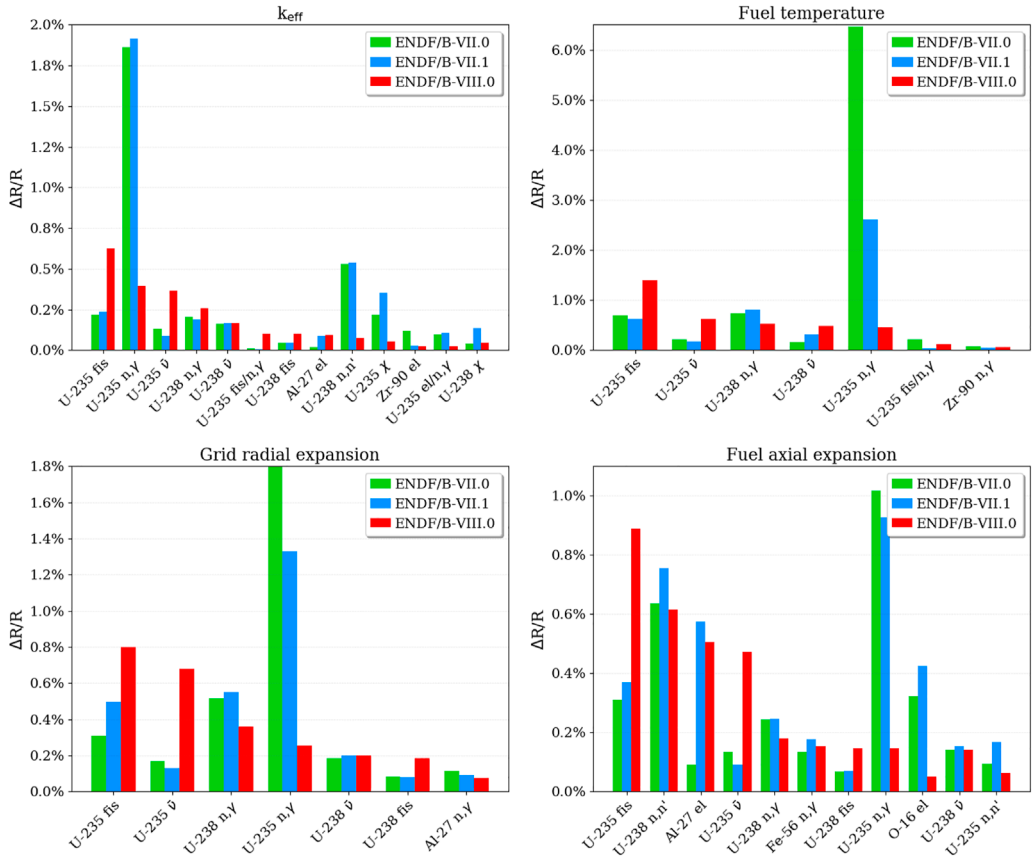

FIGURE 2
Relative contributions to the output uncertainties of the INL Design A HPR (as obtained with TSUNAMI in ΔR/R, R: response).

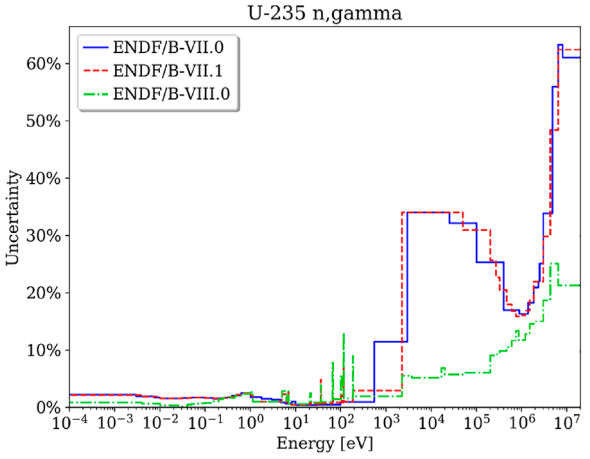

FIGURE 3
Relative uncertainty of the ^{235}U (n,γ) cross section in different ENDF/B library releases.

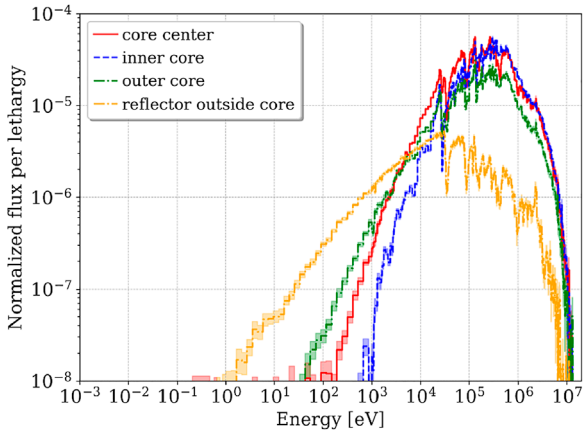

FIGURE 4
Normalized neutron flux of the INL Design A HPR at the core axial midline, at different radial positions.

are fairly similar, a significant reduction in uncertainty was observed with the ENDF/B-VIII.0 library (Table 3). It is noted that even with the ENDF/B-VIII.0 library, the k_{eff} uncertainty is about twice as large as the typical k_{eff} uncertainty of an LWR system.

To understand which cross sections are the major contributors to the observed uncertainties and why there is this significant

TABLE 4 UCB PB-FHR uncertainties[†] in quantities of interest due to nuclear data uncertainty, for different ENDF/B library versions.

Quantity	VII.1 (%)	VIII.0 (%)	$\frac{\text{VIII.0}}{\text{VII.1}} - 1$
k_{eff}	1.38	1.43	3.6%
$\Delta\rho$ fuel temperature	3.11	2.79	−10.2%
$\Delta\rho$ salt temperature	5.54	7.13	28.7%
$\Delta\rho$ salt density	35.65	36.80	3.2%

[†]1-σ relative standard deviation of normal distribution.

difference with the latest ENDF/B release, sensitivity analyses were performed by investigating the top contributions to the uncertainty provided by TSUNAMI. TSUNAMI determines these individual contributions through the multiplication of the cross section–specific sensitivity with the corresponding covariance matrix. Figure 2 presents these top contributions in the unit ΔR/R, R being the response of interest (e.g., k_{eff}).

It is easily visible that the uncertainty in the ^{235}U (n,γ) cross section is the top contributor to all output uncertainties in the ENDF/B-VII.0 and ENDF/B-VII.1 calculations. The associated uncertainty in this reaction was dramatically reduced in the ENDF/B-VIII.0 calculation, which led to a significant reduction in the overall output uncertainty. This reduction is the largest for k_{eff} because ^{235}U (n,γ) was the dominating contributor to the k_{eff} uncertainty with ENDF/B-VII.0 and ENDF/B-VII.1. Slightly larger contributions from ^{235}U fission and the neutron multiplicity $\bar{\nu}$ due to their increased uncertainty in ENDF/B-VIII.0 caused a slight offset.

To further explain the large impact of the ^{235}U (n,γ) cross section uncertainty on the INL Design A reactivity results, the uncertainty of this reaction and the neutron flux in this reactor were examined. Figure 3 shows that the ^{235}U (n,γ) uncertainty is large, with up to 34% in the fast energy range; that is, in the energy range with many neutrons. Since the uncertainty is reduced in this energy range in ENDF/B-VIII.0, the overall contribution of this reaction to the output uncertainty is reduced. Figure 4 clearly illustrates the differences in the fast neutron spectrum in various regions of the reactor.

This example of analysis demonstrates 1) how to identify top-contributing nuclide reactions to an output uncertainty of interest and 2) the strong impact of reductions of important cross section uncertainties for the overall output uncertainty. Given that the ^{235}U

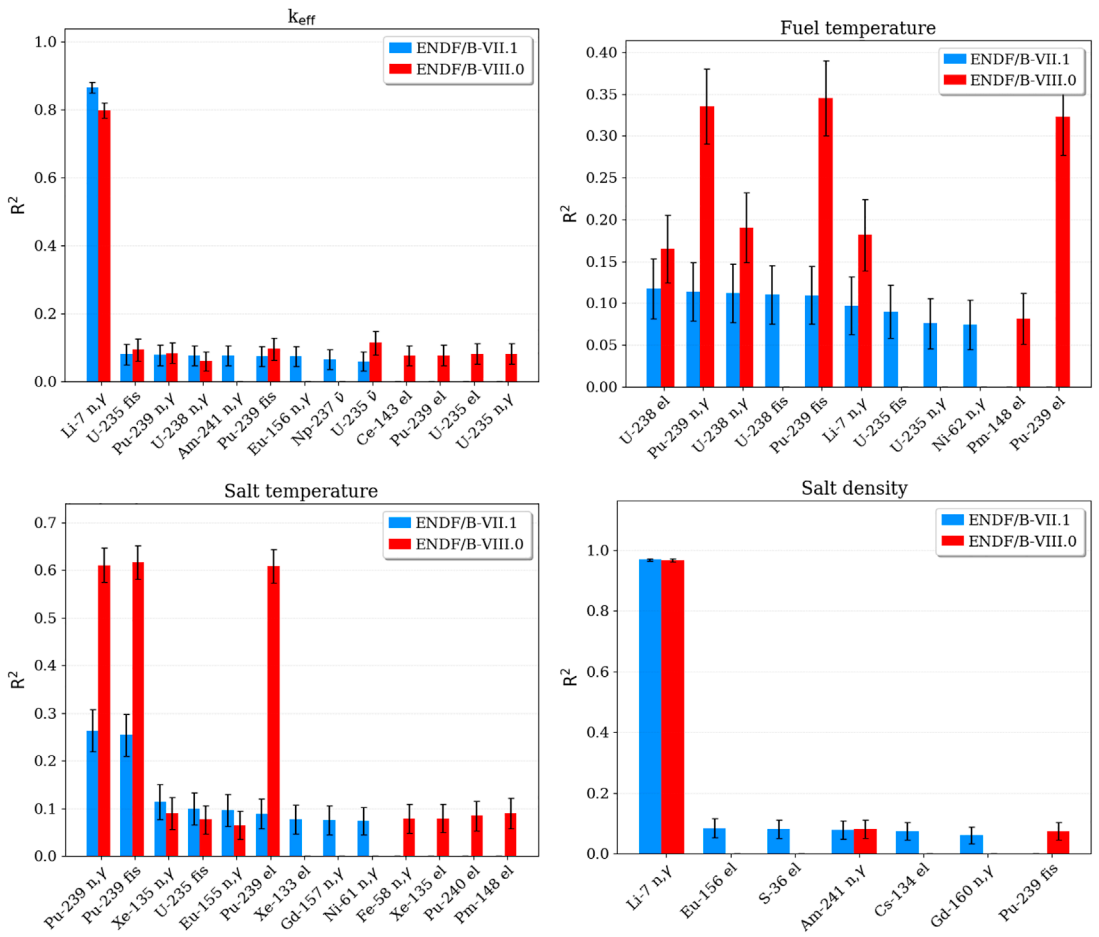

FIGURE 5
Top contributor to the output uncertainties of the UCB PB-FHR in terms of R^2 (as obtained with Sampler, accompanied by 95% confidence intervals).

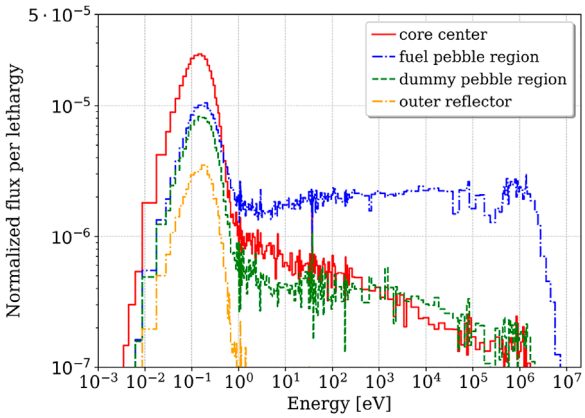

FIGURE 6
Normalized neutron flux of the UCB PB-FHR at the core axial midline, at different radial positions.

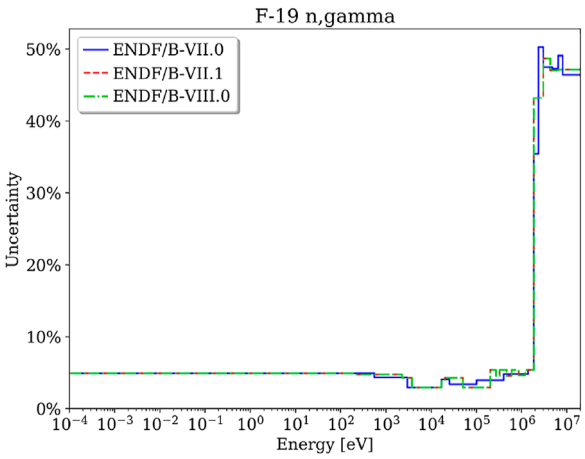

FIGURE 7
Relative uncertainty of the ^{19}F (n,γ) cross section in different ENDF/B library releases.

(n,γ) uncertainty was reduced in ENDF/B-VIII.0, the identification of top contributors in this case would result in recommendations for further measurements and evaluations of ^{235}U fission, inelastic scattering (n,n′), and $\bar{\nu}$. These conclusions were drawn upon the fact the INL Design A is a fast spectrum system based on ^{235}U-enriched fuel. The top contributors of mixed U/TRU-fueled fast spectrum reactors (such as those assumed in SFRs) do not include ^{235}U (n,γ) as the dominant contributing reaction (Bostelmann et al., 2021b).

4.2 UCB PB-FHR

Based on a SCALE full core model initially developed for a different project (Bostelmann et al., 2021a), the sensitivity and uncertainty analyses for the equilibrium core of the UCB PB-FHR were performed with Sampler and KENO-VI in MG mode for the following quantities of interest.

1 k_{eff}
2 $\Delta\rho$ fuel temperature: reactivity change from increasing fuel temperature by 500 K
3 $\Delta\rho$ coolant salt temperature: reactivity change from increasing salt temperature by 300 K
4 $\Delta\rho$ coolant salt density: reactivity change from increasing salt density by 50%

The temperature increases and the density multiplier were chosen to obtain statistically distinguishable results with the Monte Carlo approach, but they do not correspond to actual changes during reactor operation. Sampler was chosen due to convergence challenges of sensitivities for important scattering reactions of the graphite reflector and the salt components in the fast energy range when using the perturbation theory–based approach for this reactor. Furthermore, only this approach can be used for the analysis of output quantities such as a power distribution (not presented here). A sample size of 1,000 was used with Sampler to allow sufficient confidence in the obtained uncertainties of the reactivity differences. Sampler calculations were limited to ENDF/B-VII.1 and ENDF/B-VIII.0 since Sampler's sensitivity analysis is currently enabled only for these two libraries.

The relative uncertainties obtained with these two libraries are fairly similar (Table 4). The relative uncertainty of the salt density reactivity stands out, with an uncertainty larger than 35%, and the k_{eff} uncertainty is about three times as large as the typical k_{eff} uncertainty of an LWR system.

To understand which cross sections are the major contributors to the observed uncertainties and why the salt density uncertainty is significantly larger than the other uncertainties, sensitivity indices R^2 were calculated for all reactions of all nuclides in the system. Figure 5 presents the largest obtained R^2 values found to be statistically significant (above a statistical significance level).

It is easily visible that the top contributor to the k_{eff} and the salt density reactivity uncertainty is the uncertainty in the ^{7}Li (n,γ) cross section. ^{7}Li is one of the major components of the coolant salt; therefore, ^{7}Li reactions have an especially large influence on the salt density reactivity. The uncertainty of this (n,γ) reaction is significant in the thermal region in which most of the neutrons can be found (Figure 6), with an approximate value in this energy range of 5% (Figure 7). The value for this uncertainty is identical between ENDF/B-VII.1 and ENDF/B-VIII.0. If the uncertainty of this single reaction could be reduced with further measurements and evaluations, then the uncertainties of these key reactivities would dramatically decrease. The relevant nuclide reactions for the other reactivity uncertainties are spread out over various reactions, mainly U and Pu reactions. Since many of these reactions' uncertainties varied between ENDF/B-VII.1 and ENDF/B-VIII.0, their relative contributions and the total output uncertainties show larger variations.

In the ENDF/B-VIII.0 calculations of the fuel and salt temperature reactivities, large R^2 values of the ^{239}Pu elastic scattering reaction stand out. For the interpretation of R^2, it has to be considered that R^2 includes correlations between the different reactions. For example, in the case of ^{239}Pu elastic scattering, this reaction is not itself contributing significant uncertainty to the total output uncertainty, but its R^2 value is the result of correlations with both the ^{239}Pu fission and (n,γ) reaction which show larger relative

TABLE 5 Summary of key observations.

All considered non-LWRs	FHR
• Large differences exist between ENDF/B library releases for relevant nominal and uncertainty data: neutron multiplicity, fission, capture, scattering for ^{235}U, ^{238}U, and major Pu isotopes • Reactivity uncertainty is driven by fission, capture and scattering reactions of ^{235}U, ^{238}U, and major Pu isotopes	• No graphite thermal scattering data uncertainties are available • No thermal scattering data for salts (e.g., FLiBe) are available • Significant update from ENDF/B-VII.0 to VII.1 in the carbon (n,γ) cross section • Large ^{7}Li (n,γ) cross section uncertainty • Significant update from ENDF/B-VII.0 to VII.1 in the ^{6}Li (n,t) cross section
HPR and SFR	**Graphite-moderated MSR**
• No angular scattering uncertainties are available • Large ^{235}U (n,γ) cross section uncertainty causes large uncertainties in system using ^{235}U-enriched fuel • Large ^{238}U inelastic scattering uncertainty causes large uncertainties in U/TRU-fueled systems • Large impact of scattering reactions of coolant and structural materials	• No cross section data are available for ^{135m}Xe • No thermal scattering data are available for salts (e.g., FLiBe) • No graphite thermal scattering data uncertainties are available • Large ^{7}Li (n,γ) cross section uncertainty • Significant update from ENDF/B-VII.0 to VII.1 in the ^{6}Li (n,t) cross section
HTGR	**Fast spectrum MSR**
• Significant update from ENDF/B-VII.0 to VII.1 in the carbon (n,γ) cross section • No graphite thermal scattering data uncertainties	• Significant update from ENDF/B-VII.0 to VII.1 in the ^{35}Cl (n,p) significant cross section • Large impact of ^{24}Mg elastic scattering uncertainty on uncertainties

contributions in ENDF/B-VIII.0. In contrast, in the ENDF/B-VII.1 calculation, the R^2 for ^{239}Pu elastic scattering is below the statistical significance level because of the smaller importance of ^{239}Pu fission and (n,γ) reaction relative to other contributors. More detailed explanations on the interpretation of R^2 in such analyses can be found in (Bostelmann et al., 2022).

This example analysis demonstrates 1) how the large uncertainty of one cross section can dominate the uncertainty of important output quantities and that 2) analysis of non-LWRs can lead to the identification of unexpected, important cross section uncertainties of nuclides that were never found relevant for LWR analysis.

5 Key observations for the studied non-LWRs

The following provides an overview of the most relevant observations for the considered non-LWRs, focused on the ENDF/B evaluated data library. Comparisons of the data between the different ENDF/B libraries led to observations on important differences in cross sections and cross section uncertainties (e.g., ^{235}U $\bar{\nu}$). Literature research led to the identification of missing nuclear data (e.g., ^{135m}Xe) and nuclear data updates with important impact on key output quantities (e.g., ^{35}Cl (n,p)). Our own uncertainty and sensitivity studies confirmed the impact of nuclear data updates and identified further relevant nuclear data uncertainties (e.g., ^{7}Li (n,γ)).

5.1 Nuclear data for neutron transport calculations

For neutron transport calculations to determine output quantities such as reactivity and power distributions, the observations with respect to nuclear data and non-LWRs are summarized in **Table 5**.

5.2 Nuclear data for time-dependent analyses

The time-dependent behavior of any reactor type requires more than just cross section data. For the following important data, limited or no data are available in the latest ENDF/B release.

- Fission yields: Uncertainties available, correlations not available
- Decay constants: Uncertainties available, correlations not available
- Branching ratios: No uncertainty or correlation data available
- Recoverable energy for fission and capture: No uncertainty or correlation data available
- Delayed neutron fractions and decay constants: No uncertainty or correlation data available

Data on recoverable energy for fission and capture reactions are in fact often hard-coded in neutron transport codes; this data is, for example, important to determine the material power. The same is

valid for delayed neutron fractions and decay constants, which are especially important for transient analyses and which are further relevant in systems with flowing fuel (MSRs) due to the delayed neutron precursor drift.

6 Conclusion

This paper reviews an assessment of key nuclear data, nuclear data uncertainties, and nuclear data gaps that are relevant for reactor safety analysis in non-LWRs, recently concluded at ORNL. The study involved a literature review, examination of available evaluated nuclear data libraries, and sensitivity and uncertainty analyses with SCALE for six non-LWR benchmarks to quantify the impact of the identified key nuclear data on several key metrics. The nuclear data uncertainty propagation is highlighted herein for two of the six non-LWRs, and the summary of observations for all non-LWRs are presented.

SCALE's approaches to study the impact of nuclear data uncertainties on the uncertainties of key metrics of interest—particularly the ranking of contributions to the output uncertainties—can be used to guide future measurement and evaluation efforts to reduce the significant nuclear data uncertainties and thereby significantly reduce the overall observed uncertainties. However, to perform such uncertainty assessments, SCALE (just as any other uncertainty analysis tool) relies on the availability of complete and reliable nuclear data.

Besides observing major cross section and uncertainty updates between the different ENDF/B nuclear data library releases that can have major influence on reactivities, various data gaps were identified, especially for missing uncertainties. These gaps must be addressed to improve prediction of key metrics and to avoid unknown biases. Furthermore, this study identified several large cross section uncertainties. A reduction of these specific large uncertainties is needed to significantly reduce the overall output uncertainty of key metrics. It is noted that no statement on the performance or recommendation of a specific ENDF/B library are made given the limited amount of experimental measurement data for non-LWRs to allow a thorough validation.

This study focused on key figures of merit obtained with neutron transport calculations at a single point in time. This type of systematic approach to assess nuclear data performance should be continued in the depletion simulations space to determine uncertainties in nuclide inventories, as well as in transient analysis space, in which key nuclear data include delayed neutron data. All of these studies will greatly benefit from the availability of additional non-LWR reactor physics benchmarks as a basis to fill in the gaps for validating computational tools and data for various safety relevant quantities.

Data availability statement

The datasets presented in this study can be found in online repositories. The names of the repository/repositories and accession number(s) can be found in the article/Supplementary Material.

Author contributions

WW and GI provided the outline of study and provided supervision throughout. FB developed the models and performed the computational analyses. FB, GI, and WW collected the nuclear data gaps. FB wrote the first draft of the manuscript. All authors contributed to manuscript revision, read, and approved the submitted version.

Funding

This work was supported by the US Nuclear Regulatory Commission.

Acknowledgments

The authors would like to acknowledge Cihangir Celik's (ORNL) contribution during the development of the SCALE model of the pebble-bed fluoride salt-cooled high temperature reactor. The discussions with Andrew Holcomb (OECD/NEA) about ENDF/B nuclear data libraries and analysis results are much appreciated.

Conflict of interest

The authors declare that the research was conducted in the absence of any commercial or financial relationships that could be construed as a potential conflict of interest.

Publisher's note

References

Andreades, C., Cisneros, A. T., Choi, J. K., Chong, A. Y. K., Fratoni, M., Hong, S., et al. (2014). *Technical description of the "mark 1" pebble-bed fluoride-salt-cooled high-temperature reactor (PB-FHR) power plant*. Berkeley, CA: University of California. Tech. Rep. UCBTH-14-002.

Aures, A., Bostelmann, F., Hursin, M., and Leray, O. (2017). Benchmarking and application of the state-of-the-art uncertainty analysis methods XSUSA and SHARK-X. *Ann. Nucl. Energy* 101, 262–269. doi:10.1016/j.anucene.2016.11.025

Bostelmann, F., Celik, C., Kile, R., and Wieselquist, W. (2021a). *SCALE analysis of a fluoride salt cooled high temperature reactor in support of severe accident analysis*. Oak Ridge, TN: Oak Ridge National Laboratory. Tech. Rep. ORNL/TM-2021/2273.

Bostelmann, F., Ilas, G., Celik, C., Holcomb, A. M., and Wieselquist, W. (2021b). *Nuclear data assessment for advanced reactors*. Oak Ridge, TN: Oak Ridge National Laboratory. ORNL/TM-2021/2002Tech. Rep. NUREG/CR-7289.

Bostelmann, F., Wiarda, D., Arbanas, G., and Wieselquist, W. A. (2022). Extension of SCALE/Sampler's sensitivity analysis. *Ann. Nucl. Energy* 165, 108641. doi:10.1016/j.anucene.2021.108641

Broadhead, B. L., Rearden, B. T., Hopper, C. M., Wagschal, J. J., and Parks, C. V. (2004). Sensitivity- and uncertainty-based criticality safety validation techniques. *Nucl. Sci. Eng.* 146, 340–366. doi:10.13182/NSE03-2

Brown, D., Chadwick, M., Capote, R., Kahler, A., Trkov, A., Herman, M., et al. (2018). ENDF/B-VIII.0: The 8th major release of the nuclear reaction data library with CIELO-project cross sections, new standards and thermal scattering data. *Nucl. Data Sheets* 148, 1–142. doi:10.1016/J.NDS.2018.02.001

Buiron, L., Rimpault, G., Sciora, P., Stauff, N., Kim, T. K., Taiwo, T., et al. (2019). "Benchmark for uncertainty analysis in modeling (UAM) for design, operation and safety analysis of SFRs, core definitions,". Version 1.6. Tech. rep., OECD/NEA.

Chadwick, M., Herman, M., Obložinský, P., Dunn, M., Danon, Y., Kahler, A., et al. (2011). ENDF/B-VII.1 nuclear data for science and technology: Cross sections, covariances, fission product yields and decay data. *Nucl. Data Sheets* 112, 2887–2996. doi:10.1016/j.nds.2011.11.002

Chadwick, M., Obložinský, P., Herman, M., Greene, N., McKnight, R., Smith, D., et al. (2006). ENDF/B-VII.0: Next generation evaluated nuclear data library for nuclear science and technology. *Nucl. Data Sheets* 107, 2931–3060. doi:10.1016/j.nds.2006.11.001

Delipei, G. K., Hou, J., Avramova, M., Rouxelin, P., and Ivanov, K. (2021). Summary of comparative analysis and conclusions from OECD/NEA LWR-UAM benchmark Phase I. *Nucl. Eng. Des.* 384, 111474. doi:10.1016/j.nucengdes.2021.111474

Hu, G., Hu, R., Kelly, J., and Ortensi, J. (2019). *Multi-physics simulations of heat pipe micro reactor*. Argonne, IL: Argonne National Laboratory. Tech. Rep. ANL-NSE-19/25.

Lum, E. S., Pope, C. L., Stewart, R., Byambadorj, B., and Beaulieu, Q. (2018). *Evaluation of run 138B at experimental breeder reactor II, a prototypic liquid metal reactor*. France: Organisation for Economic Co-operation and Development/Nuclear Energy Agency. Tech. Rep. EBR2-LMFR-RESR-001, CRIT, NEA/NSC/DOC(2006)1.

National Academies of Sciences Engineering, and Medicine (2023). *Merits and viability of different nuclear fuel cycles and technology options and the waste aspects of advanced nuclear reactors*. Washington, DC: Tech. rep.

NEA (2014). *Technology roadmap update for generation IV nuclear energy systems. Tech. Rep*. Paris, France: Nuclear Energy Agency.

Rearden, B. T., Williams, M. L., Jessee, M. A., Mueller, D. E., and Wiarda, D. A. (2011). Sensitivity and uncertainty analysis capabilities and data in SCALE. *Nucl. Technol.* 174, 236–288. doi:10.13182/NT174-236

Shen, D., Fratoni, M., Ilas, G., and Powers, J. J. (2019). "*Molten-Salt Reactor Experiment (MSRE) zero-power first critical experiment with U-235*. Tech,". Rep. MSRE-MSR-EXP-001, NEA/NSC/DOC(2006)1, Rev. 0, OECD/NEA.

Sterbentz, J. W., Werner, J. E., Hummel, A. J., Kennedy, J. C., Brien, R. C. O., Dion, A. M., et al. (2018). "Preliminary assessment of two alternative core design concepts for the special purpose reactor,". Tech. Rep. INL/EXT-17-43212, Rev. 1. Idaho National Laboratory, Idaho Falls, ID.

Terry, W. K., Montierth, L. M., Kim, S. S., Cogliati, J. J., and Ougouag, A. M. (2007). "Evaluation of the initial critical configuration of the HTR-10 pebble-bed reactor,". Tech. Rep. HTR10-GCR-RESR-001, NEA/NSC/DOC(2006)1, Rev. 0, OECD/NEA.

Us, N. R. C. (2022). Pre-application activities for advanced reactors. https://www.nrc.gov/reactors/new-reactors/advanced/licensing-activities/pre-application-activities.html. (Accessed: 2022-09-07).

Walker, E., Skutnik, S., Wieselquist, W. A., Shaw, A., and Bostelmann, F. (2022). *SCALE modeling of the fast-spectrum heat pipe reactor*. Oak Ridge, TN: Oak Ridge National Laboratory. Tech. Rep. ORNL/TM-2021/2021.

Wieselquist, W. A., Lefebvre, R. A., and Jessee, M. A. (2020). *SCALE code system*. Oak Ridge, TN: Oak Ridge National Laboratory. Version 6.2.4. Tech. Rep. ORNL/TM-2005/39.

Williams, M. L., Broadhead, B. L., and Parks, C. V. (2001). Eigenvalue sensitivity theory for resonance-shielded cross sections. *Nucl. Sci. Eng.* 138, 177–191. doi:10.13182/NSE00-56

Williams, M. L., Ilas, G., Jessee, M. a., Rearden, B. T., Wiarda, D., Zwermann, W., et al. (2013). A statistical sampling method for uncertainty analysis with SCALE and XSUSA. *Nucl. Technol.* 183, 515–526. doi:10.13182/NT12-112

Williams, M. L. (1986). "Perturbation theory for nuclear reactor analysis," in *Handbook of nuclear reactors calculations*. Editor Y. Ronen (United States: CRC Press).

Williams, M. L. (2007). Sensitivity and uncertainty analysis for eigenvalue-difference responses. *Nucl. Sci. Eng.* 155, 18–36. doi:10.13182/NSE06-11

frontiers | Frontiers in Energy Research

TYPE Original Research
PUBLISHED 09 May 2023
DOI 10.3389/fenrg.2023.1099584

OPEN ACCESS

EDITED BY
John Darrell Bess,
JFoster & Associates, LLC (JFA),
United States

REVIEWED BY
Pavel Tsvetkov,
Texas A&M University, United States
Orest Kochan,
Lviv Polytechnic, Ukraine
Alexey Soldatov,
Tomsk Polytechnic University, Russia
Bojan Petrovic,
Georgia Institute of Technology,
United States

*CORRESPONDENCE
Richard Skifton,
richard.skifton@inl.gov

RECEIVED 16 November 2022
ACCEPTED 13 April 2023
PUBLISHED 09 May 2023

CITATION
Skifton R (2023), High-temperature irradiation-resistant thermocouple instability model for in-pile reactor use. *Front. Energy Res.* 11:1099584. doi: 10.3389/fenrg.2023.1099584

High-temperature irradiation-resistant thermocouple instability model for in-pile reactor use

Richard Skifton*

Idaho National Laboratory, Measurement Science Laboratory, Idaho Falls, ID, United States

This article presents an instability model for the high-temperature irradiation-resistant thermocouple (HTIR-TC). Here the term instability defines the superposition of both drift and inhomogeneity of TC thermoelements occurring simultaneously. The HTIR-TC is an advanced thermocouple (TC) that uses the refractory metals niobium and molybdenum as sensing thermoelements for generating electromotive force (EMF) in a field of neutrons and at temperatures upward of 1,600°C. In the Advanced Gas Reactor (AGR) 5/6/7 tests conducted at Idaho National Laboratory's Advanced Test Reactor (ATR), the HTIR-TCs showed low to moderate instability throughout the life of the test. The instability model reveals that HTIR-TCs can, when the operating temperature of the reactor fuel is normal, maintain performance throughout an 18-month refueling cycle typical of nuclear power plants, reflecting an instability of less than ±1%. The HTIR-TC is also qualified for incorporation into a test fixture during the testing of new fuels.

KEYWORDS

thermocouple, in-pile, sensor, irradiation resistant, high temperature, nuclear, reactor temperature, fuel qualification test

1 Introduction

Extensive research and development have been performed on Idaho National Laboratory's high-temperature irradiation-resistant thermocouple (HTIR-TC) design, extending as far back as 1988 (Wilkins, 1988). The initial research by Wilkins showed that, when it came to selecting the thermocouple (TC) thermoelements, molybdenum (Mo) and niobium (Nb) were the top candidates in terms of resisting TC decalibration (i.e., drift) during any long-term tests in which they were placed near or inside nuclear fuel. Since that time, every aspect of the HTIR-TC has been closely studied, including the thermoelements (Wilkins, 1988; Wilkins and Schooley, 1992; Rempe and Wilkins, 2005a; Rempe and Wilkins, 2005b; Wilkins and Evans, 2005; Rempe et al., 2006a; Rempe et al., 2006b) and associated dopants, formation of TC junctions, insulation (Daw et al., 2007), sheath (Rempe et al., 2007), long-term effects of exposure to high temperatures (Rempe et al., 2008; Daw, 2009), extension wiring (Daw et al., 2008), manufacturing and heat treatment processes (Daw et al., 2008), calibration and associated electromotive force (EMF) (Skifton et al., 2018), out-of-pile performance (Riley et al., 2019; Skifton, 2019; Skifton et al., 2019; Riley et al., 2020), transmutation affects (Skifton, 2021a), fuels and reactor temperatures (Jensen, 2007; Palmer, 2015; Palmer et al., 2019a; Palmer et al., 2019b; Palmer et al., 2021), and improved optimizations (Skifton, 2021c; Skifton et al., 2021).

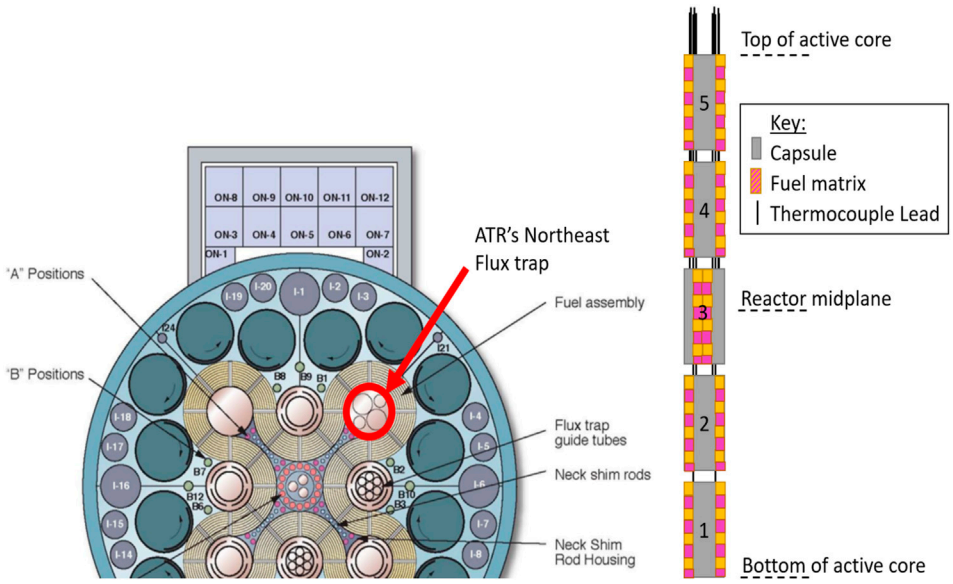

FIGURE 1
ATR layout of northeast flux trap utilized in the AGR 5/6/7 experiment and elevation of capsules within active core (not to scale).

The HTIR-TC consists of two thermoelements (i.e., one being Mo and the other Nb), an insulator (either alumina or magnesia), and an outer sheath of pure Nb. A successful qualification test was performed for the HTIR-TC through the Nuclear Energy Enabling Technologies Advanced Sensors and Instrumentation program (Dayal and Jensen, 2019; Skifton, 2021b). For this qualification test, the HTIR-TC underwent in-reactor testing for over 12 months in the Advanced Test Reactor (ATR)'s high-neutron-flux, high-temperature environment, as part of the Advanced Gas Reactor (AGR) 5/6/7 fuel test (Palmer et al., 2014). In this test, several HTIR-TCs were placed at various locations around the fuel fixtures to evaluate the performance of new advanced fuel designs for the AGR program.

As all TC types show some form of instability with use, quantifying the total amount experienced by a TC within neutron flux fields and high-temperature tests are the main objective of the present work. The instability of a TC signal derives from the inhomogeneity (White, 1906; Kim et al., 2009; Sloneker, 2009) and eventual drift of the nuclear TCs during the unique circumstance of long-term exposure to neutron bombardment and/or excessive high temperatures. Excessive high temperature leads to solid-state diffusion of atoms into the thermoelements. Strictly in nuclear applications, exposure of the TC thermoelements to the neutron field eventually leads to a significant amount of transmutation. Both phenomena are represented in the developed instability model. The developed instability model for HTIR-TCs can be directly applied to other nuclear experiments, and even to different TC types, builds, and applications. The drift should be small enough that the temperature measurements can be accepted as reasonable, and that the TC is shown to survive for extended periods of time (i.e., a nuclear power plant's 18-month refueling cycle). It is important to understand the basic principles of this instability model, as it is applicable to all TC types employed in measuring reactor core temperatures, even when the temperatures are low.

2 Experimental setup

Comprised of five capsules, the AGR-5/6/7 fuel test fixture was inserted into the ATR's northeast flux trap—with an inside diameter of 13.34 cm (5.25 in). Each capsule was ~7 cm (2.75 in) in diameter and with all five capsules welded together gave an overall test train length of 1.22 m (Test train orientation and further details on TC placement can be seen in Figure 1 and are found in greater detail in (Palmer et al., 2014; Hawkes, 2019).) The capsules were positioned in ascending order, with Capsule 1 being located at the bottom of the active core and Capsule 5 at the top. The capsules contained varying amounts of test fuel that, in interacting with the neutron flux, produced varying degrees of temperature. These temperatures were then measured by the TCs, thus generating the required test data on fuel—and in turn, TC—performance.

ATR's overarching thermal neutron flux follows a symmetrical, cosine-squared profile, with a maximum, perturbed, thermal, neutron flux value of ~2.8×10^{14} n/cm^{2}s existing at the reactor height midplane (estimated from (ATR National Scientific User Facility, 2009)), along with a fast (i.e., E > 1 MeV) neutron flux value of approximately 2.25×10^{14} n/cm^{2}s (ATR National Scientific User Facility, 2009). The neutron flux then follows the cosine-squared profile outwards from centerline decaying rapidly to the top and bottom of the reactor height. The temperature range of each capsule varied according to total irradiation and capsule fuel placement. Capsule 3 was expected to show the highest temperatures—mainly as a result of being placed at the reactor height midplane.

Of the five capsules, only Capsules 1 and 3 contained HTIR-TCs for measuring the experimental temperatures. However, the lead

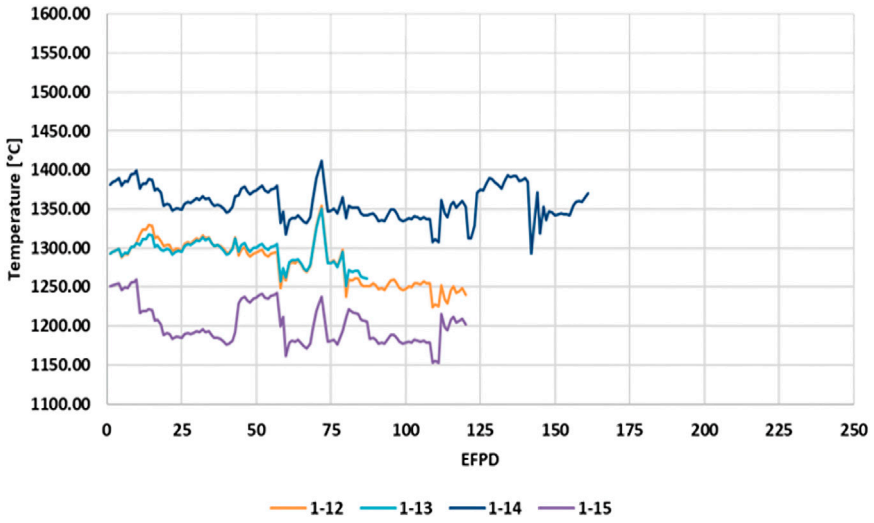

FIGURE 2
Temperatures indicated by HTIR-TCs 1-12, 1-13, 1-14, and 1-15 in Capsule 1 of the AGR-5/6/7 fuel test.

wires for each TC must exit the reactor core by passing upward through designated channels inside capsule located above. This means, for example, that the HTIR-TCs positioned to measure temperatures in Capsule 1 must pass through the higher neutron flux regions of the reactor core. Thus, although the HTIR-TCs in Capsule 1 measure a lower temperature, the TC cable drift caused by thermal- and fast-neutron-flux-induced changes (discussed in Section 3.3) would be similar for all the TCs placed in Capsules 1 and 3.

The test fixture also had provision to pass a small, adjustable He-Ne mixture gas flow around the inside of the capsules to maintain a constant temperature and minimize the effect of power fluctuations on the TC temperature readings (Scates et al., 2020). The gas flow was kept at a minimal value and did not remove heat by convection; instead, it merely provided a high thermal conduction path leading directly to the cooler high-water flow of the reactor coolant outside the capsule.

3 AGR 5/6/7 temperature data

The following data were collected from the AGR 5/6/7 test conducted at Idaho National Laboratory's ATR (ATR National Scientific User Facility, 2009). With respect to reactor core height, Capsule 1 and Capsule 3 in the AGR-5/6/7 fuel test were the bottommost capsule and the midplane capsule, respectively. The HTIR-TCs were positioned in the hottest region of each capsule—for an average measured temperature of about 1,300°C for Capsule 1, and 1,500°C for Capsule 3.

HTIR-TCs 1-12, 1-13, 1-14, and 1-15 each measured the hottest regions of Capsule 1 by being positioned within the inner circle of temperature sensors closest to the fuel. The data were collected over approximately 425 calendar days, covering the operating lifetimes of all Capsule 1 HTIR-TCs in the AGR-5/6/7 test fixture. Figure 2 shows the daily temperature averages of each HTIR-TCs' operational lifetimes, in ATR equivalent full-power days (EFPDs), as calculated by noting the length of time each TC was operational, in conjunction with how long the ATR was at full power. The operational lifetimes of HTIR-TCs 1-12, 1-13, 1-14, and 1-15 were 120, 87, 161, and 120 EFPDs, respectively. The EFPD range that each individual thermocouple experienced stems from random effects that the heat treatment, calibration, and physical handling of each TC underwent prior to installment into the AGR 5/6/7 capsules. The main failure mechanism was the stochastic process of reactor shutdown and restart that causes a sharp temperature gradient on the thermocouples leading to a guillotine total failure of the sensor.

Figure 3 shows the daily averaged temperature data collected at full reactor power from all three Capsule 3 HTIR-TCs throughout their operational lifetimes. The operational lifetimes of HTIR-TCs 3-5, 3-12, and 3-14 were 125, 166, and 164 EFPDs, respectively.

The highest temperature reached during the AGR 5/6/7 campaign was ~1,550°C, as measured by HTIR-TC 3-12 toward the end of irradiation period. This is believed to be the highest temperature ever withstood and measured by a TC within the reactor core (i.e., in-pile TC). Though the temperature in the experimental test fixture was lower than the HTIR-TC's specified maximum temperature of 1,600°C, the preliminary, out-of-pile test data suggest that the HTIR-TCs can indeed accurately measure temperatures all the way up to 1,600°C. However, the instability that would occur at that high a temperature is uncertain and would have to be analyzed and/or measured.

Capsule 1 contained four operating HTIR-TCs around the inside perimeter of the test fuel. These measured slightly lower temperatures than those in Capsule 3. A comparison between these HTIR-TC temperature readings and the temperatures predicted by the thermal model is given in (Pham et al., 2020).

Placed in the center of Capsule 3's hot zone, HTIR-TC 3-5 measured temperatures of around 1,453°C for the first few weeks of operation at full reactor power. The theoretically

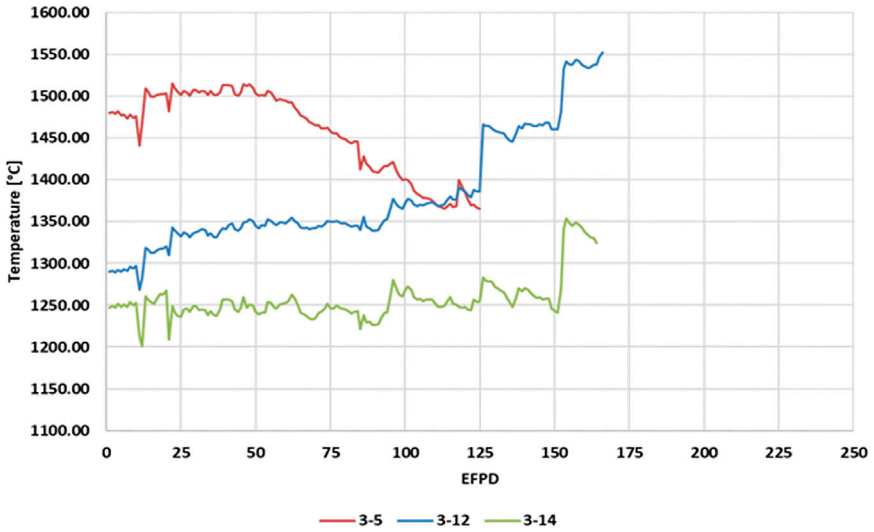

FIGURE 3
Temperature indicated by HTIR-TCs 3-5, 3-12, and 3-14 in Capsule 3 of the AGR-5/6/7 fuel test.

calculated temperature at that location was 1,436°C. The difference is around 17°C (or ~1.2%) lower than the measured temperature.

Capsule 3 contained three type-N TCs in the same lower temperature zone as HTIR-TC 3-14, and all four of these TCs gave similar temperature measurements, further evidencing the HTIR-TC's accuracy at lower temperatures (see Section 3.2.2 for further details). For comparison purposes, the type-N TCs are included in this discussion, though they can only measure temperatures of up to 1,260°C (or 1,290°C over a very short period) before nearing their melting point restrictions. On the other hand, as already stated, the HTIR-TCs can measure temperatures of up to 1,600°C.

3.1 HTIR-TC temperature range and accuracy

The HTIR-TC temperature range was established through several years of out-of-pile testing (Wilkins, 1988; Wilkins and Schooley, 1992; Rempe and Wilkins, 2005a; Rempe and Wilkins, 2005b; Wilkins and Evans, 2005; Rempe et al., 2006a; Rempe et al., 2006b; Daw et al., 2007; Rempe et al., 2007; Rempe et al., 2008; Daw, 2009). Exhaustive preliminary out-of-pile testing is indicative of in-pile nuclear testing, as both are expensive and time consuming. In the in-pile test design, different TC types were applied to various temperature ranges to help validate neighboring measurements. The HTIR-TCs inside the AGR 5/6/7 test rig were identically constructed from a consistent batch of individual materials. From all HTIR-TCs, ten (a representative sample size) were individually calibrated, and their measured accuracy in the 0°C–1,600°C range was either ±1°C or ±0.4% of the temperature reading, whichever was greater (Skifton et al., 2018). This represents the as-manufactured accuracy of all the AGR 5/6/7 HTIR-TCs and is not to be confused with calibration instability in a neutron flux environment, discussed in below in Section 3.3.

The AGR-5/6/7 test was not configured to measure the true *in situ* accuracy of the HTIR-TCs, as it lacked a calibrated reference TC that could be dropped into the capsule(s). However, a theoretical estimate of each capsule temperature was attained using the ABAQUS finite element model (Pham, 2021). Over the first 14 days of operation, a temperature deviation of less than ±5% between the ABAQUS model and the temperature measured directly by the HTIR-TCs was observed. The constancy of the temperature measurements made early in life—prior to any appreciable drift—by the HTIR-TCs in both Capsules 1 and 3 gave indication of what the baseline temperature measurements were. A summary of comparisons between TC measurements and calculations can be seen in Table 1.

3.2 AGR 5/6/7 drift and inhomogeneity results

3.2.1 Capsule 1 HTIR-TC drift and inhomogeneity trends

According to the data in Figure 2, the four HITR-TCs in Capsule 1 apparently experienced a small downward drift of 3%–4% after residing in ATR for 150 EFPDs; however, this could not be well quantified over the noise in the data, which resulted from experimental error. The capsule temperatures fluctuated around approximately ±2% and appeared to be synchronized, indicating it was caused by changes in the ambient temperature, not in the TC response. These fluctuations can be sourced to a culmination of phenomenon like overall gas flow, vibrations in the TC junction location, reactor power fluctuations, among other secondary sources like thermal expansion and contraction of the fuel matrix. The sharp spatial temperature gradient of each capsule grossly exaggerates each phenomenon, as well. Figure 4 reveals this trend more clearly, as a function of time, with the TC daily averaged temperature measurements being normalized to

TABLE 1 HTIR-TC measured vs. calculated temperature results.

Capsule	HTIR-TC #	Measured temperature [°C]	Calculated temperature [°C]	Difference [°C]	Difference [%]
1	1-12	1,250	1,271	−21	−1.7
1	1-13	1,250	1,279	−29	−2.3
1	1-14	1,323	1,328	−5	−0.4
1	1-15	1,219	1,208	11	0.9
3	3-5	1,453	1,436	17	1.2
3	3-12	1,278	1,327	−49	−3.6
3	3-14	1,200	1,185	15	1.3
—	Type N #	—	—	—	—
3	3-7	1,163	1,168	−5	−0.4
3	3-13	1,154	1,182	−28	−2.4
3	3-15	1,156	1,188	−32	−2.7

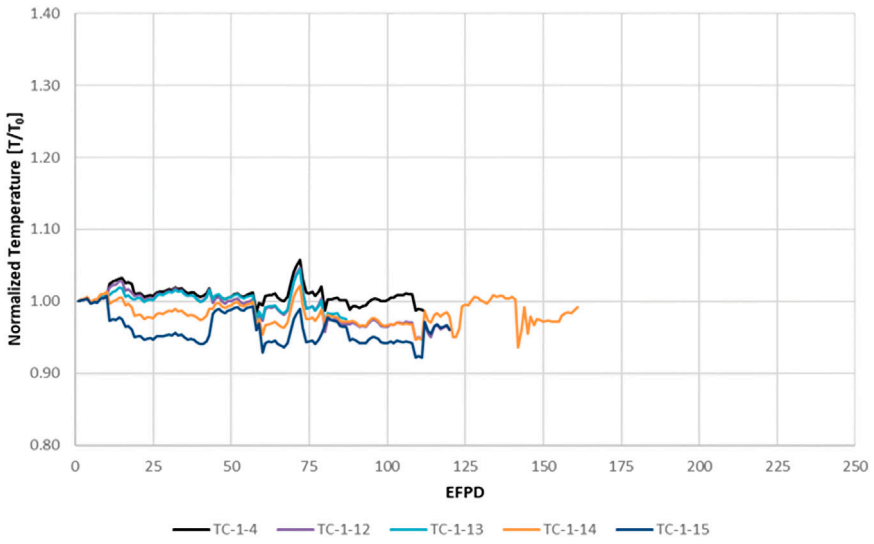

FIGURE 4
Temperature measurements from the HTIR-TCs and type-N TC in AGR-5/6/7 Capsule 1, normalized by the initial *in situ* temperature measurement, T_{INT}. The HTIR-TCs are in color, and the type-N TC (1-4) is in black.

their initial value, T_0. A collocated type-N TC is also shown for comparison purposes. These data reveal the HTIR-TCs in Capsule 1 to have performed as expected. Operating for that length of time at a temperature of 1,280°C generally produced a downward drift of −3.5%.

3.2.2 Capsule 3 HTIR-TC drift and inhomogeneity trends

The data in Figure 3 show different temperature measurement trends for the three HTIR-TCs in Capsule 3 (i.e., 3-5, 3-12, and 3-14). Figure 5 more clearly shows these trends as a function of time, with the TC daily averaged temperature measurements being normalized to T_0. HTIR-TC 3-14 showed no change in trend, either up or down, whereas 3-12 showed an upward trend. An examination of type-N TCs in a temperature location similar to that of 3-12 (i.e., same capsule but a lower temperature region) also revealed the same upward trend. HTIR-TC 3-5, on the other hand, showed a significant downward trend.

These data indicate that the noise in the measured temperatures for all the TCs is synchronized in their local regions, meaning they do not reflect true TC drift but rather a trend indicative of changes in the ambient temperature environment.

Figure 5 reveals the three types of measured temperature trends exhibited by the TCs in Capsule 3:

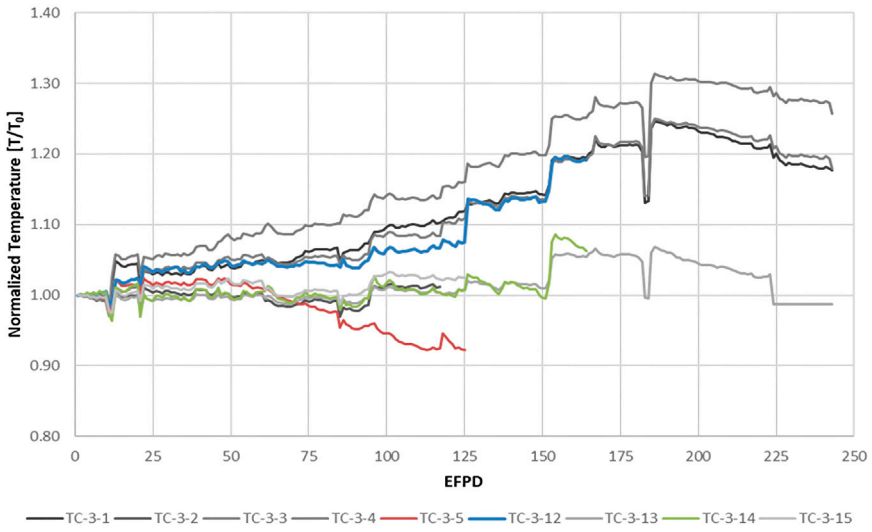

FIGURE 5
Temperature measurements from the HTIR-TCs and type-N TCs in Capsule 3 of AGR-5/6/7, normalized by the initial *in situ* temperature measurement, T_{INT}. The HTIR-TCs are in color, and the type-N TCs are in grayscale.

1. The first trend is the relatively constant temperatures exhibited by HTIR-TC 3-14 and type-N TCs 3-2, 3-13, and 3-15 at up to 150 EFPDs. In particular, note that type-N TC 3-13 was the "control" TC for the entirety of the experiment, meaning that the reactor power and gas flow mixture was adjusted based on its temperature readings. After 150 EFPDs, all the TCs noted a synchronized temperature increase, indicating a sudden increase in the surrounding temperature.
2. The second trend is that a cluster of TCs (specifically HTIR-TC 3-12 and type-N TCs 3-1, 3-3, and 3-4) all showed a gradual increase in temperature measurement readings with time once the specified lifetime of the TCs was reached, and this increase lasted all the way until shortly after the 175 EFPD mark. There is no physical reason why the sensitivity of this entire type-N/HTIR-TC group would synchronously increase. This rise in measured temperatures was not due to any TC sensitivity change (i.e., drift), but rather an actual temperature increase in this region of Capsule 3. It is also likely that this ambient temperature increase cancelled out the expected downward drift. The reason for this increase is not well understood, but likely relates to the difficulty of maintaining a constant temperature for the Capsule 3 design and is under further review. One reason why the measurements from type-N TCs 3-1, 3-3, and 3-4 trended upward is because they were in the outer of the capsule's two graphite layers. As the fuel reduces over time, less heat flux moves from the fuel to the capsule wall, which is cooled by water. To maintain a constant temperature in the fuel, a larger temperature increase begins to manifest between the wall and the inner layer of graphite. Thus, these three TCs can be expected to climb in temperature as the fuel decays. A second reason for the temperature rise is that the concentration of He and Ne gases flowing through the capsule was altered so as to maintain a constant temperature—potentially affecting an increase in the temperatures read by the TCs. Thirdly, examination of the experimental test data showed that the TC used to control the test capsule temperature (i.e., TC-3-13) was losing sensitivity. This would cause an increase in Capsule 3's ambient temperature.
3. The third trend pertains to the measurements from HTIR-TC 3-5. Being the only TC located in the center of Capsule 3, HTIR-TC 3-5 had no other similarly located TCs against which it could be compared. HTIR-TC 3-5 showed a relatively constant reading at up to approximately 75 EFPDs, at which point its temperature readings started to decrease, leading to a 125°C change (8.7%) at 125 EFPDs. If the capsule was increasing in temperature, as is suggested by the data from HTIR-TC 3-12 and the similarly located type-N TCs, this downward drift could have exceeded 10%. It is unlikely that this large downward drift was due to a large temperature decrease at this location. It is also unlikely to have been caused by fast neutron damage or thermal neutron transmutations, since the cables of all the other HTIR-TCs experienced similar thermal and fast neutron fluxes without registering the same large downward drift. It is more likely that this drift was due to a real decrease in TC sensitivity, caused by prolonged residence time at high temperature (~1,500°C). It is possible that, although HTIR-TC 3-5 was heat treated to 1,450°C for several hours during manufacturing, it needed to be instead heat treated to a higher temperature and for a longer time to become stabilized for long-term operation at higher temperatures (i.e., 1,500°C–1,600°C).

3.3 HTIR-TC instability analysis

The following general factors apply to our understanding of the drift that results when HTIR-TCs in the ATR test fixture are exposed to neutron fluxes and high temperatures:

1. Neutron-fluence-induced TC drift is primarily due to neutron-fluence-induced transmutations and neutron bombardment effects in the thermoelement cables (Scervini et al., 2013). These effects lead to Seebeck coefficient changes as a function of residence time in the reactor. The TC measurements are affected only in regions where temperature gradients exist. Thus, the instability in the Capsule 1 TCs was mainly caused by the neutron fluence effects in the Capsule 1 cable sections that pass through the large temperature change region of Capsule 1, the smaller temperature changes in the cable transport regions of Capsules 2–5, and the cooler intermediate regions between Capsules 1-2, 2-3, 3-4, and 4-5. Similarly, the instability in the Capsule 3 TCs was caused by neutron fluence effects on the TC cables as they pass through the high-temperature region of Capsule 3, the smaller temperature changes in the cable transport regions of Capsules 4 and 5, and the cooler intermediate regions between Capsules 3-4 and 4-5.

Note that because the temperature fluctuations in these intermediate capsule regions are approximately equal, the generated EMF tends to cancel each other out and does not significantly affect the measured TC EMF prior to irradiation. However, post-irradiation, the Seebeck coefficient in the cables is affected differently, due to the TCs being asymmetrically located in the neutron field. The EMFs due to temperature fluctuations do not cancel each other out, and must be computed to enable accurate drift data analysis. The Seebeck coefficient change due to neutron fluence can be estimated from theoretical considerations backed by experimental data, as described in the HTIR-TC instability model (see Section 3.4).

2. Drift due to prolonged high-temperature operation is mainly caused by impurities that intercalate into the thermoelement microstructure. The thermoelements are located near the alumina insulation, and at excessive temperatures, the aluminum disassociates from the alumina and travels into the Nb thermoelement via solid-state diffusion (Riley et al., 2023). This is most prominent when the measured temperature (T_M) nears or exceeds the heat treatment temperature (T_{HT}). It has been observed that when T_{HT}-T_M < ~400°C, the drift increases as T_M approaches T_{HT}, and increases dramatically when $T_M > T_{HT}$. The Seebeck coefficient change caused by high-temperature operation can be estimated from the experimental data as a function of time in operation at high temperature. The rest of the TC cable outside the capsule reflects a negligeable change in the Seebeck coefficient, as the temperature in these regions is well below the heat treatment temperature.

Both neutron-flux- and high-temperature-operation-induced drift cause a downward drift in the HTIR-TC signal. This leads to the drift being generally negative in magnitude.

For a standalone HTIR-TC application, the neutron-fluence-induced drift in a commercial power reactor must be less than approximately −1% of the measured temperature over a period of 18 months—and under a conservatively estimated thermal neutron exposure of 3.8×10^{21} n/cm^2, which corresponds to an average thermal neutron flux of approximately 8×10^{13} n/cm^{2}s. Similarly, the drift requirement for a 24-month cycle under the same degree of neutron flux would be −1.5%. A drift of < -1% over 18 months (or −1.5% over 24 months) of reactor operation is considered acceptable for installing the HTIR-TC as a standalone TC in a light-water power reactor (e.g., a boiling-water reactor [BWR] or pressurized-water reactor [PWR]), where the TC would primarily be used for high-temperature measurements in the event of an accident. The drift of the HTIR-TC in the ATR AGR-5/6/7 test fixture was specified at a higher value (−3.5%) for 125 EFPDs. This is because, in addition to the drift caused by neutron fluence, there is also drift due to prolonged high-temperature operation. The HTIR-TC instability model was developed to use calculated temperature and neutron flux profiles in order to determine the drift due to neutron fluence, and it uses experimentally measured drift at high temperatures (no radiation) to estimate the expected high-temperature drift in the ATR test fixture. The HTIR-TC instability model produces results that approximately match the observed drift data from the ATR qualification test, and extrapolates the data in order to approximately match the drift data found in the literature.

3.4 HTIR-TC instability model

A general model and procedure were developed for calculating HTIR-TC drift in the ATR AGR-5/6/7 test fixture. Boise State University developed a first-principles model (Sikorksi, 2021) by looking closely at the EMF generated by each HTIR-TC thermoelement (i.e., doped versions of Nb and Mo). As a follow-on to this model, the data collected from the AGR 5/6/7 experiment were empirically fit, then modeled to a general scope of TC drift occurring during an irradiation experiment (i.e., exposure to thermal/fast neutrons and higher-than-allowable temperatures). These models are briefly described in the sections that follow.

3.4.1 Model of instability due to neutron fluence

A common misconception about TC sensors is that their temperature measurements are generated in the junctions where dissimilar lead wires intersect. In fact, EMF is generated over the length of thermoelement (or cabling) exposed to a thermal gradient. It is important that this be understood whenever TCs are being used, but in the context of utilizing them in a nuclear reactor, it is paramount that the entire cable length be considered. By their very nature, reactors entail a spectrum of thermal and fast neutrons that can transmute and/or damage the TC cabling. Minimizing the cable length will help prevent a unique form of long-term drift not seen in virtually any other application.

Neutrons affect the entire length of a TC thermoelement—not just the location of the TC junction or where the TC passes through the maximum neutron flux. With that in mind, the following steps can be used to model the neutron-fluence-induced drift over the full length of the TC thermoelements—specifically utilizing the AGR 5/6/7 test as an example.

The following steps provide a consistent method of estimating the drift of in-pile HTIR-TCs. The method follows the AGR 5/6/7 test and configuration but can be generalized to apply in any experiment and/or reactor test bed.

1. Estimate the high temperatures measured at the TC junctions in the approximate mid-regions of Capsules 1 and 3, where the HTIR-TCs are located.
2. Estimate the slight reduction in temperature as the cables reach the capsule exit.
3. Estimate the sharp decrease in temperature as the cables enter the gap between one capsule and the next.
4. Estimate the temperature increase as the cables enter and travel through the cable bypass region of the upper neighboring capsule, where they are exposed to high temperatures.
5. Estimate the temperature decrease as the cables leave the cable bypass region of the neighboring capsule and enter the gap region between the upper neighboring capsules.
6. Repeat Steps 4 and 5 and estimate the cable temperatures as the cables pass through all the in-between capsule regions and finally reach the topmost capsule (i.e., Capsule 5).
7. The temperature then decreases to the reference ice temperature (0°C).

For the drift calculation, it is assumed that the temperature profiles of the HTIR-TCs in Capsules 1 and 3 are constant regardless of the number of EFPDs, and do not change with time/residence in the reactor.

After determining the temperature profile for the entire length of the TC cable, the local Seebeck coefficient must be estimated. The following steps enable estimation of the local Seebeck coefficient prior to irradiation:

8. The HTIR-TC instability model determines the TC's EMF by integrating the Seebeck coefficient multiplied by the change in temperature with respect to distance over the length of the cable, as per the following equation:

$$EMF = \int_0^L S_{eff}(T,x) \times \frac{dT(x)}{dx} dx, \quad (1)$$

where:

x = Distance along the TC cable [m], measured from the top of the reactor.

$S_{eff}(T,x)$ = Effective Seebeck coefficient of the Mo/Nb TC [mV/°C], which is a function of the temperature. And since the temperature varies along the length of the TC wires, it is also a function of distance along the TC wires.

dT/dx = Rate of temperature change with distance [°C/m].

L = Full length of the TC cable [m].

Note that, since each thermoelement generally has its own Seebeck coefficient, S(T), the Seebeck coefficient is combined or is deemed the effective Seebeck coefficient, $S_{eff}(T,x)$, of the Mo and Nb thermoelement wires. This effective Seebeck coefficient is equal to the difference between the Seebeck coefficients for Mo and Nb. The Seebeck coefficient for Mo, $S_{Mo}(T,x)$, is positive for all temperatures, and has a much larger magnitude than the Seebeck coefficient for Nb, $S_{Nb}(T,x)$. On the other hand, $S_{Nb}(T,x)$ is negative at low temperatures and positive at high ones, and at all temperatures its magnitude is significantly less than that of $S_{Mo}(T,x)$. The value of $S_{eff}(T,x)$ varies with temperature and is positive for all temperatures in the given measurement range. The magnitude of $S_{eff}(T,x)$ slightly varies for each HTIR-TC and depends on the heat treatment of the TC as well as on the thermal and fast neutron fluence it eventually experiences in the reactor. The $S_{eff}(T,x)$ value can be estimated from the literature, but is more accurately estimated from the test data by using the HTIR-TC instability model.

9. Determine the unirradiated effective Seebeck coefficient as a function of temperature. Note that, since the HTIR-TCs were individually calibrated after heat treatment, the unirradiated effective Seebeck coefficient, $S_{eff}(T,x)$, as a function of temperature and distance can be determined from the HTIR-TC calibration data. Numerically, this is the slope (or tangent) of the measured voltage [mV] vs. temperature [°C] polynomial curve at various temperatures. A polynomial can be fit to these data so that the unirradiated effective Seebeck coefficient can be determined for all temperatures within the measurement range. That is, $S_{eff}(T,x)$ equals a polynomial fit of dV/dT as function of temperature, based on the HTIR-TC calibration data. The Seebeck coefficient is then used in the following manner to calculate the total EMF generated in the thermoelements:

$$EMF(T) = \sum_0^L S(T,x) \frac{dT(x)}{dx} dx. \quad (2)$$

10. By integrating Eq. 1, determine the unirradiated EMF of the HTIR-TCs in Capsules 1 and 3. This integration is accomplished numerically by dividing the TC length into small increments, determining the temperature change by referring to the temperature profile obtained in Step 1, and then multiplying by the average unirradiated effective Seebeck coefficient for that temperature and spatial increment from Step 3 in order to produce the incremental EMF generated by that small incremental distance. Next, add up the incremental EMFs for the entire TC length. This value should approximately equal the measured EMF value for that temperature in the calibration test.

Now the effect of irradiation on the TC thermoelements Mo and Nb—and in turn the Seebeck coefficient—must be estimated via a reduction factor that accounts for the thermal and fast neutron profiles:

11. Use ATR documentation to determine the thermal neutron and fast neutron flux profile across all capsules, then modify the result per the experimentally determined factors for the test fixture.
12. Estimate the effective Seebeck coefficient reduction due to thermal and fast neutron irradiation. The HTIR-TC instability model assumes that the Seebeck coefficient reduction due to neutron fluence has the following form:

$$Reduction\ Factor = e^{-(C_1\varphi_{Thermal} + C_2\varphi_{Fast})t}, \quad (3)$$

where $C_{1\&2}$ are the correction factor coefficients for both thermal and fast neutrons, respectively; φ is the neutron flux for thermal and fast neutrons, and t is the total irradiation time in seconds. This converts the Seebeck coefficient, reduced by nuclear irradiation, into to a new irradiated Seebeck coefficient, S*(T,x), where the * represents the reduced, irradiated version:

$$S^{*}(T,x) = S(T,x) \times Reduction\,Factor. \quad (4)$$

A conservatively high estimate of the neutron flux reduction factor constant, C_1, for thermal flux is obtained by first adding the 2,200 m/s thermal neutron absorption cross sections (in barns, b, where 1 b = 10^{-24} cm^2) of the Mo and Nb, where the Mo absorption coefficient is the sum of the absorption coefficients of the Mo isotopes, as weighted by their fractional abundance (2.48 b), and the Nb cross section is 1.48 b. Thus, the conservatively high thermal neutron 2,200 m/s cross section of the Mo/Nb TC is 3.63 b. The reason for choosing a conservatively high value for the 2,200 m/s thermal neutron absorption cross section is to provide a conservatively high drift estimate for HTIR-TC applications in commercial BWRs/PWRs, where the neutron flux is primarily thermal. The constant C_1 is then obtained by converting this 2,200 m/s cross section (corresponding to an average thermal neutron temperature of ~20°C) into the cross section observed at the ATR's average thermal neutron temperature of 60°C (Wescott, 1962). The constant C_2 for fast flux is generally much smaller than the C_1 for thermal flux; and for the HTIR-TC instability model, it is assumed to be 0.5 b.

Using S^{*}_{eff} (T,x), the effective EMF generated by irradiated TCs is then calculated via the following method, which is similar to Step 11:

13. Determine the irradiated EMF of the Capsule 1 and Capsule 3 HTIR-TCs in the test fixture by numerically integrating the incremental EMF values for the irradiated TCs. Note that this irradiated EMF is only due to the Seebeck coefficient reduction caused by thermal and fast neutron fluence and does not include the Seebeck coefficient change caused by prolonged high-temperature operation. The incremental EMFs for the irradiated TCs are calculated by multiplying the incremental temperature change for each incremental distance along the TC by the reduced effective Seebeck coefficient at that location and temperature. The incremental EMFs are then added together to give the total irradiated EMF:

$$EMF^{*}(T) = \sum_{0}^{L} S^{*}(T,x)\frac{dT}{dx}dx. \quad (5)$$

14. The neutron-fluence-induced HTIR-TC drift calculated by the instability model is then determined via the following equation, comparing the EMF generated from both the unirradiated and irradiated thermoelements:

$$Instability\,(neutron\,fluence)\,(\%) = \frac{EMF^{*}(T) - EMF(T)}{EMF(T)}100\%. \quad (6)$$

3.4.2 Model of instability due to high-temperature operation

In the past, experiments were conducted in test ovens to determine the HTIR-TC drift caused by high-temperature operation, leaving out the drift due to reactor neutrons. These experiments proved that drift occurred, and that it was due to changes in the TC's metallurgical structure as well as the potential introduction of impurities into the TC. Both the data and the cause of this drift suggest that the drift depends on the difference between the TC heat treatment temperature, $T_{HT,}$ and the measured temperature, T_M, and that it can occur whenever the T_M nears or exceeds T_{HT}. The greater the temperature difference (i.e., T_{HT}–T_M > 400°C), the less the drift.

The data reveal that every TC showed drift when measuring temperatures exceeding ~1,200°C. The drift was more severe for type-K and type-N TCs than for HTIR-TCs; however, HTIR-TCs heat treated at 1,500°C showed a significant drift of −1.6% when exposed to 1,200°C for 4,000 h. Furthermore, preliminary out-of-pile data show the drift leveling off to zero after experiencing a severe drop. From a technical standpoint, this is understandable, as the TC is not expected to continue to drift once the metallurgical structure has stabilized at the operating temperature.

As all HTIR-TCs were heat treated during manufacturing to 1,450°C, the high temperature instability model was first based on a heat-treatment to measured temperature difference of 300°C, (i.e., T_{HT}–T_M = 300°C). Next, the drift data were extrapolated to a temperature difference of 157°C to match the measured temperature of HTIR-TCs 1-12 and 1-13, then extrapolated to a temperature difference of 169°C for HTIR-TC 1-14, and to a temperature difference of −50°C to match the measured temperature for HTIR-TC 3-5 at 1,500°C. For such extrapolations, it is necessary to ensure that, when adding the extrapolated high-temperature drift at 3,000 h to the neutron fluence drift at 3,000 h, the result approximately matches the observed 3000-h (125 EFPD) ATR test drift of −3.3% for HTIR-TCs 1-12 and 1-13, −3.7% for HTIR-TC 1-14, and −8.7% for HTIR-TC 3-5. These curves are represented nominally in Figure 6, which also shows that if the operating temperature is lower than the heat treatment temperature by more than 400°C (i.e., T_{HT}–T_M > 400°C), the drift due to high-temperature operation becomes negligeable. The data also show that if the TC is operating at a higher temperature than the heat treatment temperature (i.e., T_M–T_{HT} > 0°C), the magnitude of the drift due to high-temperature operation can exceed 10% for an exposure of greater than 3,000 h.

3.5 Results of the HTIR-TC instability model calculations

The total instability (in percent, as calculated by the HTIR-TC instability model) caused by neutron fluence and high-temperature operation over 125 EFPDs was obtained by adding the percent change due to neutron fluence and the percent change due to high-temperature operation.

Comparison of these results (calculated by the HTIR-TC instability model) against the observed instability can be made by examining the instability data obtained for HTIR-TCs 1-12, 1-13, 1-14, and 3-5 in the AGR 5/6/7 test, in which the instability was caused by both neutron fluence and high-temperature operation.

The data show that, for 125 EFPDs, the total instability due to neutron fluence and high-temperature operation was approximately −3.3% for HTIR-TCs 1-12 and 1-13, −3.5% for HTIR-TC 1-14, and −8.7% for HTIR-TC 3-5. Note that there was no apparent instability for HTIR-TC 3-5 over the first 1,200 h at ~1,500°C, meaning that HTIR-TCs can be used to measure such high temperatures without experiencing drift and

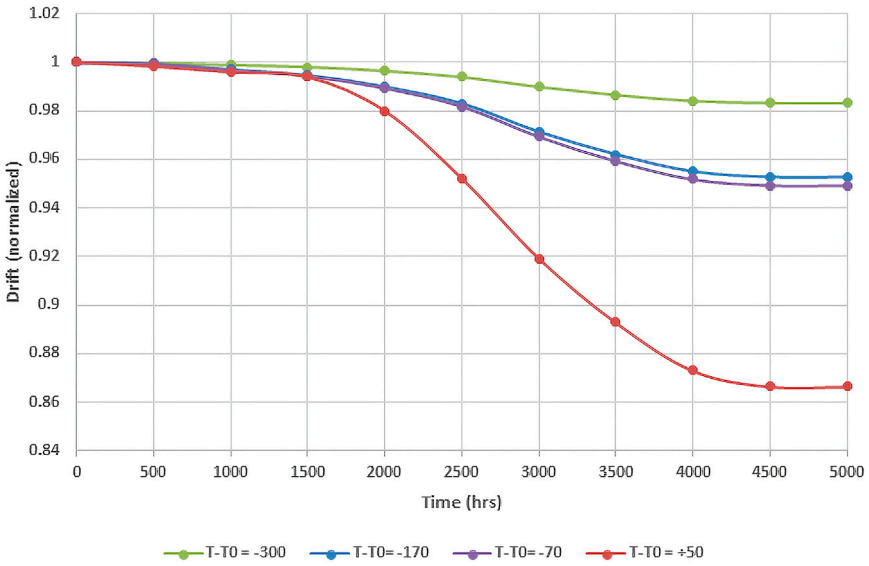

FIGURE 6
Extrapolation of the drift (normalized) due to high-temperature operation.

TABLE 2 Total calculated HTIR-TC instability due to neutron fluence and high-temperature operation. Comparison between instability model and actual measured drift is shown.

HTIR-TC #	Operating temperature [°C]	Time in ATR (EFPD)	Calculated instability due to neutron fluence [%]	Calculated instability due to high-temperature operation [%]	Total calculated instability [%]	Observed drift of HTIR-TC in ATR test [%]	Difference between calculated and observed [%]
1-12	1,293	125	−0.43	−2.86	−3.29	−3.33	~ −0.03
1-13	1,293	125	−0.43	−2.86	−3.29	−3.33	~ −0.03
1-14	1,280	125	−0.43	−3.07	−3.50	−3.48	~ −0.02
3-5	1,500	125	−0.57	−8.08	−8.65	−8.67	~ −0.02

inhomogeneity. These values compare well with the calculated values shown in Table 2.

4 HTIR-TC instability model applied to operating thermal BWR or PWR

HTIR-TC drift in commercial, well-moderated thermal power reactors can be conservatively estimated by employing the HTIR-TC instability model and the same 2,200 m/s thermal neutron cross section for determining the Seebeck coefficient reduction factor as was used for the ATR HTIR-TC drift calculation. As described in Step 9 of Section 3.4.1, the average cross section for determining the reduction factor in a reactor is obtained by modifying the 2,200 m/s cross section, using Equation 9 to account for the power reactor's thermal neutron temperature. The cross-section coefficient, C_1, for calculating drift due to neutrons thermalized at BWR and PWR temperatures is shown in Table 3. Since commercial BWRs and PWRs are primarily thermal flux reactors, the drift due to fast neutron irradiation can be neglected.

The expected thermal neutron fluence, φ_t, for a TC located in-core in a commercial power reactor is approximately 3.8×10^{21} n/cm^2 for an 18-month refueling cycle and ~5.1×10^{21} n/cm^2 for a 24-month cycle, based on the average thermal neutron flux of 8×10^{13} n/cm^{2}s. The expected TC drift for this level of thermal neutron exposure in a BWR or PWR can be calculated by assuming the TC to have been installed as a standalone TC, and the neutron flux incident on the TC to be constant in the region where the temperature is changing. For such an installation in a BWR or PWR, the drift can be calculated using the following simplified equation:

$$Drift\,(\%) = \left(e^{C_1 \varphi t} - 1\right) \times 100\,\% \tag{7}$$

where C_1(BWR) = 2.33×10^{-24} cm^2, C_1(PWR) = 2.27×10^{-24} cm^2. The results of this calculation are shown in Table 4. Another option to consider is the removal of the Nb neutron absorption cross section, as a negligible amount of EMF is generated in that

TABLE 3 Calculated instability in a commercial power reactor.

Power plant	Total cross section [barns]	Refueling cycle [months]	Average thermal flux [n/cm^2]	Thermal neutron fluence [n/cm^{2}s]	C_1 [cm^2]	Instability [%]
BWR	3.63	18	8×10^{13}	3.79×10^{21}	2.33×10^{-24}	−0.86
BWR		24		5.05×10^{21}	2.33×10^{-24}	−1.17
PWR		18		3.79×10^{21}	2.27×10^{-24}	−0.88
PWR		24		5.05×10^{21}	2.27×10^{-24}	−1.14
BWR	2.48[a]	18		3.79×10^{21}	2.33×10^{-24}	−0.60
BWR		24		5.05×10^{21}	2.33×10^{-24}	−0.80
PWR		18		3.79×10^{21}	2.27×10^{-24}	−0.59
PWR		24		5.05×10^{21}	2.27×10^{-24}	−0.78

[a]Niobium neutron cross section removed from total cross section as minimal EMF is contributed.

TABLE 4 Summary of HTIR-TC performance in Capsule 1 during the AGR 5/6/7 test.

Parameter	Requirement	Measured value of HTIR-TCs in capsule 1			
		1-12	1-13	1-14	1-15
Temp Range Min [°C] Max [°C]	Room Temp 1550°C	21.31 1,354	22.96 1,350	21.45 1,412	21.20 1,259
Accuracy [%]	±1%	Test not designed to measure TC accuracy to within 1%. HTIR-TC temperatures agreed to within 5% of the theoretically calculated temperatures, which is within the accuracy of the theoretical calculations			
Repeatability [%]	±1%	±1%	±1%	±1%	±1%
Instability in ATR due to neutron fluence (calculated)	−3.5% (For 125 EFPDs)	−0.43% (calc)	−0.43% (calc)	−0.43% (calc)	—
Instability in ATR due to high temperature (calculated)		−2.9%	−2.9%	−3.1%	—
Total instability in ATR (calculated)		−3.3% (calc)	−3.3% (calc)	−3.5% (calc)	—
Total instability in ATR [%] (measured)	−3.5% (for 125 EFPDs of exposure at ATR when operating at less than the heat treatment temperature)	−3.3% at 125 EFPDs (Note: The drift value at 125 EFPD is extrapolated, since the TC only survived to 120 EFPDs)	−3.3% at 125 EFPDs (Note: The drift value at 125 EFPD is extrapolated, since the TC only survived to 87 EFPDs)	−3.5% at 125 EFPDs	Not measurable due to noise in the data
Instability in BWR [%]	<1%	−0.86% (calculated)			
Instability in PWR [%]	<1%	−0.86% (calculated)			
End-of-Life					
Exposure (EFPD)	125	120	87	161	120
Thermal transients	5	10	7	8	7
Reactor startups					
Reactor shutdowns	5	9	7	8	7

TABLE 5 Summary of HTIR-TC performance in Capsule 3 during the AGR 5/6/7 test.

Parameter	Requirement	Measured value of HTIR-TCs in capsule 3		
		3-5	3-12	3-14
Temp Range Min [°C] Max [°C]	Room Temp 1550°C	23.12 1,515	22.97 1,552	22.70 1,353
Accuracy (%)	±1%	Test not designed to measure TC accuracy to within 1%. HTIR-TC temperatures agreed to within 5% of the theoretically calculated temperatures, which is within the accuracy of the theoretical calculations		
Repeatability (%)	±1%	±1%	±1%	±1%
Instability in ATR due to neutron fluence (calc)	−3.5% (For 125 EFPDs)	−0.57%	—	—
Instability in ATR due to high temperature (calc)		−8.1%	—	—
Total instability in ATR (calc)		−8.7%	—	—
Total instability in ATR (%) (measured)	−3.5% (for 125 EFPDs of exposure at ATR when operating at less than the heat treatment temperature)	−8.7% at 125 EFPDs (due mainly to prolonged operation at a temperature 50°C higher than the heat treatment temperature)	Virtually no measurable drift at up to 125 EFPDs, but likely −3 or −4% drift, which was undetected since the temp was controlled by a TC whose sensitivity was decreasing	Drift not measurable due to an increase in ambient temperature. Would likely meet the drift req't of −3 or −4% if the ambient temp was constant
Instability in BWR (%)	<1%	0.86% (calculated)		
Instability in PWR (%)	<1%	0.88% (calculated)		
End-of-Life				
Exposure (EFPD)	125	125	166	164
Thermal transients Reactor startups Reactor shutdowns	5 5	11 10	11 11	11 10

thermoelement. Mo would then be considered the sole EMF generator, leaving the neutron absorption cross section of the HTIR-TC as 2.48 b.

Note that for HTIR-TCs operating in a BWR or PWR, the only drift that occurs is due to neutron exposure. The drift due to high-temperature operation in a BWR or PWR is negligible since the operating temperature is far below the heat treatment temperature. The typical operating reactor temperature at 100% power is 300°C for a BWR and 315°C for a PWR, while the heat treatment temperature for these HTIR-TCs is 1,450°C. Thus, for normal full-power operation, the difference between the heat treatment temperature and the operating temperature (>1,100°C) is very large and would produce a negligible high-temperature drift. Also note that even if the TC was measuring a BWR/PWR accident temperature of 1,000°C, the difference with the heat treatment temperature would be > 400°C. Therefore, according to the HTIR-TC instability model, the high-temperature drift would be negligible, especially since the accident time is generally brief.

5 Summary of HTIR-TC instability performance

Tables 4, 5 summarize the results of the HTIR-TC test measurements and the requirements for the HTIR-TC calibrations. Tables 4, 5 are associated with the AGR 5/6/7 Capsule 1 results, and the AGR 5/6/7 Capsule 3 results, respectively.

Results of the qualification test enabled the following observations:

1. **Range**: The HTIR-TCs were able to measure temperatures ranging from room temperature to ~1,550°C. That was the highest temperature ever measured and withstood by any TC in a high-flux reactor environment. Note that, due to melting point restrictions, type-N TCs, which are typically used for high-temperature measurements, can only measure temperatures of up to approximately 1,300°C—nearly 300°C lower than for the HTIR-TCs.
2. **Accuracy**: The accuracy of the HTIR-TCs was determined via an out-of-pile calibration test in which the HTIR-TC temperature measurement was compared to that of a type-B TC National Institute of Standards and Technology (NIST) standard (Skifton et al., 2018) utilizing ASTM comparative methods under ASTM E220. The general accuracy of each HTIR-TC was statistically found to be either ±1°C or ±0.4% of the temperature reading, whichever was greater.
3. **Instability**: This aspect of performance could not be accurately determined, due to random fluctuations in the data caused by variations in ambient temperature–arising from the capsule

blanket He/Ne gas mixture and/or flow rate. The four HTIR-TCs in Capsule 1 behaved as expected regarding drift. The drift of the HTIR-TCs in Capsule 1 (i.e., 1-12, 1-13, and 1-14) met the −3.5% requirement at 125 EFPDs, though some failed prior to the 125 EFPD period, having been subjected to a large (more than the specified) number of severe thermal transients. The three HTIR-TCs in Capsule 3 reflected different drift performance trends. HTIR-TC 3-14 showed an upward trend that was synchronous with four similarly located type-N TCs—a trend attributed to a gradual ambient temperature increase caused by changes in the passive gas system. The performance data indicate that, had this increase in ambient temperature not occurred, the TC would have behaved as expected. HTIR-TC 3-12, along with two other type-N TCs, behaved normally and showed virtually no drift and inhomogeneity. HTIR-TC 3-5 behaved as expected for an exposure of 50 EFPDs. The performance data indicate that HTIR-TC 3-5 would have instead shown between −3% and −4% instability at an exposure of 125 EFPDs had the ambient temperature held steady, but instead showed a large drop of −8.7% at 125 EFPDs. The cause of this large sensitivity decrease was due to prolonged operation at a temperature 50°C higher than the heat treatment temperature. The technical reason for this is not well understood but is likely due to diffusion of impurities into the thermoelements, due to prolonged operation at high temperatures. Note that the instability measurements were made at high ATR power, and that the HTIR-TC drift and inhomogeneity values calculated by the instability model described in this report apply only to high-temperature operation (>1,050°C). No HTIR-TC drift measurements were made at low ATR power, and no experimental results are available regarding low-temperature operation.

6 Conclusion

The HTIR-TC instability model was developed to calculate TC drift and inhomogeneity. It was determined that, based on the experimental data, HTIR-TC instability was due to both thermal and fast neutrons having caused a reduction in the thermoelements' Seebeck coefficients, as well as to prolonged high-temperature operation. The thermal neutrons change the Seebeck coefficient by transmuting the thermoelements via absorption of thermal neutrons, and the fast neutrons change the Seebeck coefficient primarily by altering the thermoelements' lattice structure through fast neutron bombardment. In addition, prolonged high-temperature operation can change the metallurgical structure of the thermoelements and cause drift and inhomogeneity. Constants for these effects were determined from the available experimental data and then used, along with estimates of the temperature and neutron flux profiles across the TC cables, to determine the pre- and post-irradiation TC EMFs and calculate the TC drift and inhomogeneity due to neutron fluence and prolonged high-temperature operation. The calculation showed that, for 125 EFPDs of exposure in the ATR test fixture, the drift was −3.3% for HTIR-TCs 1-12 and 1-13 in Capsule 1, -3.5% for HTIR-TC 1-14 in Capsule 1, and -8.7% for HTIR-TC 3-5 at a higher temperature in Capsule 3. The calculated instability matched the observed drift for the HTIR-TCs in Capsule 1, though this was not the case for Capsule 3, due to the uncontrolled temperature increase it underwent.

Data availability statement

The raw data supporting the conclusion of this article will be made available by the authors, without undue reservation.

Author contributions

RS designed the entirety of the instability model utilized in mapping HTIR-TC use in the reactor and/or fuels experiments. He designed each figure and table to provide clarification to the text.

Funding

United States Department of Energy—Office of Nuclear Energy. Under the Nuclear Energy Enabling Technology (NEET) Advanced Sensors and Instrumentation (ASI) program. Nuclear grade sensors are developed to high TRL level under this program. Prepared for the U.S. Department of Energy Office of Nuclear Energy Under DOE Idaho Operations Office Contract DE-AC07-05ID14517.

Conflict of interest

The author declares that the research was conducted in the absence of any commercial or financial relationships that could be construed as a potential conflict of interest.

Publisher's note

Author disclaimer

References

ATR National Scientific User Facility (2009). *Advanced test reactor national scientific user facility users guide*. Idaho National Laboratory. INL/EXT-08-14709. Available at: https://nsuf.inl.gov/File/ATRUsersGuide.pdf.

Daw, J. E., Crepeau, J. C., Rempe, J. L., Wilkins, S. C., Knudson, D. L., and Condie, K. G. (2007). "Initial results from investigations to enhance the performance of high temperature irradiation-resistant thermocouples," in *J jpn soc mech eng (JSME), invited paper for 15th international conference on nuclear engineering (ICONE15) special edition* (Nagoya, Japan. April 22-26, 2007. Available at: https://www.researchgate.net/publication/282614012_Initial_Results_from_Investigations_to_Enhance_the_Performance_of_High_Temperature_Irradiation-Resistant_Thermocouples.

Daw, J. E. (2009). "High temperature irradiation-resistant thermocouple performance improvements," in *Proc. Sixth American nuclear society international topical meeting on nuclear plant instrumentation, control, and human-machine interface Technologies* (Knoxville, TN: NPIC&HMIT). April 5-9, 2009. Available at: https://inldigitallibrary.inl.gov/sites/sti/sti/4235634.pdf.

Daw, J. E., Rempe, J. L., Knudson, D. L., Wilkins, S. C., and Crepeau, J. C. (2008). Extension wire for high temperature irradiation resistant thermocouples. *Meas. Sci. Technol.* 19, 045206. doi:10.1088/0957-0233/19/4/045206

Dayal, Y., and Jensen, C. (2019). *Guidelines for developing and qualifying instrumentation systems at Idaho national laboratory*. Idaho National Laboratory. Document ID: GDE-947 Rev 0, Available upon request.

Hawkes, G. L. (2019). "Thermal model details and description of the AGR-5/6/7 experiment," in *Proc. International congress on advances in nuclear power plants, ICAPP 2019* (France, Juan-les-pins. May 12-15, 2019. Available at: https://www.osti.gov/biblio/1599861-thermal-model-details-description-agr-experiment.

Jensen, C. (2007). *FY17 report for instrumentation for the transient testing program*. Idaho National Laboratory. INL/EXT-17-43444. Available at: https://inldigitallibrary.inl.gov/sites/sti/sti/Sort_3449.pdf.

Kim, Y. G., Song, C. H., Gam, K. S., and Yang, I. (2009). Change in inhomogeneity with temperature between 180° C and 950° C in base-metal thermocouples. *Meas. Sci. Technol.* 20 (7), 075102. doi:10.1088/0957-0233/20/7/075102

Palmer, A. J., Petti, D., and Grover, S. B. (2014). "Advanced gas reactor (AGR)-5/6/7 fuel irradiation experiments in the advanced test reactor," in *International congress on advances in nuclear power plants* (ICAPP), 1, 257–266. Available at: https://inldigitallibrary.inl.gov/sites/sti/sti/6064457.pdf.

Palmer, A. J., Skifton, R. S., Haggard, D. C., and Swank, W. D. (2019). "Performance of custom-made very high temperature thermocouples in the advanced gas reactor experiment AGR-5/6/7 during irradiation in the advanced test reactor," in *Animma 2019 - international conference on advancements in nuclear instrumentation measurement methods and their applications* (Portoroz, Slovenia. Jul 17-21, 2019. Available at: https://www.aconf.org/conf_161818.html.

Palmer, A. J., Skifton, R. S., Haggard, D. C., Swank, W. D., and Scervini, M. (2019). "Development and testing of thermocouples for the advanced gas reactor fuel experiment AGR-5/6/7," in *Proc. 11th nuclear plant instrumentation, control and human-machine interface Technologies (NPIC&HMIT 2019)* (Orlando, FL, 1013–1027. (February). Available at: https://www.ans.org/pubs/proceedings/article-45868/.

Palmer, A. J. (2015). "Summary of thermocouple performance during advanced gas reactor fuel irradiation experiments in the advanced test reactor and out-of-pile thermocouple testing in support of such experiments," in *Proc. 2015 4th international conference on advancements in nuclear instrumentation measurement methods and their applications (ANIMMA)* (Lisbon: Portugal), 1–9. (April). doi:10.1109/ANIMMA.2015.7465501

Palmer, J., Skifton, R. S., Pham, B., and Hawkes, G. (2021). "Summary of thermocouple performance in the advanced gas reactor experiment AGR-5/6/7 during irradiation in the advanced test reactor," in *ANIMMA international conference* (Prague, Czech Republic. (June). Available at: https://www.osti.gov/servlets/purl/1822921.

Pham, C. B. T. (2021). *AGR 5/6/7 irradiation test final as-run report*. Idaho National Laboratory. INL/EXT-21-64221. Available at: https://inldigitallibrary.inl.gov/sites/sti/sti/Sort_52944.pdf.

Pham, C. B. T., Sterbentz, J. W., Hawkes, G. L., Scates, D. M., and Palmer, J. (2020). *AGR-5/6/7 experiment monitoring and simulation progress*. Idaho National Laboratory. INL/EXT-19-55429. Available at: https://www.osti.gov/servlets/purl/1689160.

Rempe, J. L., Knudson, D. L., Condie, K. G., Wilkins, S. C., and Daw, J. E. (2008). "Long duration performance of high temperature irradiation resistant thermocouples," in *Proc. International conference on advanced power plants (ICAPP 2007)* (Nice, France. May 2008. Available at: https://inldigitallibrary.inl.gov/sites/sti/sti/3693710.pdf.

Rempe, J. L., Knudson, D. L., Condie, K. G., and Wilkins, S. C. (2006). "Evaluation of specialized thermocouples for high-temperature in-pile testing," in *Proc. 2006 int. Congress advances in nuclear power plants (ICAPP'06)* (Reno, Nevada. June 4–8, 2006. Available at: https://www.osti.gov/servlets/purl/911567.

Rempe, J. L., Knudson, D. L., Condie, K. G., and Wilkins, S. C. (2007). "Long duration performance of high temperature irradiation resistant thermocouples." INL/CON-06-11879," in *Proc. International conference on advanced power plants (ICAPP 2007)* (Nice, France. May 13-18, 2007. Available at: https://www.osti.gov/biblio/912437.

Rempe, J. L., Knudson, D. L., Condie, K. G., and Wilkins, S. C. (2006). Thermocouples for high-temperature in-pile testing. *Nucl. Technol.* 156 (3), 320–331. doi:10.13182/NT06-A3794

Rempe, J. L., and Wilkins, S. C. (2005). "High temperature thermocouples for in-pile applications," in *Proc. 11th int. Topl. Mtg. On nuclear reactor thermal-hydraulics (NURETH-11)* (Avignon, France. October 2–6, 2005. Available at: https://www.researchgate.net/publication/238099701_HIGH_TEMPERATURE_THERMOCOUPLES_FOR_IN-PILE_APPLICATIONS.

Rempe, J. L., and Wilkins, S. C. (2005). *Specialized thermocouples for high temperature in-pile applications*. Idaho National Laboratory. INEEL/EXT-05-02576. Available at: https://www.researchgate.net/publication/286778226_Specialized_Thermocouples_for_High_Temperature_In-Pile_Applications.

Riley, B. P., Sikorski, E., Skifton, R., Li, L., and Jaques, B. J. (2019). "Development and performance of high temperature irradiation resistant thermocouples," in *Materials for nuclear applications* (Portland, OR: Materials Science & Technology). September 29 – October 3, 2019.

Riley, S., Holloway, K., Bateman, A., Skifton, R., and Jaques, B. J. (2023). Influence of microstructure and phase morphology on the stability of high temperature irradiation resistant thermocouples. *Mat Sci Eng A* 112. doi:10.1016/j.mtcomm.2023.105972

Riley, S., Perrine, B., Sikorski, E., Li, L., Skifton, R., and Jaques, B. (2020). "Performance of niobium and molybdenum alloys for high temperature sensing applications," in *Proc. 2020 TMS annual meeting & exhibition* (San Diego, CA: Refractory Metals).

Scates, D., Reber, E. L., and Miller, D. (2020). Fission gas monitoring for the AGR-5/6/7 experiment. *Nucl. Eng. Des.* 358, 110417. doi:10.1016/j.nucengdes.2019.110417

Scervini, M., Rae, C., and Lindley, B. (2013). "Transmutation of thermocouples in thermal and fast nuclear reactors," in *Proc. 2013 3rd international conference on advancements in nuclear instrumentation, measurement methods and their applications (ANIMMA)* (Marseille, France, 1–8. doi:10.1109/ANIMMA.2013.6727900

Sikorksi, E. (2021). *Computational modeling towards accelerating accident tolerant fuel concepts and determining in-pile fuel behavior*. Ph.D. Thesis. Boise State University, 93–117. Chapter 5. doi:10.18122/td.1873.boisestate

Skifton, R. (2021a). "A first principle look at the electromotive force generation from molybdenum and niobium alloys," in *Proc. 12th nuclear plant instrumentation, control and human-machine interface Technologies (NPIC&HMIT 2021)* (Providence, RI, 585–591. (June 2021). doi:10.13182/T124-34537

Skifton, R. (2021b). *High temperature irradiation resistant thermocouple qualification requirement report*. Idaho National Laboratory. INL/EXT-21-63269, 2021. Available at: https://inldigitallibrary.inl.gov/sites/sti/sti/Sort_53355.pdf.

Skifton, R., Palmer, J., and Hashemian, A. (2021). Optimized high-temperature irradiation resistant thermocouple for fast-response measurements. *EPJ Web Conf.* 253, 06004. doi:10.1051/epjconf/202125306004

Skifton, R. S. (2021c). *Function and operational requirements for high temperature irradiation resistant thermocouples (No. INL/EXT-21-63173-Rev001)*. Idaho Falls, ID (United States): Idaho National Lab.(INL.

Skifton, R. S. (2019). *Out-of-pile performance of high temperature irradiation resistant and cladding thermocouples*. Idaho National Laboratory. INL/EXT-19-55295, 2019. Available at: https://inldigitallibrary.inl.gov/sites/sti/sti/Sort_19912.pdf.

Skifton, R. S., Palmer, A. J., Davis, K., Calderoni, P., Sikorski, E., and Corbett, D. (2019). "Summary of high temperature irradiation resistant thermocouple standardization tests," in *Proc. 11th nuclear plant instrumentation, control and human-machine interface Technologies (NPIC&HMIT)* (Orlando, FL. INL/CON-18-51789-Rev. 0 (February). Available at: https://www.osti.gov/biblio/1497074.

Skifton, R. S., Palmer, J., and Calderoni, P. (2018). Optimization of heat treatment and calibration procedures for high temperature irradiation resistant thermocouples. *Instrum. Sci. Techno* 46 (4), 349–363. doi:10.1080/10739149.2017.1389754

Sloneker, K. C. (2009). Thermocouple inhomogeneity. *Ceram. Ind.* 159 (4), 13–18.

Wescott, C. H. (1962). *Effective cross section values for well-moderated thermal reactor spectrum*. Atomic Energy of Canada Limited. AECL-1101. Available at: https://inis.iaea.org/search/search.aspx?orig_q=RN:41057250.

White, W. P. (1906). The constancy of thermoelements. *Phys. Rev. Ser. I)* 23 (6), 449–474. doi:10.1103/physrevseriesi.23.449

Wilkins, S. C., and Evans, R. P. (2005). *Assessment of high-temperature measurements for use in the gas test loop*. Idaho National Laboratory. INL/EXT-05-00298. Available at: https://inldigitallibrary.inl.gov/sites/sti/sti/3480227.pdf.

Wilkins, S. C. (1988). "Low cross-section Mo-Nb thermocouples for nuclear application: The-State-of-the-Art," in *5th symp of space nuclear power systems* (Albuquerque, NM, 1. (January). Available at: https://www.osti.gov/servlets/purl/5651355.

Wilkins, S. C., and Schooley, J. F. (1992). "Characterization and materials-compatibility tests of molybdenum-niobium thermocouples," in *Proc. 7th int. Symp. Temperature: Its meas and control in science and industry* (Toronto, Canada, 728–630. 6, no. 1, (January). Available at: https://www.tib.eu/en/search/id/BLCP:CN005065549/Characterization-and-material-compatibility-tests?cHash=7aa5d556756a2bfc53f39937b7c35b3d.

Frontiers in Energy Research

Advances and innovation in sustainable, reliable and affordable energy

Explores sustainable and environmental developments in energy. It focuses on technological advances supporting Sustainable Development Goal 7: access to affordable, reliable, sustainable and modern energy for all.

Discover the latest Research Topics

See more →

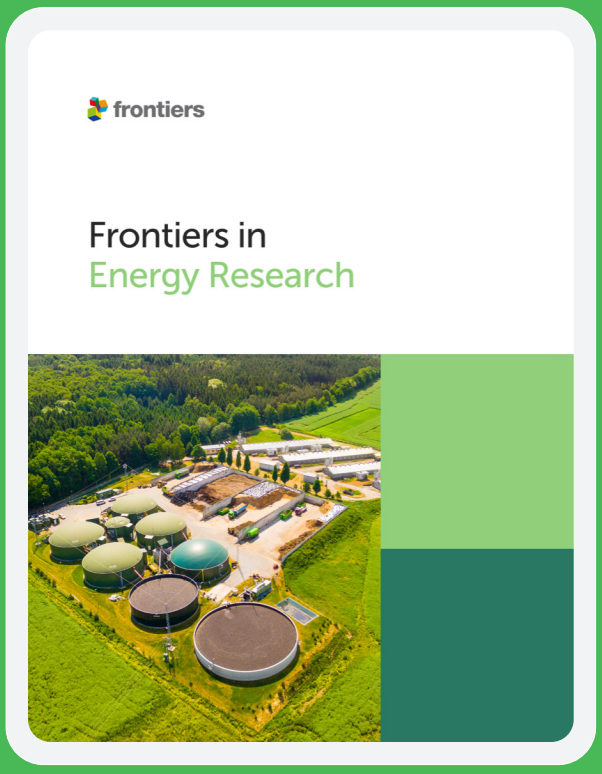

Frontiers

Avenue du Tribunal-Fédéral 34
1005 Lausanne, Switzerland
frontiersin.org

Contact us

+41 (0)21 510 17 00
frontiersin.org/about/contact